Leaders in Deep Exploration

Quantec Geoscience

TITAN-24 DC - IP - MT SURVEY

GEOPHYSICAL REPORT

ELK GOLD PROJECT

(BRITISH COLUMBIA, CANADA)

ON BEHALF OF

GOLD MOUNTAIN MINING CORPORATION

(BRITISH COLUMBIA, CANADA)

QUANTEC GEOSCIENCE LTD
146 SPARKS AVE, TORONTO, ONTARIO, M2H 2S4, CANADA
PHONE: (416) 306-1941 / FAX: (416) 306-1949
WWW.QUANTECGEOSCIENCE.COM

BENOIT TOURNERIE
WADE LEE

08/11/2011

EXECUTIVE SUMMARY

INTRODUCTION

A Titan-24 DCIP survey was undertaken on behalf of Gold Mountain Mining Corporation, Vancouver, Canada, from September 24th to October 10th, 2011, over the Elk Gold Project property.

The survey is located approximately 45 km Southeast of Merritt, British Columbia, and includes two lines with azimuth 0°. Each line was surveyed using 3 spreads, for a total length of 7.1km each. For each spread, the DC-IP utilized a pole-dipole configuration with 100m dipoles. Current and station overlap were used to ensure better continuity between spreads. The magnetotelluric data were collected using the same DCIP dipoles, plus another set of 100m dipoles oriented perpendicular to the profile, for frequencies ranging from 10kHz down to 0.01Hz. The final coverage of the survey is 14.1km of DCIP, and 14.1km on MT, without current extensions and overlap.

SURVEY OBJECTIVES

The main objective of the survey is to detect gold-bearing quartz veins to depth for drill targeting, and delineation of mineralization and alteration.

RESULTS

The data were inverted using 2D inversion algorithms to produce sections of the resistivity and chargeability distributions of the subsurface. The final interpretation is based on the integration and comparison of the IP, the DC, and the MT results.

The MT inversion results highlight on the two profiles a deep conductive structure at depth located between 5523500N and 5525500N. The results on the first hundreds of meters display a relative good correlation between the MT and the DC results, delineating several structural contacts along the two profiles. Two strong IP zones located on the northern end of the two profiles have been identified. It is not clear what can be the cause of these anomalies and ground sampling or DDH follow is recommended to better identify these structures. Except these IP zones, only a few weak to medium chargeability high zones were identified. We note however that these IP weak anomalies delineate some gradient zones on the IP models that correlate with the more conductive zones that are associated with the structural zones.

From the analysis of all the results, a total of 16 targets zones had been identified along the two profiles, with 6 as high priority, 6 as medium priority, and 4 as low priority. It is important to note here that several of the target zones identified here have already DDH information over them. It will be them important to complete the integration of the Titan-24 results with the known geology, the existing drilling information, and other geophysical results (i.e., magnetics, ground or airborne EM) to further enhance the interpretation and drill targeting.

We also recommend future follow up over the property with Titan-24 profiles east and west of the current profiles, at regular 200m line spacing, and then consideration for 3D inversion of the data to better delineate the geometry of the main target zone. A more detailed and high resolution survey over the *Pit Outline zone* might be also considered on the exploration program.

TABLE OF CONTENTS

LIST OF FIGURES

LIST OF TABLES

1 INTRODUCTION

This report presents the logistics and the results of the analysis of the Titan-24 DC - IP - MT data acquired from 2011/09/24 to 2011/10/10 over the Elk Gold Project, on behalf of Gold Mountain Mining Corporation.

The first part of this report presents the inversion results, their geophysical interpretation, and some recommendations for future follow-up on the property.

The second part of the report presents the logistics of the survey, including the survey parameters and methodology, and the survey results (data) in digital documents.

1.1 SURVEY OBJECTIVES

The exploration objectives of the Titan 24 DCIP & MT survey at Elk Gold Project are to detect gold-bearing quartz veins to depth for drill targeting, and delineation of mineralization and alteration.

The Titan 24 **D**istributed **A**cquisition **S**ystem (**DAS**; Sheard, 1998) employs a combination of multiplicity of sensors, 24-bit digital sampling, and advanced signal processing. It provides three in-dependent datasets capable of measuring subsurface resistivity's (structure, alteration & lithology) and chargeability (mineralization) to depth.

The DC/IP component of the survey should provide an excellent means of delineating target mineralization within the top 500m to 750m pending geologic and cultural environment. The MT resistivity provides additional resistivity information from surface to depths beyond 1km. The MT resistivity is useful for mapping geological contacts with resistivity contrasts and deep conductors that may potentially represent alteration or mineralization.

1.2 GENERAL SURVEY INFORMATION

Quantec Project No.:	CA00900T
Client:	Gold Mountain Mining Corporation
Client Address:	Suite 1700 – 700 West Pender Street, Vancouver, British Columbia, Canada V6C 1G8
Client representative:	Peter Thiersch Phone: (604) 558 4653 x237 Email: PeterT@aumtn.com
Project Name:	Elk Gold Project
Survey Type:	Titan-24 DC - IP - MT
Project Survey Period:	2011/09/24 to 2011/10/10

General Location:	Approximately 45 km Southeast of Merritt
Province	British Columbia
Nearest Settlement:	Merritt
Datum & Projection:	NAD83 – Zone 10 North Hemisphere
Latitude & Longitude:	Approx. 49°48’24”N, 120°19'13”W
UTM position:	Approx. 692800m E, 5525150m N
List of Claims Surveyed	516755; 516750; 516740; 516743; 517116; 308695

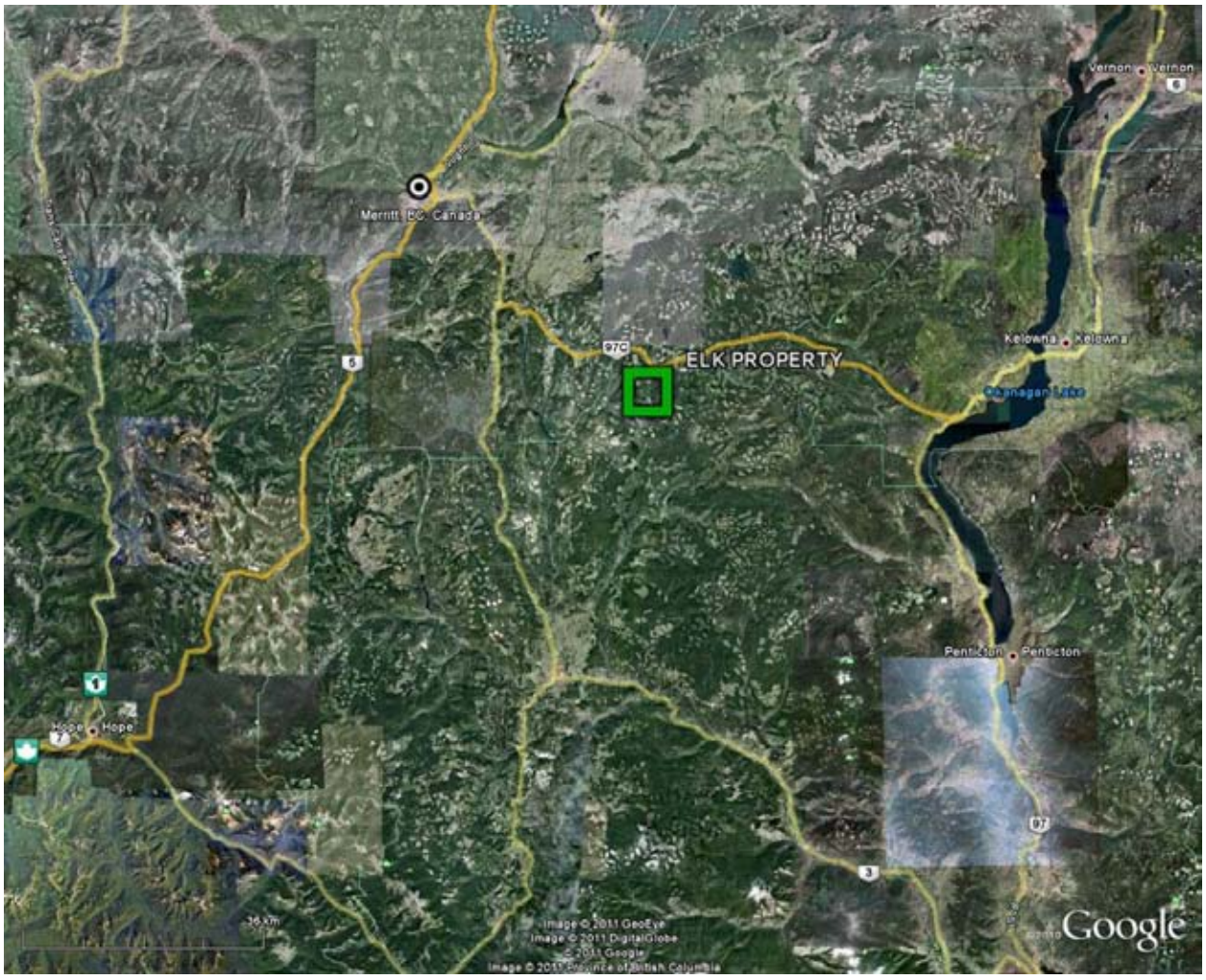

Figure 1-1: General Project Location[1].

[1] Image from Google Earth

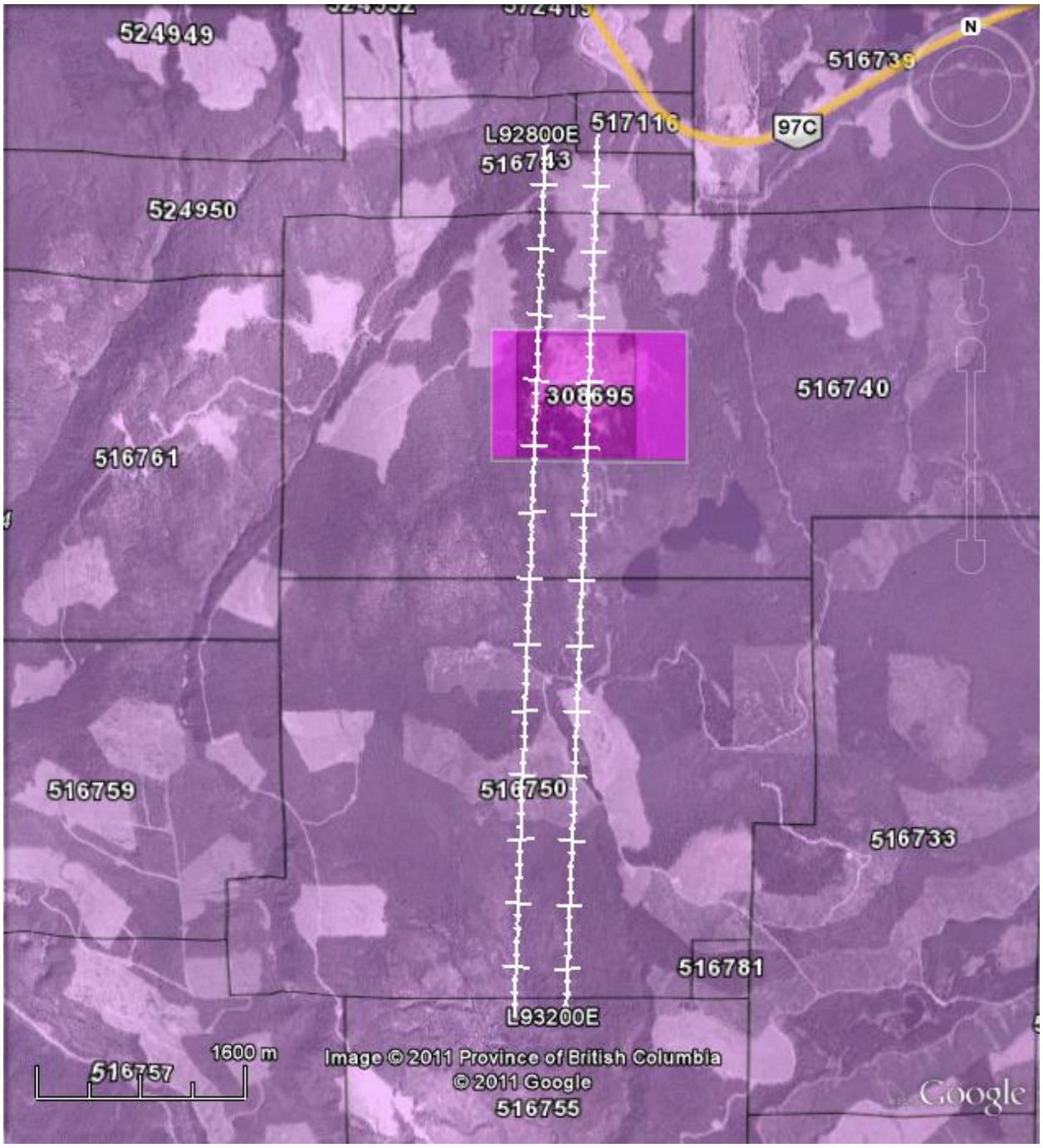

Figure 1-2: Surveyed Location Map with Property Claims[2].

[2] {2011/10/31} Google Earth with Claim map from GeoBC-Information Services [http://archive.ilmb.gov.bc.ca/dm/wms/index.html]

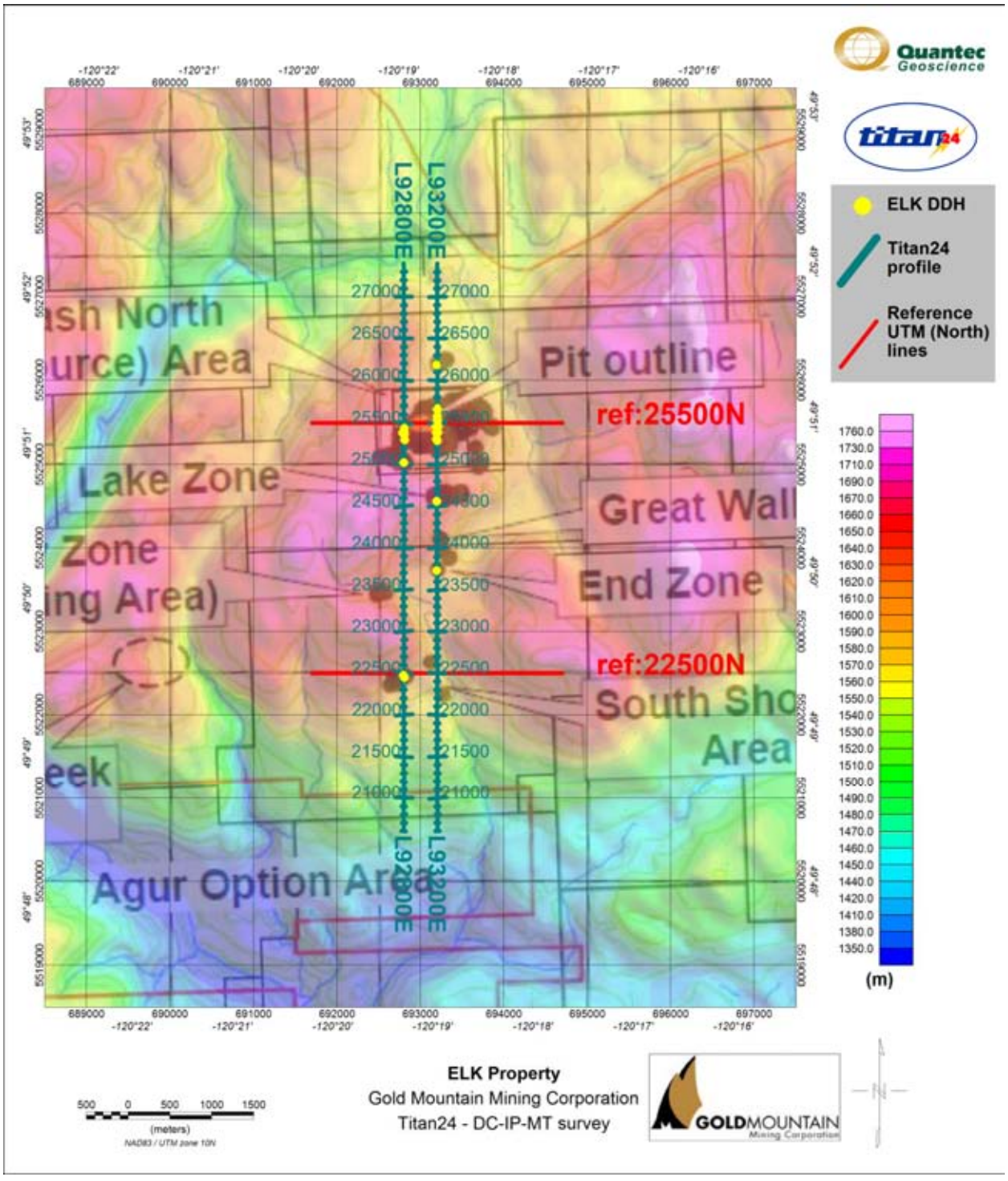

Figure 1-3: Detailed Surveyed Location Map.

2 PREVIOUS WORK & GEOLOGY

2.1 GEOLOGY OF THE AREA[3]

The Elk Property lies within the Intermontane tectonic belt of south-central British Columbia. Upper Triassic magmatic arc sequence volcanic rocks and sediments of the Nicola Group cover the western third of the project area. The eastern two-thirds is covered by Middle Jurassic age intrusive rocks of the Osprey Lake Batholith (see Figure 2-1). The contact between the Nicola andesite and basalt and the Osprey Lake granite and granodiorite trends NNE across the western part of the claim block. Early Tertiary quartz-feldspar-porphyry dykes and stocks from the Otter Intrusive occur within the property. The youngest units mapped are andesite dykes which cross cut all other lithologies.

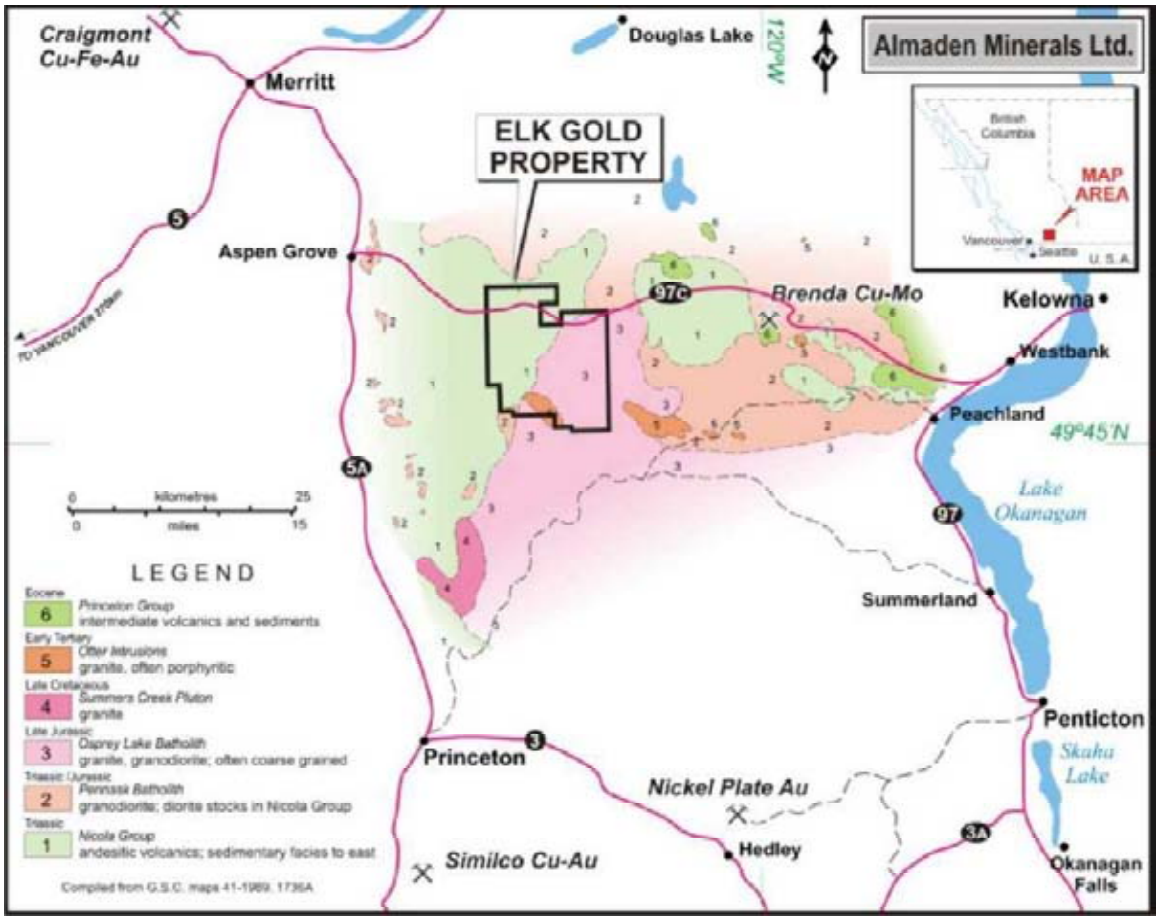

Figure 2-1: Property location and geology.

[3] R.Pooley, s-Lomas, G-Hawthorn, and RB-Alexander; NI 43-101 Technical Report for a Preliminary Economic Assessment on the Elk Gold Project, Merritt, British Columbia, Canada, for almaden Minerals. January, 2011.

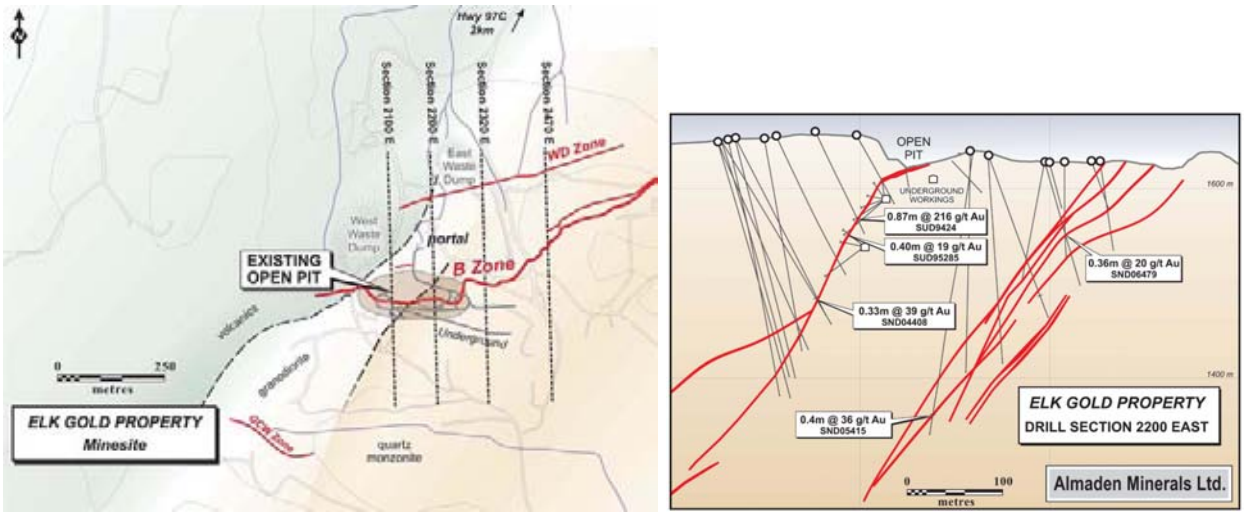

Figure 2-2: Detail view of the Geology over the open pit zone – Elk Property[4].

The Elk project is a gold-bearing ***mesothermal[5] quartz + sulphide vein deposit****. This depositional environment is characterised by deep circulation and evolution of meteoric water in structures associated with major, strike-slip fault zones.*

The ***B*** *and* ***WD*** *Vein Complex (historically called the Siwash Vein, Almaden Minerals) is emplaced within a fault / fracture zone that strikes east-northeast and dips moderately to steeply southward. Most of the previous mine production occurs within the granodiorite border phase of the batholiths (Lewis, 2000).*

Gold mineralization occurs within quartz-sulphide veins and stringers most often within altered granite and occasionally within the adjacent volcanics. Vein widths range from a few centimetres to several meters wide. Pyrite is the most common sulphide (Conroy, 1994), ranging from 5 to 80% with higher grades associated with chalcopyrite and tetrahedrite.

2.2 OTHER GEOLOGICAL/GEOPHYSICAL/DDH

Collar information on a total of 52 drill holes located along the two surveyed profiles over the survey area had been provided. Figure 2-3 present the plan maps of the collars of these DDH. No assay information along these DDH had been provided.

Trace of these DDH will be included in the 2D sections.

[4] Images from Almaden Mineral web site: http://www.almadenminerals.com/Projects/Siwash.html
[5] See Dubé et al, 2007 for a review of mesothermal gold deposit type.

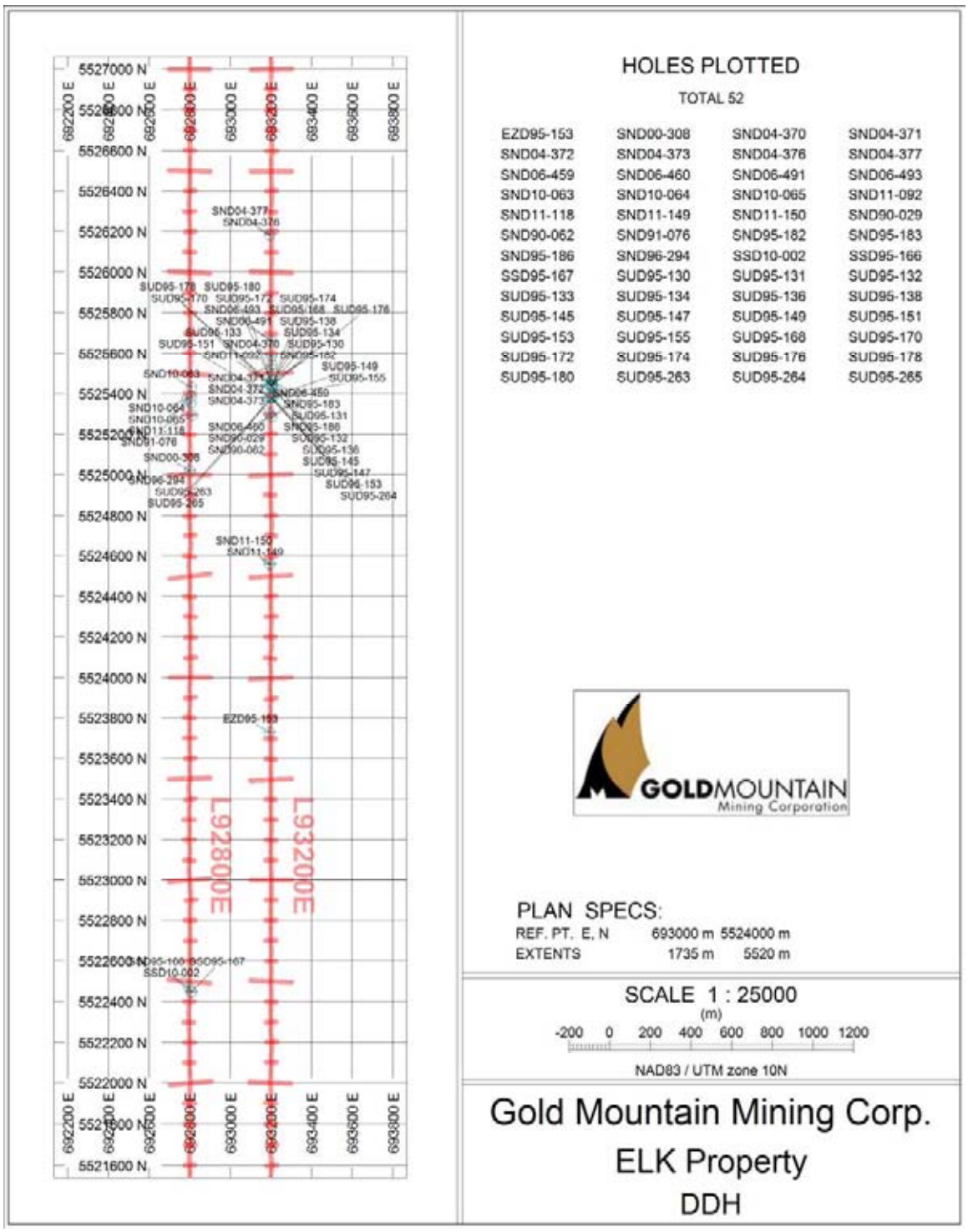

Figure 2-3: Collar information of the DDH –over the two Titan24 profiles.

3 RESULTS AND INTERPRETATION

This section presents the results of the 2D inversion of the Titan-24 data and interpretation in context with the survey objectives and significance to future exploration at Elk Gold Project.

The Titan-24 system acquires three types of geophysical data – magnetotelluric (MT), direct current resistivity (DC), and induced polarization (IP).

The MT and DC methods are used to resolve the resistivity distribution of the subsurface by measuring the electric potential (DC) and the variation of natural source electric and magnetic fields (MT). Resistivity can be an indicator of metallic mineralization, but is more often than not controlled by rock porosity and is therefore an indirect indicator of alteration and mineral grain fabric.

In the induced polarization method, electrical capacitance or chargeability of the subsurface is measured. Chargeability is a near-direct indicator of the presence of sulphide mineralization, in both massive and disseminated forms. Chargeable mineralization is most commonly various sulphides and graphite, but also includes clay-type minerals potentially making it a useful tool for base-metals exploration.

For each line surveyed, the DC-IP utilized a pole-dipole configuration with 100m dipoles with the current injection points located at every 100m between the potential dipoles along the lines. Each profile was surveyed using 3 spreads. Current overlap and station overlap was used between the spreads to assure continuity over the measurement.

The MT utilized the same DC-IP dipoles, plus another set of 100m dipoles oriented perpendicular to the profile at every second site to acquire electric field data. One set of high-frequency and one set of low frequency magnetic sensors was used on the line. A remote site with the same magnetic sensor configuration was used to improve processing of the MT data.

Detailed information on the survey logistics, acquisition parameters and screen capture of the acquired data for the survey are provided in appendices at the end of this report.

The final inversion models are presented graphically in Geosoft plot format along with an interpretation overlay and comments on the most significant results and recommended targets. Scaled sections and plan maps of the resistivity (DC and MT) and of the chargeability models are also provided at the end of this report.

Detail results, i.e. observed DC-IP-MT data and equivalent calculated responses for each model, are presented on a line per line basis in PowerPoint (PDF) documents delivered in the digital archive (CD/DVD) attached to this report.

3.1 OVERVIEW OF INVERSION PROCEDURE

3.1.1 DC RESISTIVITY & INDUCED POLARIZATION INVERSIONS

DC-IP is an electrical method that uses the injection of current and the measurement of voltage difference along with its rate of decay to determine the subsurface resistivity and chargeability, respectively. Depth of investigation is mainly controlled by the array geometry, but may also be limited by the received signal, which is dependent on transmitted current, and ground resistivity. The chargeability parameter is particularly susceptible to cases with a low signal-to-noise ratio. In its

standard configuration (a=100m / n=0.5-23.5) the Titan-24 surveys typically image DC resistivity to depths of 500-750m, and the IP typically images to 500-750m, in sub-vertical tabular geologic settings and up to 50% more for sub-horizontal. The differences in penetration are a function of the relative property contrasts and relative signal-to-noise levels between the two measurements. decreases or increases proportionally to the dipole-size (i.e., 300-500m for 50m dipoles, and 1000-1500m for 200m dipoles). A detailed introduction to DC-IP is given in Telford, et al. (1976).

The primary tool for evaluating the Titan-24 data is through the inversion of the data in two-dimensions (2D). An inversion model depends not only on the data collected, but also on the associated data errors in the reading and the "model norm". Inversion models are not unique and may contain "artefacts" from the inversion process. The inversion model may not accurately reflect all of the information apparent in the actual data. Inversion models must be reviewed in context with the observed data, model fit, and with an understanding of the model norm used.

The Titan-24 DC and IP data were inverted to produce cross-sections of the resistivity and chargeability variations along the survey lines. The UBC DCIP2D inversion code (Oldenburg & Li, 1994) was used for the 2D inversion of the DC and IP data.

Potential difference (voltage) and phase values were used as input data in the DC and IP inversions, respectively. DC Resistivity and induced polarization (IP) data are first pre-conditioned; the error of each data point is adjusted for the inversion process using a general error equation similar to:

$$errors\begin{pmatrix} Vp \\ IP \end{pmatrix} = \mathrm{A}\% \begin{vmatrix} Vp \\ IP \end{vmatrix} + B \times \mathrm{Acq\_Error}\begin{pmatrix} Vp \\ IP \end{pmatrix} + C\,(\mathrm{floor})$$

with the set of parameters $\{A, B, C\}$ adjusted (and large errors data points removed) for each dataset until we achieve convergence with relaxation of the DC or IP models (see example of Model Norm fit curve on Figure 3-1).

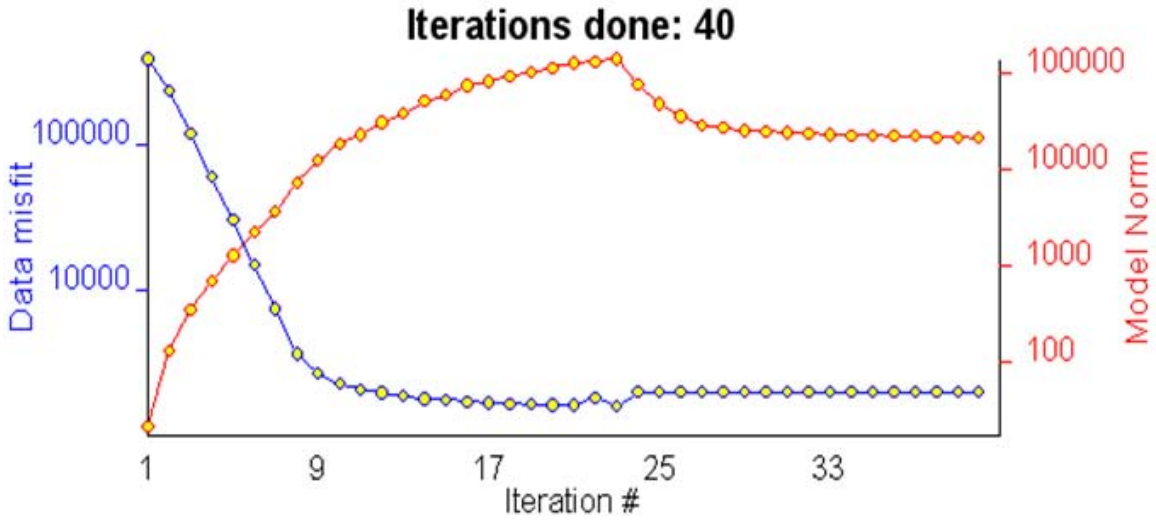

Figure 3-1: Example of DC-IP misfit curves showing relaxation of the model after iteration #40.

Three 2D inversions were carried out along each line.

The DC data was inverted using an unconstrained 2D inversion with a homogenous half-space of average input data as starting model. The DC models are labelled as 'smDC'.

Two IP inversions are calculated from the same data set and parameters, but they use a different reference model[6]. The first inversion of the IP data uses the previously calculated DC model as the reference model, and is labelled the 'IP *dcref* model'. The second IP inversion uses a homogeneous half-space resistivity model as the reference model and is labelled 'IP *hsref* model' or 'IP *nullcon'* model. This model is included to test the validity of chargeability anomalies, and to limit the possibility of inversion artefacts in the IP model due to the use of the DC model as a reference.

The DC and IP inversion use the same mesh. The horizontal mesh was set as 2 cells between electrodes on the double spread lines, and as 3 cells between electrodes on the single spread lines. The vertical mesh was designed with a cell thickness from 10 to 15m for the first 200-300m to accommodate the topographic variation along the profile, and then it increases from 20 to 100m with depth. The inversions were generally run for a maximum of 50 iterations.

3.1.2 AUDIO-MAGNETOTELLURIC INVERSIONS

The Audio-Magnetotelluric (AMT) method is a natural source method that measures the variation of both the electric (E) and magnetic (H) field on the surface of the earth in order to determine the distribution at depth of the resistivity of the underlying rocks. A complete review of the method is presented in Vozoff (1972) and Orange (1989).

The measured MT impedance Z, defined by the ratio between the E and H fields, is a tensor of complex numbers. This tensor is generally represented by its two off-diagonal elements. In a 1D earth model, i.e. the resistivity varies only with depth, there is no strike direction and the two off-diagonal impedances are equal. In the 2D case, i.e. when the resistivity varies with depth and perpendicularly to the strike, and when the profile is set perpendicular to the strike direction, the two off-diagonal elements are not equal but reflect the variation of the resistivity along two directions, one parallel and the other perpendicular to the strike, i.e., the TE (Transverse Electric; E parallel to the strike) and the TM (Transverse Magnetic; E perpendicular to the strike) modes.

Both TE and TM impedances are represented by an apparent resistivity (a parameter proportional to the modulus of Z) and a phase (argument of Z). The variation of those parameters with frequency relates the variations of the resistivity with depth, the high frequencies sampling the sub-surface and the low frequencies the deeper part of the earth. However the apparent resistivity and the phase have an opposite behaviour. An increase of the phase indicates a more conductive zone than the host rocks, and is associated with a decrease of the apparent resistivity. The objective of the inversion of MT data is to compute a distribution of the resistivity of the surface that explains the variations of the MT parameters, i.e. the response of the model that fits the observed data. The solution however is not unique and different inversions must be performed (different programs, different conditions) in order to test and compare solutions for artefacts versus a target anomaly.

The primary tool for evaluating the Spartan MT data is 1D, 2D, and 3D inversion.

The depth of investigation is determined primarily by the frequency content of the measurement. Depth estimates from any individual sounding may easily exceed 20 km. However, the data can only be confidently interpreted when the aperture of the array is comparable to the depth of investigation.

The inversion model is dependent on the data, but also on the associated data errors and the model norm. The inversion models are not unique, may contain artefacts of the inversion process and may not therefore accurately reflect all of the information apparent in the actual data. Inversion models need to

[6] The reference model is used to calculate the sensitivity matrix used at each iteration for the IP inversion.

be reviewed in context with the observed data, model fit. They must have an understanding of the model norm used and if the model is geologically plausible.

For this study, 1D and 2D inversions were performed on the data.

A 1D model at each MT site and for each mode (TE, TM, and DET-determinant[7]) has been calculated as a QA/QC tool using a Occam layered inversion program. This inversion calculates a 1D resistivity earth model (i.e., the resistivity varies only with depth) that best fits the data. Geosoft plot of the Stitched 1D models calculated from the determinant of the impedances is presented in the Appendix I.

The 2D inversions were completed on each profile using the "un-rotated" data which assumes the strike direction is perpendicular to the profile for all sites: the TM mode is then defined by the inline E-field (and cross line H-field), and the TE mode is defined by the cross line E-field (and inline H-field) data.

Two different 2D inversion algorithms were used to invert the MT data. The first inversion procedure was carried out using the Quantec proprietary Phil Wannamaker inversion algorithm (PWm). The second inversion was carried out using the Randy Mackie inversion code (RLM). From previous work, we noticed that the PWm code has a tendency to accentuate anomalies with sharp vertical boundaries and to locate these anomalies at a greater depth than the RLM code. In contrast, the RLM code has a tendency to accentuate anomalies with a layered (horizontal) aspect resulting in a smooth lateral variation and lower depth to top of the anomalous bodies. Therefore, the choice of the inversion algorithm and the inversion results to be used in interpretation is generally dataset definitive and must confirm with the geological setting of the survey area.

All inversions used the TE and TM resistivity and phase from 10kHz to 0.01Hz and 10kHz to 0.1Hz (b models), interpolated at 6 frequencies per decade, assuming 5% error for the resistivity and 3 degrees error for the phase.

The different models calculated are:

The inversion model MUH4b and PUH4 were derived from inverting the TE and TM apparent resistivity and phase MT data starting from a half space model of 100 Ohm-m, no topography, using the RLM and PWM program respectively.

The PWm inversion model PUTH4 and PUTH4b were derived from inverting the TE and TM apparent resistivity and phase MT data starting from a half space model of 100 Ohm-m, including topography. The model PUTH4b is the inversion completed using data between 10kHz to 0.1Hz.

Finally, the model PUTD4b was derived from inverting the TE and TM apparent resistivity and phase MT data starting from the smooth stitched 1D DET inversion model (model m1d).

[7] The determinant of the impedances is defined as: $\mathrm{DET}=\sqrt{Z_{xy}Z_{yx}-Z_{xx}Z_{yy}}$

3.2 DISCUSSION OF RESULTS

The interpretation results described and presented in this section are interpreted as the most significant geophysical anomalies and potential targets from the final DC, IP, and MT inversion models. The DC model, IP (DC referenced) model, and the MT PUTH4b models are used for presenting the interpretation results. These inversion models were found to produce consistent results along the survey lines and illustrate the resistivity and chargeability distribution of subsurface structures and occurrence of potential mineralized zones in the property.

On the graphics, variations of the geophysical parameters are:

- IP Chargeability model Values from 0 to 60mrads;
- DC & MT Resistivity models Values from 10 to 1000 Ohm-m.

The main objective of the survey is to detect gold-bearing quartz veins to depth for drill targeting, and delineation of mineralization and alteration.

The zones of anomalous resistivity and chargeability are classified and assigned a target type according to amplitude, size and IP Chargeability and DC Resistivity association as follows:

T1: Strong IP response located coincidently with DC resistivity low, interpreted to be consistent with sulphide mineralization;

T2: Moderate to high IP response located at the edges and/or over DC resistivity moderate to high gradient zones, interpreted to be consistent with geological structures and represent disseminated mineralization and/or alteration zones;

T3: Weak IP response coincident with DC resistivity high, interpreted to be consistent with the leached cap consisting of remnant silicification.

Analysis of the 2D results with the DDH information tend to indicate that main target type, as delineated by the results over the current open pit zone, seem to be correlated to type T2, with a resistivity low associated with a weak or gradient chargeability zone. Other type or association should be reviewed, and analysed, accordingly to local geology.

3.2.1 L28000E

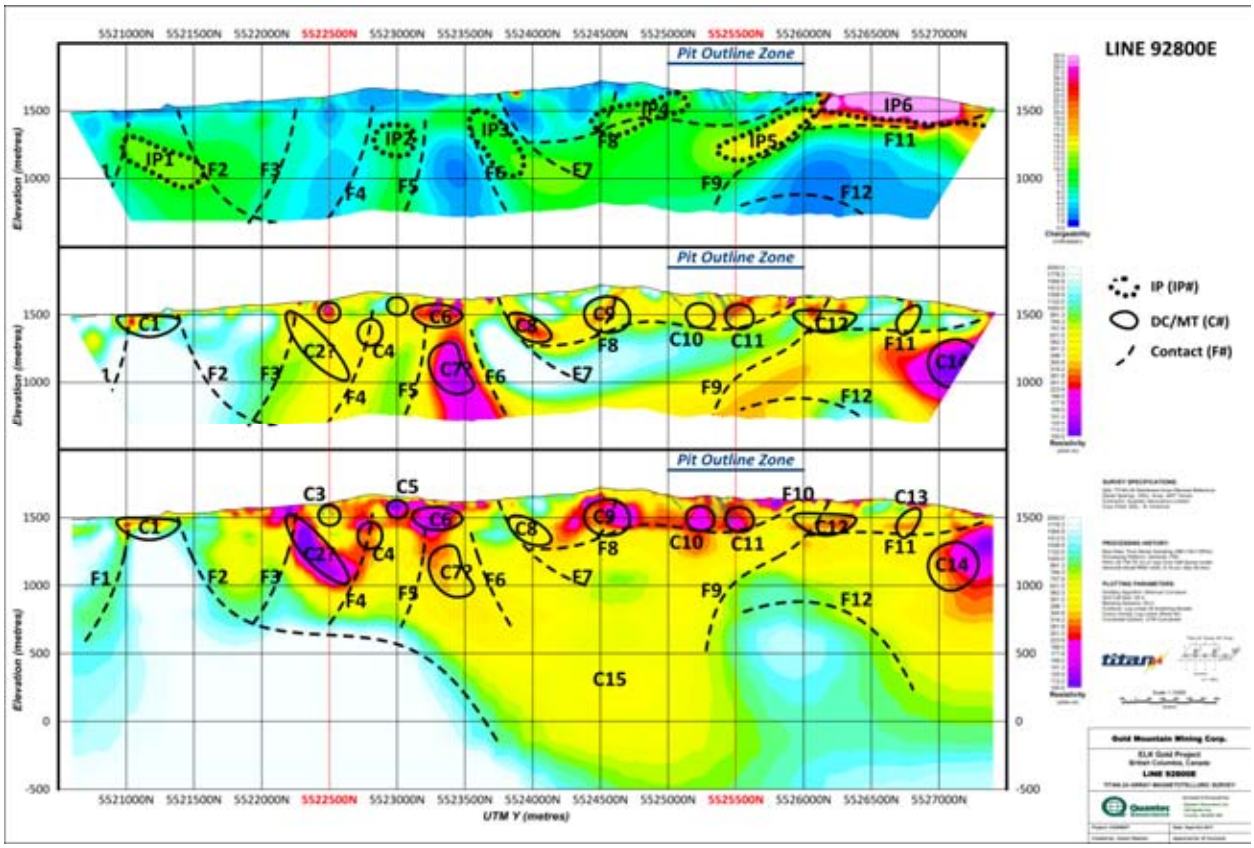

Figure 3-2: DC-IP-MT 2D results over line L28000E, with interpretation.

Figure 3-2 presents the DC and MT (resistivity) and IP (chargeability) results on line L28000E.

We observe that the MT and DC sections display lateral variation of the resistivity; such variations are interpreted as potential contact or faults between geological units. We note that there is a good correlation regarding the location of these structural features labelled from **F1** to **F12** on Figure 3-2.

We are able to characterize on the DC and MT models several more conductive zones. They are delineated by the inferred structural features.

A first deep conductive zone **C15** is characterized between 5523500N and 5525500N; it is surrounded by two more resistive zones located at the southern and northern end of the profile. That structure is delineated by the contacts **F2** on the south and by **F9+F12** on the north. We want to indicate here that a similar structure is also observed on the profile L32000E (e.g., ***C25*** on L32000E). The southern more resistive unit is well defined on the DC model. The characterization of the northern resistive unit is however not well resolved on the DC model as its depth is at the limit of penetration of the DC method. This feature might represent a main but deep shear zone or other structural feature, or alteration zone.

Zone **C1** corresponds to a near surface more conductive zone located on top of two contacts **F1** and **F2**. The conductive zones **C2** (not well defined on the DC) and **C3** seem to be correlated with the structural zone **F2**, while the conductive zones **C4** and **C5** are apparently associated with the contact **F4**. The more conductive zones **C6** and **C7** are associated with the contacts **F5** and **F6**. We note that the DC model present a stronger signature for **C7** than the MT, suggesting that **C7** has to be taken with care.

In that area, we can identify a weak IP zone **IP1**, but it appear more like formational, i.e., a variation

between the overburden and the deeper geological units. We note however gradient on the IP model near **F3** and **F4**, that can be associated with the more conductive zones **C3** (*F3*) and **C4** (*F4*); that could represent potential area of interest, but may be with low priority. It is important to indicate here the conductive zone **C3** corresponds to an anomaly already sampled by DDH. So a review of the DDH information over **C3** might refine priority of the more conductive zones over that area.

Another weak IP zone **IP2** is identified between **F4** and **F5**; that IP gradient zone seems to correlate with two more conductive zones. The first conductive zone **C5** is a small conductive zone located near surface, and so might not represent a principal target. The second more conductive zone **C6** is well defined on both the DC and MT models, and it is located near a weak IP gradient zone; **C6** might represent a potential target zone, but as a medium priority. Following results over **C6**, the deeper conductive zone **C7** might be considered as a deep target zone, knowing that **C7** is associated with a no chargeable zone.

The conductive zone **C8** is located at the edge of the structural zone **F7**. It is also located near a week IP zone **IP3** located between **F6** and **F7**. The conductive zone **C8** is the southern of a set of more conductive zones (**C9**, **C10**, and **C11**) located between 5523750N and 5526000N, an area delineated by the structural feature **F10**. That zone includes the open pit zone (5525000N to 5526000N). Anomaly **C9** is located near a weak IP gradient **IP4**, and seems to be associated with a structural feature **F8**. The more conductive zone **C10** and **C11** are well defined on the MT model, but are 'known' zone as they are located in the *Pit Outline zone*, and so, already 'sampled' by numerous drill holes. The more conductive zones **C8**, **C9** represent potential target zones, and will be rank as first priority target due to their potential (structural) association with **C10** and **C11**.

The conductive zone **C12** is located just north of the *Pit Outline zone*. It is clearly associated with the structural zone **F9**, and can also be associated with the strong IP anomaly IP5. F9, as F2, might represent a main structural feature in the area. The conductive zone **C12** represents a first priority target due to the association conductive and chargeable.

The conductive zone **C13** is located at the northern end of the profile. It is located on top of a strong but near surface IP high zone (**IP6**). It is not clear what can be the cause of the strong IP response **IP6**, and so, **C13** remain a potential target, but as a medium to low priority: **IP6** need to be clarified.

Finally, we would like to mention a potential more conductive zone **C14**. It is located below the strong IP zone **IP6**, but at the northern end of the profile; it remains so not well resolved. We will recommend, after **IP6** being explained, to re-evaluate **C14** as potential deep target.

3.2.2 L32000E

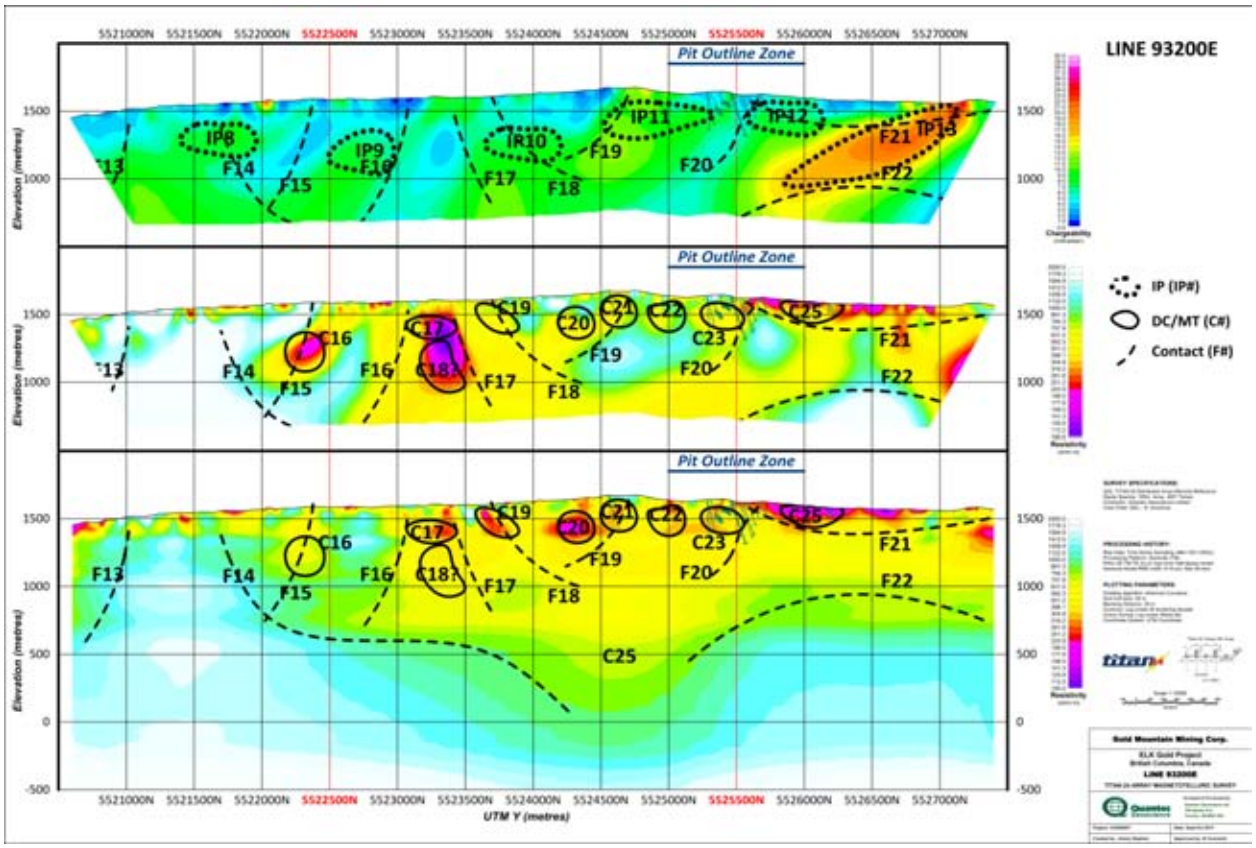

Figure 3-3: DC-IP-MT 2D results over line L32000E, with interpretation

Figure 3-3 presents the DC and MT (resistivity) and IP (chargeability) results on line L32000E.

We observe that the MT and DC sections display lateral variation of the resistivity; such variations are interpreted as potential contact or faults between geological units. We note that there is a good correlation regarding the location of these structural features labelled from **F13** to **F22** on Figure 3-3.

We are able to characterize on the DC and MT models several more conductive zones. They are delineated by the inferred structural features.

We first note a deep conductive zone **C25** centered near 5524500N. That feature is surrounded by two more resistive zones located at the southern and northern end of the profile, delineating the structural features **F14** (south) and **F22** (north). The two more resistive units are well defined on both the MT and DC models. That structure is clearly associated with the deep conductive feature ***C15*** observed on L28000E. The geometry of the **C25** conductive zone seems to indicate that we might be close to the eastern extend of that deep structure. This feature might represent a main but deep shear zone or other structural feature, or alteration zone.

The conductive zone **C16** is associated with the structural feature **F15**. That conductive zone appears well defined on both the DC and MT models. There is no clear IP high zone near that conductive zone, but we can note a gradient of the IP north of the IP weak high zone **IP8**. **C16** might represent a potential target zone, but as a medium priority.

The more conductive zone **C17** and the deeper but less well resolved **C18** one are located between two structural features: **F16**, and **F17**. These conductive zones are located, as **C16**, at the edge between a weak IP zone, **IP9**, and a no chargeable zone. **C17** might represent a potential target zone, but as a medium priority.

The more conductive zone **C19** is associated with the structural feature **F18**. That feature is better defined on the MT model. There are no clear association between **C19** and an IP high, or a gradient of the IP. **C19** might represent a potential target zone, but as a low priority. We would like to indicate there is a DDH located just north of that conductive zone. Results on that DDH should be review prior follow up on that conductive zone.

The more conductive zones **C20** and **C21** are located near the structural feature **F19**. It seems to be located near a weak IP anomaly (**IP11**), and so near a gradient of the IP. **C20** and **C21** might represent potential target zones, but as a medium priority. There is DDH information over **C21**. Results on those DDH should be reviewed prior follow up on the conductive zone.

The more conductive zone **C22** is located in the center of a weak IP zone **IP11**. There is no clear evidence for a structural zone associated to that conductive feature. However, it is located just south of the *Pit Outline zone*. It might represent potential target zones, but as a low priority.

The more conductive zone **C23** is located near the structural feature **F20**. That area is well defined on the DC and MT model, and seems associated with a small variation of the IP between **IP11** and **IP12**, coincident with **F20**. This conductive zone is located in the *Pit Outline zone*, and so, already 'sampled' by numerous drill holes.

The more conductive unit **C24** is a near surface zone delineated by **F21** that extends from the north limit of the *Pit Outline zone* to the northern end of the profile. We identify a high IP zone **IP13** below that conductive unit, just at the edge of the profile, dipping to the south. That IP zone **IP13** seems to correlate with the IP high zones **IP5-6** observed on L28000E. It could be of interest to test that strong IP zone on L32000E (IP5 on L28000E), as it seems to extend below the current *Pit Outline zone*.

4 CONCLUSIONS AND RECOMMENDATIONS

This report presents the logistics and the results of the analysis of the Titan-24 DC - IP - MT data acquired from 2011/09/24 to 2011/10/10 over the Elk Gold Project property, on behalf of Gold Mountain Mining Corporation.

The exploration objectives of the Titan 24 DCIP & MT survey at Elk Gold Project are to detect gold-bearing quartz veins to depth for drill targeting, and delineation of mineralization and alteration.

The survey is located approximately 45 km Southeast of Merritt, British Columbia, and includes two lines with azimuth 0^{o}. Each line was surveyed using 3 spreads, for a total length of 7.1km each. For each spread, the DC-IP utilized a pole-dipole configuration with 100m dipoles. Current and station overlap were used to ensure better continuity between spreads. The magnetotelluric data were collected using the same DCIP dipoles, plus another set of 100m dipoles oriented perpendicular to the profile, for frequencies ranging from 10kHz down to 0.01Hz. The final coverage of the survey is 14.1km of DCIP, and 14.1km on MT, without current extensions and overlap.

The data were inverted using 2D inversion algorithms to produce sections of the resistivity and chargeability distributions of the subsurface. The final interpretation is based on the integration and comparison of the IP, the DC, and the MT results.

The MT inversion results highlight on the two profiles a deep conductive structure at depth located between 5523500N and 5525500N. The results on the first hundreds of meters display a relative good correlation between the MT and the DC results, delineating several structural contacts along the two profiles. Two strong IP zones located on the northern end of the two profiles have been identified. It is not clear what can be the cause of these anomalies and ground sampling or DDH follow is recommended to better identify these structures. Except these IP zones, only a few weak to medium chargeability high zones were identified. We note however that these IP weak anomalies delineate some gradient zones on the IP models that correlate with the more conductive zones that are associated with the structural zones.

From the analysis of all the results, a total of 16 targets zones had been identified along the two profiles, with 6 as high priority, 6 as medium priority, and 4 as low priority. It is important to note here that several of the target zones identified here have already DDH information over them. It will be them important to complete the integration of the Titan-24 results with the known geology, the existing drilling information, and other geophysical results (i.e., magnetics, ground or airborne EM) to further enhance the interpretation and drill targeting.

We also recommend future follow up over the property with Titan-24 profiles east and west of the current profiles, at regular 200m line spacing, and then consideration for 3D inversion of the data to better delineate the geometry of the main target zone. A more detailed and high resolution survey over the *Pit Outline zone* might be also considered on the exploration program.

Table 4-1: Summary of target zones over the Elk Property.

Profile	Station (UTM north/depth)	Conductive Zone	Priority
L28000E	5522500N / 100m 5522800N / 300m	C3 (DDH available) C4	Low
	5523300 / 200m 5526750 / 170m	C6 C13	Medium
	5524000N / 275m 5524550N / 250m 5525250N / 170m 5525500N / 160m 5526100N / 160m	C8 C9 C10 (DDH available)[1] C11 (DDH available)[1] C12	High
L32000E	5523750N / 175m 5525000N /	C19 (DDH available) C22	Low
	5522300N / 360m 5523250N / 220m 5524300N / 275m 5524650N / 181m	C16 C17 C20 C21 (DDH available)	Medium
	5525425N / 200m	C23 (DDH available) [1]	High
Note 1: conductive zones located in the Pit Outline Zone			

Respectfully Submitted

Toronto, ON, the 08/11/2011,

Benoit Tournerie
Quantec Geoscience Ltd

Wade Lee
Quantec Geoscience Ltd

5 STATEMENT OF QUALIFICATIONS

BENOIT TOURNERIE

I, Benoît Tournerie, declare that:

I am a Geophysicist with residence in Toronto, Ontario and am presently employed in this capacity with Quantec Geoscience Ltd., Toronto, Ontario;

I obtained a License (equivalent to B.Sc.) in 1989, a DEA (equivalent to M.Sc.) in 1991, and a Doctorate with Honours (equivalent to Ph.D.) in December 1995, in Earth Sciences, option geophysics, from the University of Rennes 1, Rennes, France;

I am a registered geophysicist, since 2008, with license to practice in the Province of Ontario (APGO member # 1609); a registered geoscientist, since 2008 with a license to practice in the Province of Quebec (OGQ #1322); a registered geoscientist, since 2009 with a license to practice in the Province British Columbia (APEG-BC #33786);

I have practiced my profession continuously since April, 1996 in North and South America, in Europe, and in Oceania;

I am a member of the Society of Exploration Geophysicists (SEG), the European Association of Geoscientist and Engineers (EAGE), and the Canadian Exploration Geophysics Society (KEGS);

I have no interest, nor do I expect to receive any interest in the properties or securities of **Gold Mountain Mining Corporation**, its subsidiaries or its joint-venture partners;

I am the Professional Geophysicist responsible for this project and have authored this Geophysical Report;

I was in charge of the Quality Control and Assurance of the acquired data; I have reviewed the survey results and the logistics sections of the report, and can attest that these accurately and faithfully reflect the data acquired on site;

I undertook the MT inversions of the data, and have compiled the final processed data, inversions and interpretation results contained in the Geophysical Report.

The statements made in this report represent my professional opinion in consideration of the information available to me at the time of writing this report.

Toronto, Ontario, the 08/11/2011

Benoît Tournerie, D. Sc., P.Geo.
Quantec Geoscience Ltd.

JIMMY STEPHEN

I, Jimmy Stephen, declare that:

I am a Geophysicist with residence in Toronto, Ontario and am presently employed in this capacity with Quantec Geoscience Ltd., Toronto, Ontario;

I obtained my Bachelor of Science Degree (B.Sc.), Physics from Mahatma Gandhi University, India in 1994, a Master of Science and Technology Degree (M.Sc.Tech.), Marine Geophysics from Cochin University of Science and Technology, India in 1998, and Doctor of Philosophy (PhD), Geophysics from Swami Ramanand Teerth Marathwada University, India in 2004;

I have practiced my profession continuously since November 1998 in India, Middle East and North America.

I am a member of the Society of Exploration Geophysicists (SEG), and the American Geophysical Union (AGU);

I have no interest, nor do I expect to receive any interest in the properties or securities of **Gold Mountain Mining Corporation**, its subsidiaries or its joint-venture partners;

I undertook the 2D DC-IP inversions. The statements made in this report represent my professional opinion based on my consideration of the information available to me at the time of writing this report.

Toronto, Ontario, the 08/11/2011

Jimmy Stephen, PhD

Quantec Geoscience Ltd.

WADE LEE

I, Wade Lee, declare that

I am a data processor with residence in Toronto, Ontario and am presently employed in this capacity with Quantec Geoscience Ltd., Toronto, Ontario.

I obtained a Bachelor of Applied Science Degree in Chemical Engineering (B.Sc.) at Queen's University,Kingston, ON, in spring of 2009.

I have practiced my profession continuously since February, 2011 in North America, Europe and South America.

I have no interest, nor do I expect to receive any interest in the properties or securities of **Gold Mountain Mining Corporation**, its subsidiaries or its joint-venture partners;

I was the data processor on site, responsible for the quality control of data acquired throughout the survey. I compiled and edited the logistics report. The statements made in this report represent my professional opinion based on my consideration of the information available to me at the time of writing this report.

Toronto, ON, the 08/11/2011,

Wade Lee, B.Sc.

Quantec Geoscience Ltd.

6 DIGITAL ARCHIVE

The CD or DVD attached to this report contains a copy of all the inversion results, final processed data, including the survey files, the daily processing (and field) notes, and an electronic copy of this report (with all appendices).

General Description of the CD/DVD Structure

Folder	Sub level 1	Sub level 2	Description
Contract and Client Info			**Contract, technical reports, images, and other documents**
Fields Results			**Final field results CSV, EDI, surveyFiles, and Processing Notes**
Presentation of Results			**Power Points, PDF, and documents presented or emailed to client**
Geosoft			**Geosoft Files**
	Base Maps		Base maps, location, etc
	DDH		DDH info (if applicable)
	Interpretation		Interpretation
	Sections		2D sections
Gocad			**Gocad Project**
	ClientData		Client Gocad Files
	QuantecTSfiles		Quantec Gocad Files
invDCIP			**DC IP inversion**
	Line ##	data	raw data and error conditioning
		smDC	DC inversion
		smIP_dcref	IP with DC reference
		smIP_hsref	IP with Half-space reference
invMT			**MT inversions** *Data, 1D and 2D models are included in the geotools db's*

A PRODUCTION SUMMARY

Date	Field Activities and Observations	Line Spread	Line Start	Line End	Tx Start	Tx End	Read MT (km)	Read IP (km)	Read IP Current Extension (km)
23/09/2011	Mobilization to Kamloops and to Merrit (BC)								
24/09/2011	Moved all equipment to Grid, completed site orientation. Performed PST and Remote Site set up and tested. Infinite was laid out and Line 93200e was partially setup.	93200E_sp1	25100N	27600N	24050N	27650N	0.0	0.0	0.0
25/09/2011	Finished setup Line 93200E Spread 1. Long troubleshooting due to high contacts to be bought down using salt water. IP Test readings were positive. Client was moving drills and equipment around all day, had to disconnect and reconnect all (10) of the road crossings several times. Surveyed MT on line.	93200E_sp1	25100N	27600N	24050N	27650N	2.5	0.0	0.0
26/09/2011	Due to severe geo-magnetic storm active all day and weather (heavy rain and snow during the day), no valid IP data could be acquired. Data were affected by strong Telluric noise overpowering the IP signal and by power leaks. To be considered a weather day.	93200E_sp1	25100N	27600N	24050N	27650N	0.0	0.0	0.0

Date	Field Activities and Observations	Line Spread	Line Start	Line End	Tx Start	Tx End	Read MT (km)	Read IP (km)	Read IP Current Extension (km)
27/09/2011	IP completed on Line 93200E Spread 1. Due to unknown problem with doghouse location and/or infinite the data were not good enough and IP reacquisition is necessary.	93200E_sp1	25100N	27600N	24050N	27650N	0.0	0.0	0.0
28/09/2011	Resurveyed IP on line 93200E Spread 1; moved to Line 92800E (Spread 1); unable to survey MT due to incomplete troubleshooting and high contacts.	93200E_sp1	25100N	27600n	24050N	27650N	0.0	2.5	1.0
29/09/2011	Completed setup of line 92800E Spread 1. Surveyed IP and MT	92800E_sp1	25100N	27600N	24050N	27650N	2.5	2.5	1.0
30/09/2011	Due to harvesting issues at remote site, the MT was reacquired. Day shift prepared the next line, moving all power wire, rerouting the infinite wire and swapping out all discharged batteries on the line.	92800E_sp1	25100N	27600N	24050N	27650N	0.0	0.0	0.0
01/10/2011	Moved to Line 92800E Spread 2. Attempt to survey IP was not successful due to LF tellurics; MT was surveyed	92800E_sp2	22800N	25300N	21750N	26350N	2.5	0.0	0.0
02/09/2011	Surveyed IP on Line 92800E Spread 2; picked up gear and started preparation of next line; coils were moved to new line.	92800E_sp2	22800N	25300N	21750N	26350N	0.0	2.5	2.0
03/10/2011	Moved to Line 93200E Spread 2; surveyed MT.	93200E_sp2	22800N	25300N	21750N	26350N	2.5	0.0	0.0

Date	Field Activities and Observations	Line Spread	Line Start	Line End	Tx Start	Tx End	Read MT (km)	Read IP (km)	Read IP Current Extension (km)
04/10/2011	Surveyed IP on Line 92800E Spread 2; problems with power leaks due to wet weather (rain in the afternoon); 0.9Km of IP will be reacquired the next morning; surveyed more LF events for MT.	93200E_sp2	22800N	25300N	21750N	26350N	0.0	2.5	1.0
05/10/2011	Attempt to complete IP on line 93200E Spread 2 failed due to bad weather; doghouse was moved to south end of line to eliminate running power through entire array; several leaks along infinite wire.	93200E_sp2	22800N	25300N	21750N	26350N	0.0	0.0	0.0
06/10/2011	IP completed on line 93200E Spread 2; moved to Line to 93200E Spread 3 and surveyed MT	93200E_sp2 93200E_sp3	20500N	22900N	20350N	23950N	2.4	1.0	1.0
07/10/2011	Surveyed only 1.8km of IP due to declined permission by the Ministry of Transportation to cross the highway through the culver; the infinite wire needed to be rerouted and the search of access was time consuming; leaks in the line due to bad weather; extra HF events were acquired for MT.	93200E_sp3	20500N	22900N	20450N	23950N	0.0	1.8	0.0
08/10/2011	Completed IP on line 93200E Spread 3; moved to Line 92800E Spread 3 and surveyed MT.	93200E_sp3 92800E_sp3	20500n	22900N	20450N	23950N	2.4	0.6	1.0
09/10/2011	Surveyed IP on line 92800E Spread 3; pick up gear. End of Acquisition.	92800E_sp3	20500N	22900N	20450N	23950N	0	2.4	1.0

Date	Field Activities and Observations	Line Spread	Line Start	Line End	Tx Start	Tx End	Read MT (km)	Read IP (km)	Read IP Current Extension (km)
10/10/2011	Picked up all Titan equipment and performed inventory and packing. Job is completed.								
						TOTAL	**14.8**	**14.8**	**8.0**

B SURVEY LOGISTICS

B.1 ACCESS

Base of Operation: Merritt, British Columbia

Mode of Access to Grid: Truck

Mode of Access to Lines: ATV, by foot

B.2 SURVEY GRID AREA

Established by: Gold Mountain Mining Corporation.

Coordinate Reference System: Grid referenced to UTM Coordinates

Datum & Projection: NAD83 / Zone 10U

Grid Azimuth: 0^o

Magnetic Declination: 17^o E

Station Interval: 100 m

Method of Chaining: Metric, slope distance, pickets GPS surveyed

Surveyed Line-start and -end point coordinates.

Line	Grid Coordinate		UTM Coordinate Start		UTM Coordinate End	
	Start	End	Easting	Northing	Easting	Northing
L92800E	20500	27600	692800	5520500	692800	5527600
L93200E	20500	27600	693200	5520500	693200	5527600

B.3 PRODUCTION AND COVERAGE

Survey Period/days: September 24th – October 10th, 2011
17 days

Survey Days (read time): 13 days

Mob/Demob: 2 days

Parallel Sensor Test: 1 day

Weather/Down Days: 1 day

Number of Spreads surveyed: 6

Number of Lines surveyed: 2

DCIP Survey Coverage: 23.4 km (with overlap and current extensions)

MT Survey Coverage: 14.8 km

Max and Min Pole (Tx) and Potential (P1-P2) Electrode Position.

Line	Setup	Min P1	Max P2	Min Tx	Max Tx	Line Coverage (km)	Total Coverage (km)
L92800E	S1	25100	27600	24050	27650	2.5	3.6
	S2	22800	25300	21750	26350	2.5	4.6
	S3	20500	22900	20450	23950	2.4	3.5
L93200E	S1	25100	27600	24050	27650	2.5	3.6
	S2	22800	25300	21750	26350	2.5	4.6
	S3	20500	22900	20450	23950	2.4	3.5
					TOTAL	**14.8**	**23.4**

MT Survey Coverage (Electrode to Electrode).

Line	Setup	Min Extent (m)	Max Extent (m)	Coverage (km)
L92800E	S1	25100	27600	2.5
	S2	22800	25300	2.5
	S3	20500	22900	2.4
L93200E	S1	25100	27600	2.5
	S2	22800	25300	2.5
	S3	20500	22900	2.4
			TOTAL	**14.8**

B.4 PERSONNEL

Project Manager:	Kevin Blackshaw
Responsible Geophysicist:	Benoit Tournerie
Data Processing (in field):	Wade Lee William Xu
Crew Chief & IP Operator:	Nick Hnotchuk
MT operator:	Warren Gregory Steven Kana Allen Boissoneau
Remote Operator:	Matthew Cousineau
Field Technicians:	Ryan Foyle John Mantyla Luc Lafond Matt King Brian Commanda Chad Commanda Thomas Reid Luchin Thagya Steve Zuniga

B.5 INSTRUMENTATION

Receiver System:	Quantec Distributed Array Acquisition System: - 61 channels max. per system (55ch operationally with internal A/D conversion (24bit @120db / dual speed @120-48kHz), and buffer memory (6Mb). 24 x 2-channel Acquisition Modules (AMs) 13 x 1-channel Acquisition Modules (AMs) AM data transmission using LAN cabling - 2 Central Recording Units (CRU; 140 Gb data storage) at base & at MT remote reference (MT survey) - 2 GPS synchronization clocks (10nsec precision /12.3MHz clock-speed), at base & at MT remote reference (MT survey) - 2 PC-based Central Processing Units (CPU) at base & at MT remote reference (MT survey)
Transmitter (DCIP Surveys):	GDD (5kW) with frequency/waveform control, using CRU and Current Monitor (CM)
Power Supply (DCIP Surveys):	Honda 6500W generator
Transmit Electrodes	4 x 1.2cm diameter 1 meter long stainless steel rods
Receiver Electrodes:	Ground contacts using stainless steel rods

Receiver Coils (MT Surveys):

Low Frequency Range (0.0001Hz to 1kHz):
4 Magnetometers (P50 model)
{2 at base & 2 at remote}
Base: P50-2114, P50-2130
Remote: P50-2131, P50-2203

Mid to High Frequency Range (1Hz to 25kHz)
4 Magnetometers (BF-6 model)
{4 at base & 2 at remote}
Base: (Set 1) BF6-5009, BF6-6176
(Set 2) BF6-6179, BF6-6277
Remote: BF6-5007, BF6-5008

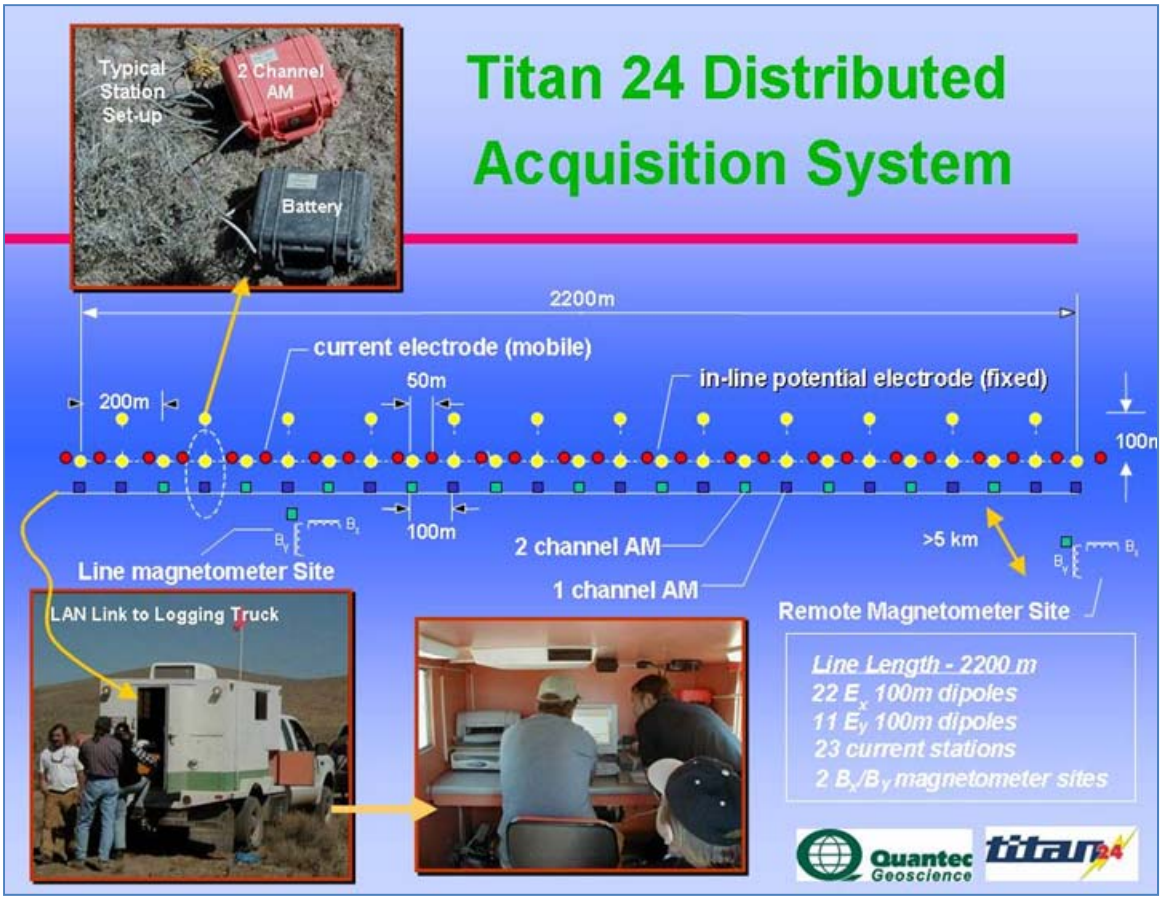

Titan-24 DCIP and MT Schematic Survey Layout.

B.6 DCIP SURVEY SPECIFICATION

B.6.1 GEOMETRY

Survey Array: Dipole-Pole-Dipole Array

Receiver Configuration: 23-24 Ex = Continuous In-line voltages,
12-13 Ey = Alternating (2-stations) cross-line voltages[8].

Array Length: 2.4 km

Number of Arrays/line: 3 arrays/line

Dipole length: Ex = 100metres
Ey = 100 metres

Sampling Interval: Ex = 100 metres
Ey = 200 metres

Rx-Tx Separation: N-spacing (Pn-Cn min)[9] = 0.5 to 23.5

Infinite Pole Location: L92800E S1, S2 & L93200E S1, S2
Grid Coordinate: 96461m E, 31958m N
696457m E, 5531959m N (WGS 84)

L92800E S3 & L93200E S3
Grid Coordinate: 93205m E, 27678m N
693201m E, 5527679m N (WGS 84)

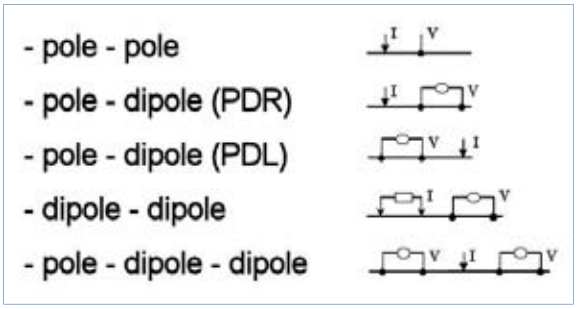

Common DCIP Survey Layouts.

[8] Note: Cross-Line (Ey) voltages obtained for future reference purposes – not presented in cross-sectional plots.
[9] Current electrodes at midpoints between potential electrodes.

B.6.2 ACQUISITION & PROCESSING

Spectral Domain:	Tx = Frequency-domain square-wave current Rx = Full waveform time-series acquisition Data processing/output in frequency-domain.
Spectral Chargeability Model[10]:	Halverson-Wait
Transmitter Waveform:	30/256 Hz square waves at 100% duty cycle (~4sec Pos./Neg.)
Transmitter Output Current:	min 0.47 Amperes to max 4.93 Amperes
Receiver Sampling Speed:	240 samples/second (24 bit A/D @ 120 db dynamic range)
Tx-Rx Synchronization:	using current monitor (10 μsec time-accuracy)
Time-Series Stacking:	20 cycles (full-waveform)
Read Time:	approx 3.0 minutes per event
Time-Domain Decay Window:	**Integration Start Time:** T_O = 0.8 seconds **Integration End Time:** T_F = 1.9 seconds
Post-Processing:	using Quantec proprietary QuickLay v.2.30.14 1) Time-series stacking 2) Robust statistics 3) Current waveform deconvolution 4) Digital filtering (60Hz + harmonics) 5) Spectral model decay-curve fitting

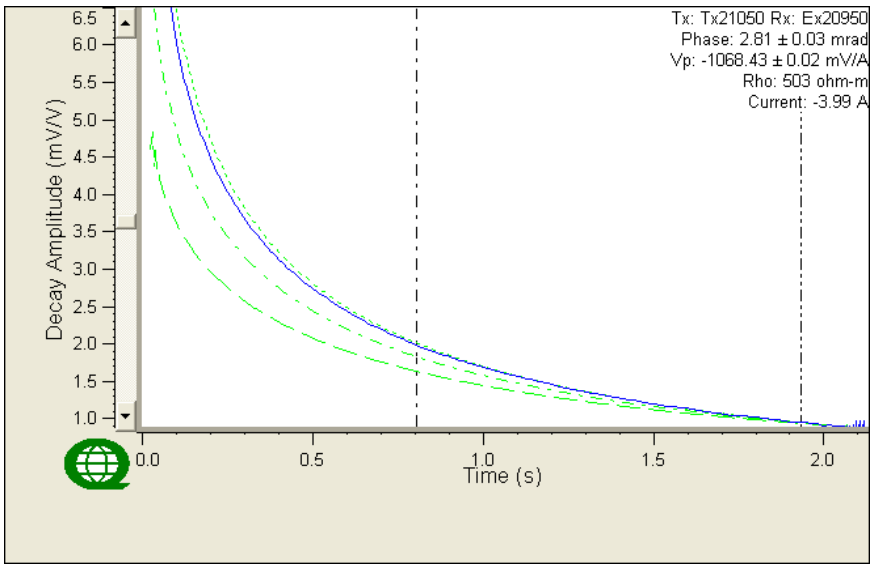

Spectral Chargeability Model and Calculated Halverson-Wait Decays[11].

[10] The Halverson-Wait model chargeability (Halverson et al., 1981) is similar to and improves upon the frequency-domain Cole-Cole model (Pelton et el., 1978) described in the time-domain by Johnson (1984).

B.6.3 DATA PRESENTATION

Accuracy and Repeatability

Measured Data average error (from CSV files) using Halverson-Wait model calculation:

Voltage Errors	0.00061mV/V (average)
Phase Errors	93.5% less than 1.0 mrad

Pseudo-Section Plots:

In-line[12] DC Resistivity and IP Chargeability pseudo sections, posted, contoured (equal area zoning) and plotted in ground units using QuickLay viewer.

Raw Data (digital):

(external Hard Drive)
Raw Event Log File Folders (eg. Eventxxxx.dat).
Also contains AU.txt and Event.log files which contain information on the location and time of the event in QuickLay digital format
(Raw data output to Matlab format upon request).

Processed Data (digital):

DC/IP Data in ASCII CSV (comma delimited) file format from QuickLay, containing final processed voltage and phase data.

CSV File Format:

Line 1:	Column headings
Column 1	Event name/number (e.g., Eventxxxx)
Column 2:	Transmitter site ID (e.g., Tx150)
Column 3:	Receiver site ID (e.g., Rx150)
Column 4-11:	C1-C2/P1-P2 positions in X and Y (m)
Column 12:	Current (Amperes)
Column 13:	Current error (Amperes)
Column 14:	Normalized voltage (Volts/Ampere)
Column 15:	Voltage error (Volts/Ampere)
Column 16:	Phase (milliradians)
Column 17:	Phase error (milliradians)
Column 18:	Apparent resistivity (Ohm-m)[13]

.

B.6.4 DATA QA/QC COMMENTS

Some spread acquisitions encountered geomagnetic storms resulting in higher IP errors in respective pseudo sections. Several event repeats were done throughout survey period to minimize any possible errors such as current leakages and local station disturbances. Overall the data for the all spreads read have low errors with majority below 2 mrad.

---

[11] Halverson-Wait (HW) model parameters calculated in frequency domain, with hatched green lines corresponding to theoretical HW decay with spectral r-factors of 0.1, 1.0 (default) & 10, k-factor of 0.2 (default).

[12] Cross-line (Ey) values not shown for presentation purposes.

[13] Apparent resistivity's are calculated in 2D space using the 4 electrodes general array configuration (as per XY electrode positioning in columns 4-11 of CSV file) – not based on pole-dipole calculations (K. Nurse, QGL, pers. comm., 07-2004).

B.7 MT SURVEY SPECIFICATION

B.7.1 GEOMETRY

Technique: Tensor soundings, remote-referenced

Line Configuration:
23-24 Ex = Continuous In-line voltages,
12-13 Ey = Alternating (2-stations) cross-line E-fields
1 pair Low Frequency coils
1 pair High Frequency coils

Remote Configuration:
1 Ex = in line E-fields
1 Ey = cross-line E fields
1 pair Low Frequency coils
1 pair High Frequency coils

Array Length: 2.4 km

Number of Arrays/line: 3 spreads/line

Dipole size:
Ex = 100 metres
Ey = 100 metres

Sampling Interval:
Ex = 100 metres
Ey = 200 metres

Ex/Ey sampling Ratio 2/1

E/H sampling Ratio
Ex: 23-24/2
Ey: 12-13/2

Remote Reference Position:
Grid Coordinates: 56682E, 106685N
UTM: 656678 mE , 5606686 mN (WGS 84 / Zone 10U)

B.7.2 ACQUISITION & PROCESSING

Data Acquisition:
Full-waveform time-series acquisition
Data processing/output in frequency-domain.

Remote-Base Synchronization: GPS clocks (10μsec time-accuracy)

Frequency Bandwidth:
Operating: 0.01 to 48000 Hz
Effective: 0.1 to 20000 Hz

Time-series Sampling:
High Range: 48000 samples/sec
Mid-Range: 12000 samples/sec
Low Range: 120 samples/sec

Time-Series Stacking:
High Range: 1,534,999 samples
Mid-Range: 2^{20} (1,048,576) samples
Low Range: 2^{19} (524,288) samples

Sample/Record Time:
High Range: min. 2 events @ 30 seconds per event
Mid Range: min. 2 events @ 2.0 minutes per event
Low Range: 1.5 - 3 events @ 80 minutes for a full event (total recording and retrieving time approx. 7 hrs)

Post-Processing: using Quantec proprietary QuickLay v.4.00.10
1) Coherent noise rejection using remote-reference
2) Proprietary digital filtering (scrubbing)
3) Coherency sorting
4) Impedance estimate stacking

B.7.3 DATA PRESENTATION

Parallel Sensor Test: Result of the test of the equipment (PST) is presented in detail in Appendix Parallel Sensor Test.

Data Error: Apparent Resistivity = <1/20TH decade average.
Phase = <3 degrees average

Sounding Curves: Apparent resistivity and phase (XY and YX) sounding curves versus the frequency (8 pts. per decade) using Geotools™ viewer.

Pseudo-Section Plots: MT Apparent Resistivity and Phase Pseudo-Sections (XY, and YX) posted, contoured (equal area zoning) and plotted in grid units using Geotools™ viewer.

Raw Data (digital): (external Hard Drive)
Base and Remote Raw Event Log File Folders
(i.e. Base-Eventxxx.dat; Remote-Eventxxxx.dat).
Also contains AU.txt and Event.log files, which contain information on the location and time of the event in QuickLay digital format (external Hard Drive).
(Raw data output to Matlab format upon request)

Processed Data (digital): MT DATA in EDI (Electronic Data Interchange) file created in Geotools™ containing Auto and Cross-power Spectral estimates for individual stations (sites) and profiles (site-sets);
Spectra are in Right Hand positive down co-ordinate system, and for profiles, EDI files are created with X as the profile direction.

For this study, final EDI have X at 90deg (ROTSPEC= 90)

EDI is a format conforming to SEG standard for the storage of magnetotelluric (MT) data
(Wight, D. E., 1987).

B.7.4 DATA QA/QC COMMENTS

Two sets of high frequency coils were used on the survey line to maximize signals acquired on either end of the line. MT data in general look good with minor scatterings in 48,000 Hz band.

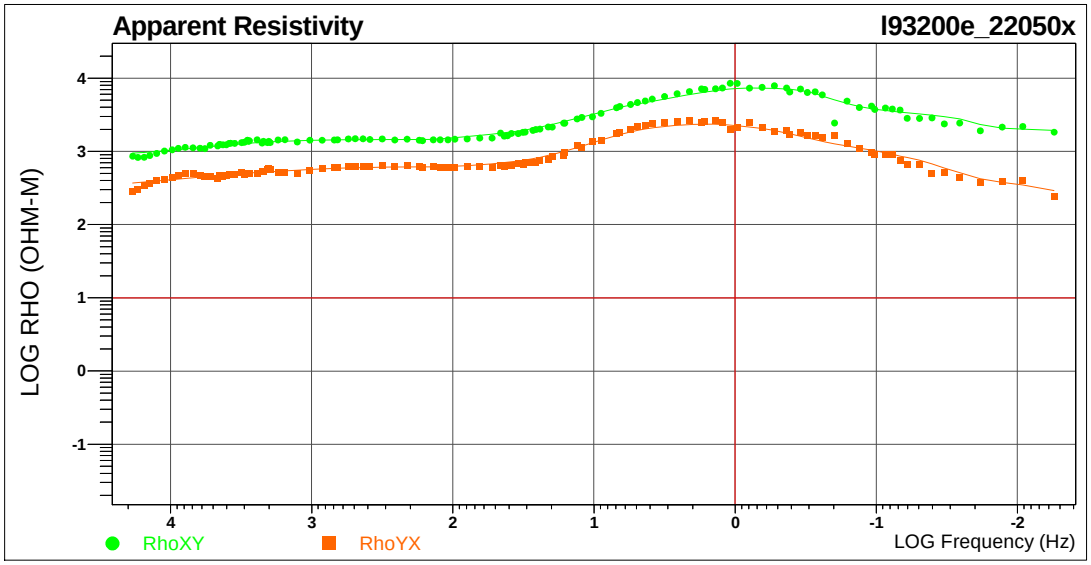

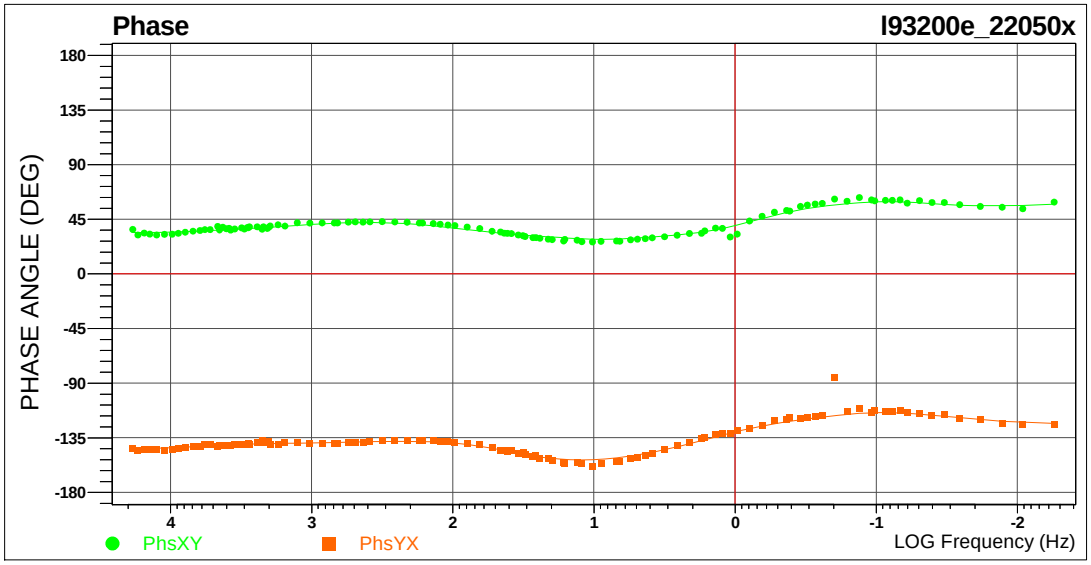

Example of Apparent Resistivity and Phase (XY and YX) Sounding Curves.

C DC – IP PSEUDO-SECTIONS OF FINAL PROCESSED DATA

C.1 LINE 92800E_S1

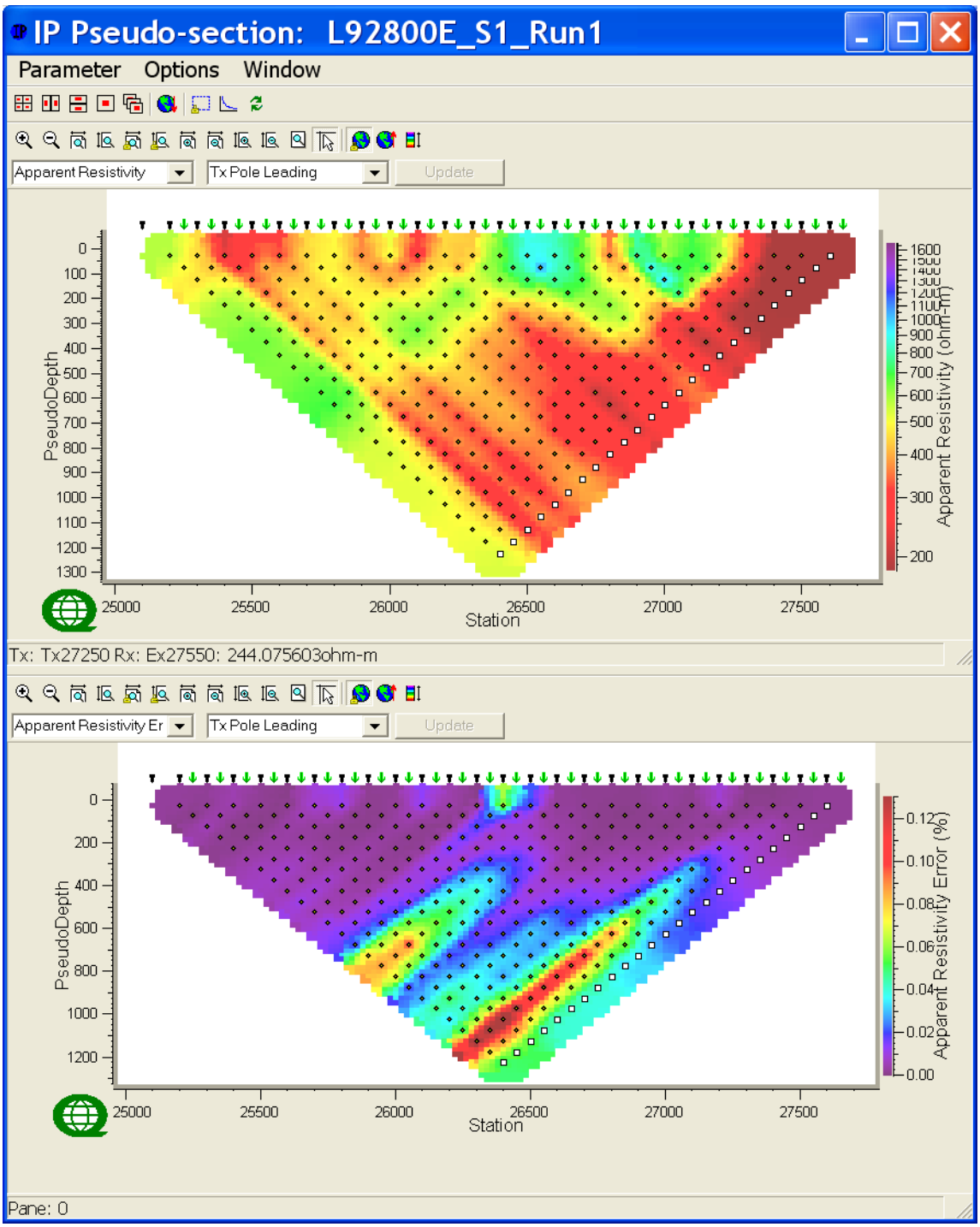

Line 92800E_S1 – Observed Apparent Resistivity Raw Data (Ohm.m) & Voltage Errors (%)-Tx Pole Leading.

☐ Tx with more than one event

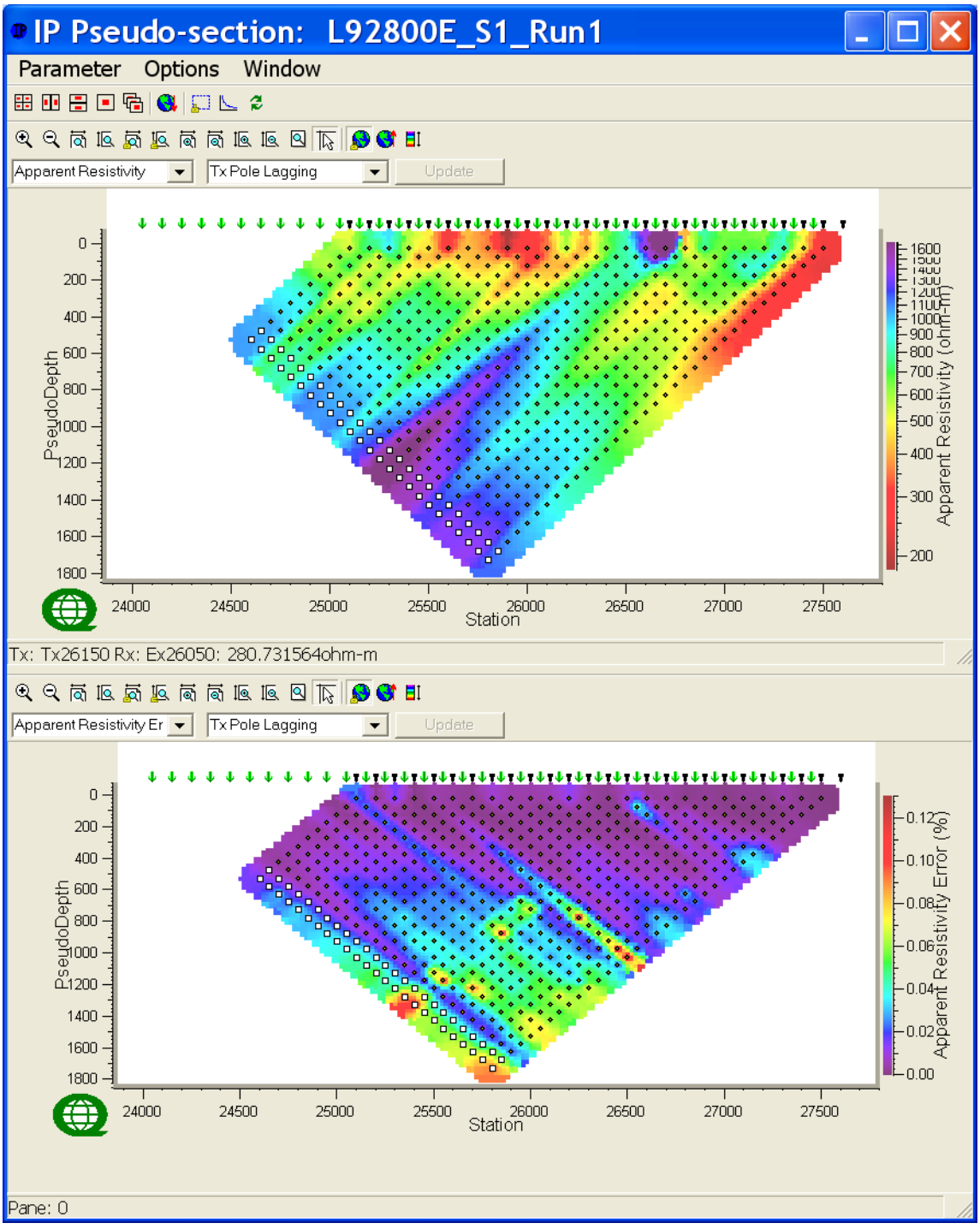

Line 92800E_S1 – Observed Apparent Resistivity Raw Data (Ohm.m) & Voltage Errors (%)-Tx Pole Lagging.

☐ Tx with more than one event

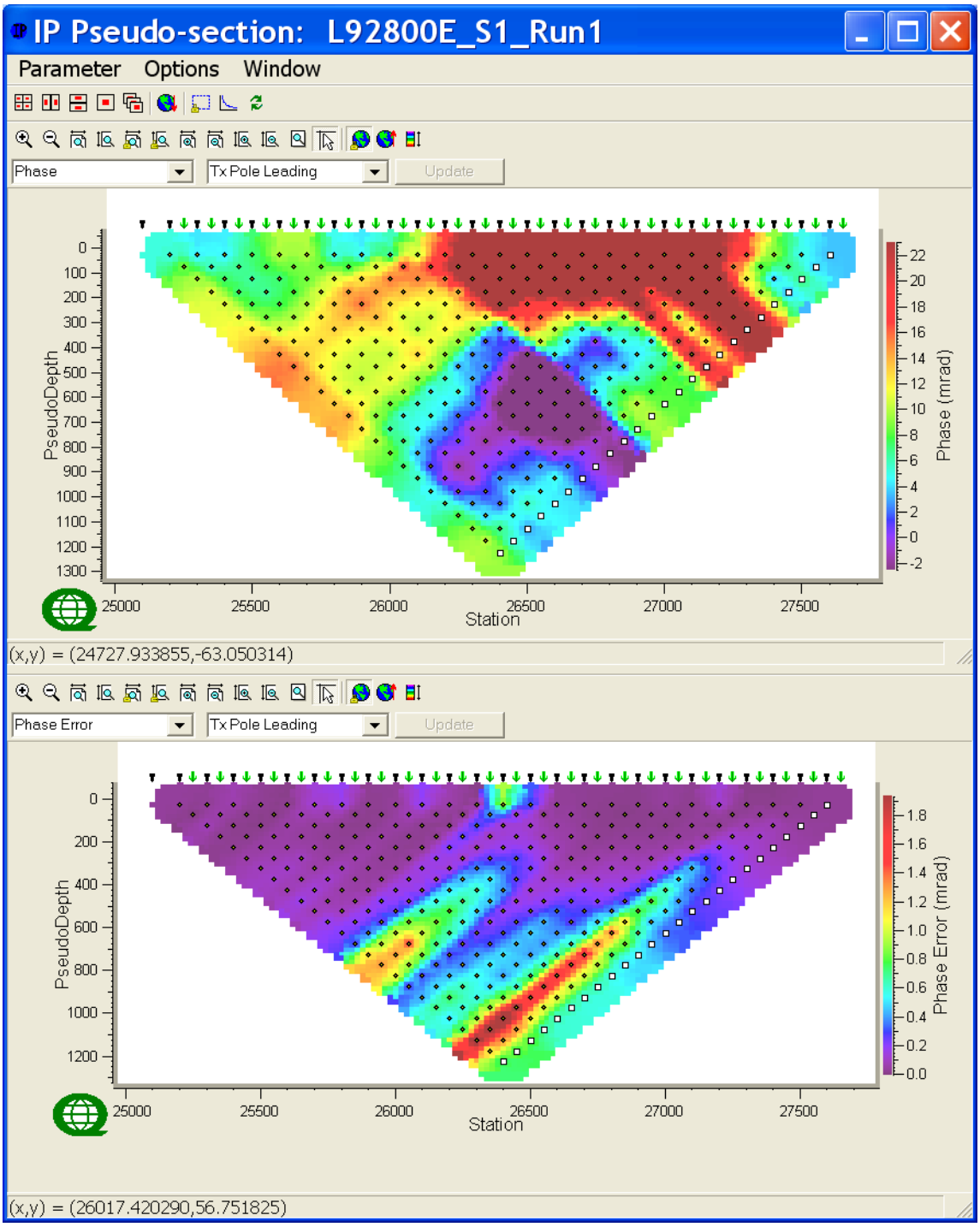

Line 92800E_S1 – Observed IP Raw Data (mrad) & IP Errors (mrads)-Tx Pole Leading.

☐ Tx with more than one event

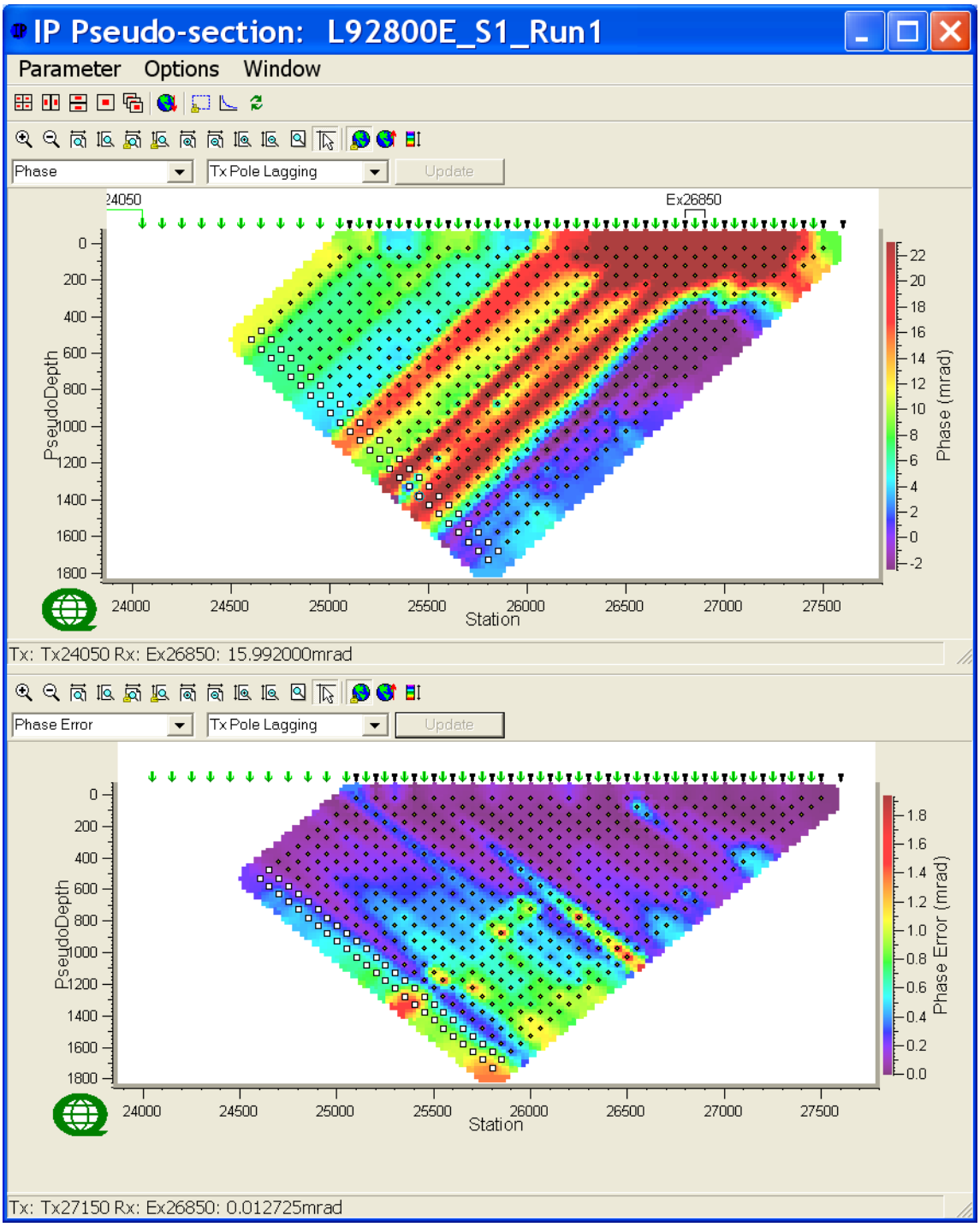

Line 92800E_S1 – Observed IP Raw Data (mrad) & IP Errors (mrads)-Tx Pole Lagging.

☐ Tx with more than one event

C.2 LINE 92800E_S2

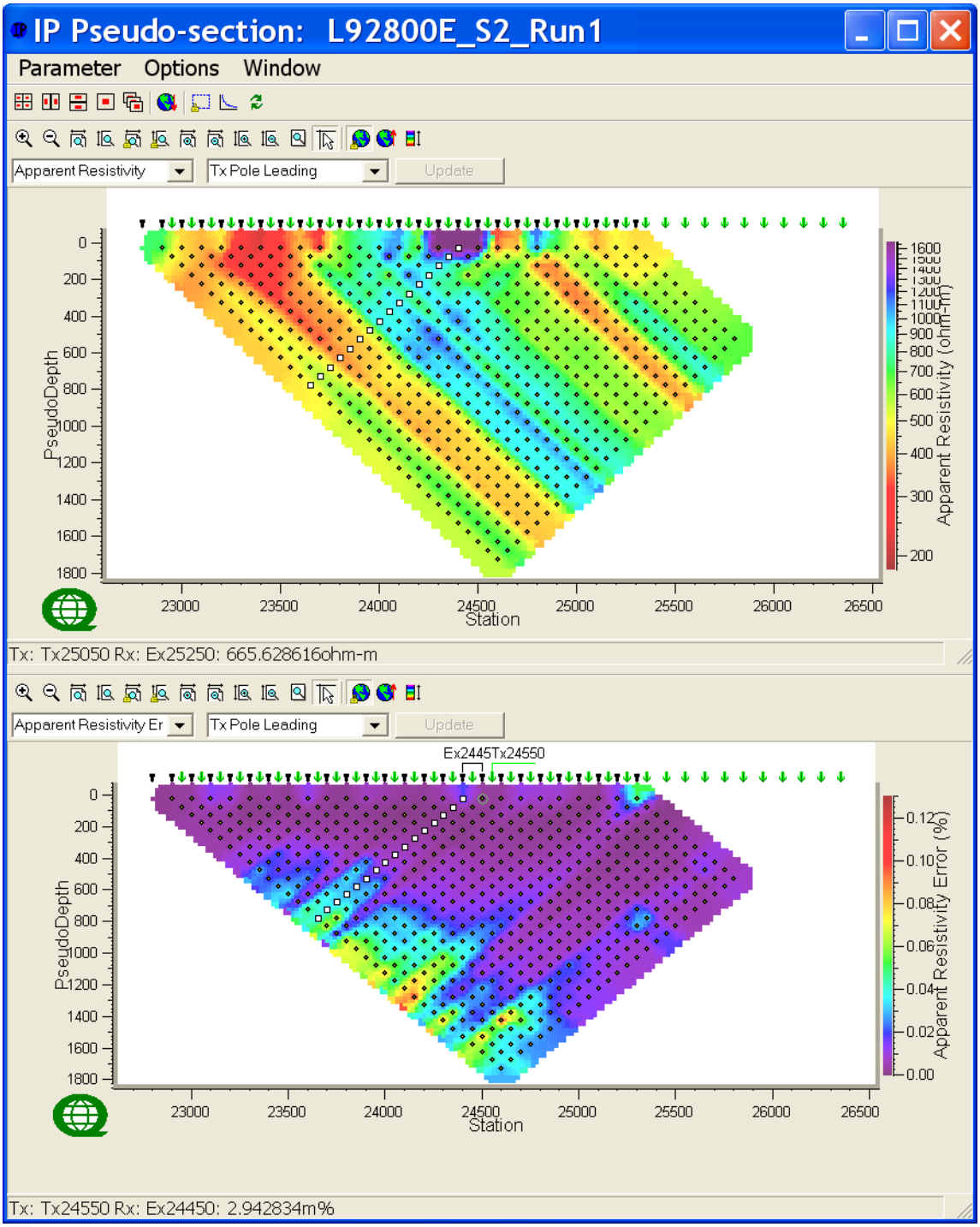

Line 92800E_S2 – Observed Apparent Resistivity Raw Data (Ohm.m) & Voltage Errors (%)-Tx Pole Leading.

☐ Tx with more than one event

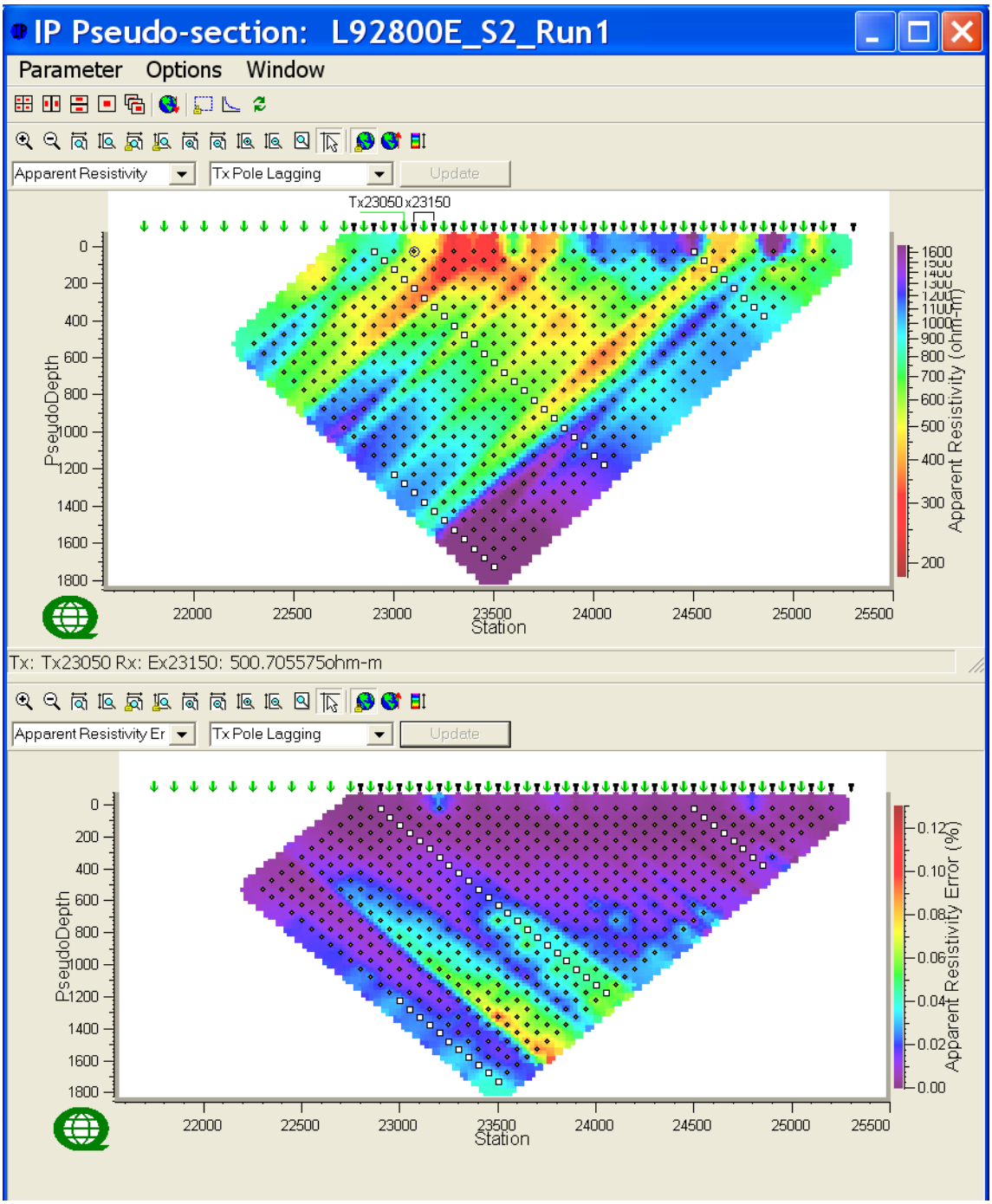

Line 92800E_S2 – Observed Apparent Resistivity Raw Data (Ohm.m) & Voltage Errors (%)-Tx Pole Lagging.

☐ Tx with more than one event

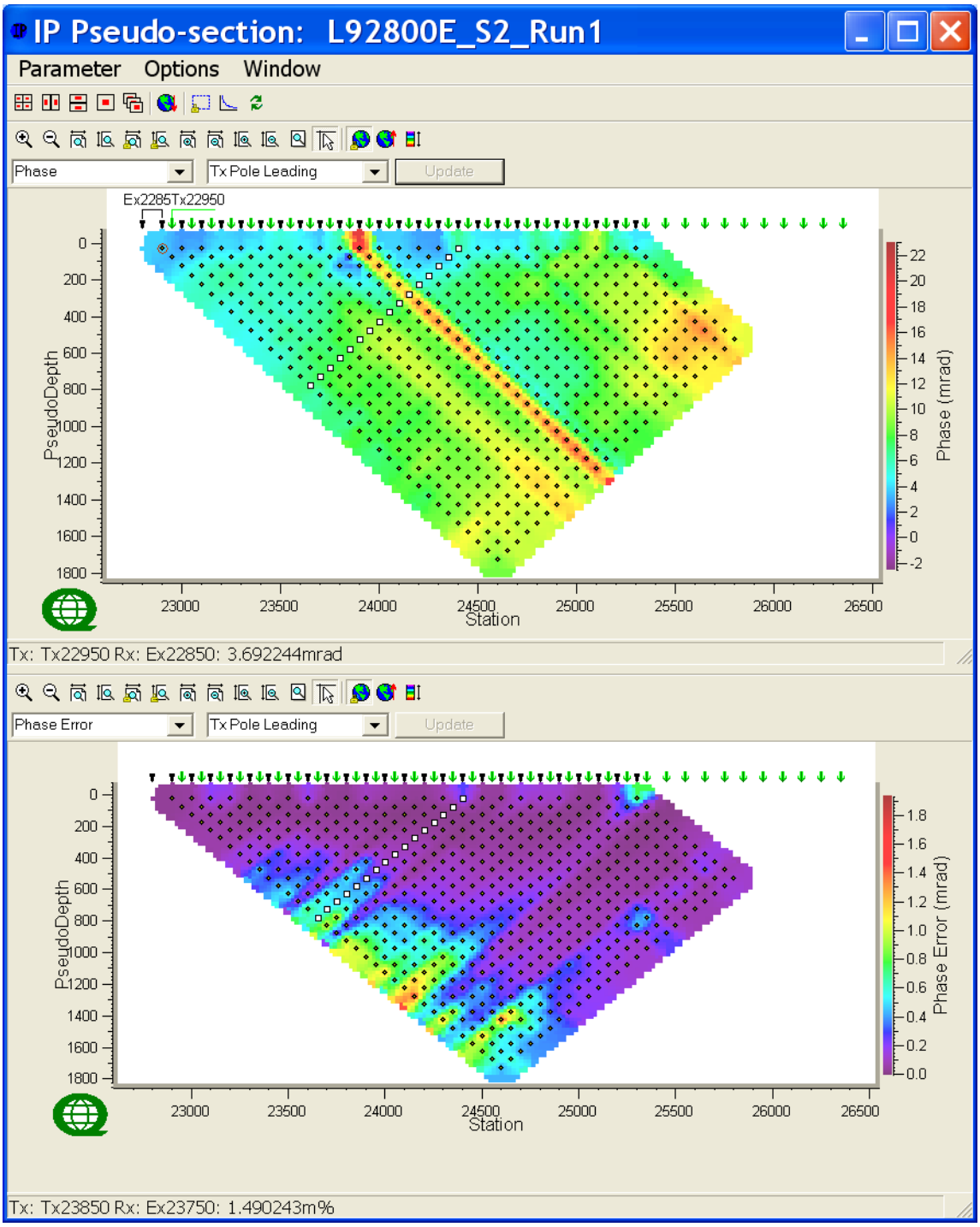

Line 92800E_S2 – Observed IP Raw Data (mrad) & IP Errors (mrads)-Tx Pole Leading.

☐ Tx with more than one event

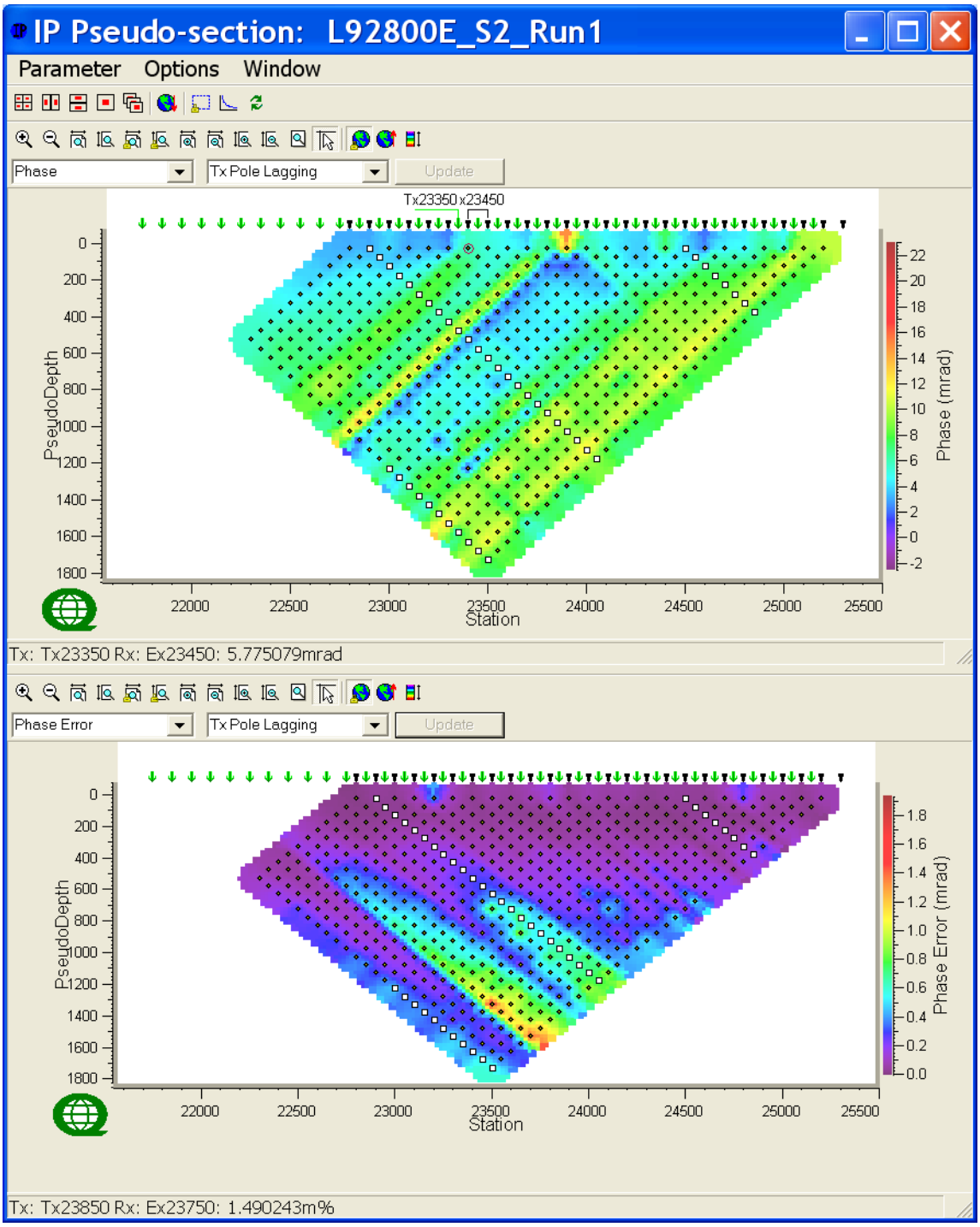

Line 92800E_S2 – Observed IP Raw Data (mrad) & IP Errors (mrads)-Tx Pole Lagging.

☐ Tx with more than one event

C.3 LINE 92800E_S3

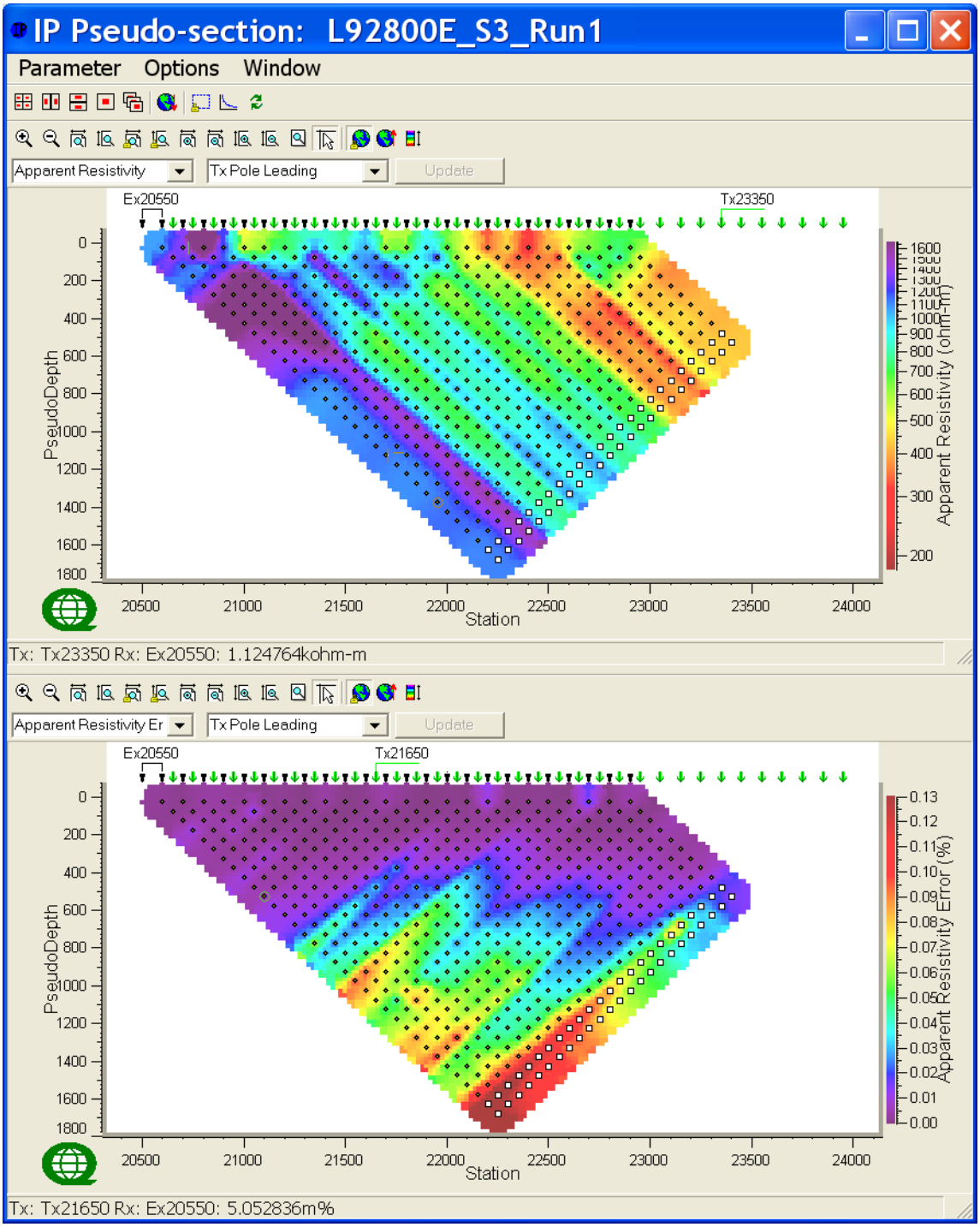

Line 92800E_S3 – Observed Apparent Resistivity Raw Data (Ohm.m) & Voltage Errors (%)-Tx Pole Leading.

☐ Tx with more than one event

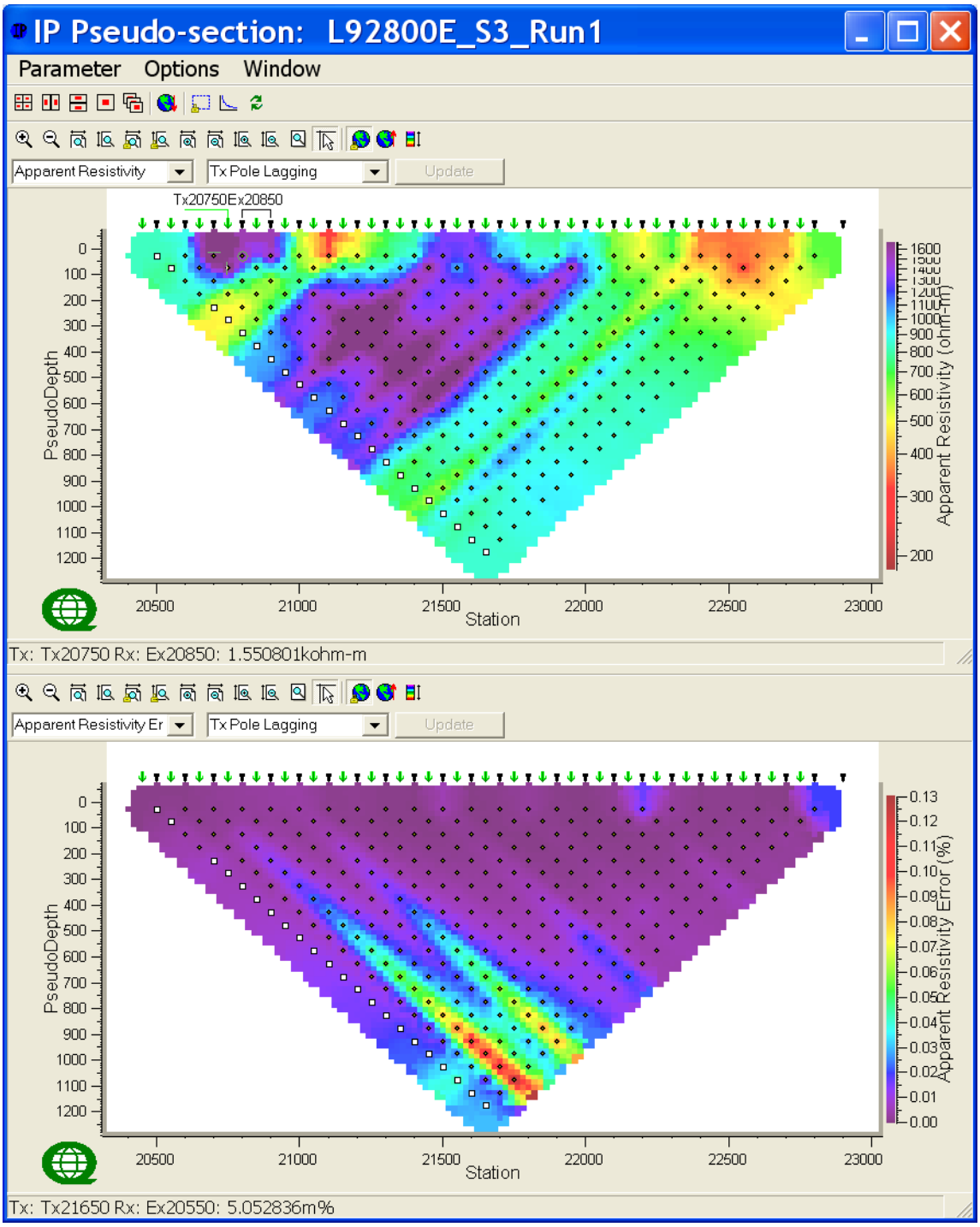

Line 92800E_S3 – Observed Apparent Resistivity Raw Data (Ohm.m) & Voltage Errors (%)-Tx Pole Lagging.

☐ Tx with more than one event

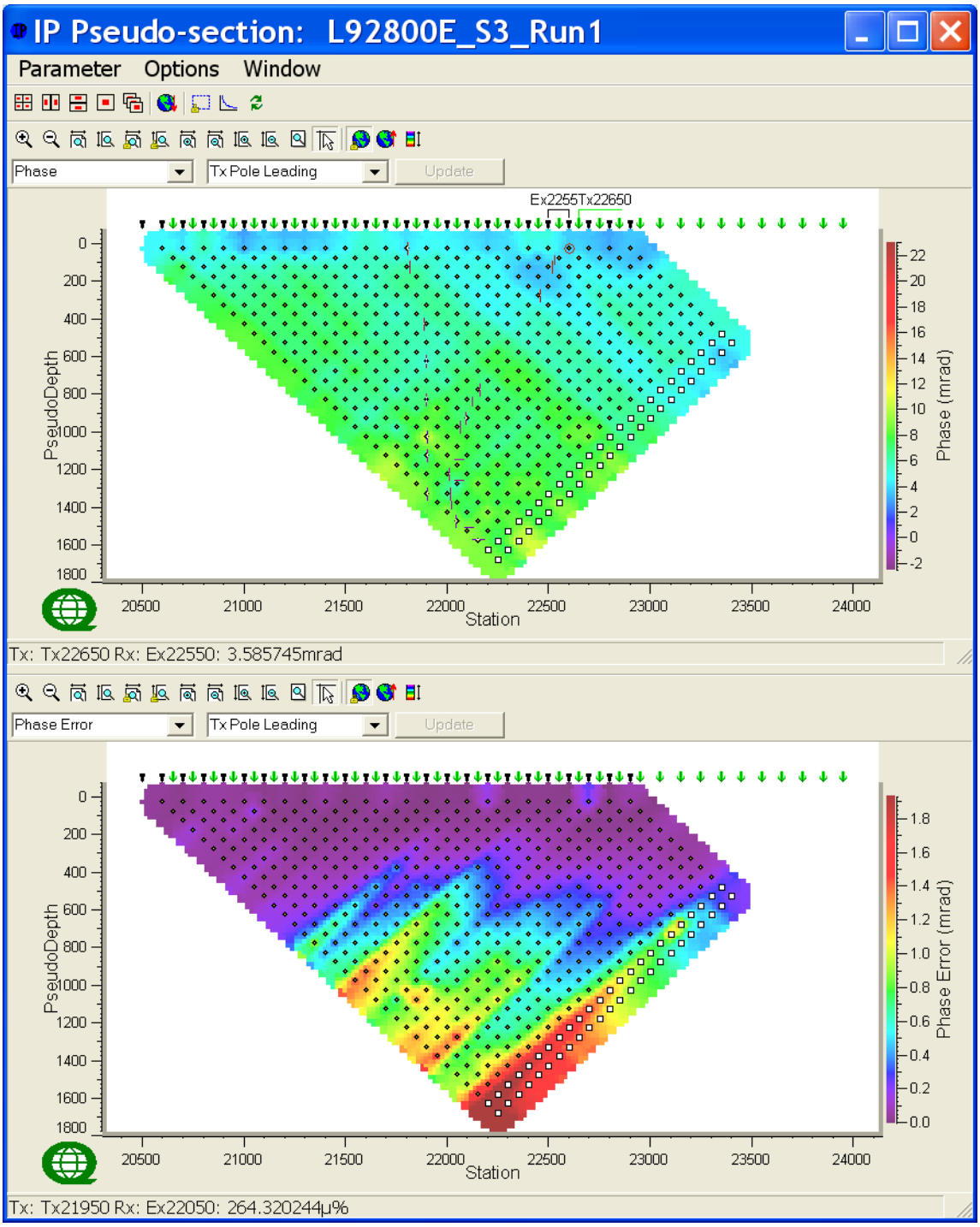

Line 92800E_S3 – Observed IP Raw Data (mrad) & IP Errors (mrads)-Tx Pole Leading.

☐ Tx with more than one event

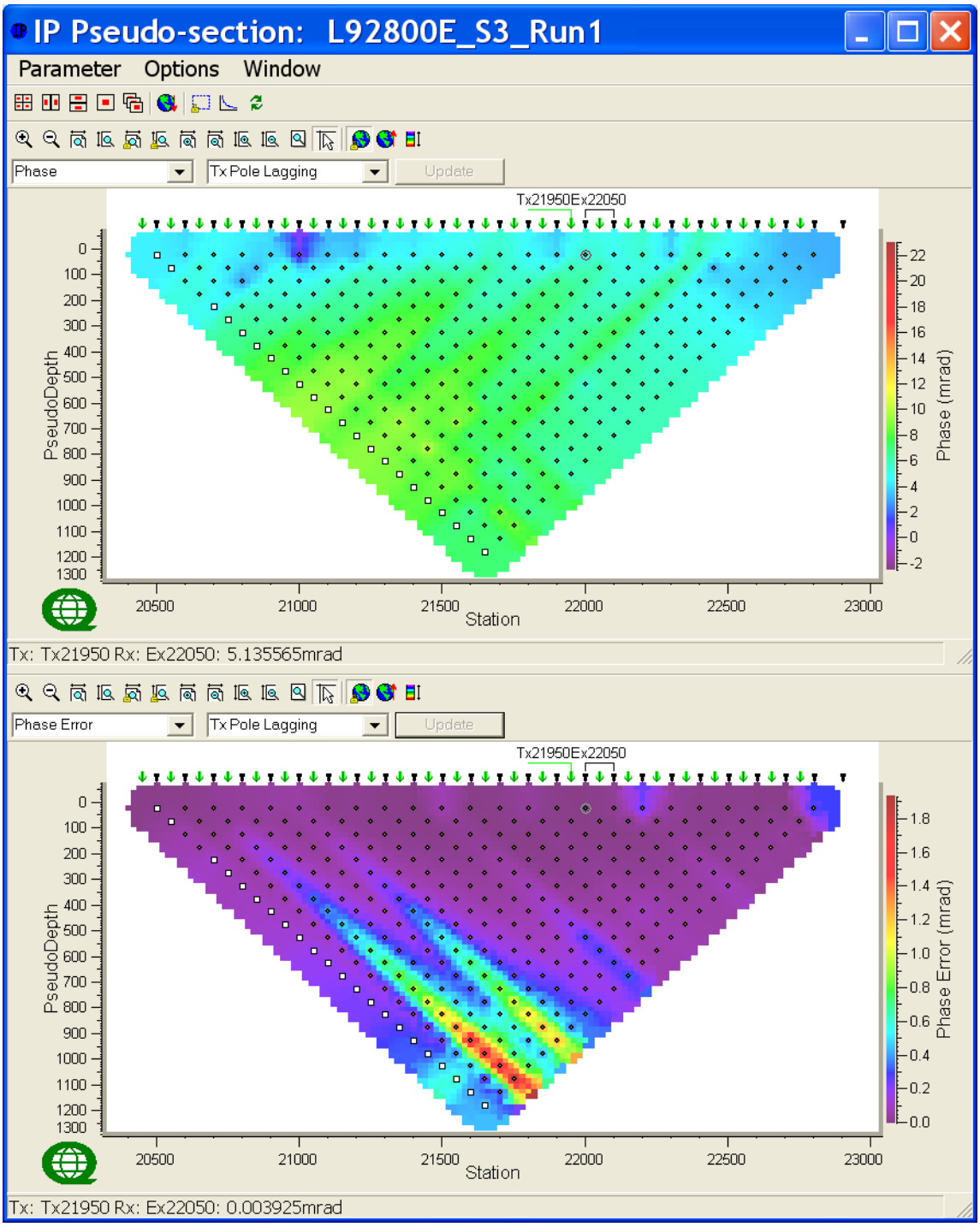

Line 92800E_S3 – Observed IP Raw Data (mrad) & IP Errors (mrads)-Tx Pole Lagging.

☐ Tx with more than one event

C.4 LINE 93200E_S1

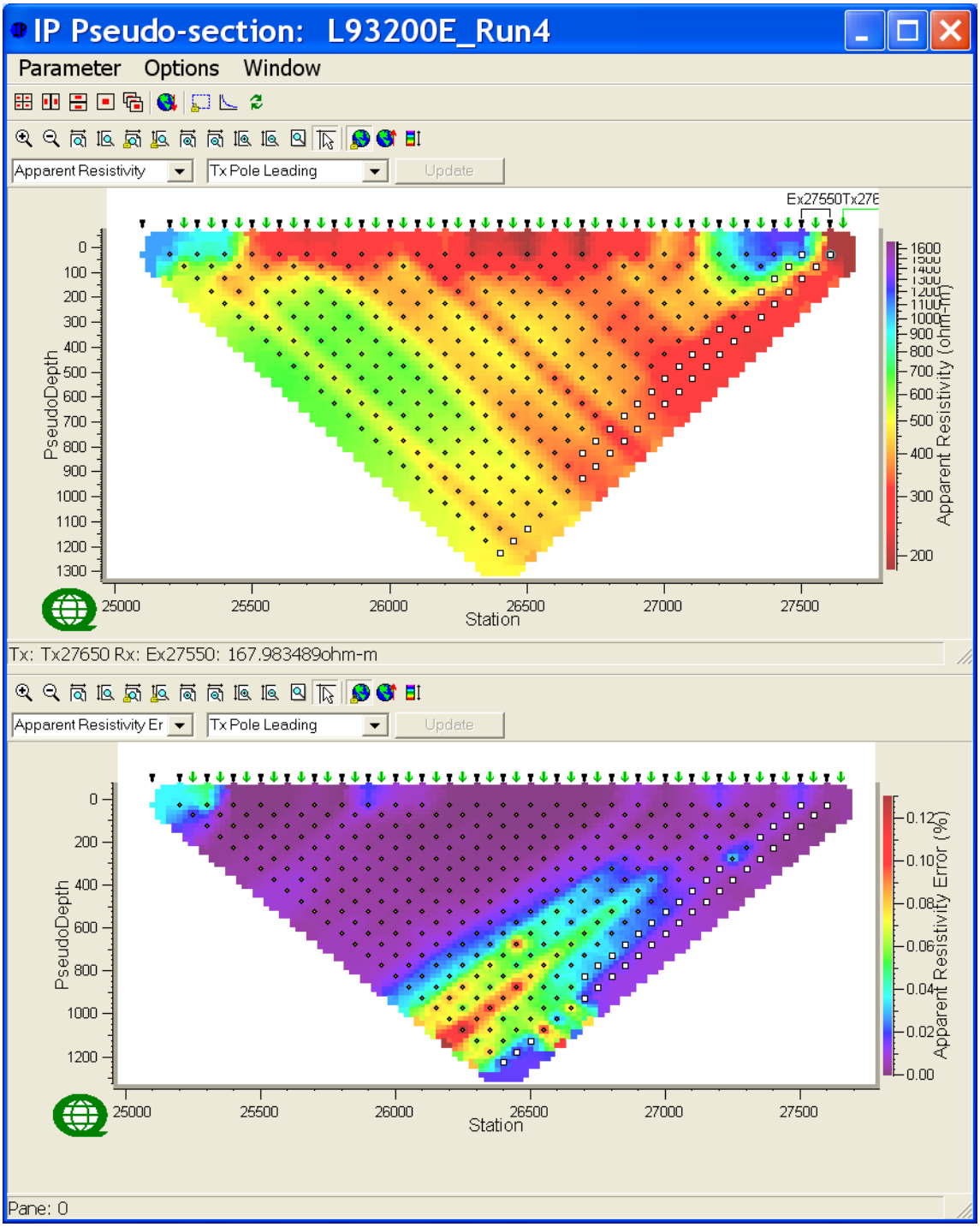

Line 93200E_S1 – Observed Apparent Resistivity Raw Data (Ohm.m) & Voltage Errors (%)-Tx Pole Leading.

☐ Tx with more than one event

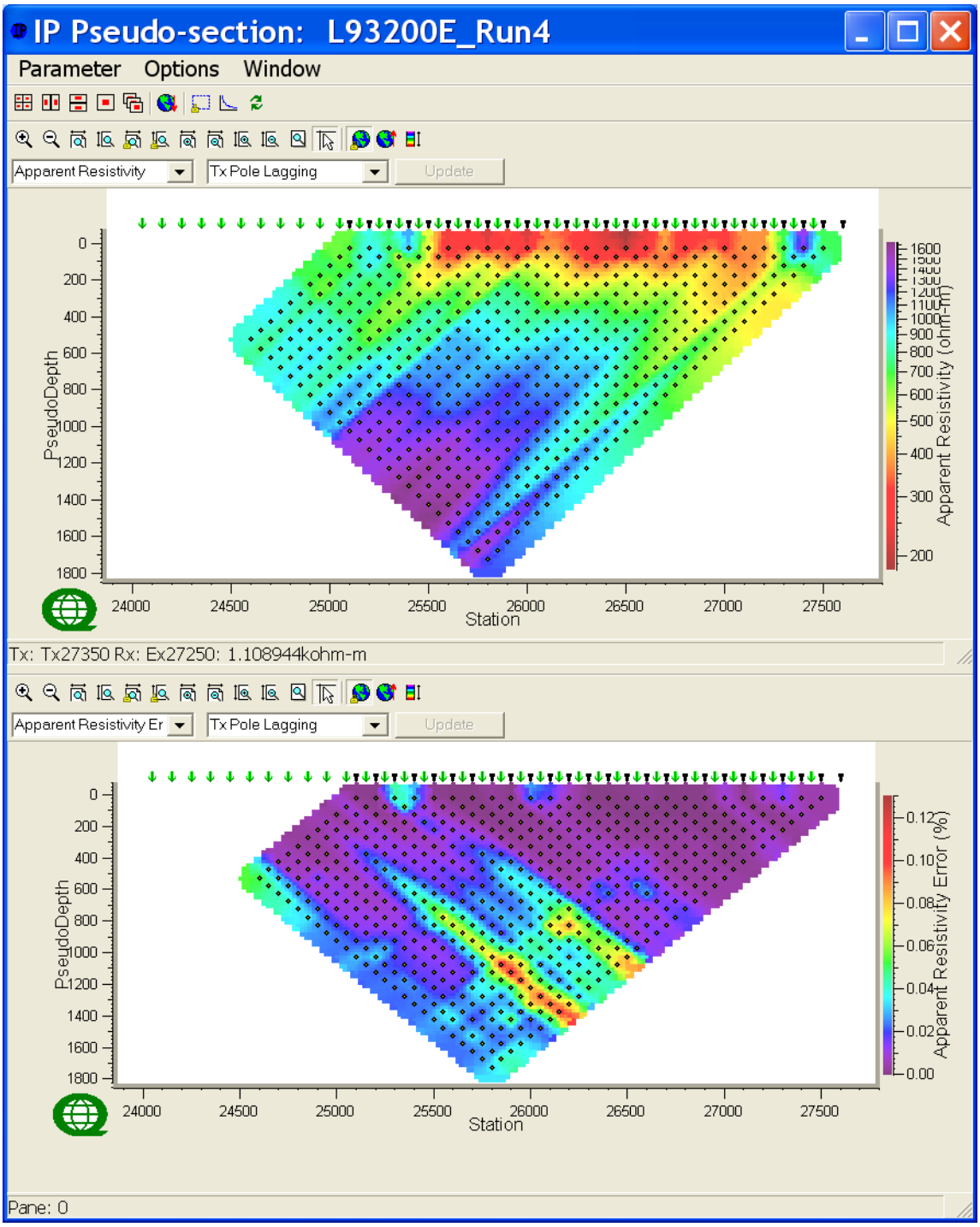

Line 93200E_S1 – Observed Apparent Resistivity Raw Data (Ohm.m) & Voltage Errors (%)-Tx Pole Lagging.

☐ Tx with more than one event

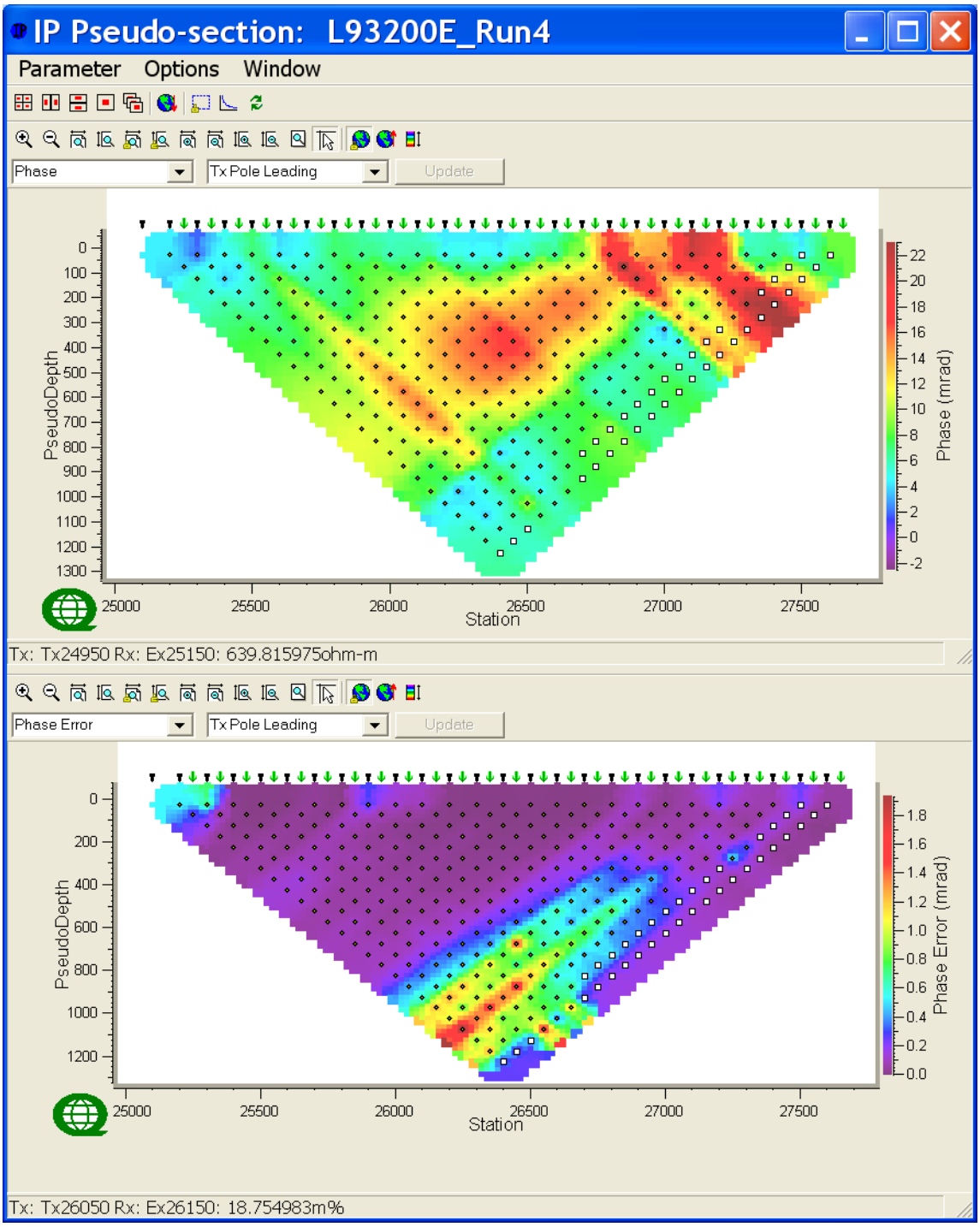

Line 93200E_S1 – Observed IP Raw Data (mrad) & IP Errors (mrads)-Tx Pole Leading.

☐ Tx with more than one event

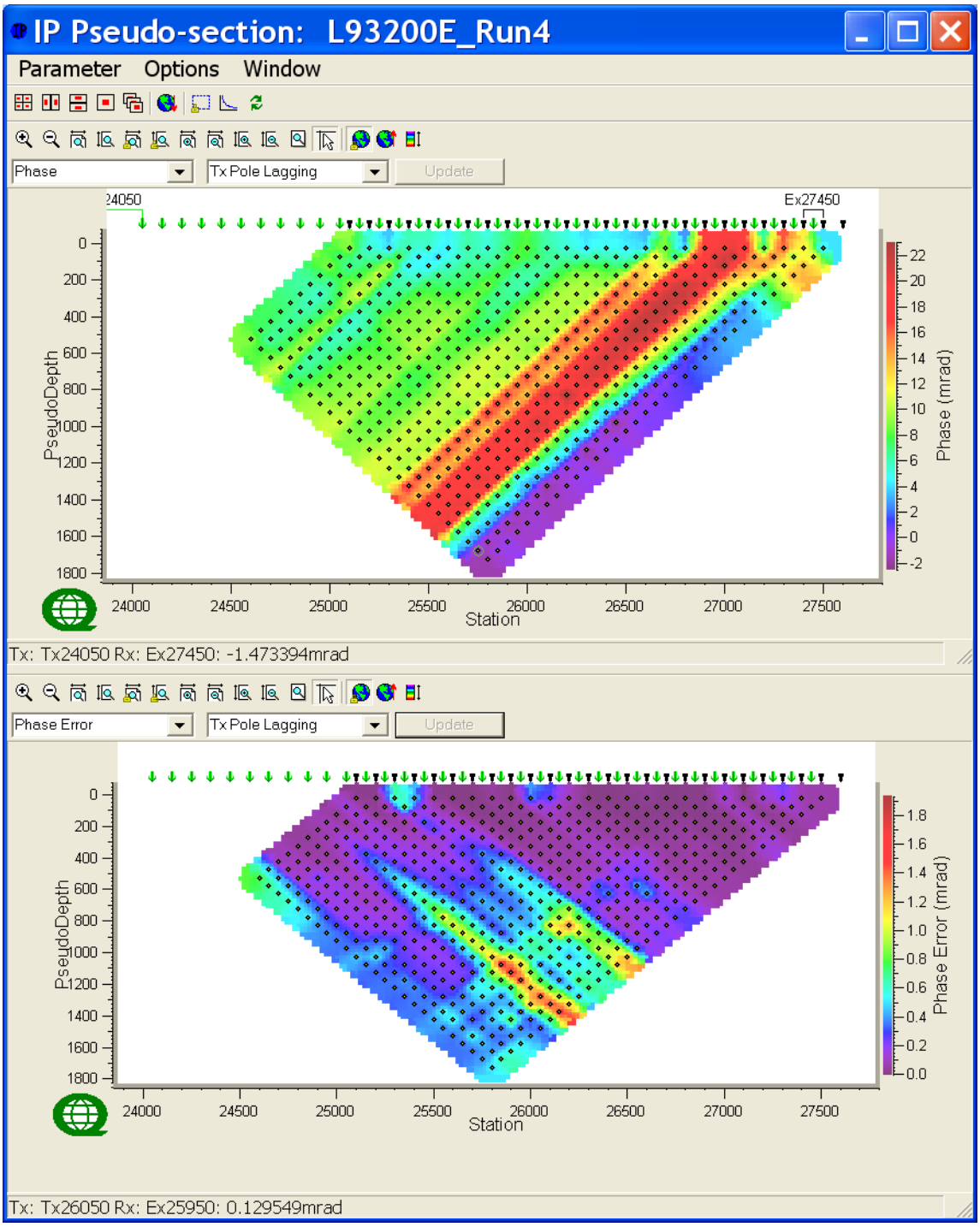

Line 93200E_S1 – Observed IP Raw Data (mrad) & IP Errors (mrads)-Tx Pole Lagging.

☐ Tx with more than one event

C.5 LINE 93200E_S2

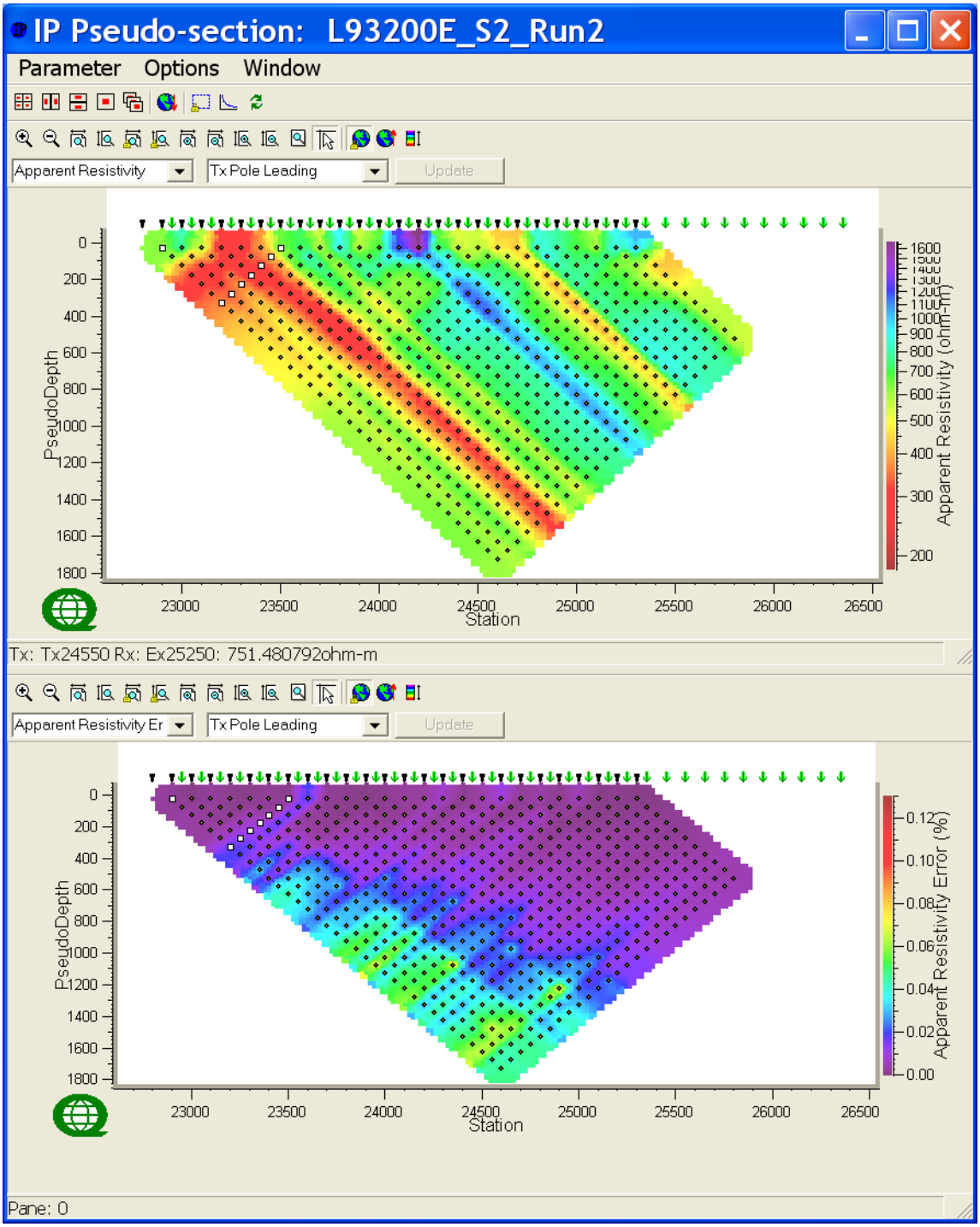

Line 93200E_S2 – Observed Apparent Resistivity Raw Data (Ohm.m) & Voltage Errors (%)-Tx Pole Leading.

☐ Tx with more than one event

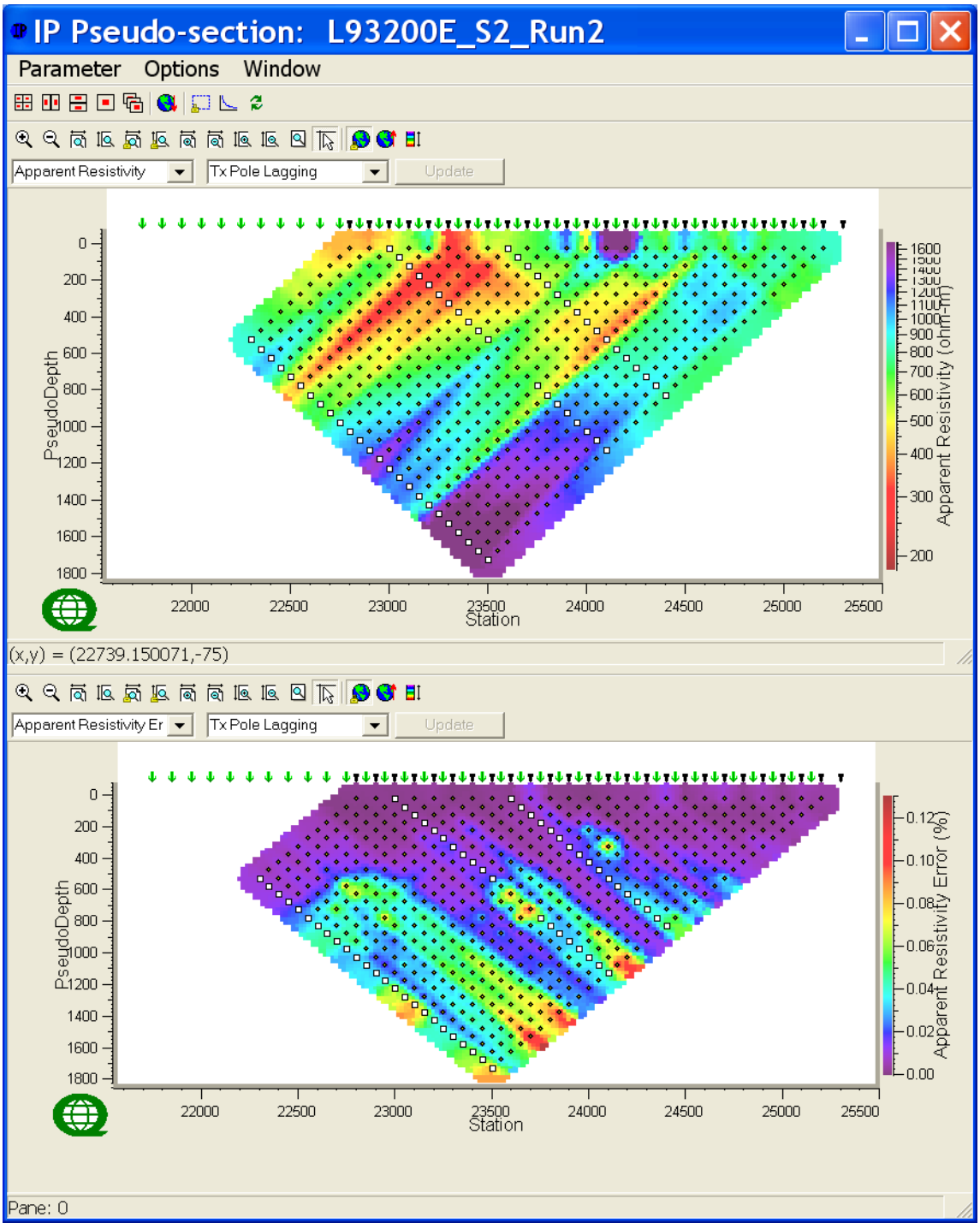

Line 93200E_S2 – Observed Apparent Resistivity Raw Data (Ohm.m) & Voltage Errors (%)-Tx Pole Lagging.

☐ Tx with more than one event

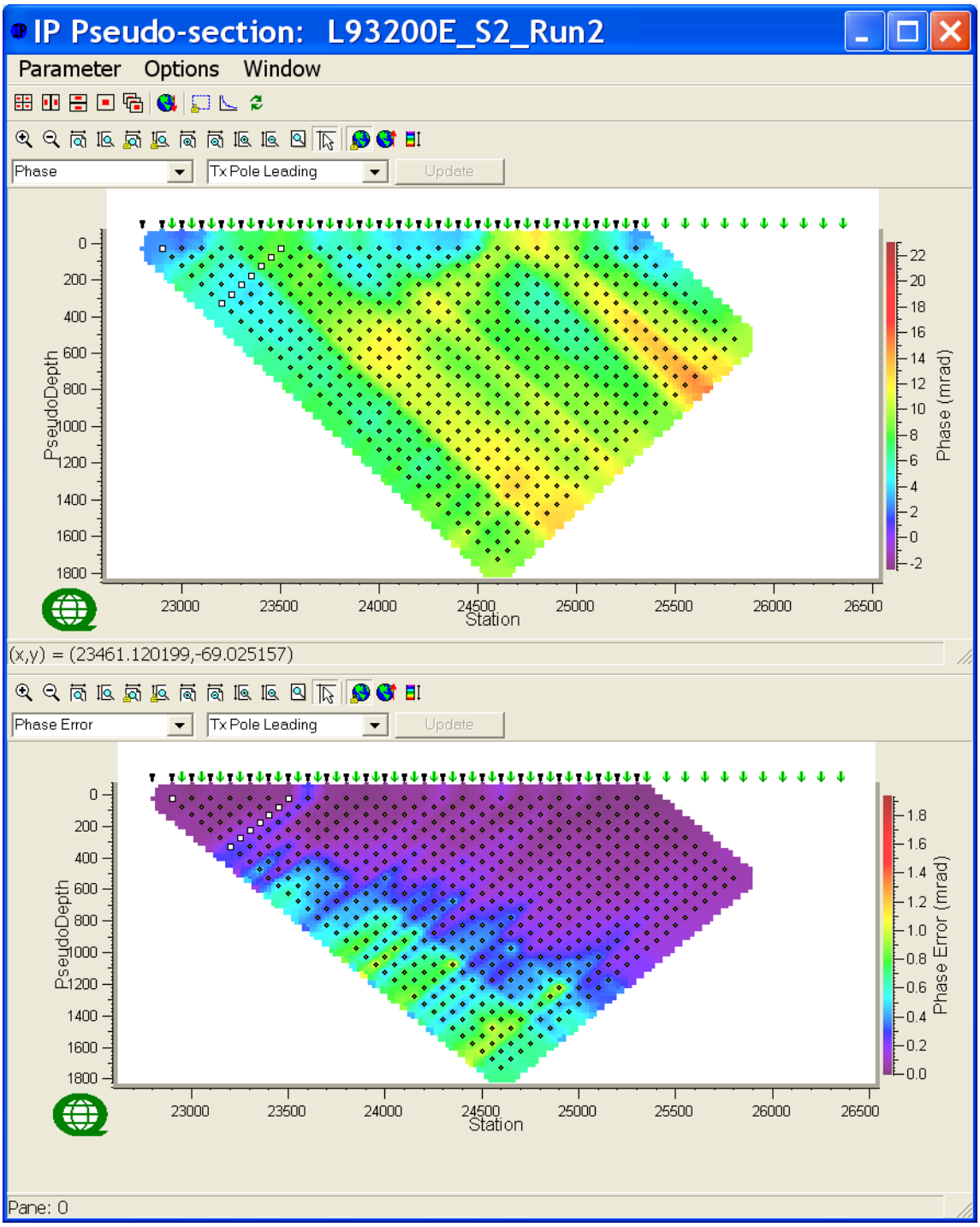

Line 93200E_S2 – Observed IP Raw Data (mrad) & IP Errors (mrads)-Tx Pole Leading.

☐ Tx with more than one event

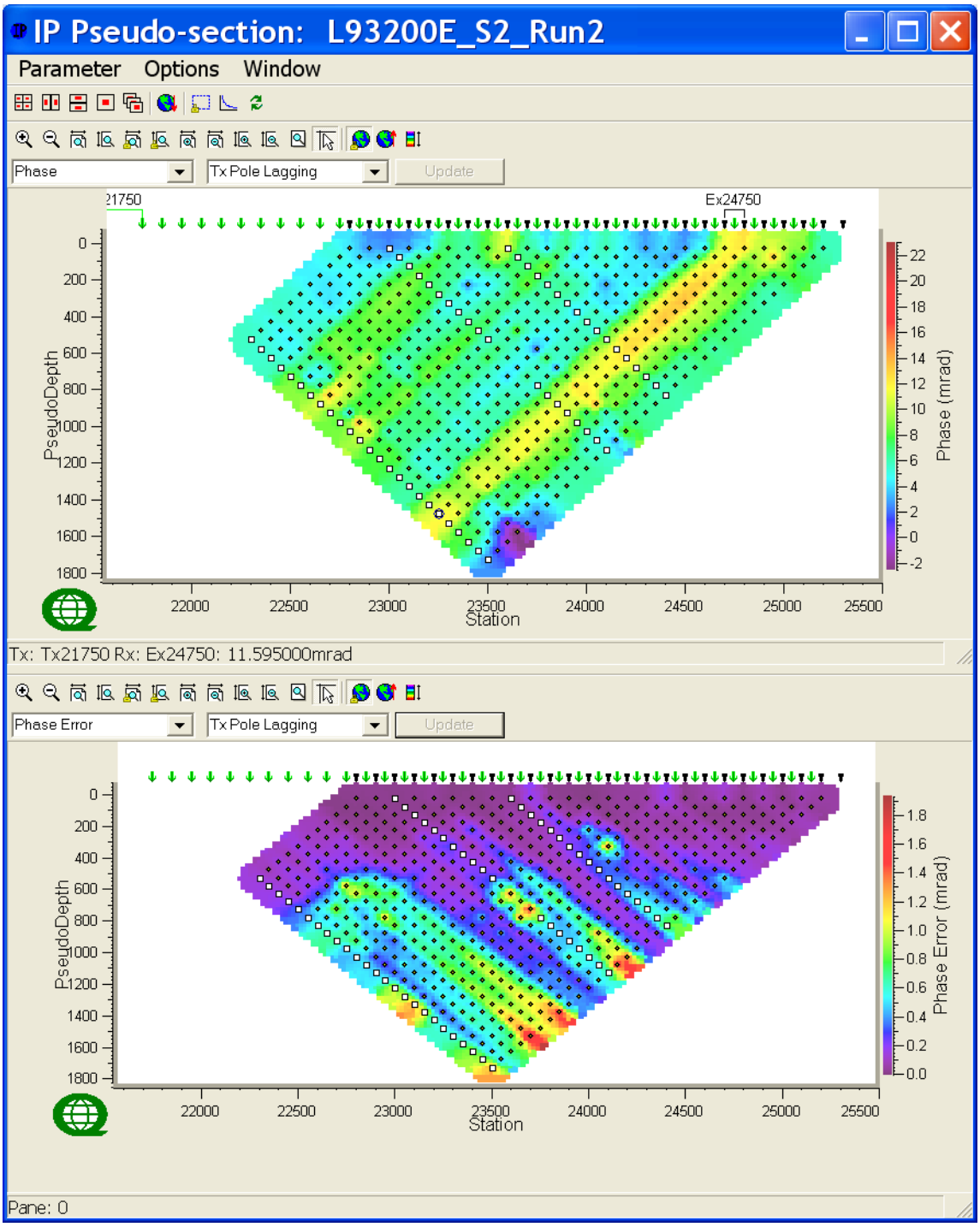

Line 93200E_S2 – Observed IP Raw Data (mrad) & IP Errors (mrads)-Tx Pole Lagging.

☐ Tx with more than one event

C.6 LINE 93200E_S3

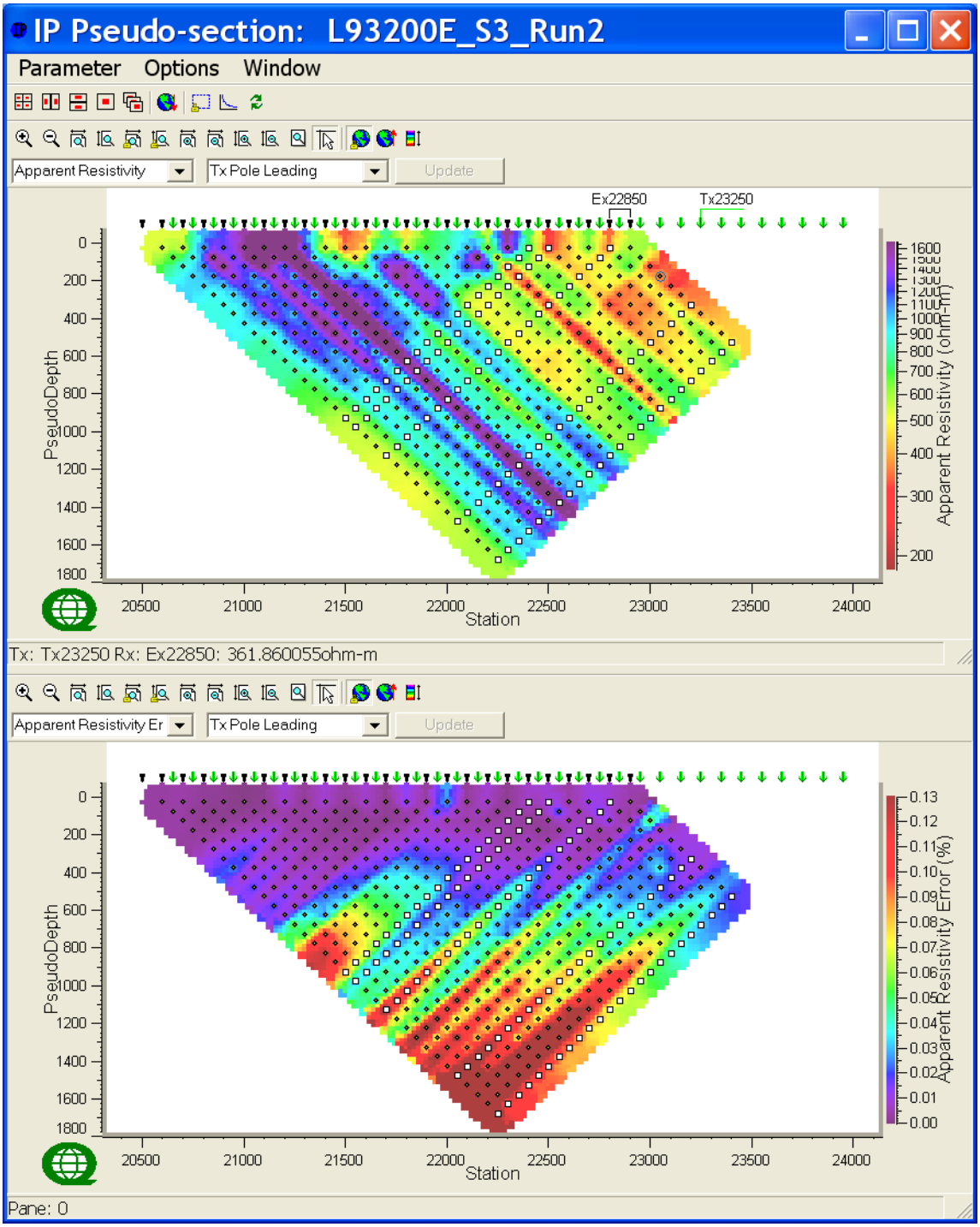

Line 93200E_S3 – Observed Apparent Resistivity Raw Data (Ohm.m) & Voltage Errors (%)-Tx Pole Leading.

☐ Tx with more than one event

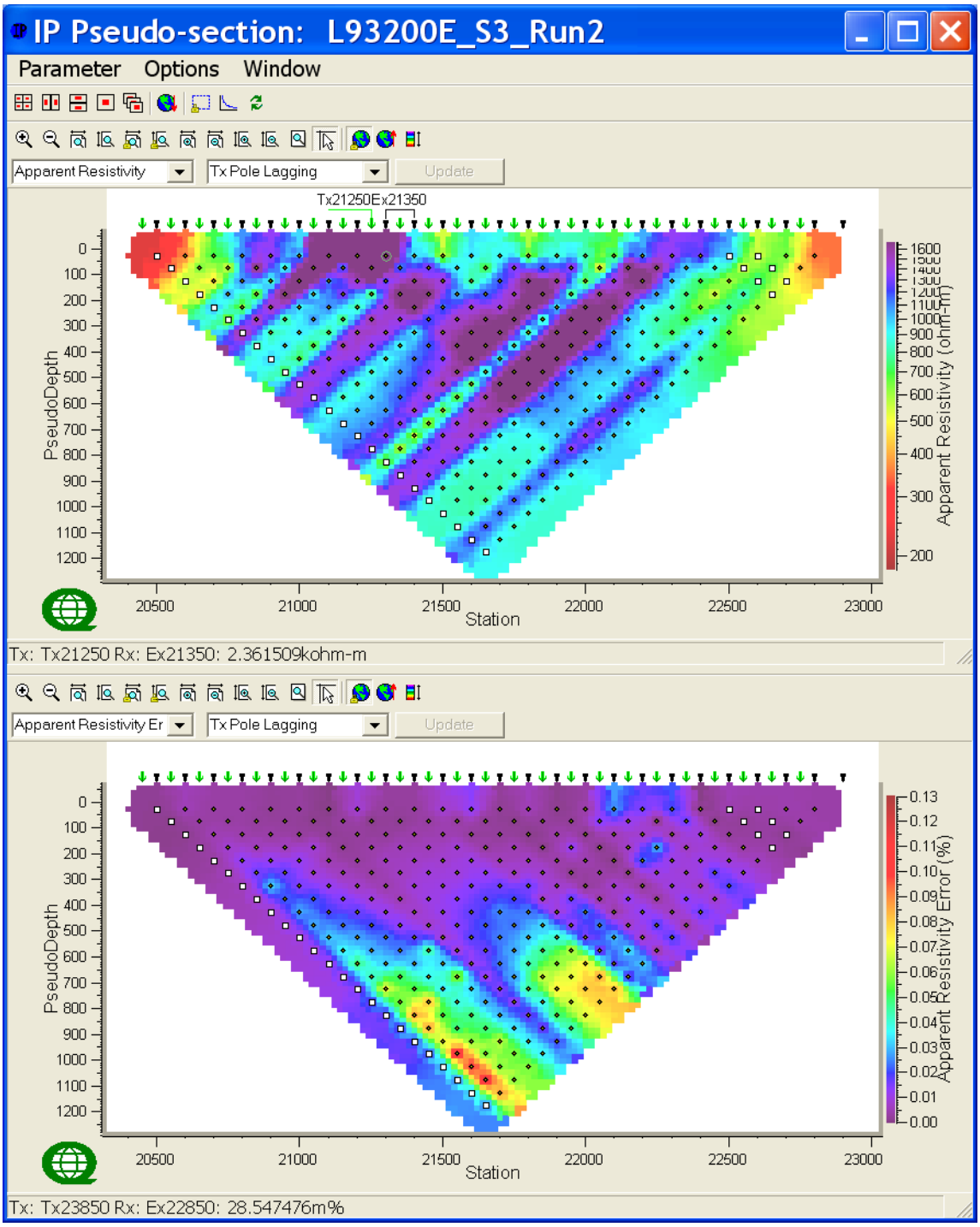

Line 93200E_S3 – Observed Apparent Resistivity Raw Data (Ohm.m) & Voltage Errors (%)-Tx Pole Lagging.

☐ Tx with more than one event

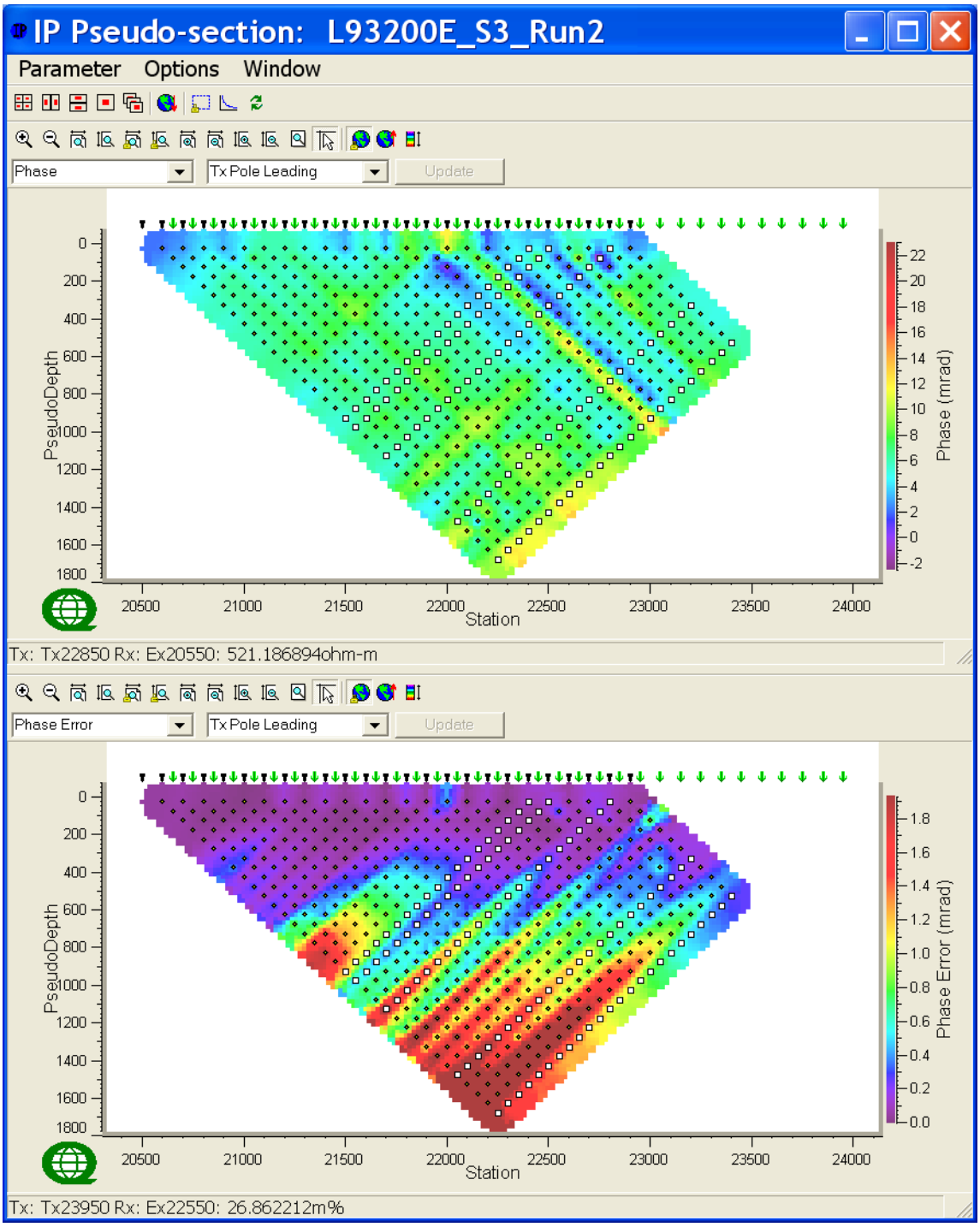

Line 93200E_S3 – Observed IP Raw Data (mrad) & IP Errors (mrads)-Tx Pole Leading.

☐ Tx with more than one event

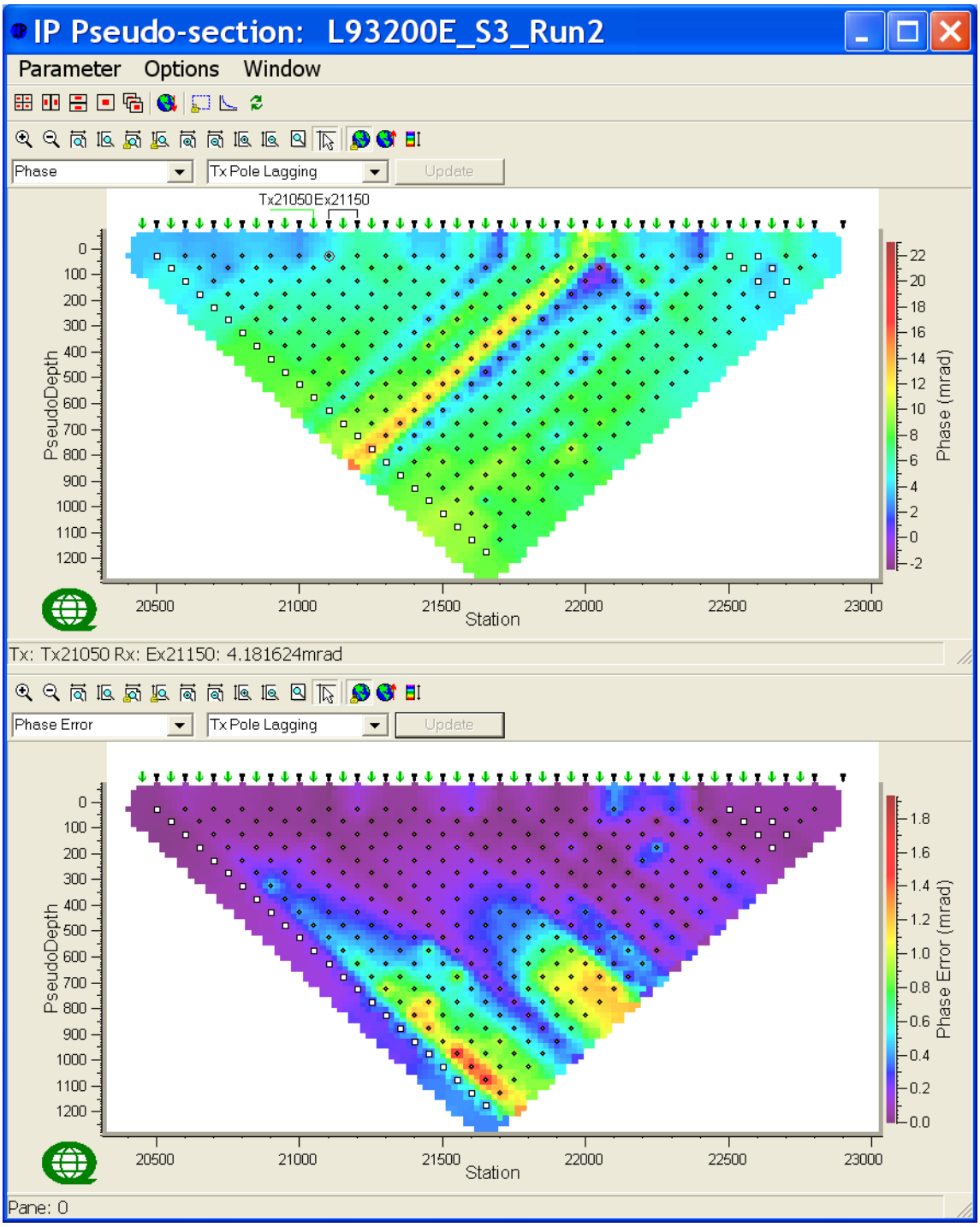

Line 93200E_S3 – Observed IP Raw Data (mrad) & IP Errors (mrads)-Tx Pole Lagging.

☐ Tx with more than one event

D MT SOUNDINGS CURVES OF FINAL AND MERGED PROCESSED DATA

Line	Spread	From	To
92800E	**MERGED**	**20550**	**27550**
	S1	25150	27550
	S2	22850	25250
	S3	20550	22850
93200E	**MERGED**	**20550**	**27550**
	S1	25150	27550
	S2	22850	25250
	S3	20550	22850

MODE XY (GREEN) DENOTES ELECTRICAL (**EX**) FIELD AND ORTHOGONAL MAGNETIC (**HY**) FIELD (=EX/HY)
MODE YX (ORANGE) DENOTES ELECTRICAL (**EY**) FIELD AND ORTHOGONAL MAGNETIC (**HX**) FIELD (=EY/HX)

D.1 LINE 92800E

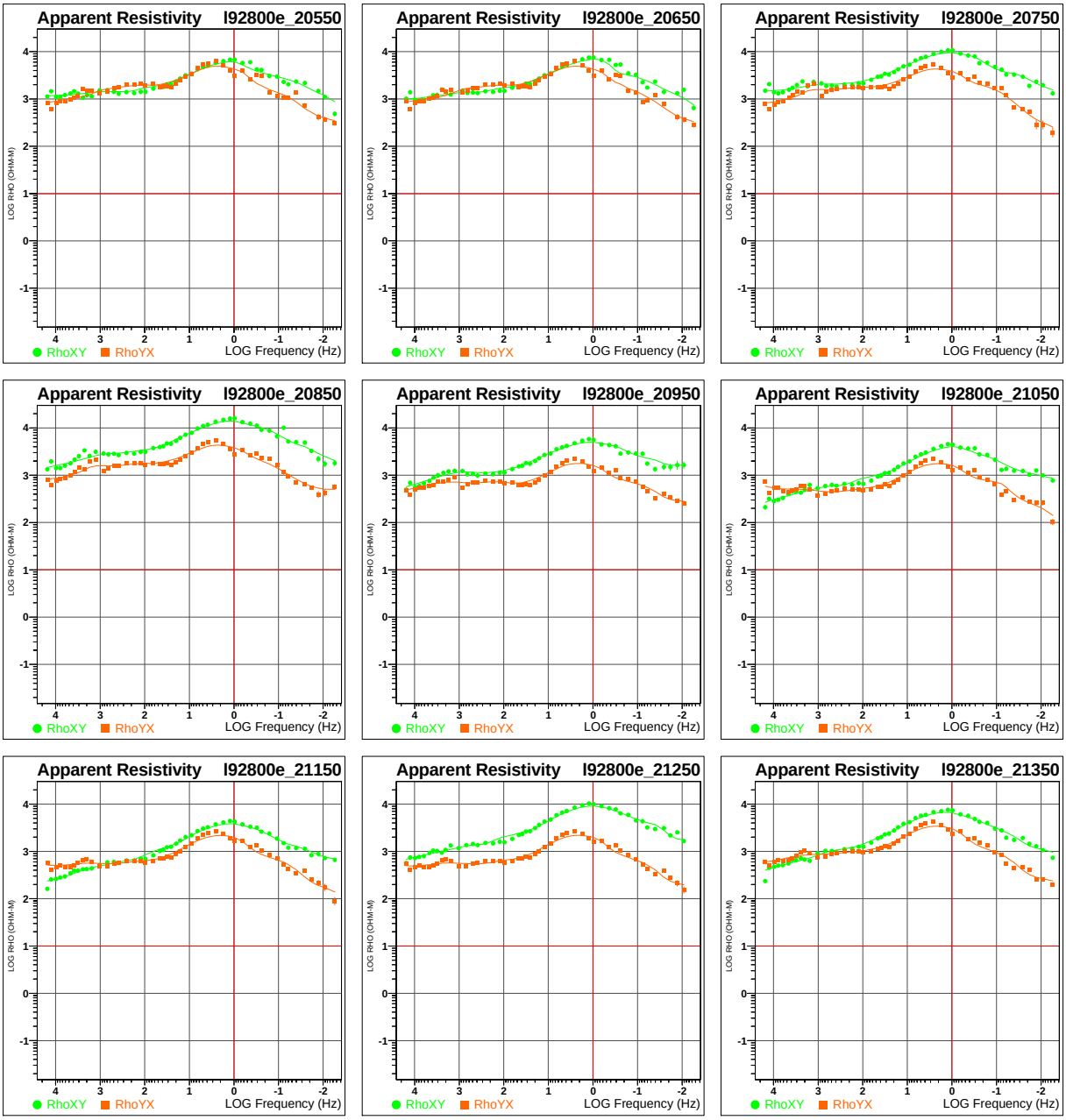

Line 92800E – Apparent Resistivity Sounding Curves vs Frequency (1 of 8).

MODE XY (GREEN) DENOTES ELECTRICAL (**EX**) FIELD AND ORTHOGONAL MAGNETIC (**HY**) FIELD (=EX/HY)
MODE YX (ORANGE) DENOTES ELECTRICAL (**EY**) FIELD AND ORTHOGONAL MAGNETIC (**HX**) FIELD (=EY/HX)

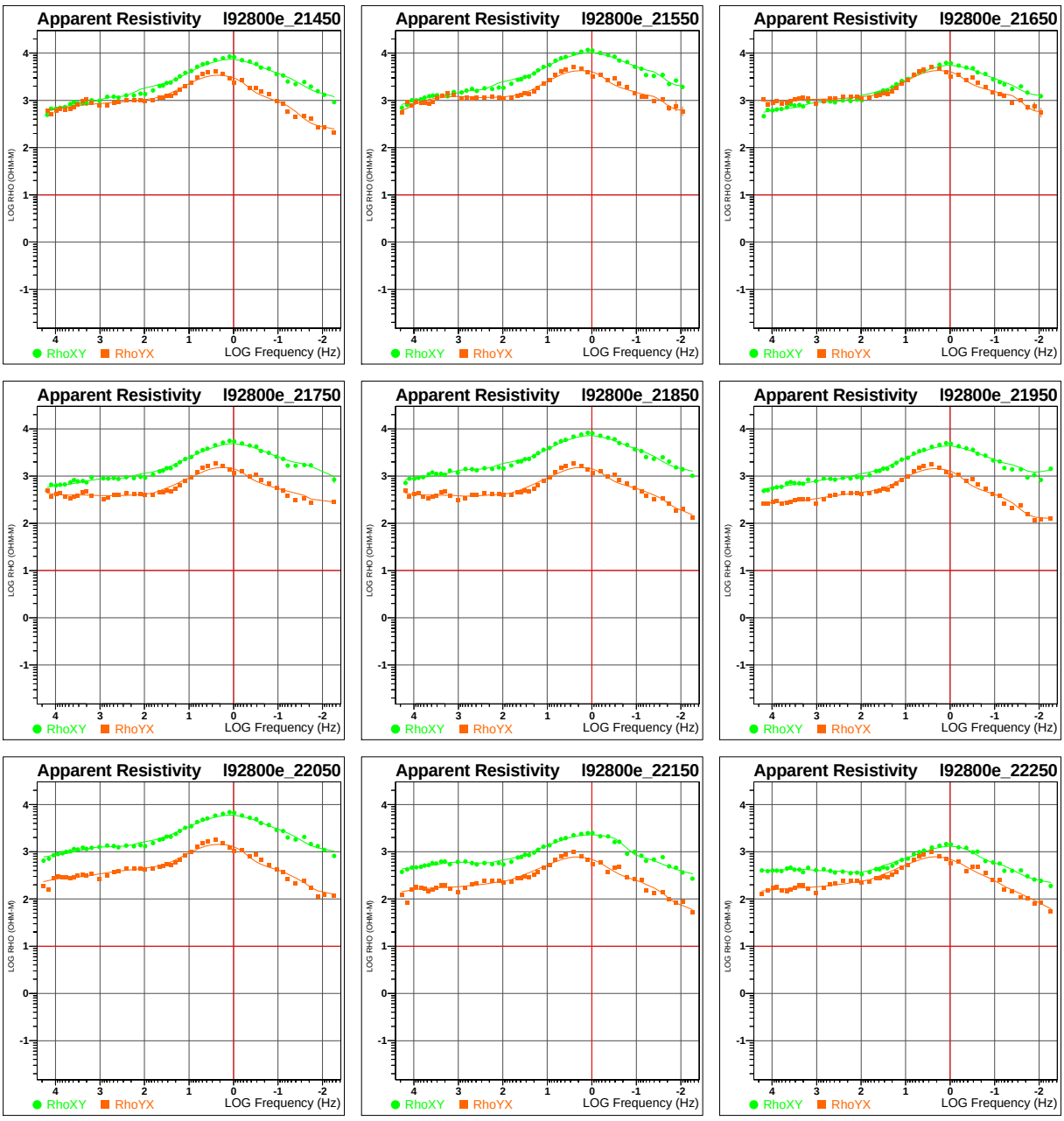

Line 92800E – Apparent Resistivity Sounding Curves vs Frequency (2 of 8).

MODE XY (GREEN) DENOTES ELECTRICAL (**EX**) FIELD AND ORTHOGONAL MAGNETIC (**HY**) FIELD (=EX/HY)
MODE YX (ORANGE) DENOTES ELECTRICAL (**EY**) FIELD AND ORTHOGONAL MAGNETIC (**HX**) FIELD (=EY/HX)

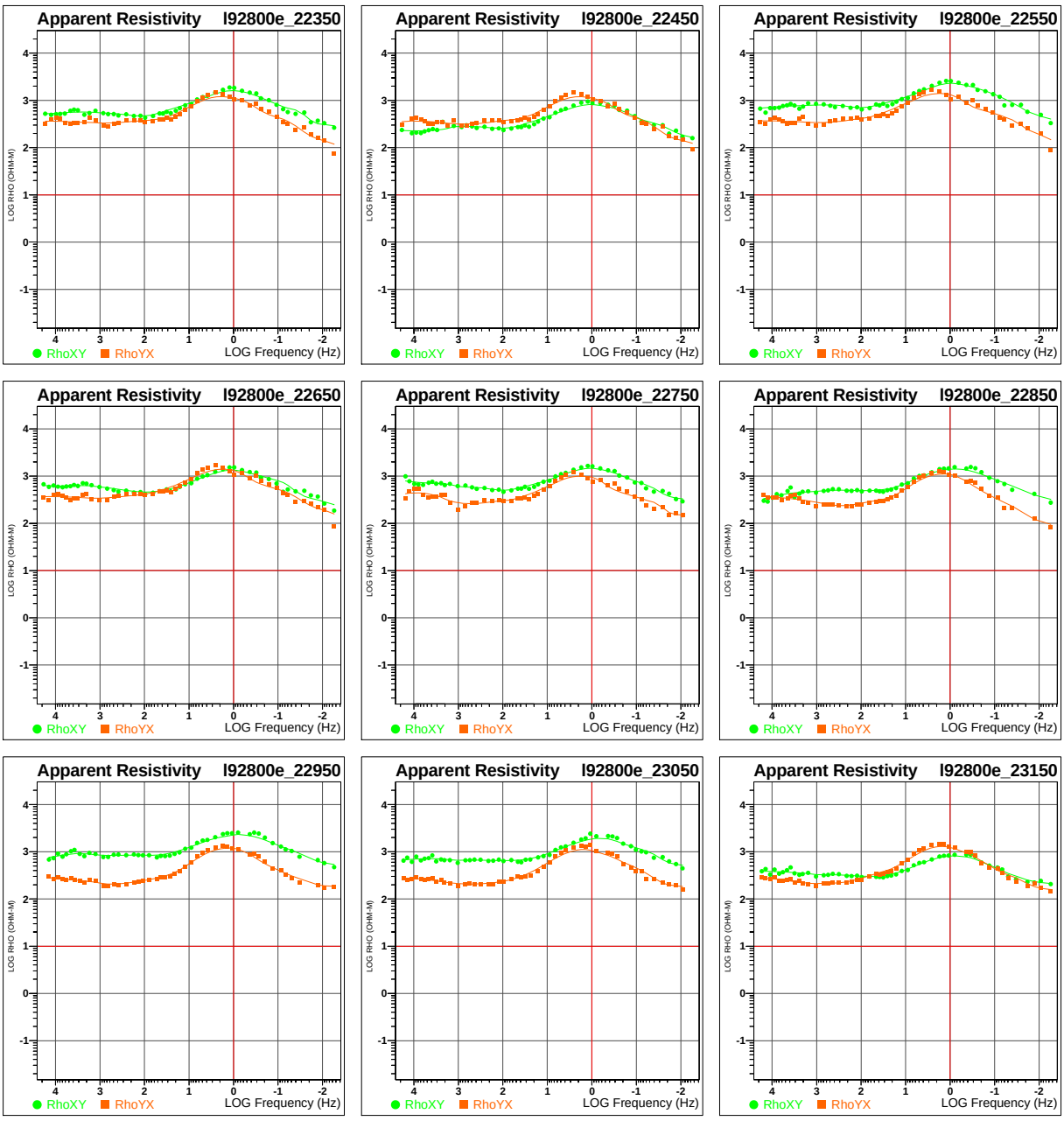

Line 92800E – Apparent Resistivity Sounding Curves vs Frequency (3 of 8).

MODE XY (GREEN) DENOTES ELECTRICAL (**EX**) FIELD AND ORTHOGONAL MAGNETIC (**HY**) FIELD (=EX/HY)
MODE YX (ORANGE) DENOTES ELECTRICAL (**EY**) FIELD AND ORTHOGONAL MAGNETIC (**HX**) FIELD (=EY/HX)

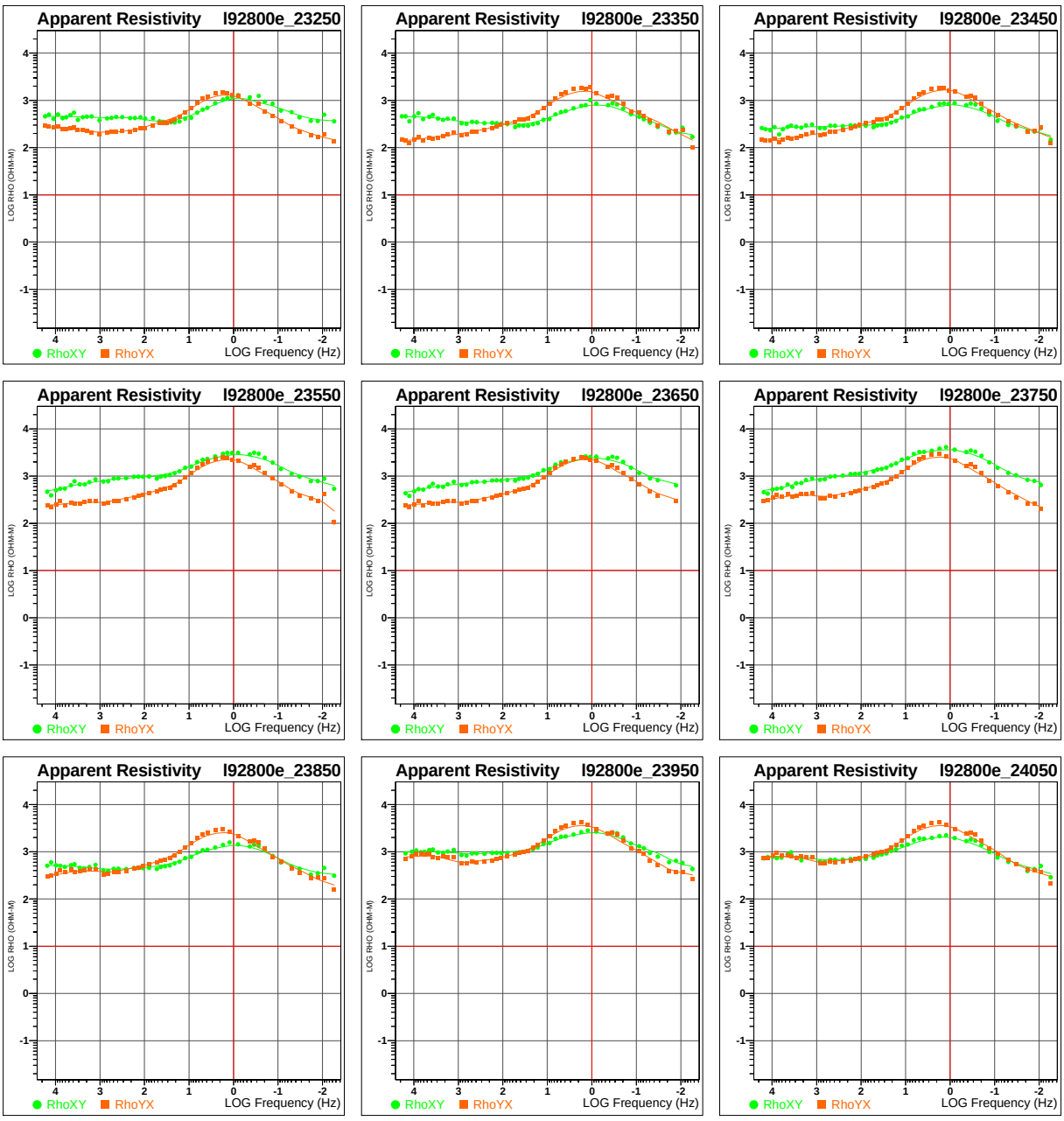

Line 92800E – Apparent Resistivity Sounding Curves vs Frequency (4 of 8).

MODE XY (GREEN) DENOTES ELECTRICAL (**EX**) FIELD AND ORTHOGONAL MAGNETIC (**HY**) FIELD (=EX/HY)
MODE YX (ORANGE) DENOTES ELECTRICAL (**EY**) FIELD AND ORTHOGONAL MAGNETIC (**HX**) FIELD (=EY/HX)

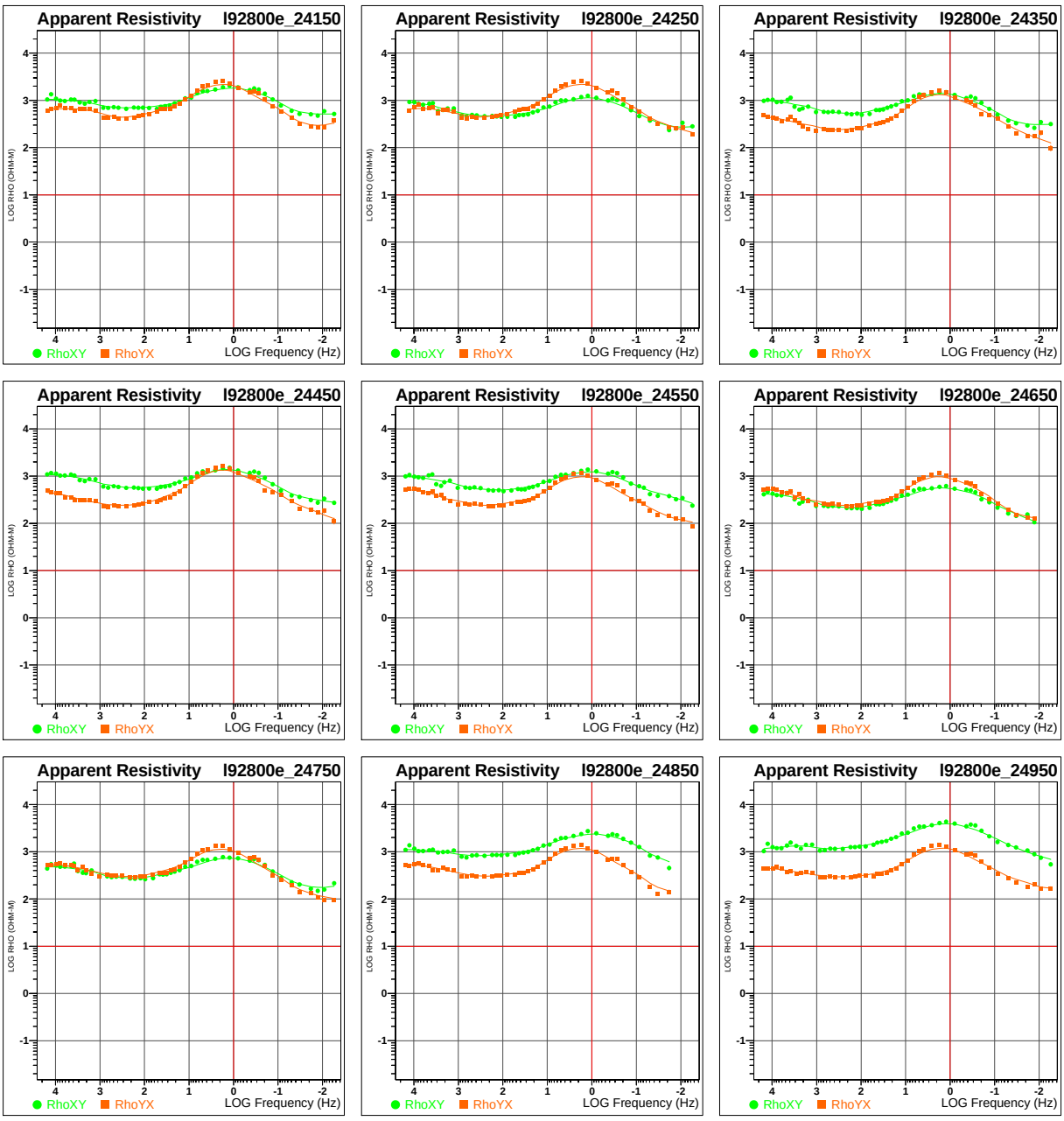

Line 92800E – Apparent Resistivity Sounding Curves vs Frequency (5 of 8).

MODE XY (GREEN) DENOTES ELECTRICAL (**EX**) FIELD AND ORTHOGONAL MAGNETIC (**HY**) FIELD (=EX/HY)
MODE YX (ORANGE) DENOTES ELECTRICAL (**EY**) FIELD AND ORTHOGONAL MAGNETIC (**HX**) FIELD (=EY/HX)

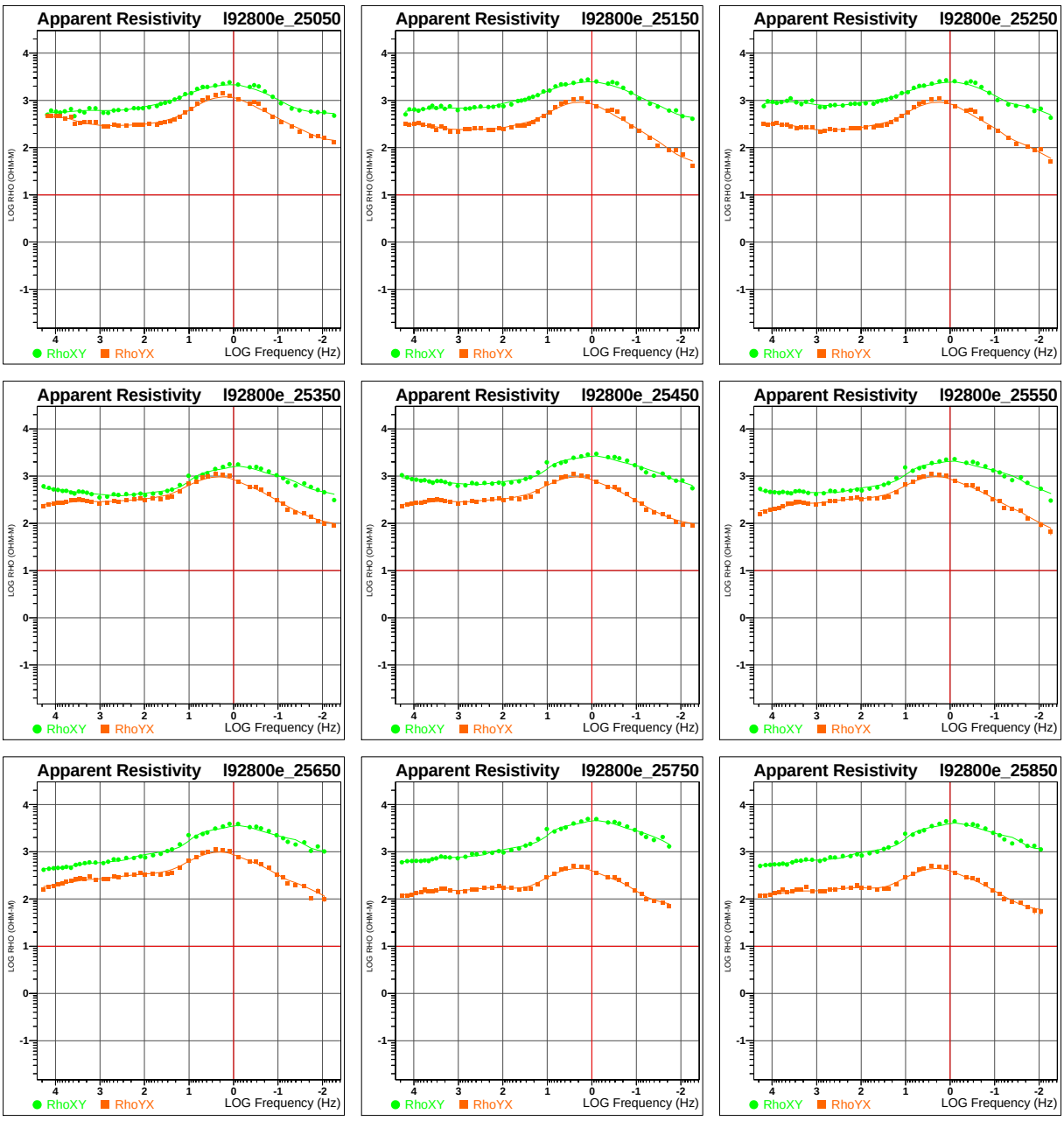

Line 92800E – Apparent Resistivity Sounding Curves vs Frequency (6 of 8).

MODE XY (GREEN) DENOTES ELECTRICAL (**EX**) FIELD AND ORTHOGONAL MAGNETIC (**HY**) FIELD (=EX/HY)
MODE YX (ORANGE) DENOTES ELECTRICAL (**EY**) FIELD AND ORTHOGONAL MAGNETIC (**HX**) FIELD (=EY/HX)

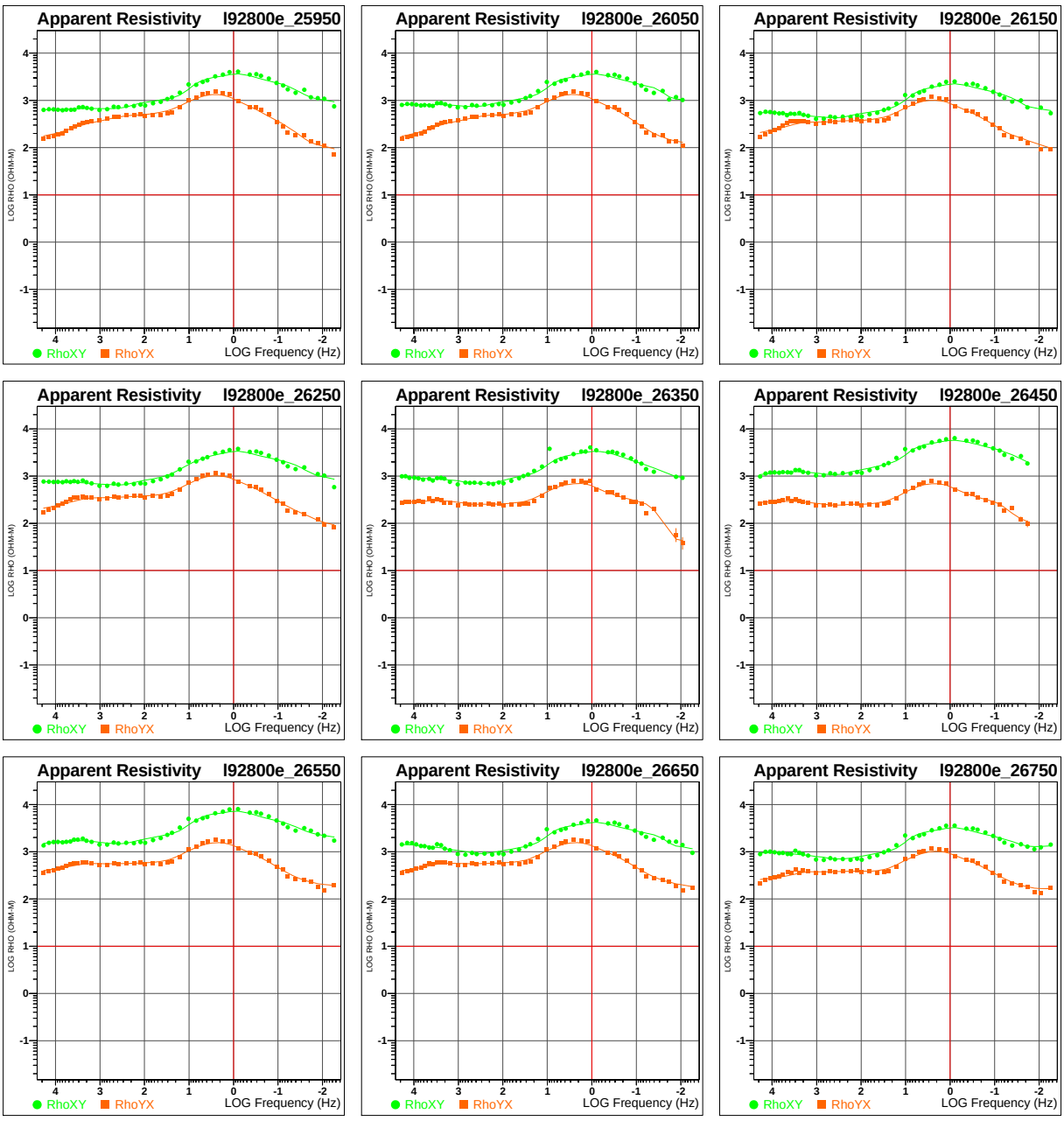

Line 92800E – Apparent Resistivity Sounding Curves vs Frequency (7 of 8).

MODE XY (GREEN) DENOTES ELECTRICAL (**EX**) FIELD AND ORTHOGONAL MAGNETIC (**HY**) FIELD (=EX/HY)
MODE YX (ORANGE) DENOTES ELECTRICAL (**EY**) FIELD AND ORTHOGONAL MAGNETIC (**HX**) FIELD (=EY/HX)

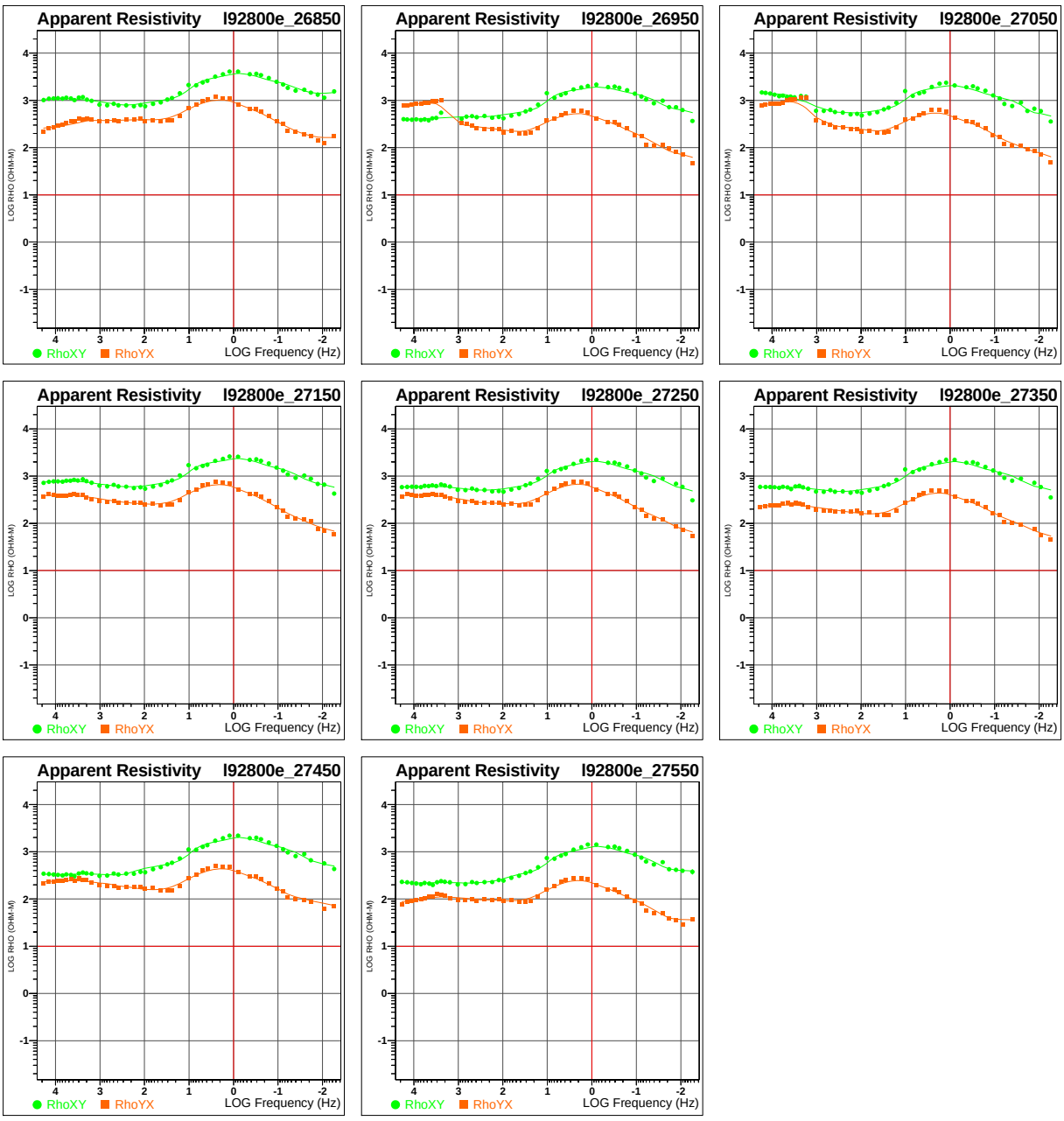

Line 92800E – Apparent Resistivity Sounding Curves vs Frequency (8 of 8).

MODE XY (GREEN) DENOTES ELECTRICAL (**EX**) FIELD AND ORTHOGONAL MAGNETIC (**HY**) FIELD (=EX/HY)
MODE YX (ORANGE) DENOTES ELECTRICAL (**EY**) FIELD AND ORTHOGONAL MAGNETIC (**HX**) FIELD (=EY/HX)

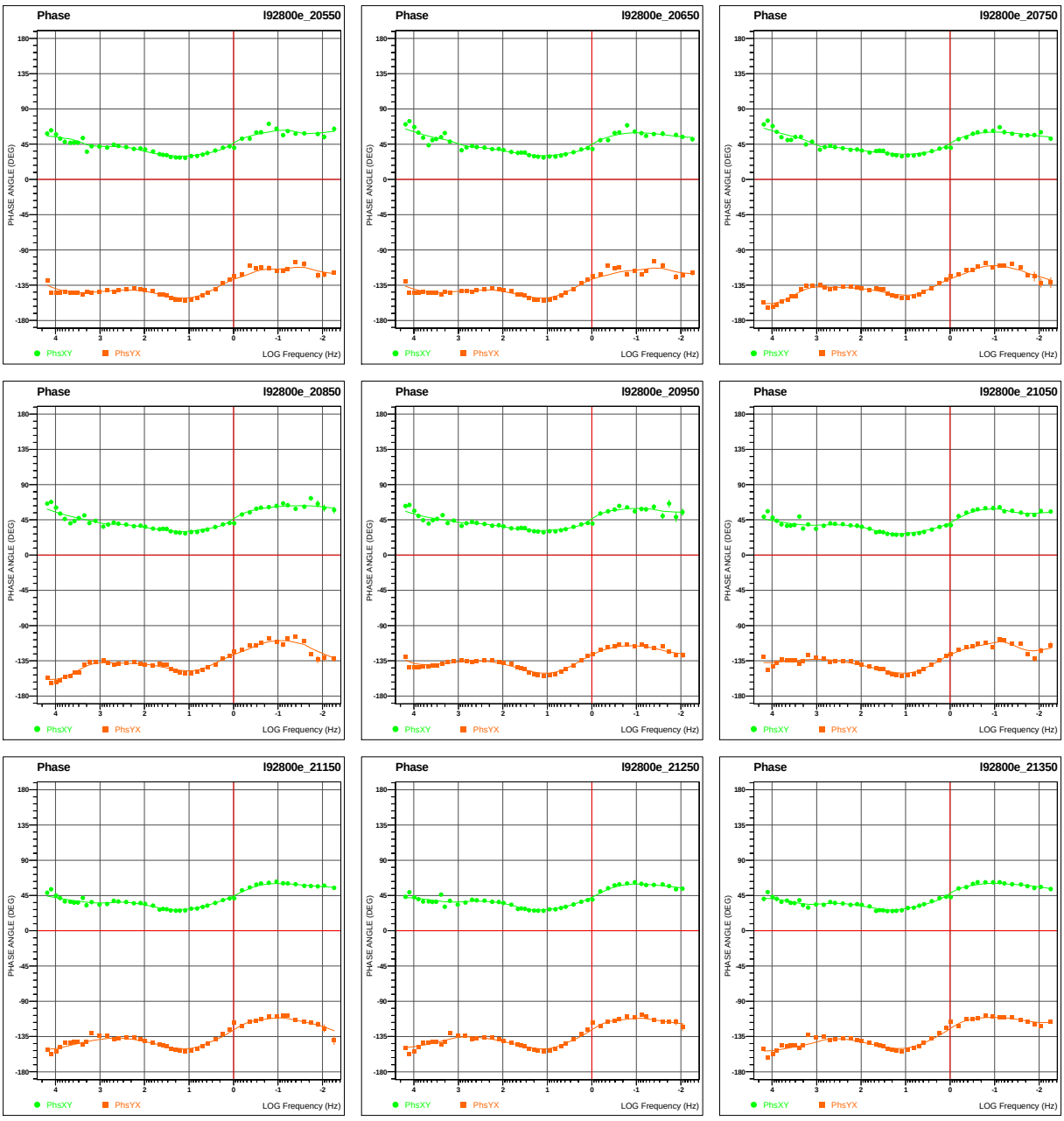

Line 92800E – Phase Sounding Curves vs Frequency (1 of 8).

MODE XY (GREEN) DENOTES ELECTRICAL (**EX**) FIELD AND ORTHOGONAL MAGNETIC (**HY**) FIELD (=EX/HY)
MODE YX (ORANGE) DENOTES ELECTRICAL (**EY**) FIELD AND ORTHOGONAL MAGNETIC (**HX**) FIELD (=EY/HX)

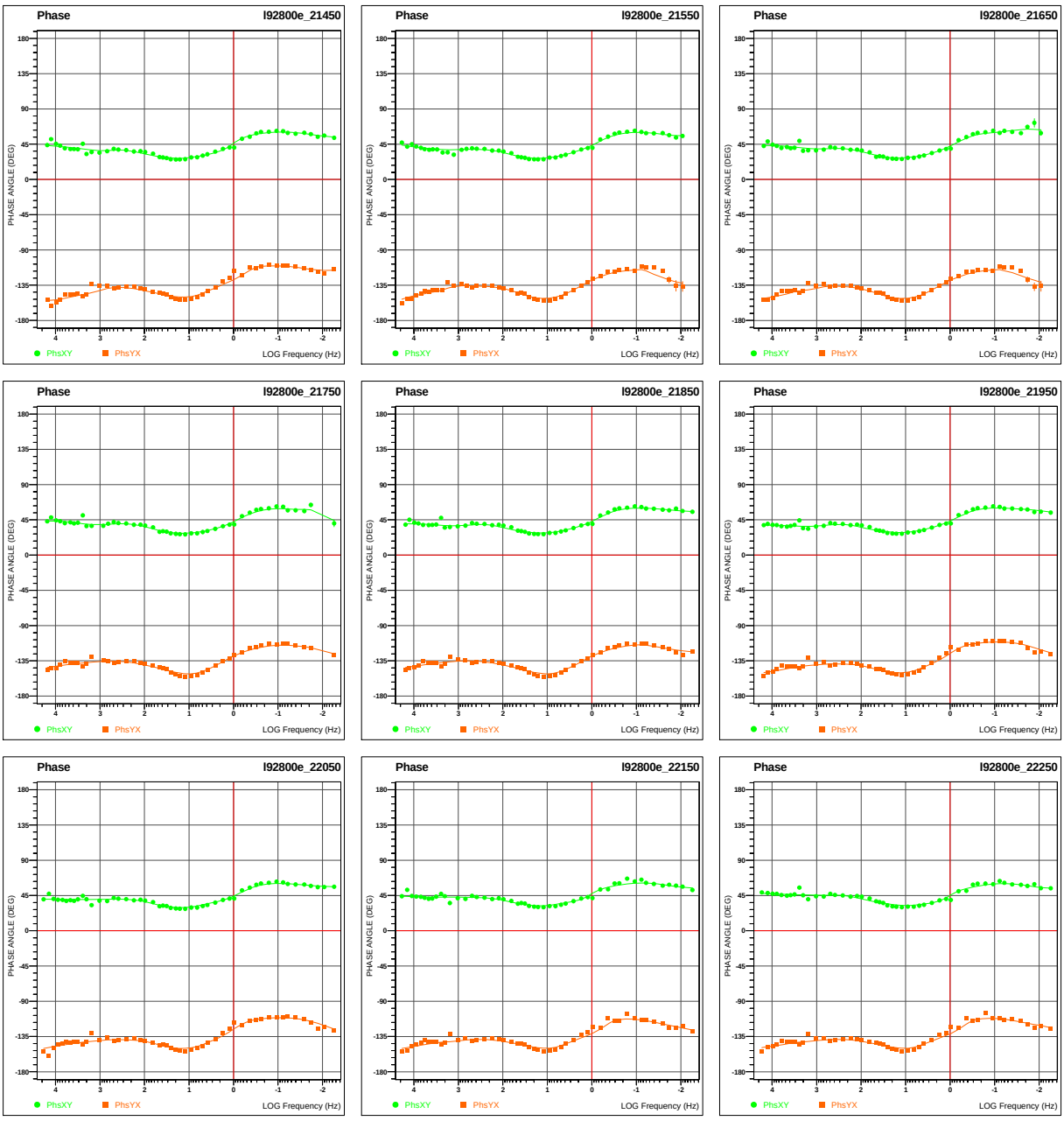

Line 92800E – Phase Sounding Curves vs Frequency (2 of 8).

MODE XY (GREEN) DENOTES ELECTRICAL (**EX**) FIELD AND ORTHOGONAL MAGNETIC (**HY**) FIELD (=EX/HY)
MODE YX (ORANGE) DENOTES ELECTRICAL (**EY**) FIELD AND ORTHOGONAL MAGNETIC (**HX**) FIELD (=EY/HX)

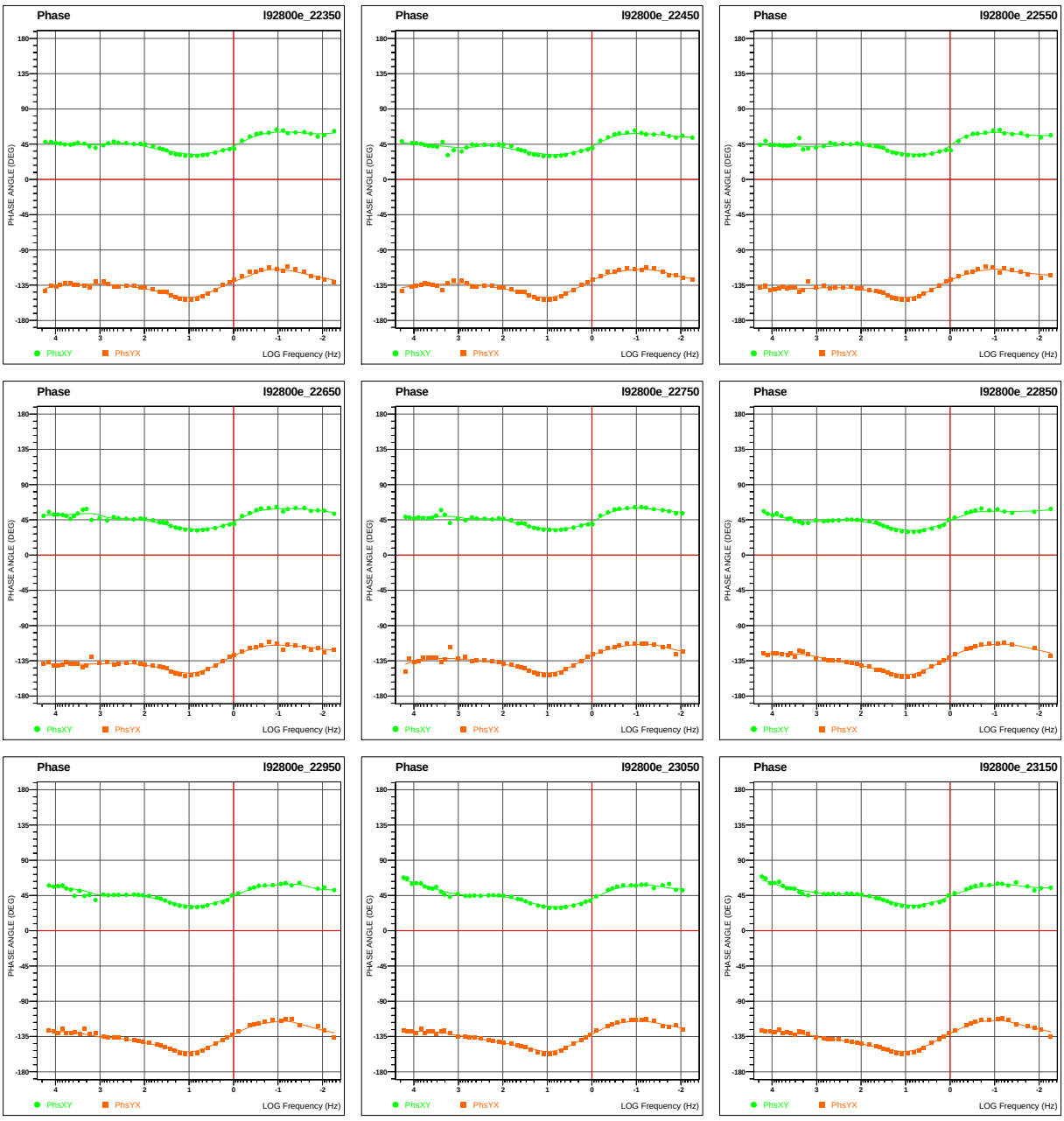

Line 92800E – Phase Sounding Curves vs Frequency (3 of 8).

MODE XY (GREEN) DENOTES ELECTRICAL (**EX**) FIELD AND ORTHOGONAL MAGNETIC (**HY**) FIELD (=EX/HY)
MODE YX (ORANGE) DENOTES ELECTRICAL (**EY**) FIELD AND ORTHOGONAL MAGNETIC (**HX**) FIELD (=EY/HX)

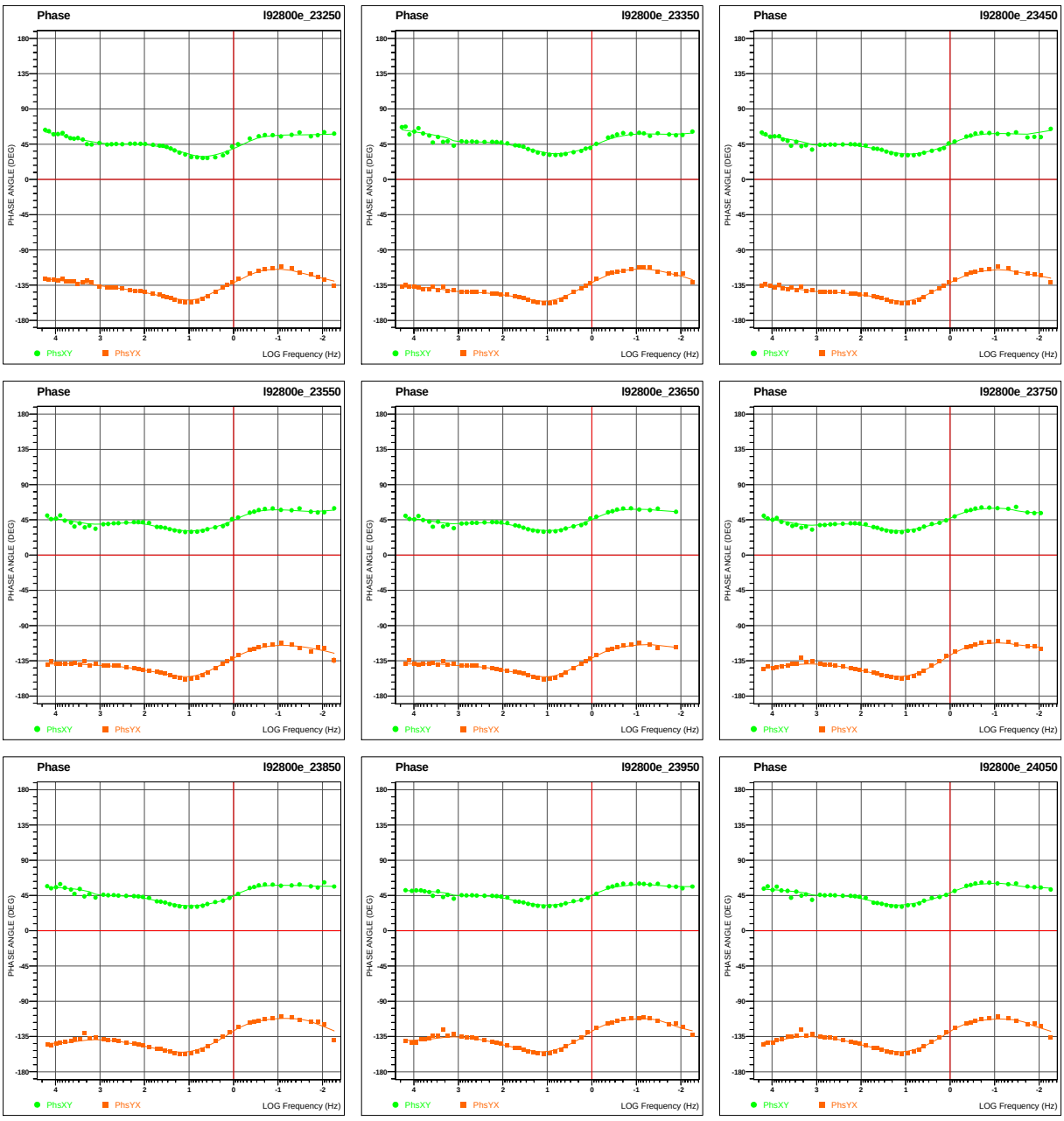

Line 92800E – Phase Sounding Curves vs Frequency (4 of 8).

MODE XY (GREEN) DENOTES ELECTRICAL (**EX**) FIELD AND ORTHOGONAL MAGNETIC (**HY**) FIELD (=EX/HY)
MODE YX (ORANGE) DENOTES ELECTRICAL (**EY**) FIELD AND ORTHOGONAL MAGNETIC (**HX**) FIELD (=EY/HX)

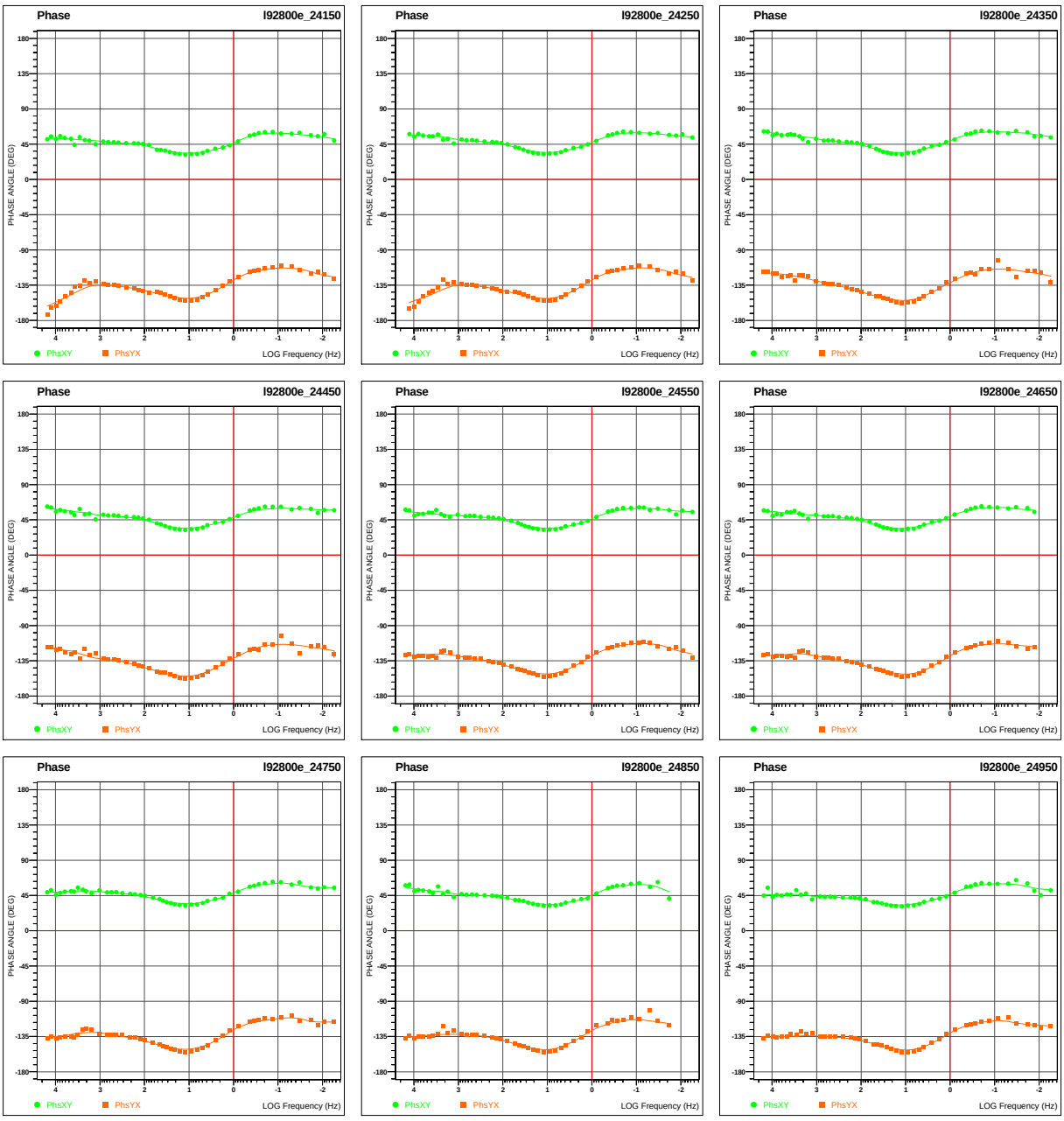

Line 92800E – Phase Sounding Curves vs Frequency (5 of 8).

MODE XY (GREEN) DENOTES ELECTRICAL (**EX**) FIELD AND ORTHOGONAL MAGNETIC (**HY**) FIELD (=EX/HY)
MODE YX (ORANGE) DENOTES ELECTRICAL (**EY**) FIELD AND ORTHOGONAL MAGNETIC (**HX**) FIELD (=EY/HX)

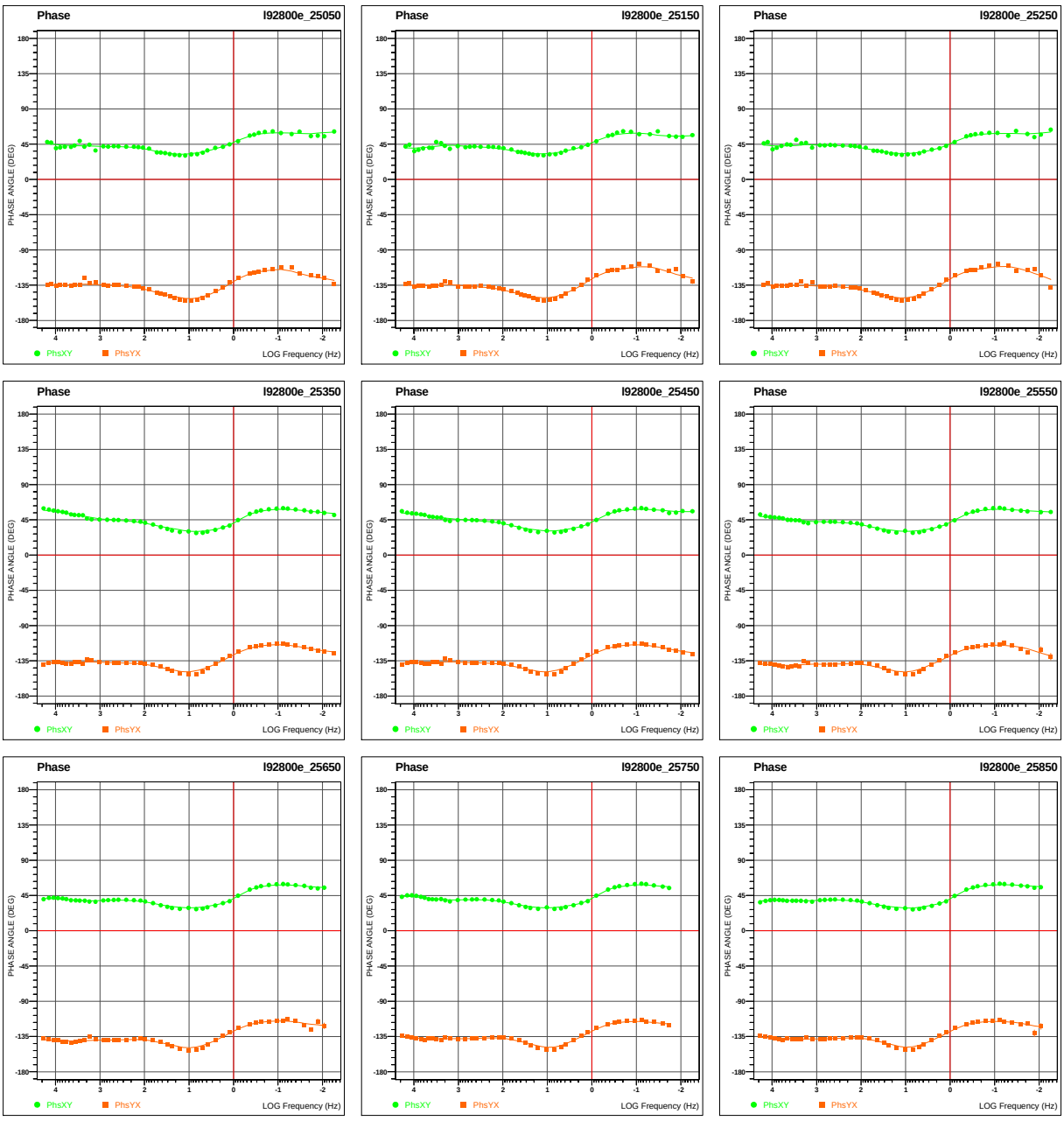

Line 92800E – Phase Sounding Curves vs Frequency (6 of 8).

MODE XY (GREEN) DENOTES ELECTRICAL (**EX**) FIELD AND ORTHOGONAL MAGNETIC (**HY**) FIELD (=EX/HY)
MODE YX (ORANGE) DENOTES ELECTRICAL (**EY**) FIELD AND ORTHOGONAL MAGNETIC (**HX**) FIELD (=EY/HX)

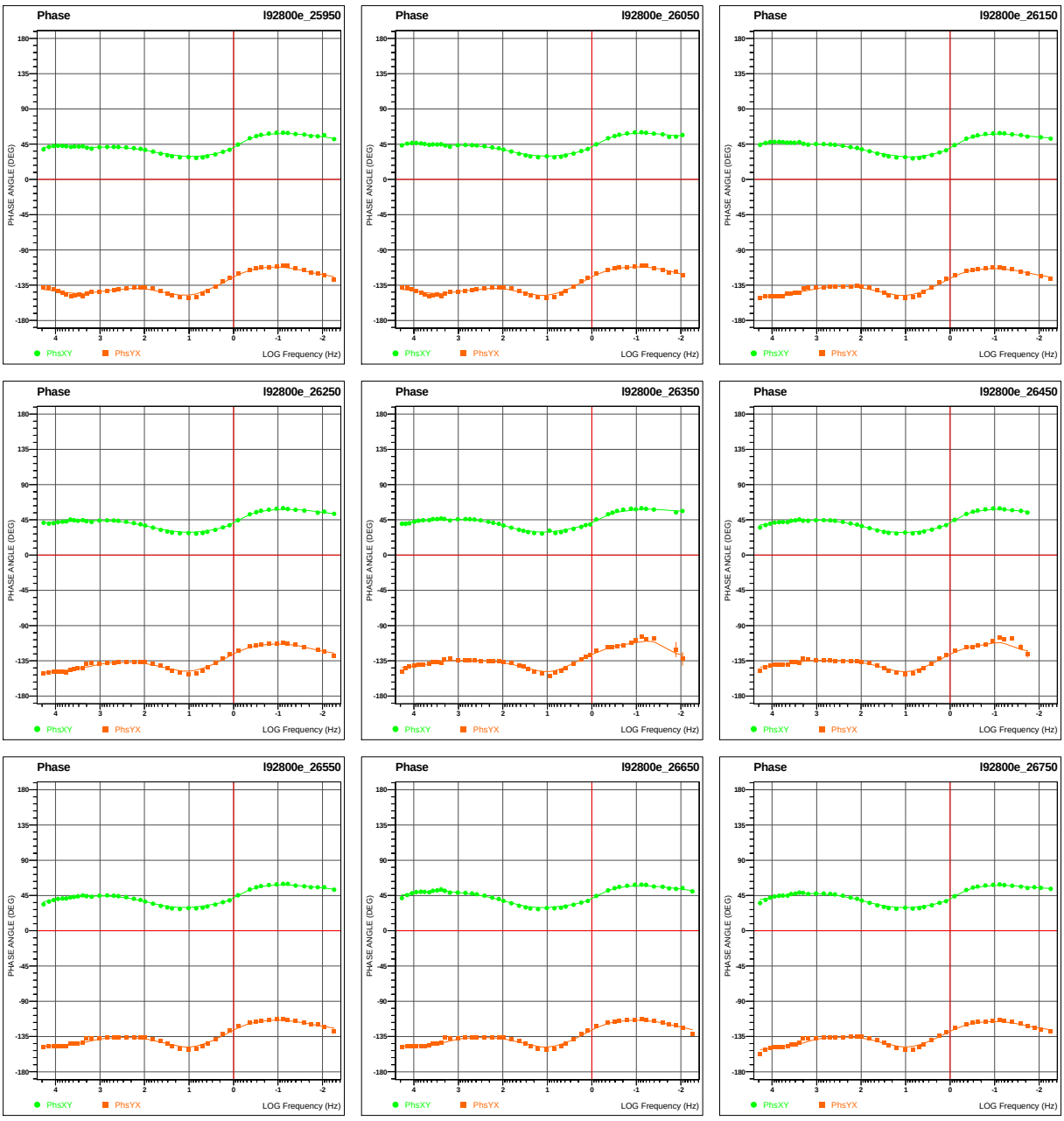

Line 92800E – Phase Sounding Curves vs Frequency (7 of 8).

MODE XY (GREEN) DENOTES ELECTRICAL (**EX**) FIELD AND ORTHOGONAL MAGNETIC (**HY**) FIELD (=EX/HY)
MODE YX (ORANGE) DENOTES ELECTRICAL (**EY**) FIELD AND ORTHOGONAL MAGNETIC (**HX**) FIELD (=EY/HX)

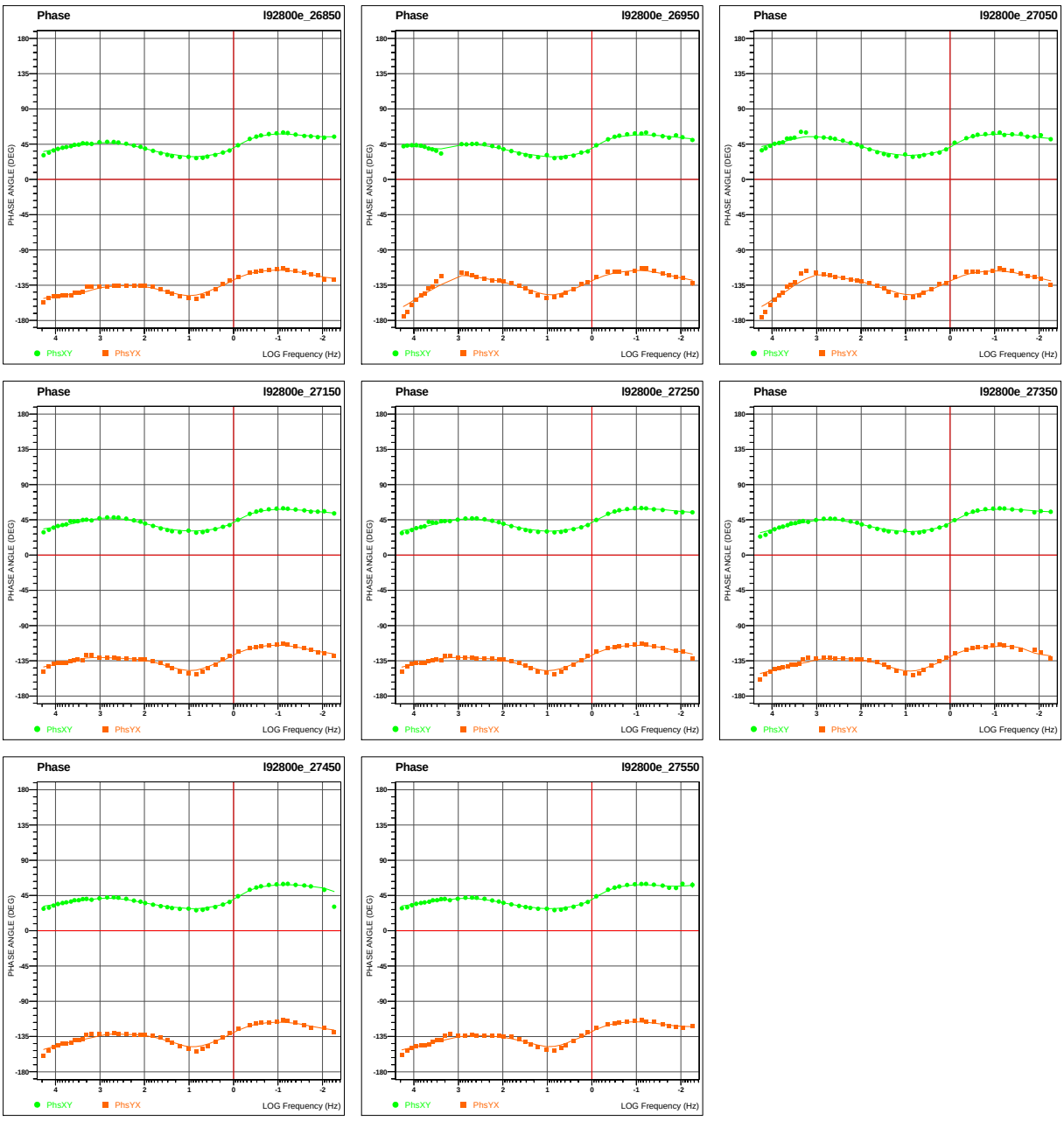

Line 92800E – Phase Sounding Curves vs Frequency (8 of 8).

MODE XY (GREEN) DENOTES ELECTRICAL (**EX**) FIELD AND ORTHOGONAL MAGNETIC (**HY**) FIELD (=EX/HY)
MODE YX (ORANGE) DENOTES ELECTRICAL (**EY**) FIELD AND ORTHOGONAL MAGNETIC (**HX**) FIELD (=EY/HX)

D.2 LINE 93200E

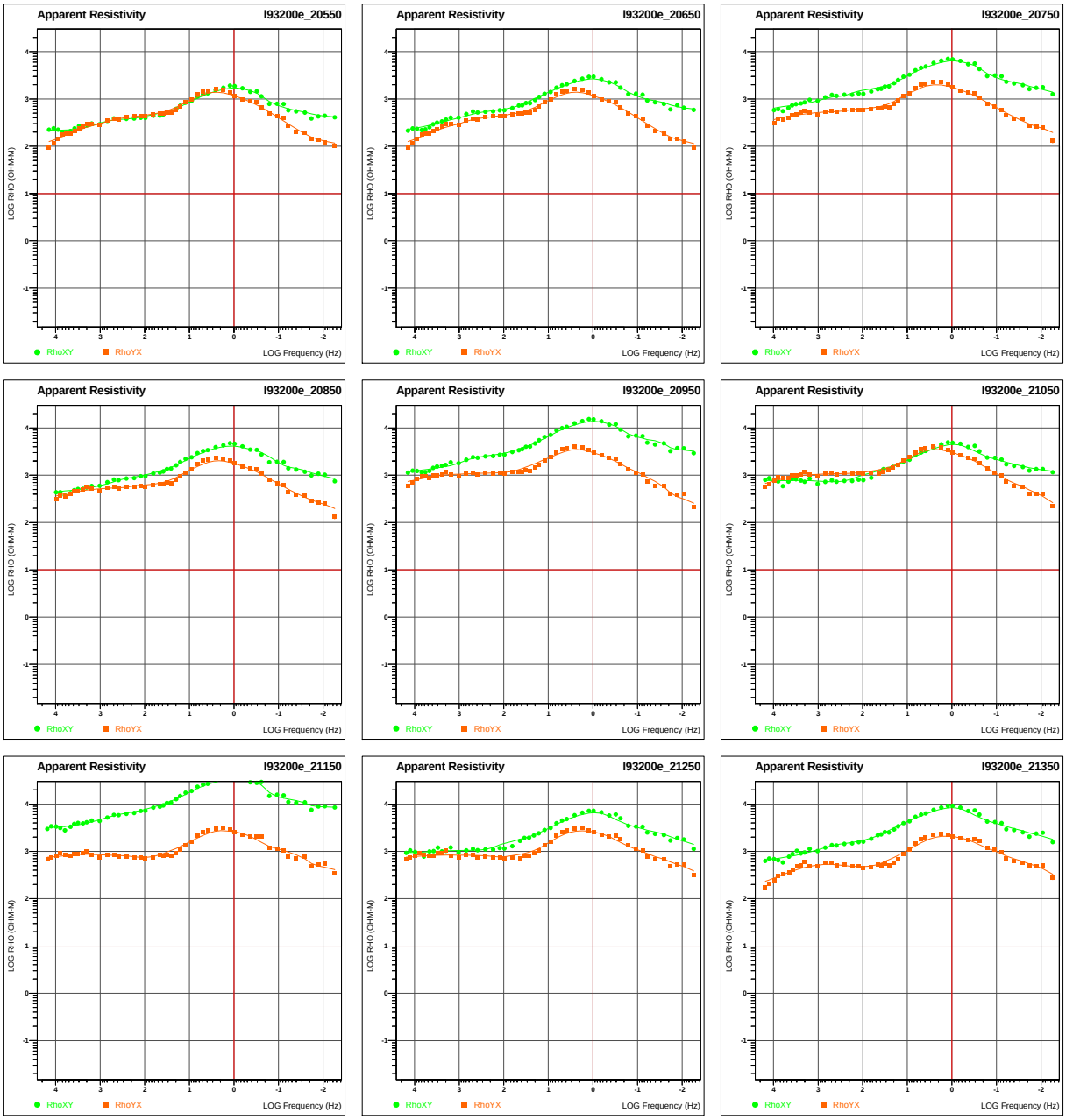

Line 93200E – Apparent Resistivity Sounding Curves vs Frequency (1 of 8).

MODE XY (GREEN) DENOTES ELECTRICAL (**EX**) FIELD AND ORTHOGONAL MAGNETIC (**HY**) FIELD (=EX/HY)
MODE YX (ORANGE) DENOTES ELECTRICAL (**EY**) FIELD AND ORTHOGONAL MAGNETIC (**HX**) FIELD (=EY/HX)

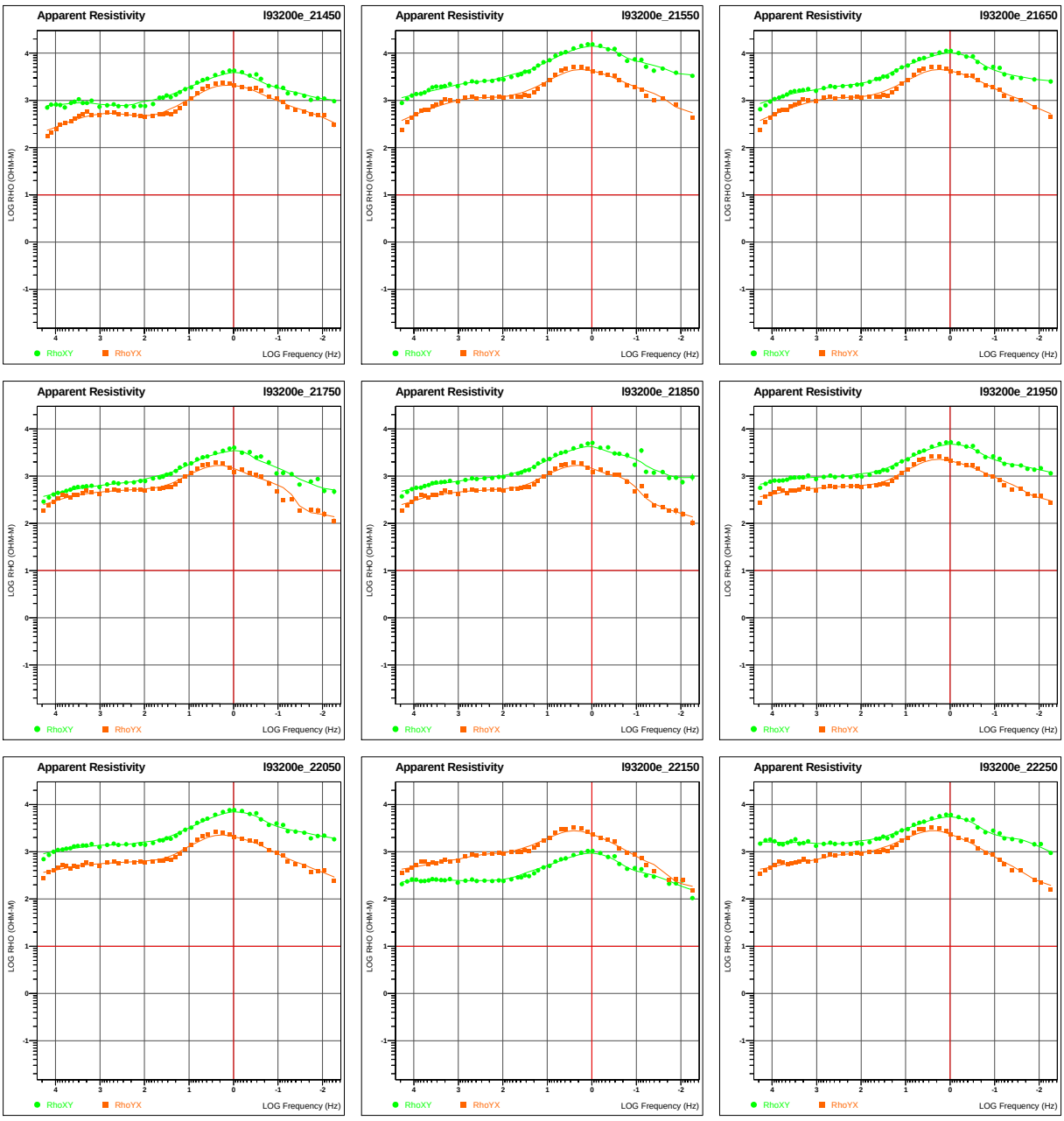

Line 93200E – Apparent Resistivity Sounding Curves vs Frequency (2 of 8).

MODE XY (GREEN) DENOTES ELECTRICAL (**EX**) FIELD AND ORTHOGONAL MAGNETIC (**HY**) FIELD (=EX/HY)
MODE YX (ORANGE) DENOTES ELECTRICAL (**EY**) FIELD AND ORTHOGONAL MAGNETIC (**HX**) FIELD (=EY/HX)

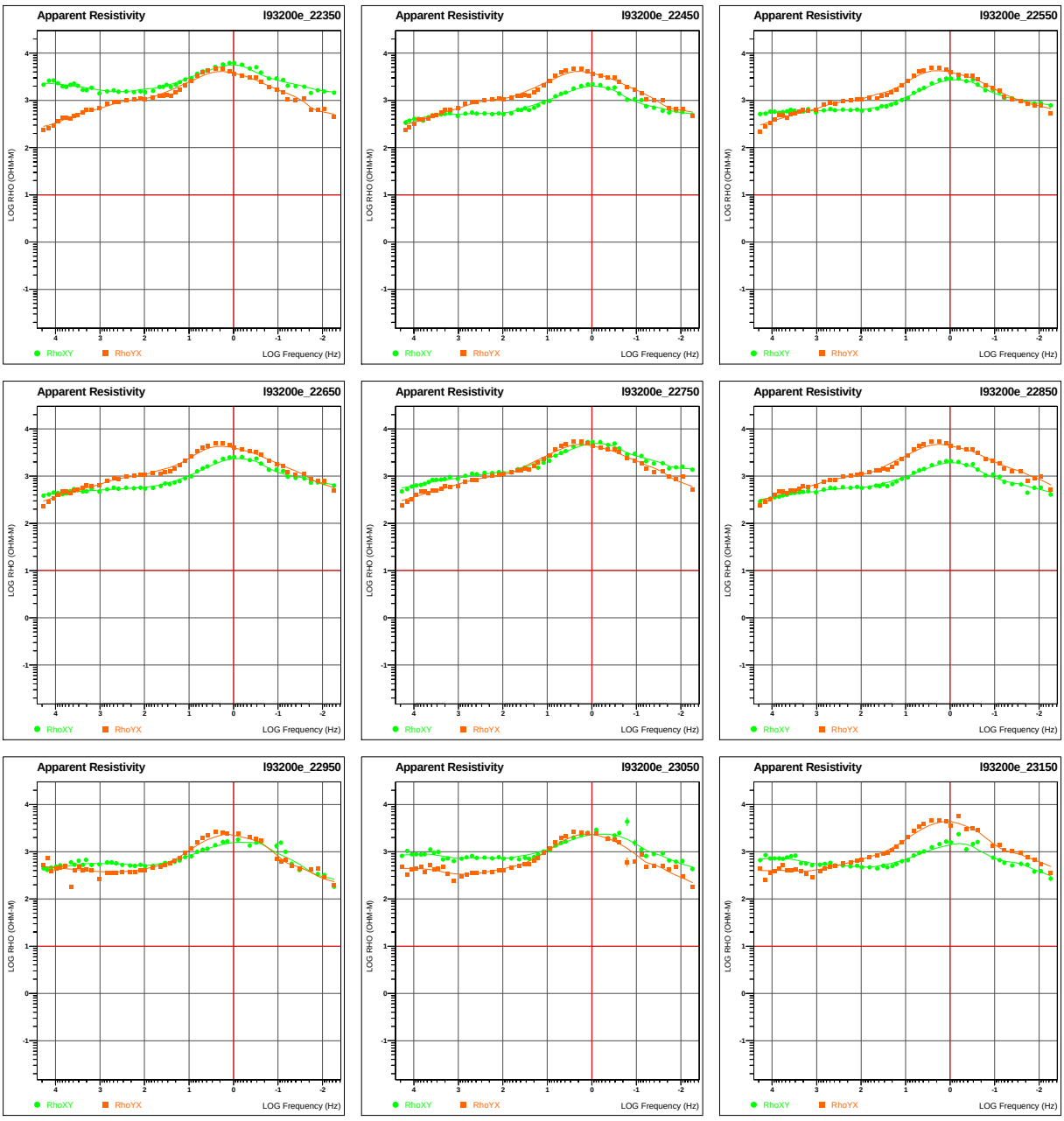

Line 93200E – Apparent Resistivity Sounding Curves vs Frequency (3 of 8).

MODE XY (GREEN) DENOTES ELECTRICAL (**EX**) FIELD AND ORTHOGONAL MAGNETIC (**HY**) FIELD (=EX/HY)
MODE YX (ORANGE) DENOTES ELECTRICAL (**EY**) FIELD AND ORTHOGONAL MAGNETIC (**HX**) FIELD (=EY/HX)

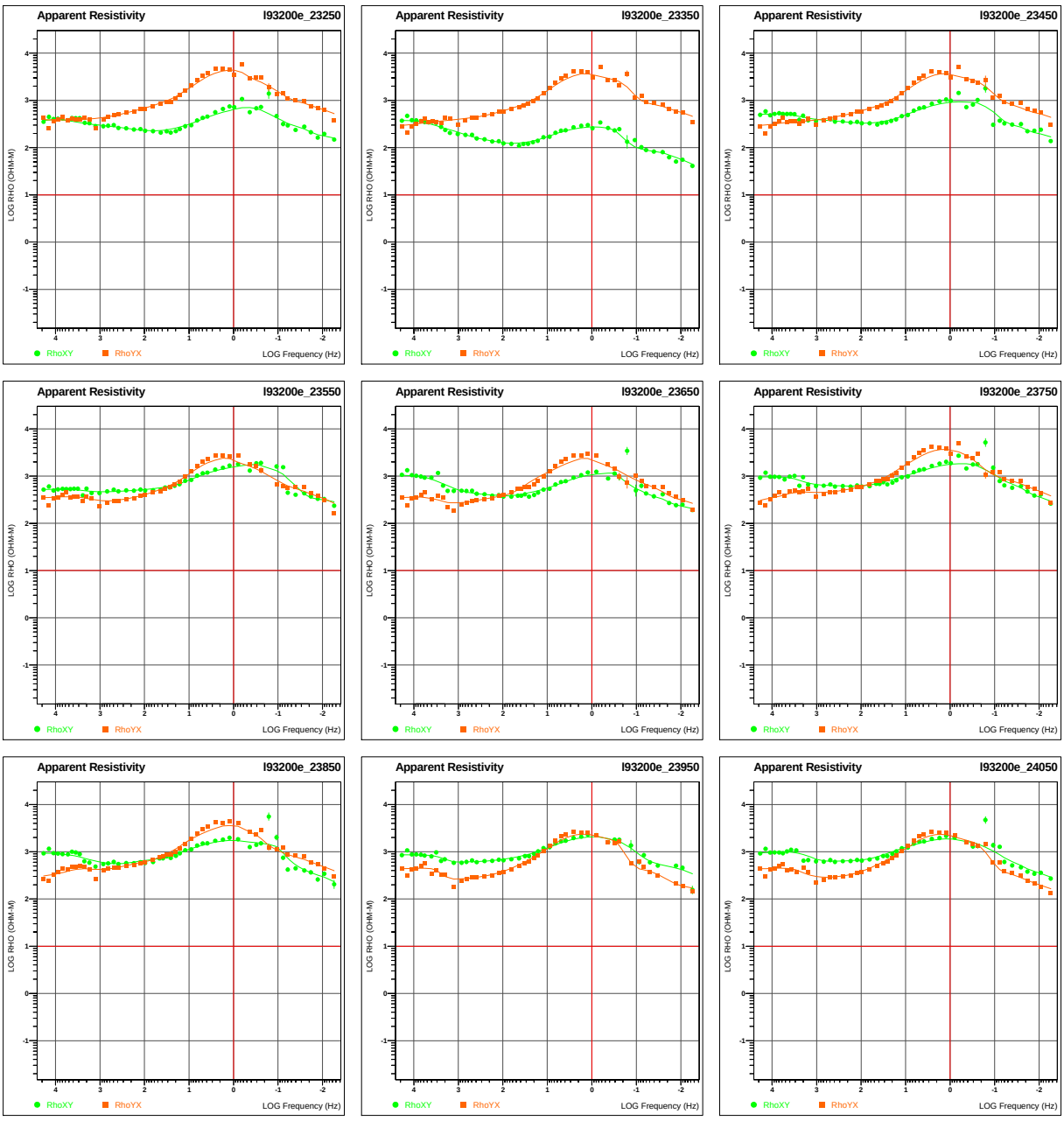

Line 93200E – Apparent Resistivity Sounding Curves vs Frequency (4 of 8).

MODE XY (GREEN) DENOTES ELECTRICAL (**EX**) FIELD AND ORTHOGONAL MAGNETIC (**HY**) FIELD (=EX/HY)
MODE YX (ORANGE) DENOTES ELECTRICAL (**EY**) FIELD AND ORTHOGONAL MAGNETIC (**HX**) FIELD (=EY/HX)

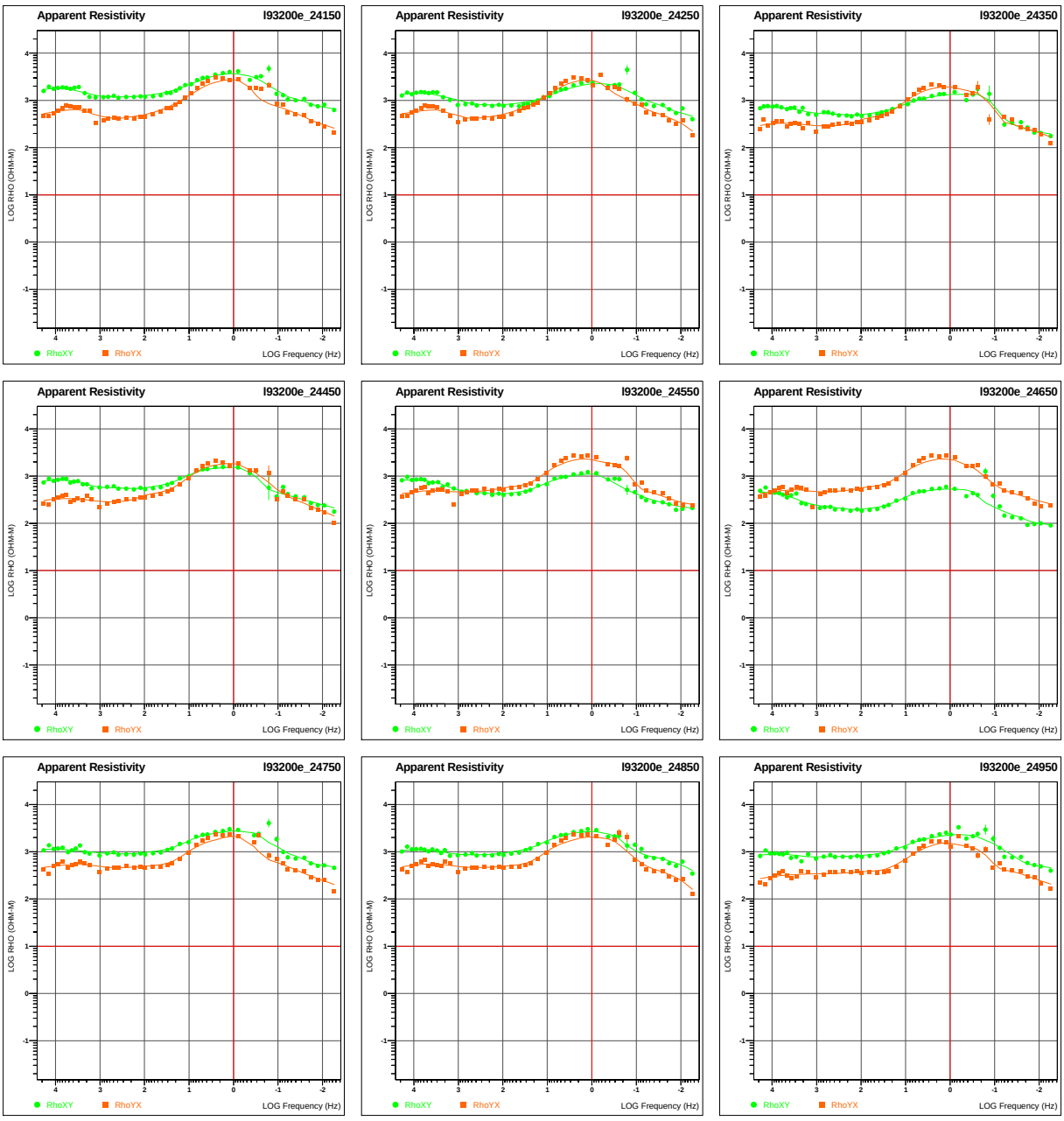

Line 93200E – Apparent Resistivity Sounding Curves vs Frequency (5 of 8).

MODE XY (GREEN) DENOTES ELECTRICAL (**EX**) FIELD AND ORTHOGONAL MAGNETIC (**HY**) FIELD (=EX/HY)
MODE YX (ORANGE) DENOTES ELECTRICAL (**EY**) FIELD AND ORTHOGONAL MAGNETIC (**HX**) FIELD (=EY/HX)

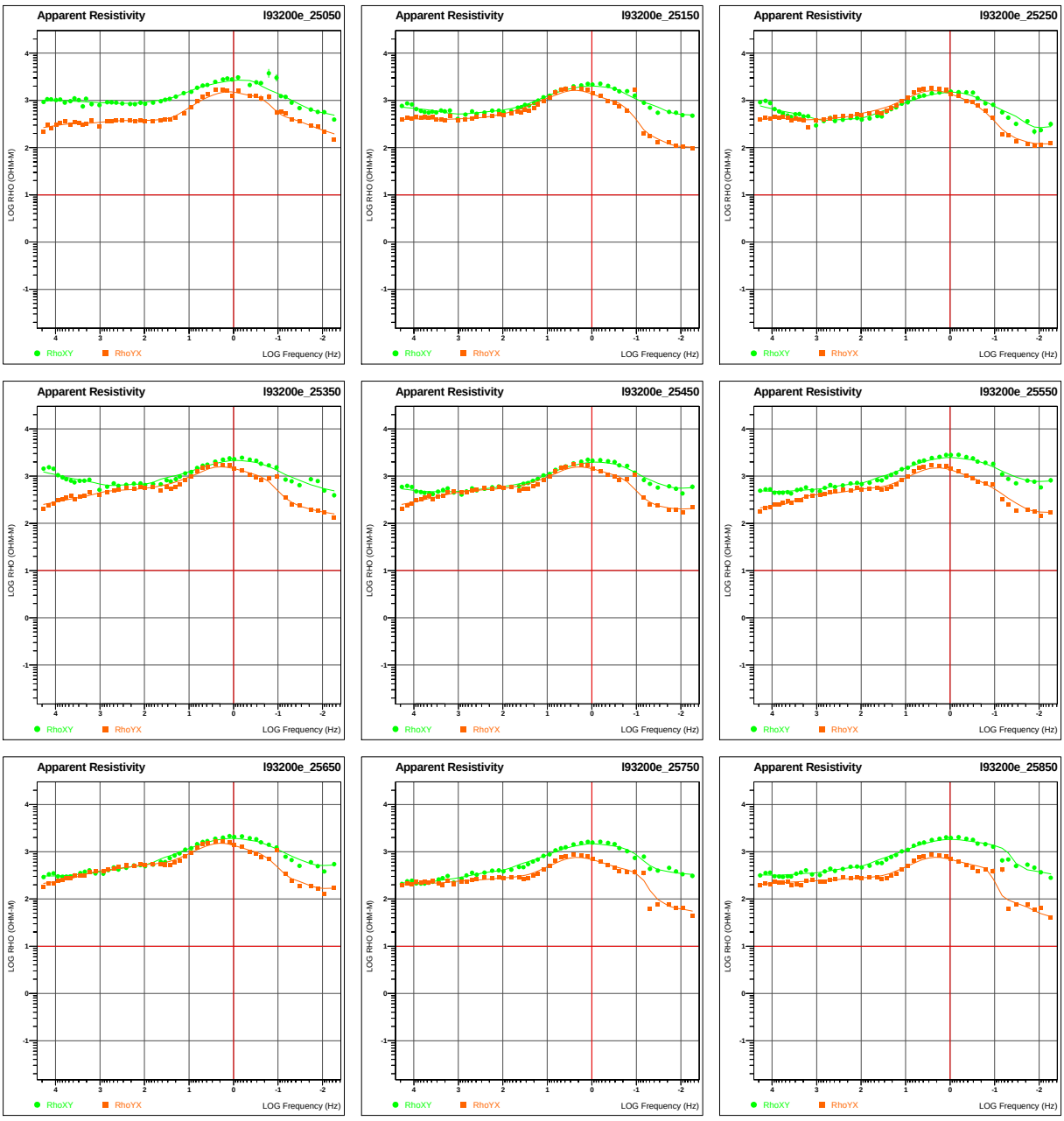

Line 93200E – Apparent Resistivity Sounding Curves vs Frequency (6 of 8).

MODE XY (GREEN) DENOTES ELECTRICAL (**EX**) FIELD AND ORTHOGONAL MAGNETIC (**HY**) FIELD (=EX/HY)
MODE YX (ORANGE) DENOTES ELECTRICAL (**EY**) FIELD AND ORTHOGONAL MAGNETIC (**HX**) FIELD (=EY/HX)

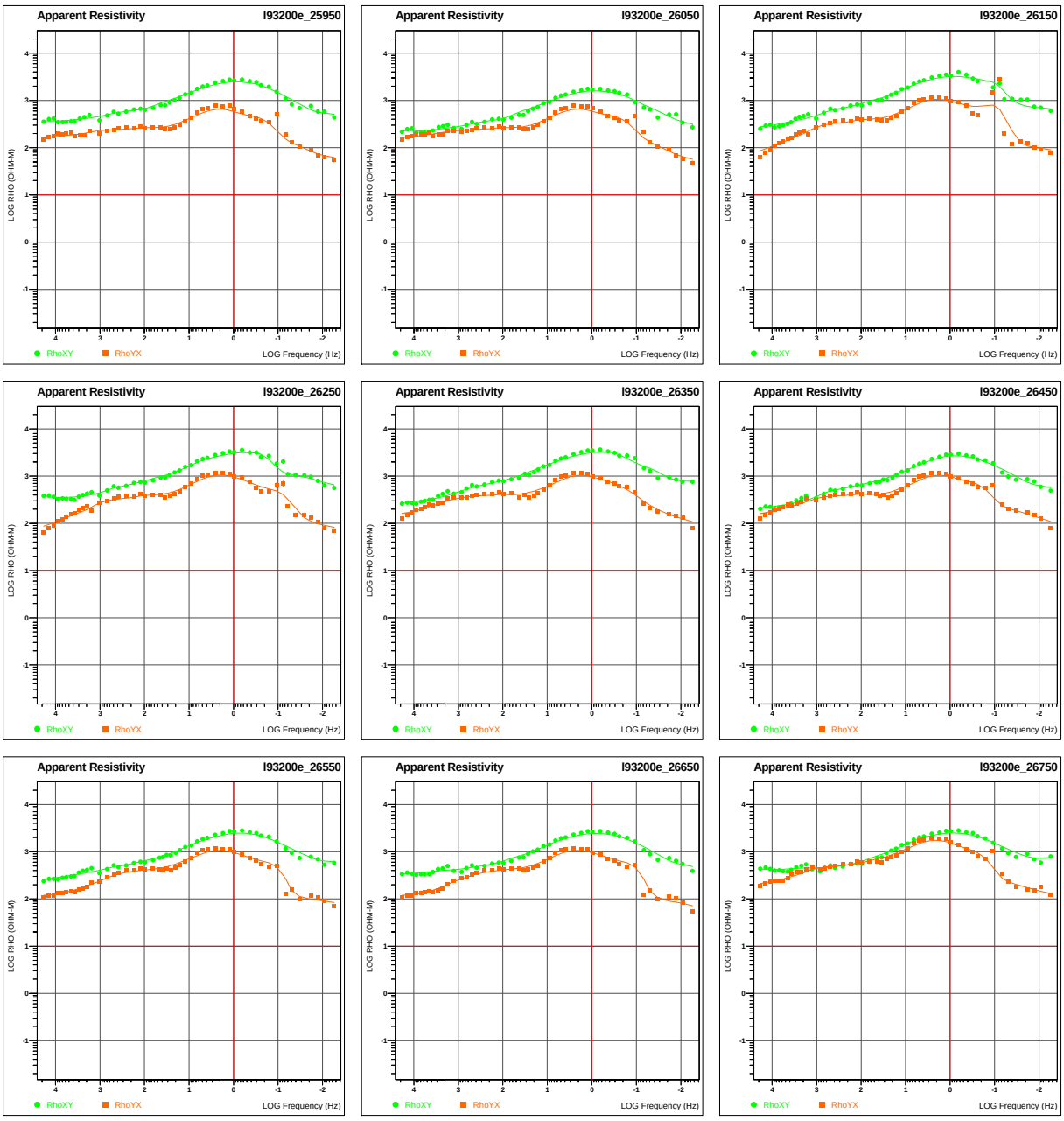

Line 93200E – Apparent Resistivity Sounding Curves vs Frequency (7 of 8).

MODE XY (GREEN) DENOTES ELECTRICAL (**EX**) FIELD AND ORTHOGONAL MAGNETIC (**HY**) FIELD (=EX/HY)
MODE YX (ORANGE) DENOTES ELECTRICAL (**EY**) FIELD AND ORTHOGONAL MAGNETIC (**HX**) FIELD (=EY/HX)

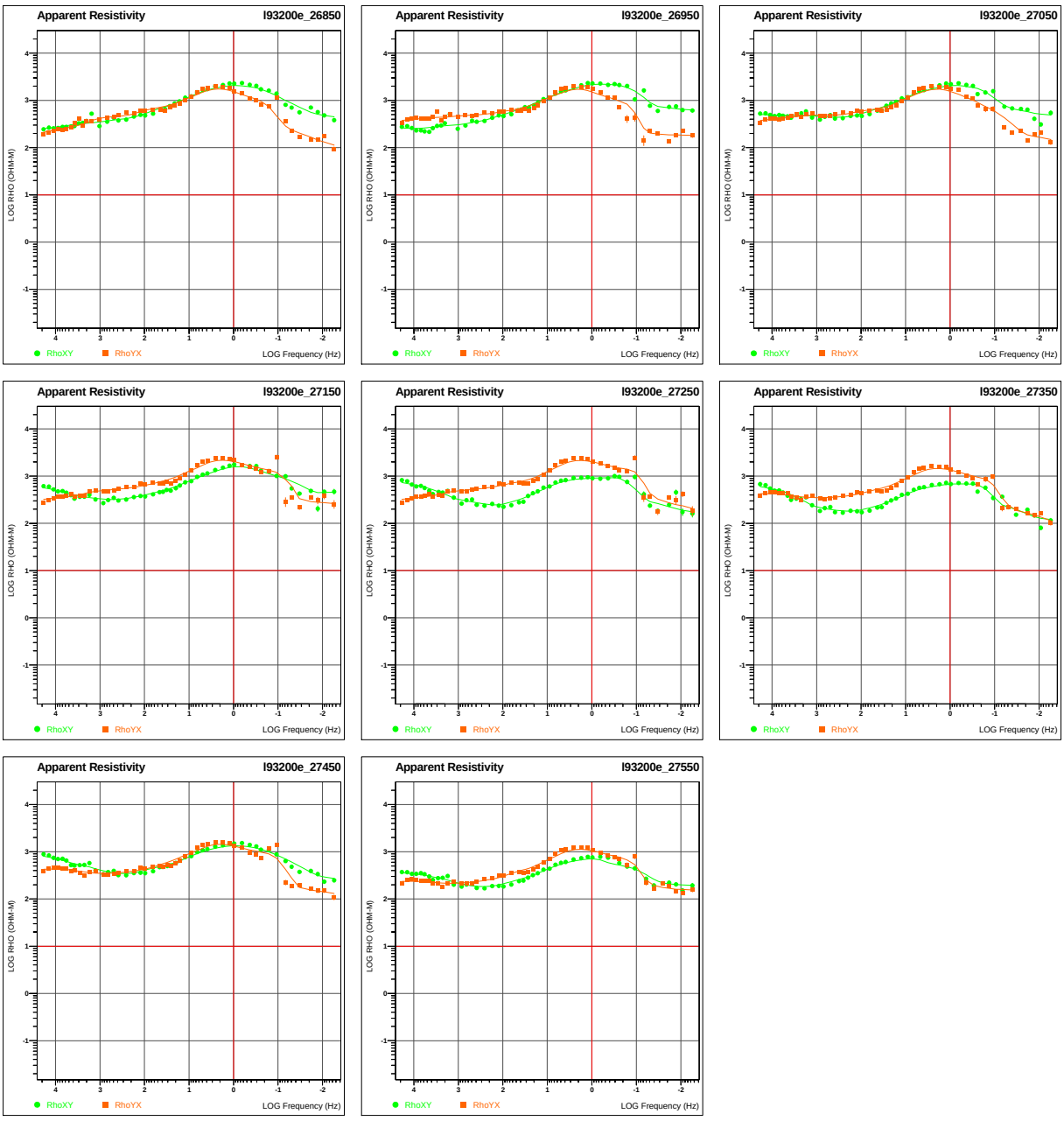

Line 93200E – Apparent Resistivity Sounding Curves vs Frequency (8 of 8).

MODE XY (GREEN) DENOTES ELECTRICAL (**EX**) FIELD AND ORTHOGONAL MAGNETIC (**HY**) FIELD (=EX/HY)
MODE YX (ORANGE) DENOTES ELECTRICAL (**EY**) FIELD AND ORTHOGONAL MAGNETIC (**HX**) FIELD (=EY/HX)

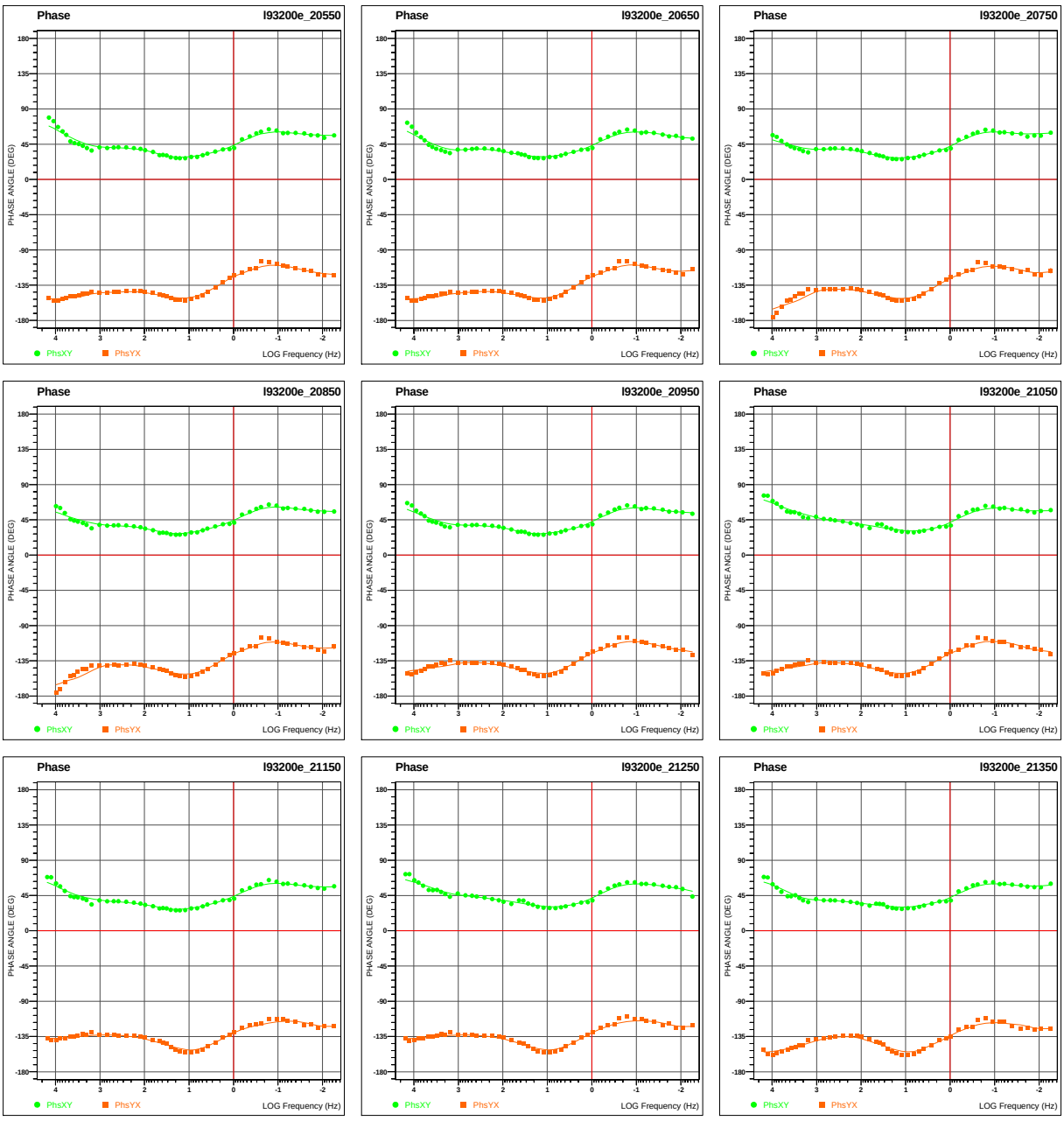

Line 93200E – Phase Sounding Curves vs Frequency (1 of 8).

MODE XY (GREEN) DENOTES ELECTRICAL (**EX**) FIELD AND ORTHOGONAL MAGNETIC (**HY**) FIELD (=EX/HY)
MODE YX (ORANGE) DENOTES ELECTRICAL (**EY**) FIELD AND ORTHOGONAL MAGNETIC (**HX**) FIELD (=EY/HX)

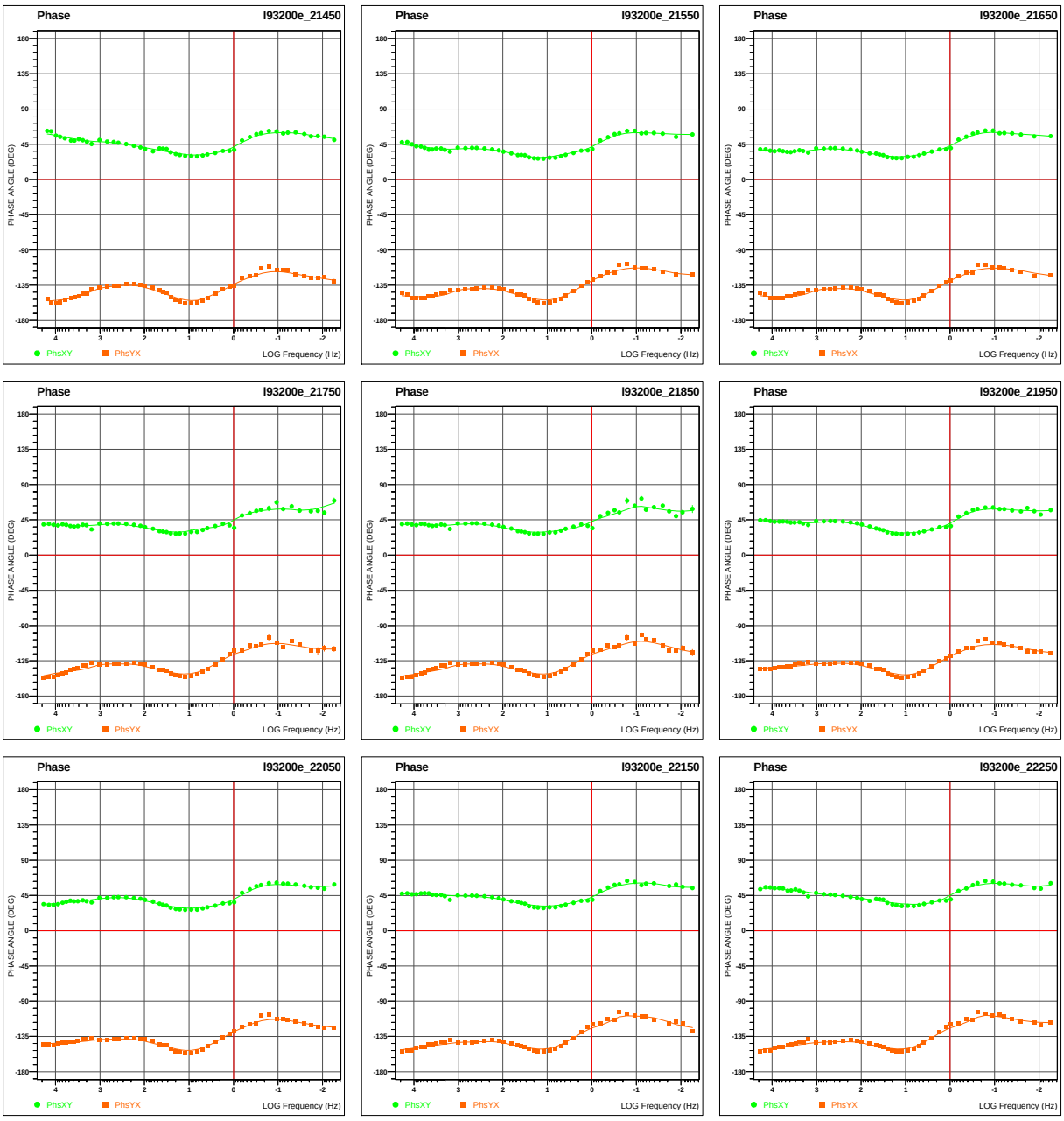

Line 93200E – Phase Sounding Curves vs Frequency (2 of 8).

MODE XY (GREEN) DENOTES ELECTRICAL (**EX**) FIELD AND ORTHOGONAL MAGNETIC (**HY**) FIELD (=EX/HY)
MODE YX (ORANGE) DENOTES ELECTRICAL (**EY**) FIELD AND ORTHOGONAL MAGNETIC (**HX**) FIELD (=EY/HX)

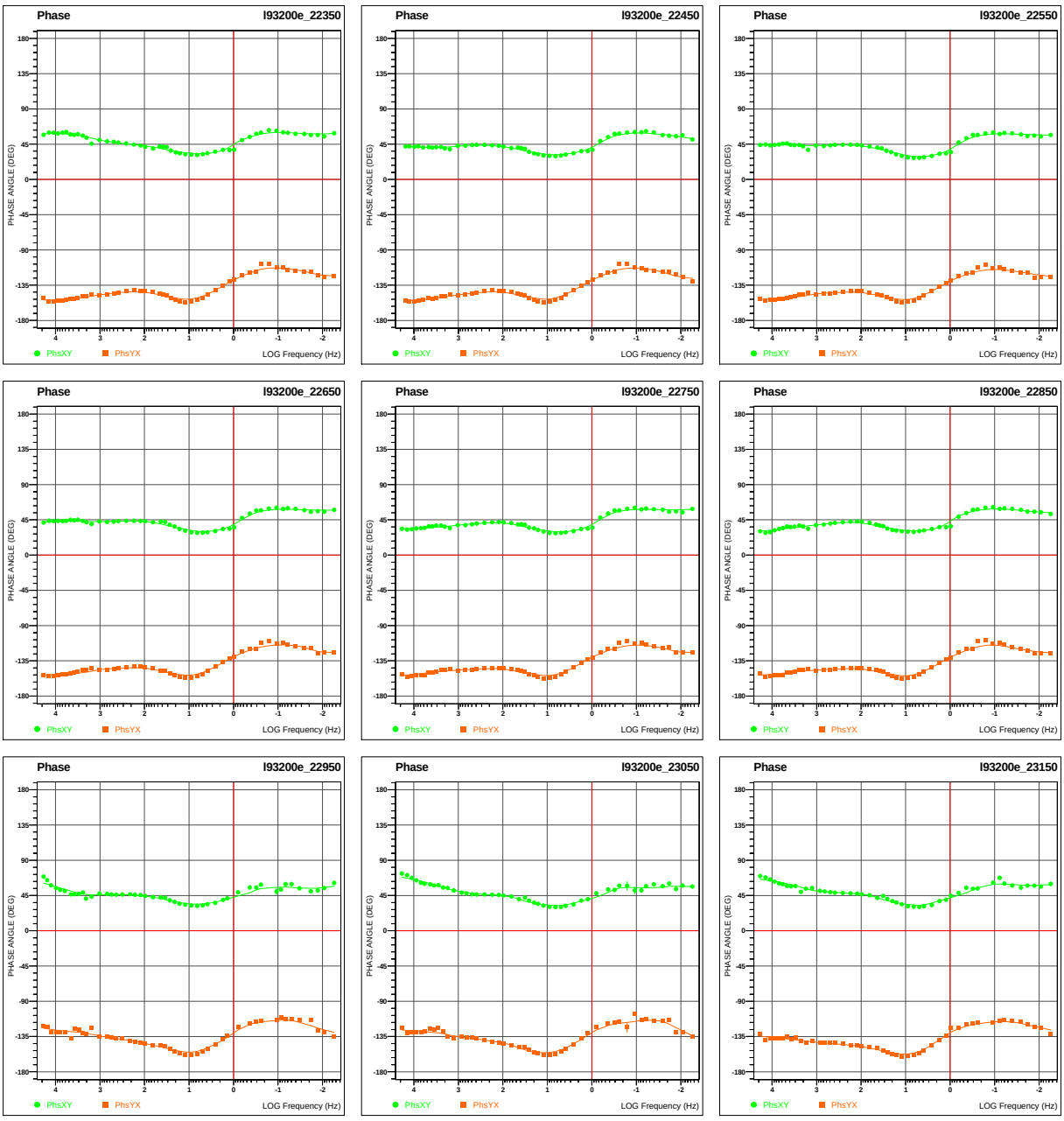

Line 93200E – Phase Sounding Curves vs Frequency (3 of 8).

MODE XY (GREEN) DENOTES ELECTRICAL (**EX**) FIELD AND ORTHOGONAL MAGNETIC (**HY**) FIELD (=EX/HY)
MODE YX (ORANGE) DENOTES ELECTRICAL (**EY**) FIELD AND ORTHOGONAL MAGNETIC (**HX**) FIELD (=EY/HX)

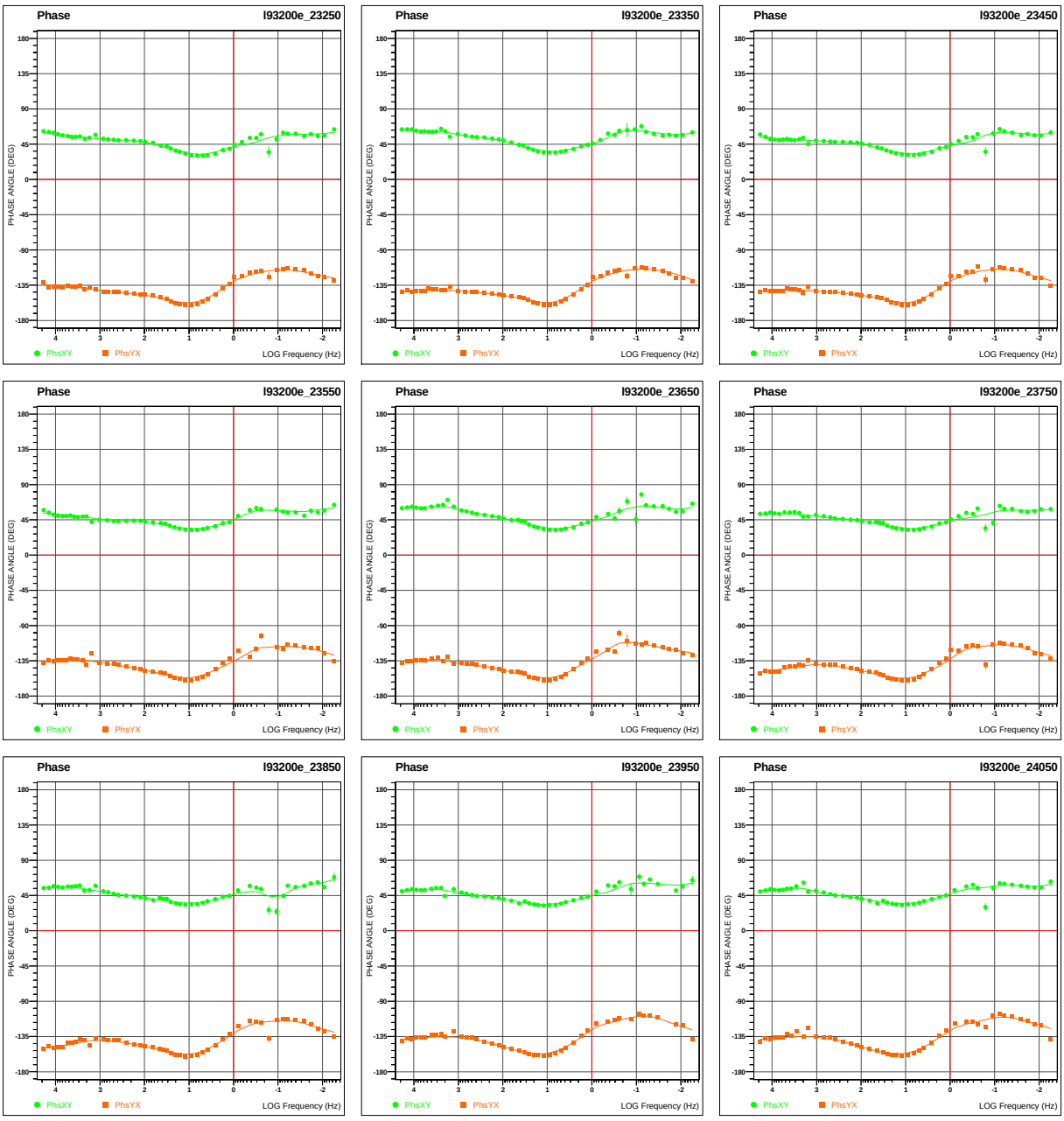

Line 93200E – Phase Sounding Curves vs Frequency (4 of 8).

MODE XY (GREEN) DENOTES ELECTRICAL (**EX**) FIELD AND ORTHOGONAL MAGNETIC (**HY**) FIELD (=EX/HY)
MODE YX (ORANGE) DENOTES ELECTRICAL (**EY**) FIELD AND ORTHOGONAL MAGNETIC (**HX**) FIELD (=EY/HX)

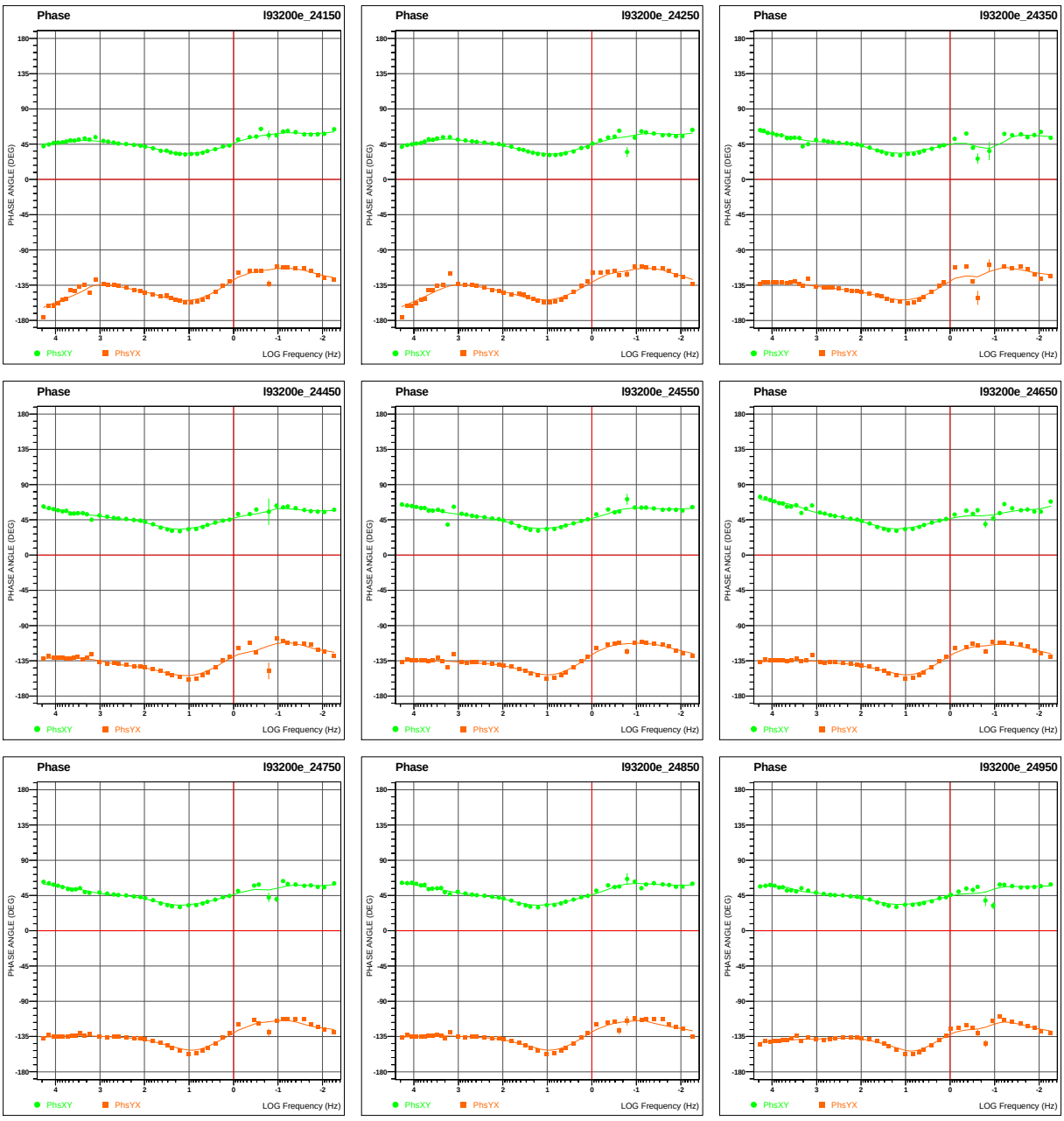

Line 93200E – Phase Sounding Curves vs Frequency (5 of 8).

MODE XY (GREEN) DENOTES ELECTRICAL (**EX**) FIELD AND ORTHOGONAL MAGNETIC (**HY**) FIELD (=EX/HY)
MODE YX (ORANGE) DENOTES ELECTRICAL (**EY**) FIELD AND ORTHOGONAL MAGNETIC (**HX**) FIELD (=EY/HX)

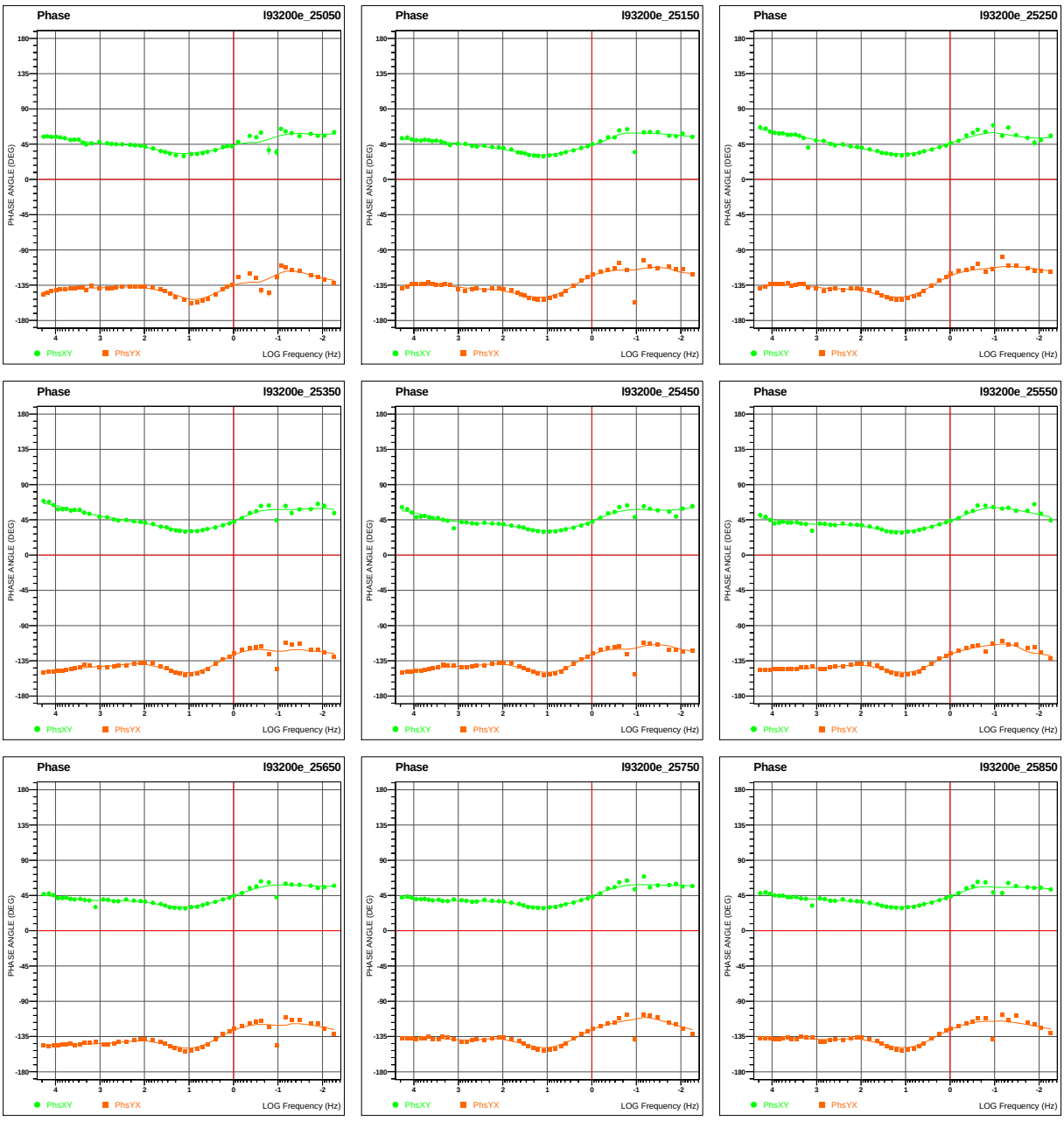

Line 93200E – Phase Sounding Curves vs Frequency (6 of 8).

MODE XY (GREEN) DENOTES ELECTRICAL (**EX**) FIELD AND ORTHOGONAL MAGNETIC (**HY**) FIELD (=EX/HY)
MODE YX (ORANGE) DENOTES ELECTRICAL (**EY**) FIELD AND ORTHOGONAL MAGNETIC (**HX**) FIELD (=EY/HX)

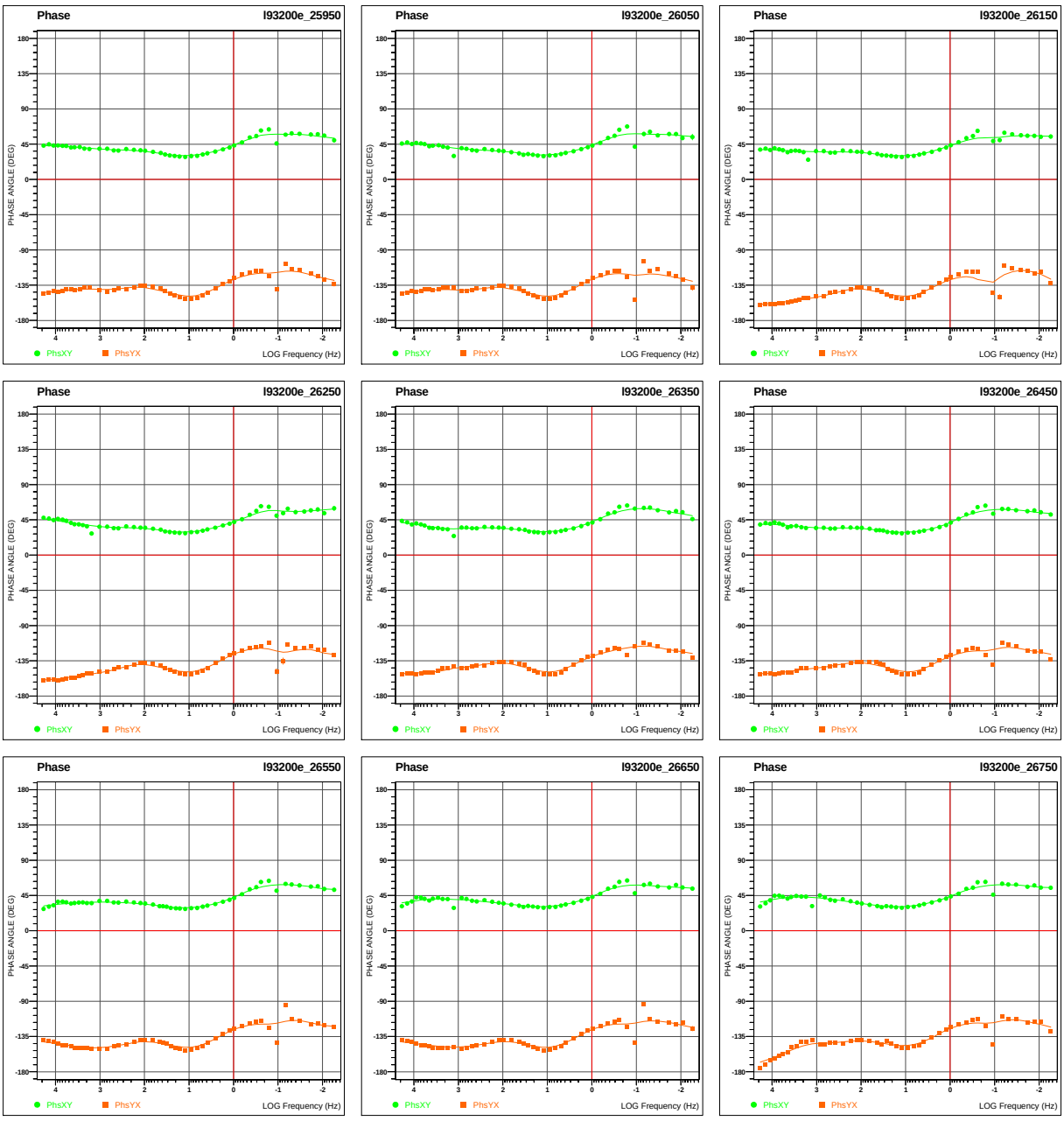

Line 93200E – Phase Sounding Curves vs Frequency (7 of 8).

MODE XY (GREEN) DENOTES ELECTRICAL (**EX**) FIELD AND ORTHOGONAL MAGNETIC (**HY**) FIELD (=EX/HY)
MODE YX (ORANGE) DENOTES ELECTRICAL (**EY**) FIELD AND ORTHOGONAL MAGNETIC (**HX**) FIELD (=EY/HX)

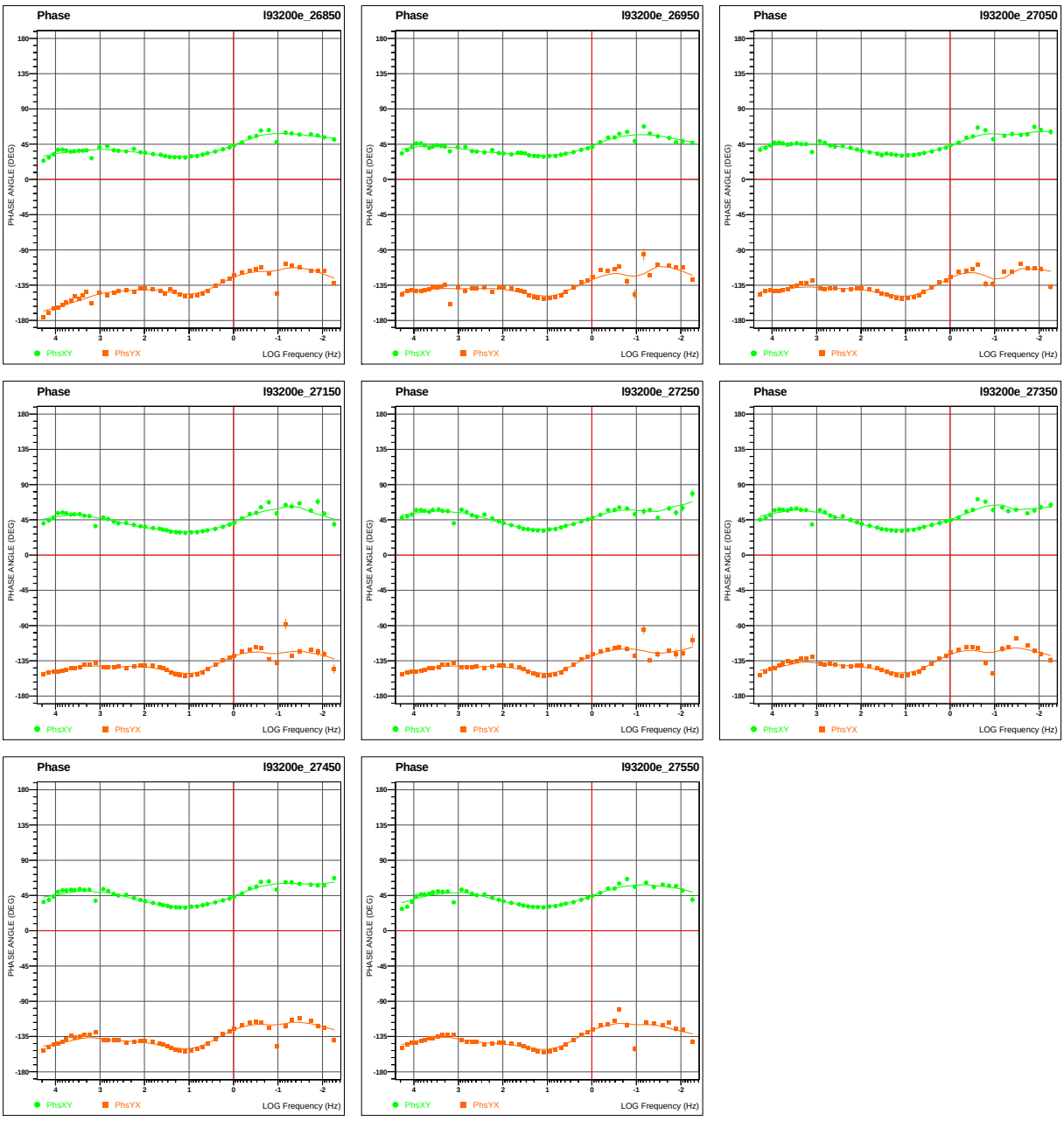

Line 93200E – Phase Sounding Curves vs Frequency (8 of 8).

MODE XY (GREEN) DENOTES ELECTRICAL (**EX**) FIELD AND ORTHOGONAL MAGNETIC (**HY**) FIELD (=EX/HY)
MODE YX (ORANGE) DENOTES ELECTRICAL (**EY**) FIELD AND ORTHOGONAL MAGNETIC (**HX**) FIELD (=EY/HX)

E MT PSEUDO-SECTIONS OF FINAL PROCESSED DATA

IMPORTANT

X IS THE DIRECTION ALONG THE PROFILE; Y IS PERPENDICULAR TO X
(RIGHT HAND POSITIVE DOWN COORDINATE SYSTEM)

GRAPHICS DISPLAYED

(top) Strip 1	**Rho XY**
Strip 2	**Phase XY**
Strip 3	**Rho YX**
(bottom) Strip 4	**Phase YX**

where **XY** denotes
Electrical (**Ex**) field and orthogonal Magnetic (**Hy**) field (=Ex/Hy)

and **YX** denotes
Electrical (**Ey**) field and orthogonal Magnetic (**Hx**) field (=Ey/Hx)

STRIP 1 (TOP): RHO XY – STRIP 2: PHASE XY – STRIP 3: RHO YX – STRIP 4 (BOTTOM): PHASE YX
WHERE XY DENOTES ELECTRICAL (**EX**) FIELD AND ORTHOGONAL MAGNETIC (**HY**) FIELD (=EX/HY)
AND YX DENOTES ELECTRICAL (**EY**) FIELD AND ORTHOGONAL MAGNETIC (**HX**) FIELD (=EY/HX)

E.1 LINE 92800E

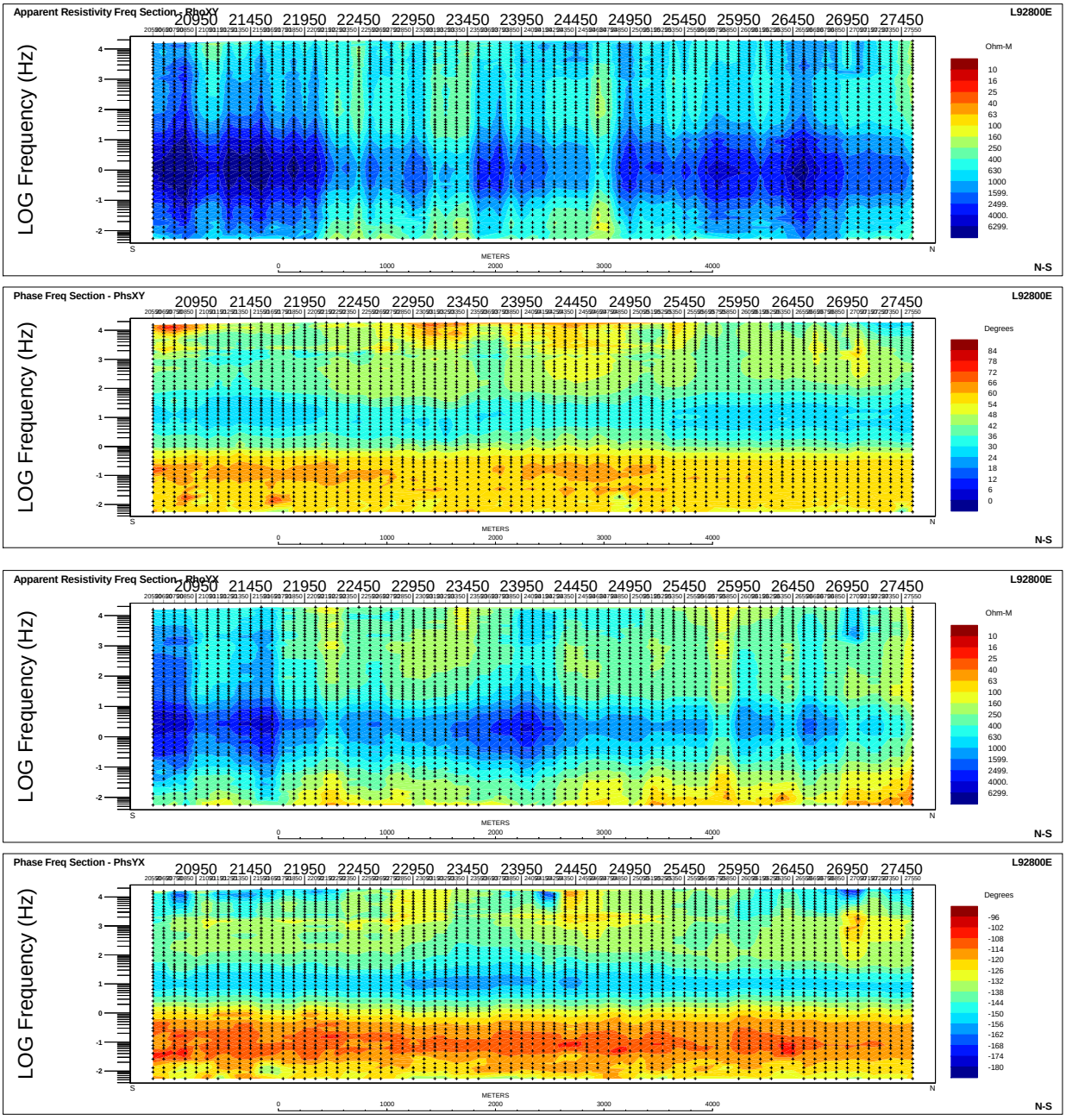

Line 92800E – Apparent Resistivity and Phase (XY & YX) Pseudo-Section.

STRIP 1 (TOP): RHO XY – STRIP 2: PHASE XY – STRIP 3: RHO YX – STRIP 4 (BOTTOM): PHASE YX
WHERE XY DENOTES ELECTRICAL (**EX**) FIELD AND ORTHOGONAL MAGNETIC (**HY**) FIELD (=EX/HY)
AND YX DENOTES ELECTRICAL (**EY**) FIELD AND ORTHOGONAL MAGNETIC (**HX**) FIELD (=EY/HX)

E.2 LINE 93200E

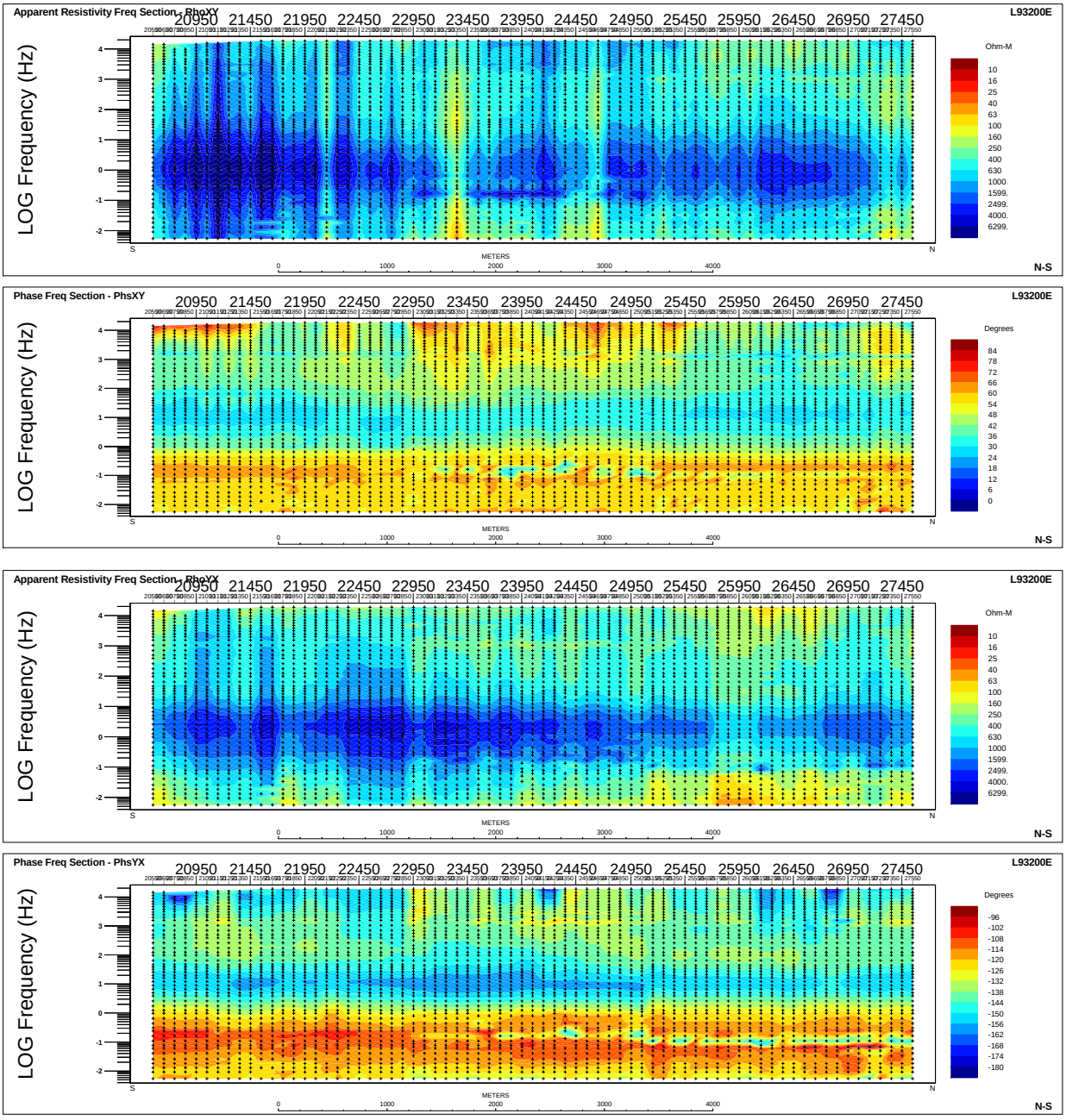

Line 93200E – Apparent Resistivity and Phase (XY & YX) Pseudo-Section.

STRIP 1 (TOP): RHO XY – STRIP 2: PHASE XY – STRIP 3: RHO YX – STRIP 4 (BOTTOM): PHASE YX
WHERE XY DENOTES ELECTRICAL (**EX**) FIELD AND ORTHOGONAL MAGNETIC (**HY**) FIELD (=EX/HY)
AND YX DENOTES ELECTRICAL (**EY**) FIELD AND ORTHOGONAL MAGNETIC (**HX**) FIELD (=EY/HX)

F PARALLEL SENSOR TEST

Project	**CA00900T**
Date:	September 25, 2011
Report by:	Wade Lee
Staff:	William Xu
	Warren Gregory
	Matt Cousineau
QuickLay Version	4.00.010
Common folder	V1.50
Datum:	UTM WGS 84 / Zone 10U
Station:	656678 m E, 5606686 m N
Coil Azimuth:	0° true
Declination	17°E

Results:

All coils tracking good.

F.1 LOW FREQUENCY COILS

Available Coils:

TS Strip	Manufacture	Serial #	Task for
1	Phoenix	P50-1963	Spare
2	Phoenix	P50-1969	Spare
3	Phoenix	P50-2114	Line Lnx
4	Phoenix	P50-2130	Line Lny
5	Phoenix	P50-2131	Remote Rmx
6	Phoenix	P50-2203	Remote Rmy

Processing Parameters:

Parameters	Values
PSD Method	Welch
Window	Hanning
Window Length	2048
Segment Overlap	50%

F.1.1 TEST RESULTS: 120SPS

Titan NetEvent:	9032.000037
Sample Rate:	120sps
TS Length:	80,000 samples (~11min)

Results:

All low frequency coils are tracking well and have good coherency

Time Series

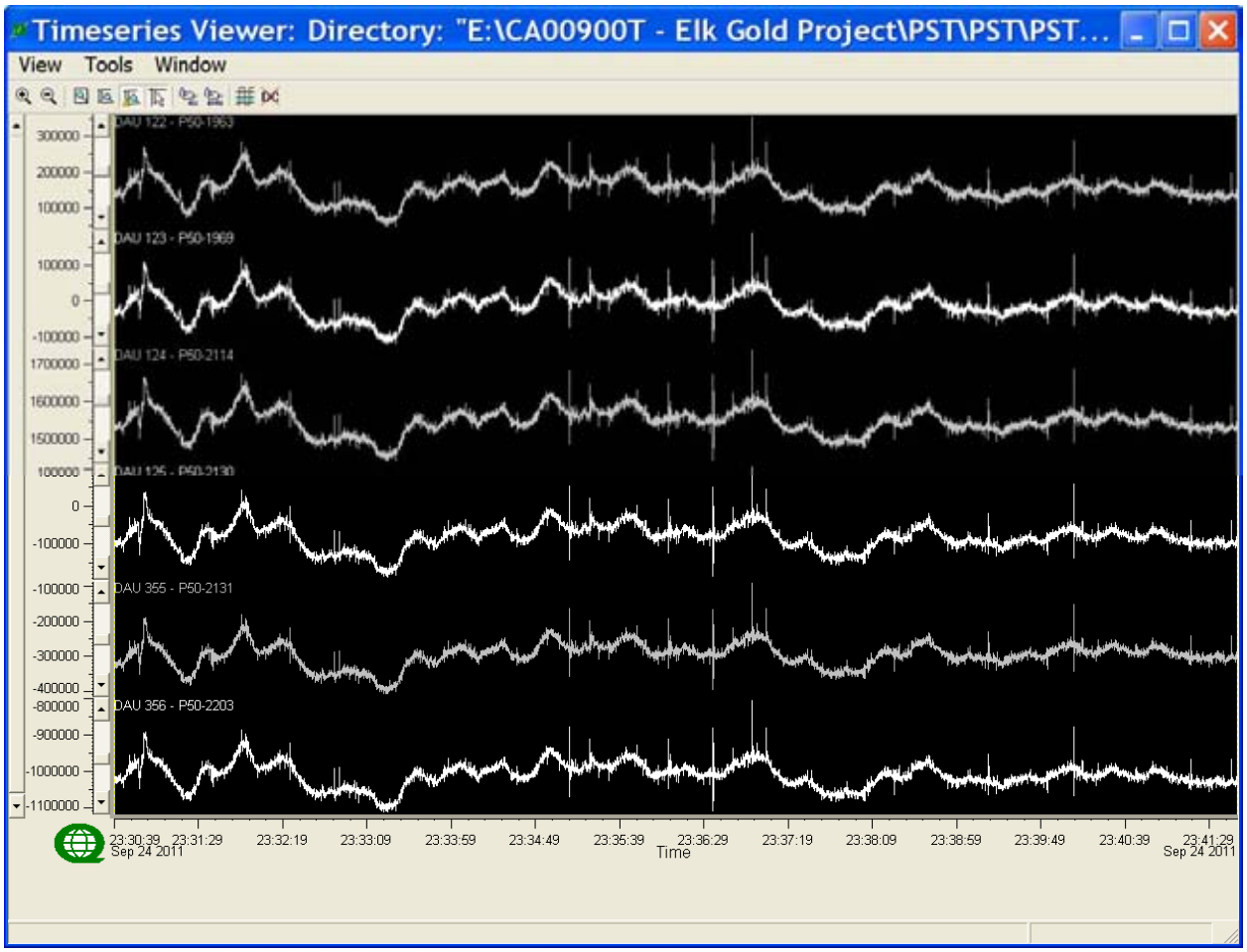

Complete time series @ 120sps

Low Frequency Coil Results **Coherency to P50-1963(Blue)**

From top to bottom: PSD of channels and Coherency and Response Function (Amplitude and Phase) compared to Reference Channel – Linear frequency scale

Low Frequency Coil Results (continued) **Coherency to P50-1963 (Blue)**

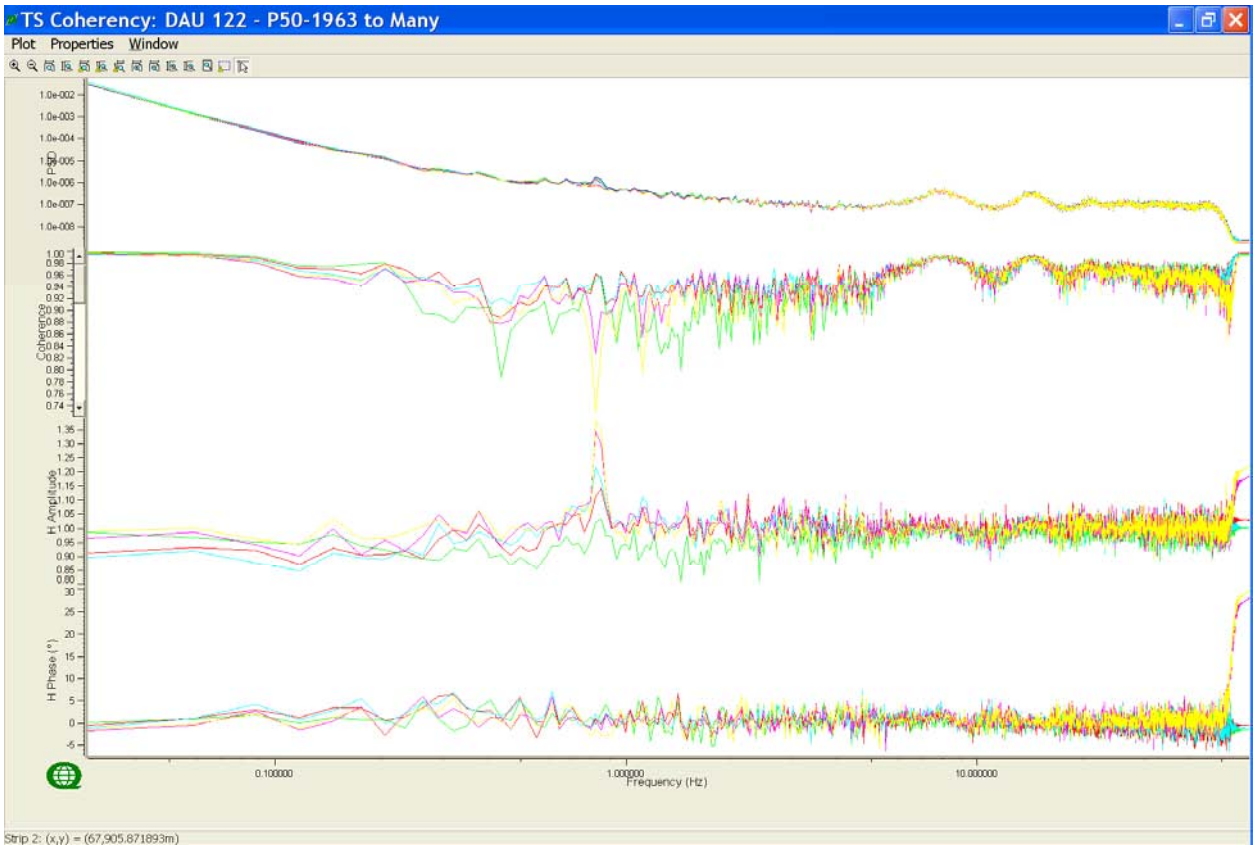

From top to bottom: PSD of channels and Coherency and Response Function (Amplitude and Phase) compared to Reference Channel – Logarithmic frequency scale

Colour	Channel	Notes
Blue	P50-1963	All OK
Green	P50-1969	
Red	P50-2114	
Cyan	P50-2130	
Magenta	P50-2131	
Yellow	P50-2203	

F.2 HIGH FREQUENCY COILS

Available Coils:

TS Strip	Manufacture	Serial #	Task for
1	EMI	BF6-5007	Remote Rmx
2	EMI	BF6-5008	Remote Rmy
3	EMI	BF6-5009	Spare
4	EMI	BF6-6176	Spare
5	EMI	BF6-6179	Line Lx
6	EMI	BF6-6277	Line Ly

Processing Parameters:

Parameters	Values
PSD Method	Welch
Window	Hanning
Window Length	2048
Segment Overlap	50%

Colour	Channel	Notes
Blue	P50-1963	All OK
Green	P50-1969	
Red	P50-2114	
Cyan	P50-2130	
Magenta	P50-2131	
Yellow	P50-2203	

F.2.1 TEST RESULTS: 48KSPS

Titan NetEvent:	9032.000025
Sample Rate:	48k sps
TS Length:	1,500,000 samples (~31s)

Results:

All coils tracking good.

Time Series

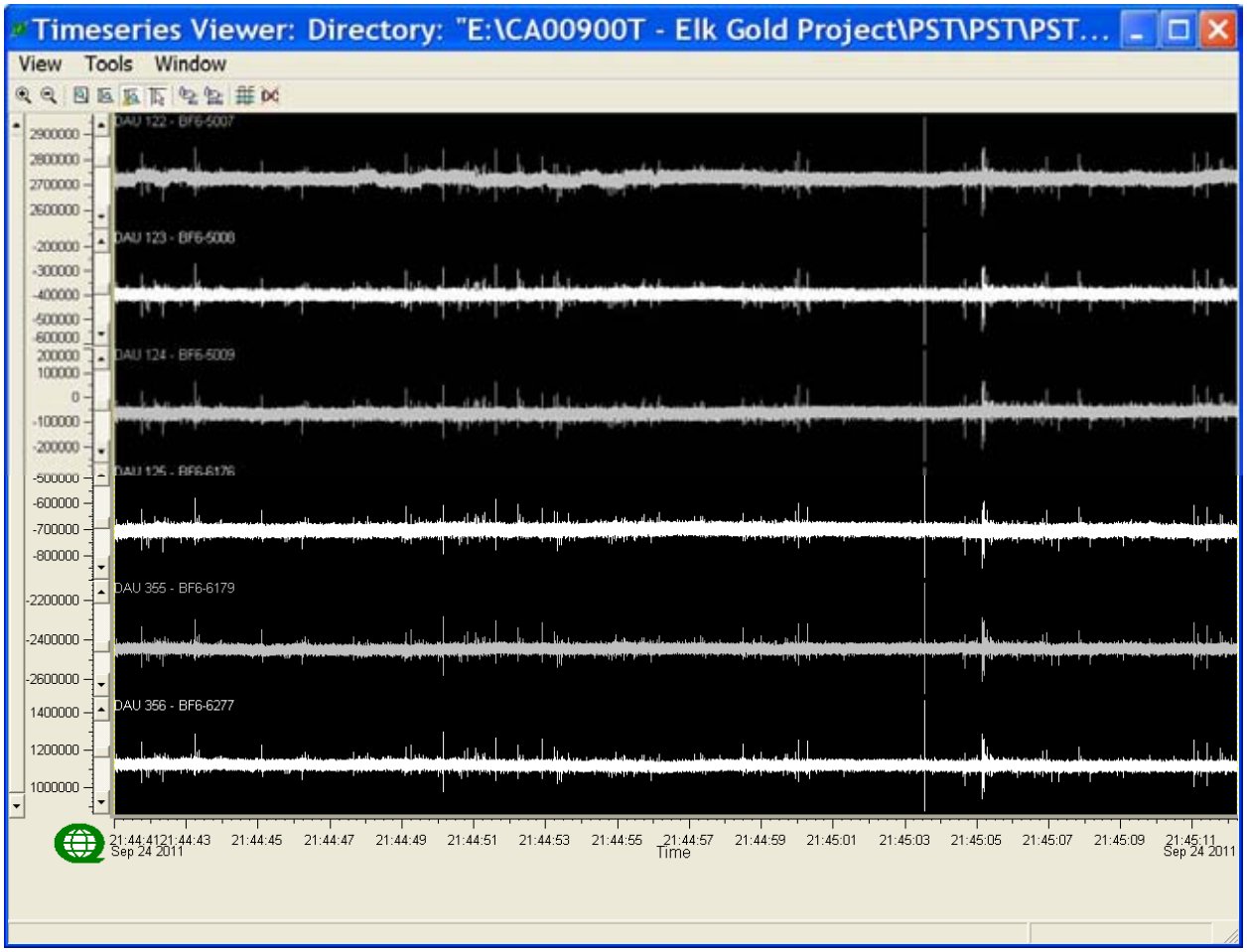

Complete time series at 48ksps.

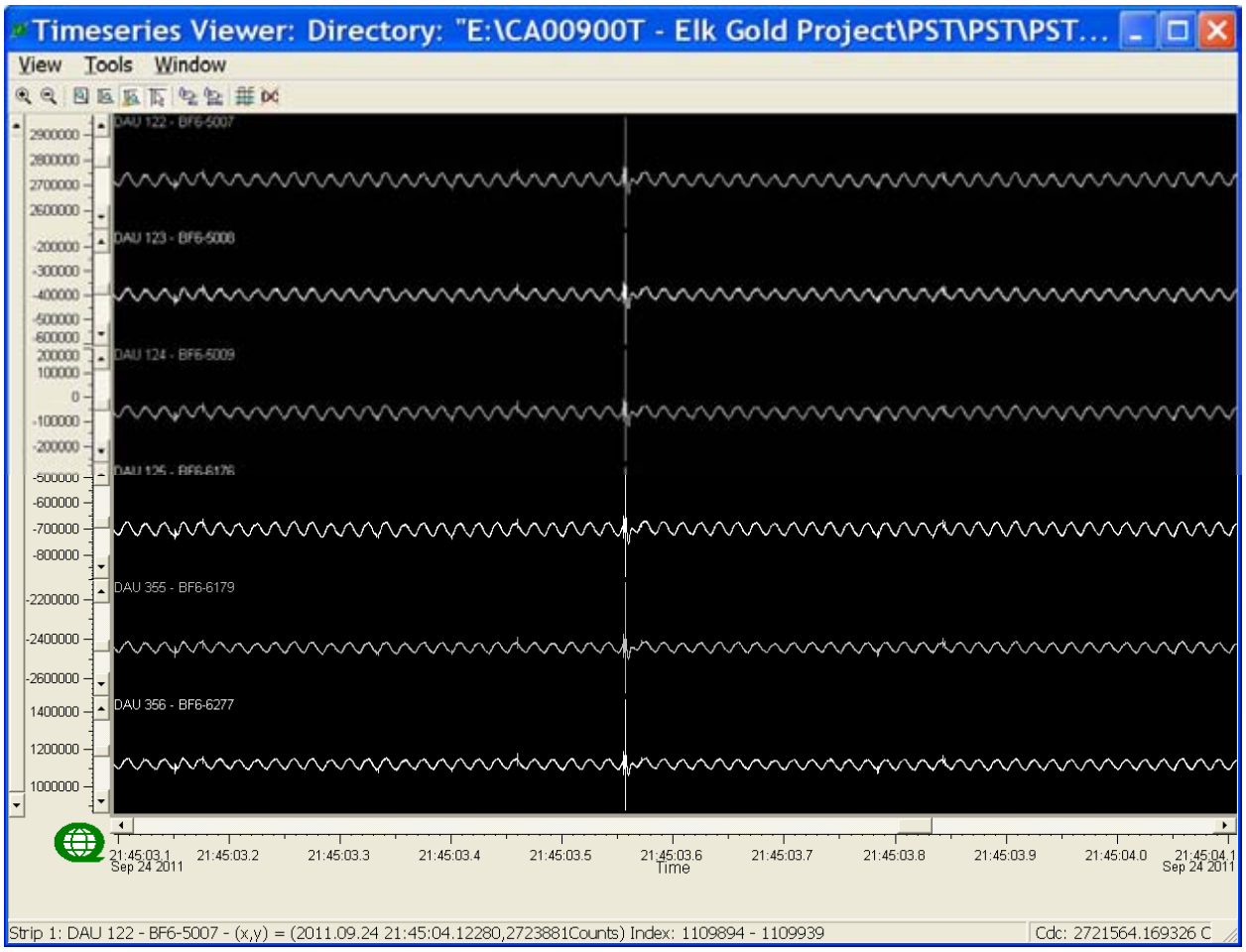

Time series focused in on ~1s at 48ksps.

High Frequency (48k) Coil Results **Coherency to BF6-5007 (Blue)**

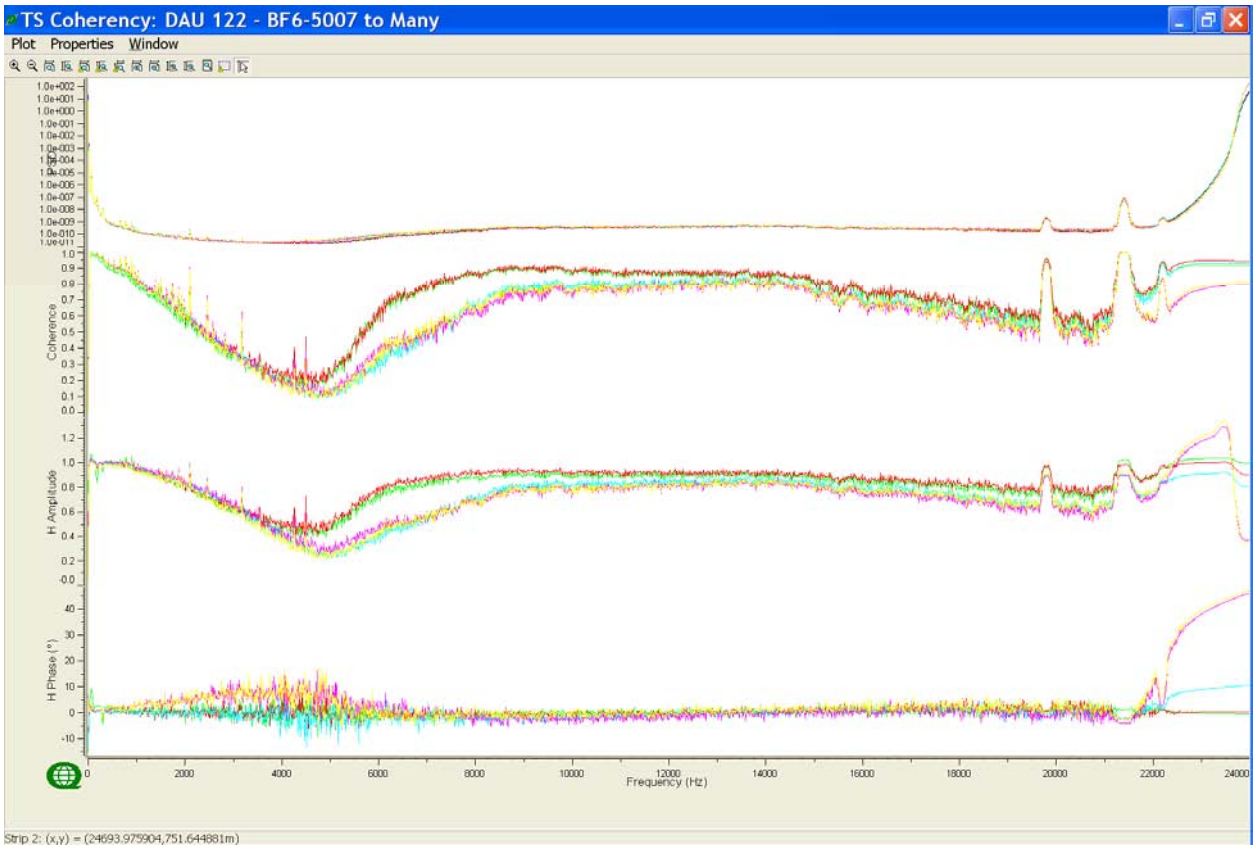

From top to bottom: PSD of channels and Coherency and Response Function (Amplitude and Phase) compared to Reference Channel – Linear frequency scale.

Colour	Channel	Notes
Blue	BF6-5007	All OK
Green	BF6-5008	
Red	BF6-5009	
Cyan	BF6-6176	
Magenta	BF6-6179	
Yellow	BF6-6277	

High Frequency (48k) Coil Results (Continued) **Coherency to BF6-5007 (Blue)**

From top to bottom: PSD of channels and Coherency and Response Function (Amplitude and Phase) compared to Reference Channel – Logarithmic frequency scale.

Colour	Channel	Notes
Blue	BF6-5007	All OK
Green	BF6-5008	
Red	BF6-5009	
Cyan	BF6-6176	
Magenta	BF6-6179	
Yellow	BF6-6277	

F.2.2 TEST RESULTS: 12K SPS

Titan NetEvent:	9032.000023
Sample Rate:	12k sps
TS Length:	1,500,000 samples (~2min)

Results:

All coils tracking good.

Time Series

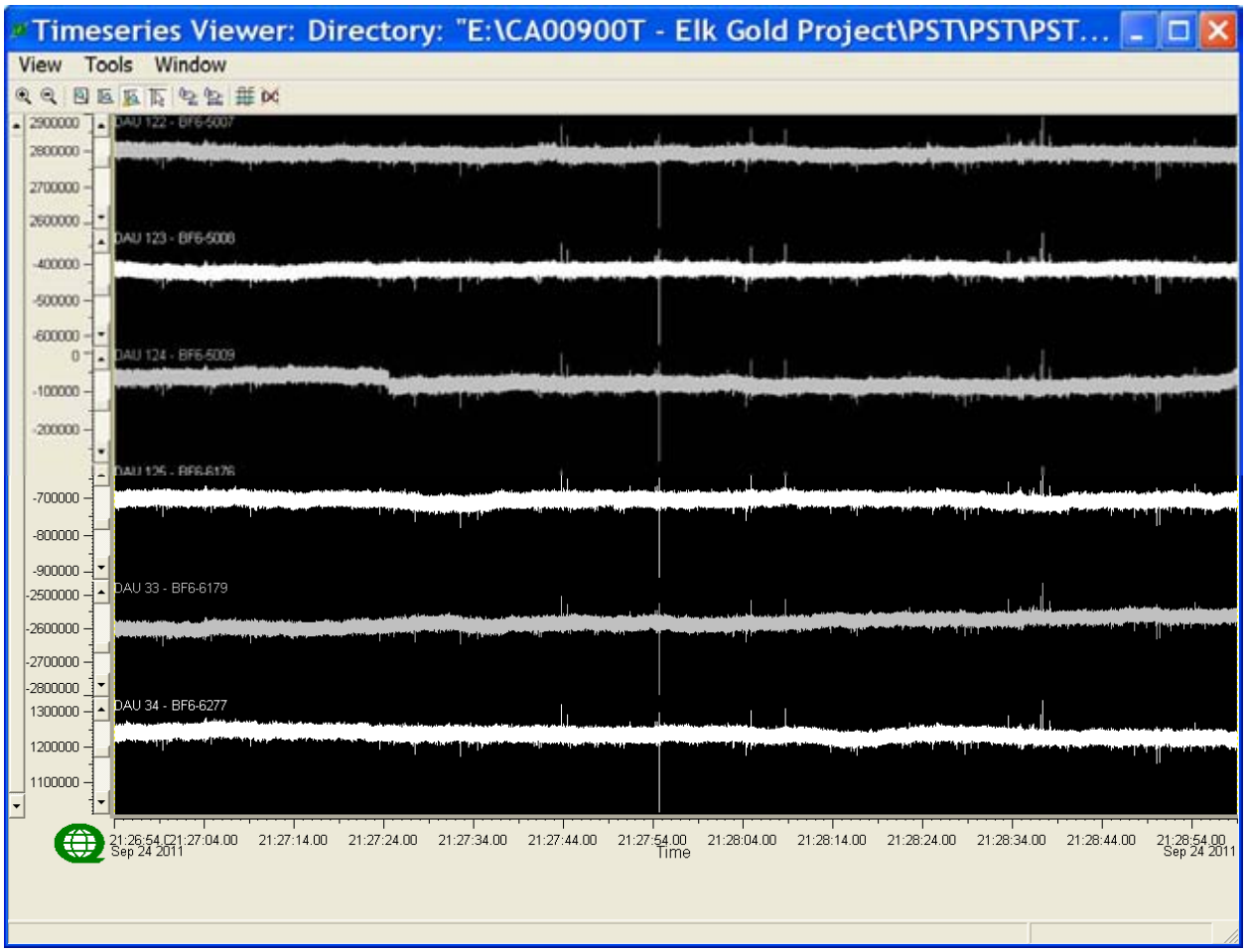

Complete time series 12ksps

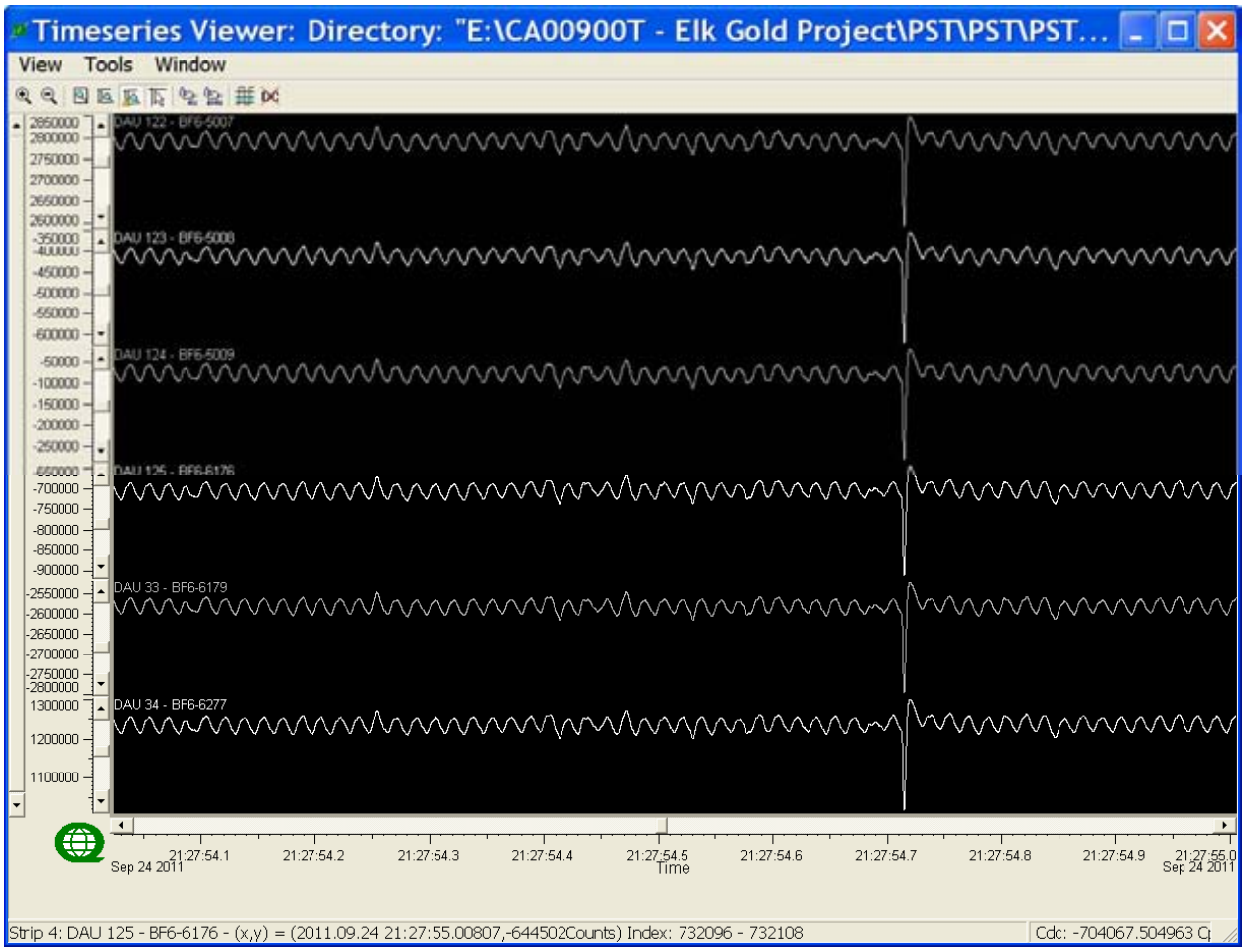

Focus on 1s of the time series 12ksps

High Frequency (12k) Coil Results **Coherency to BF6-5007 (Blue)**

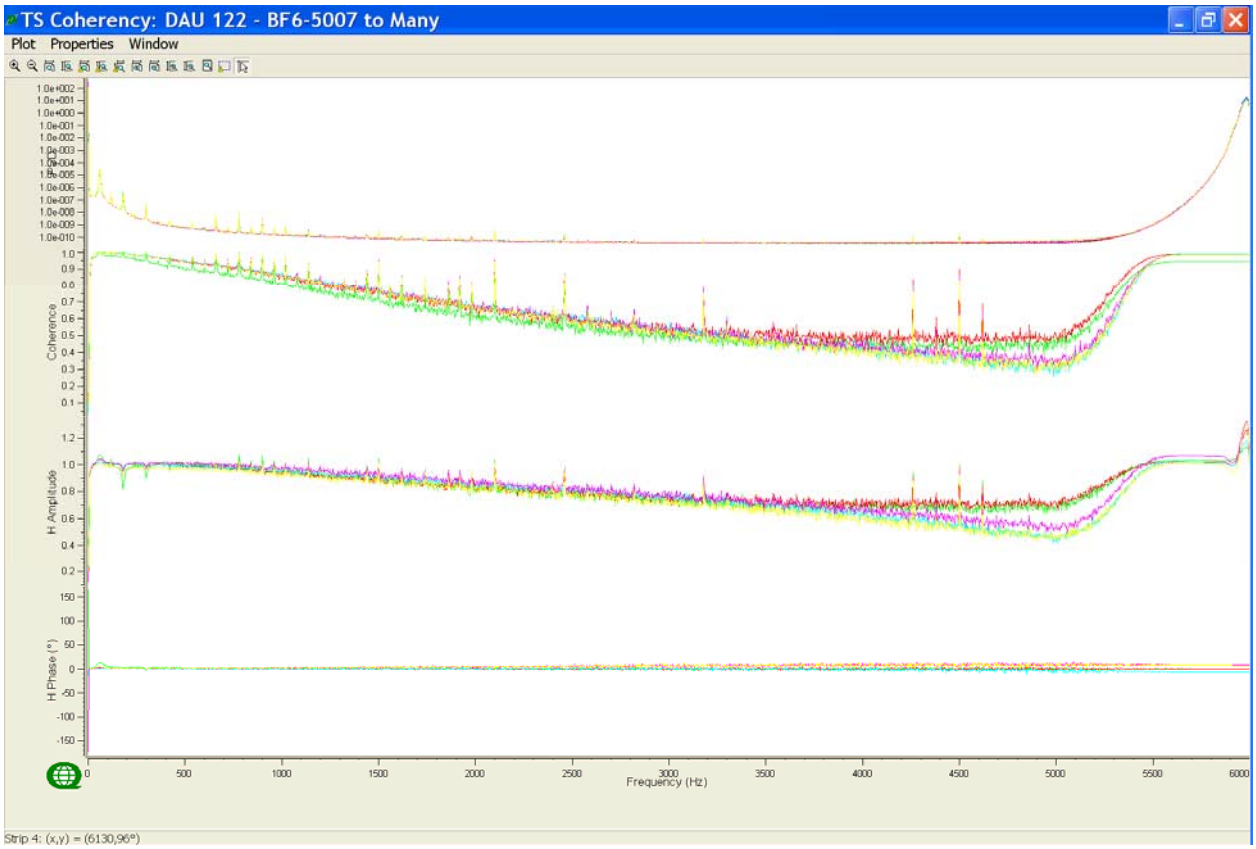

From top to bottom: PSD of channels and Coherency and Response Function (Amplitude and Phase) compared to Reference Channel – Linear frequency scale

Colour	Channel	Notes
Blue	BF6-5007	All OK
Green	BF6-5008	
Red	BF6-5009	
Cyan	BF6-6176	
Magenta	BF6-6179	
Yellow	BF6-6277	

High Frequency (12k) Coil Results (Continued) **Coherency to BF6-5007 (Blue)**

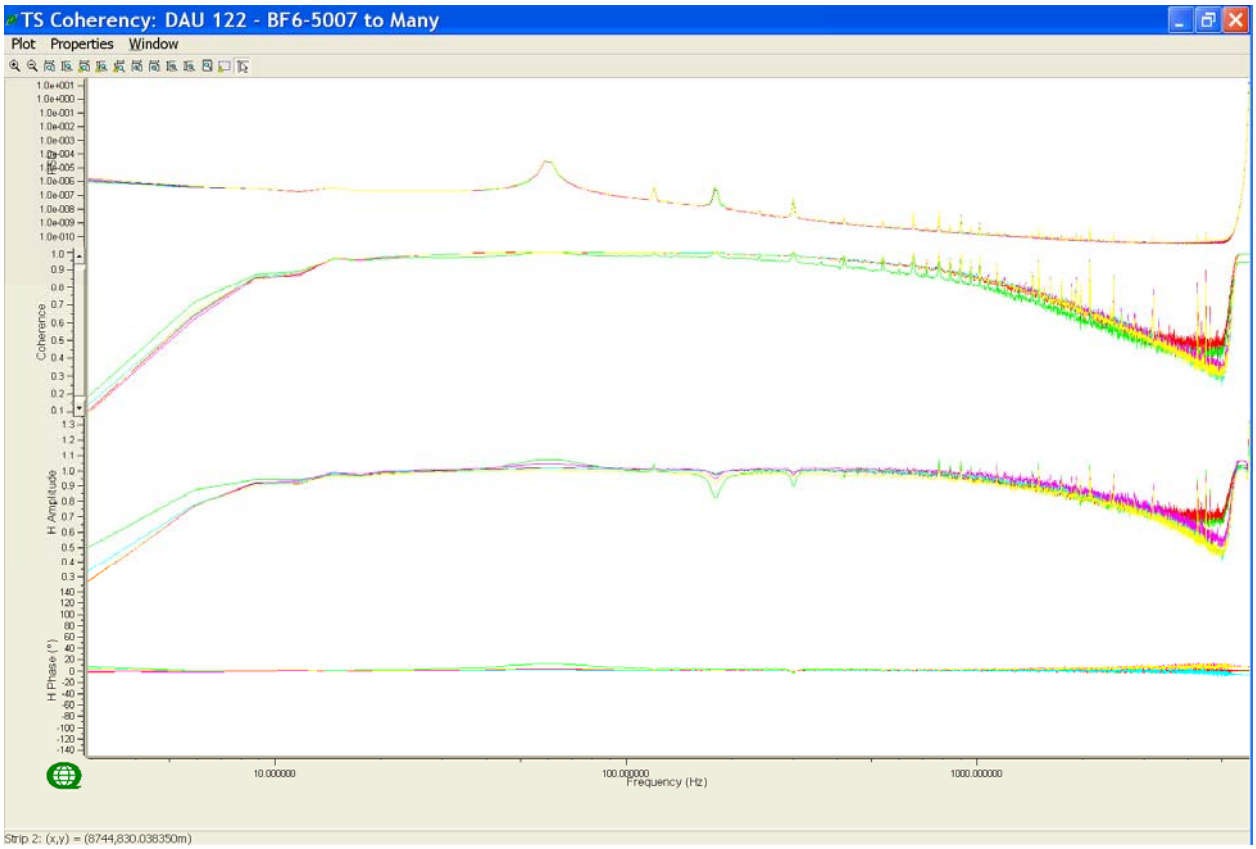

From top to bottom: PSD of channels and Coherency and Response Function (Amplitude and Phase) compared to Reference Channel – Logarithmic frequency scale

Colour	Channel	Notes
Blue	BF6-5007	All OK
Green	BF6-5008	
Red	BF6-5009	
Cyan	BF6-6176	
Magenta	BF6-6179	
Yellow	BF6-6277	

G MT REMOTE – UNREFERENCED DATA

Project	**CA00900T**		
Date:	September 25, 2011		
Report by:	Wade Lee		
QuickLay Version	4.00.010		
Common folder	V1.50		
Remote Location:	656678 mE / 5606686 mN (WGS 84 / Zone 10U) (approx. 60 km N from Merritt)		
Mag Declination:	17° East		
Sensor Azimuth:	**Ex**	00°North	dipole = 100m
	Ey	270° West	dipole = 100m
	Hx	00° North	
	Hy	270° West	
Culture:	N/A		

Details below ALL the data used and processed for the test

TITAN DATA

Sample Rate	Net Events	TS Length	Observations
48ksps	9032.000049	1,500,000	N/A
12ksps	9032.000050	1,500,000	N/A
120sps	9032.000051	80,000	Scattering below 1 Hz

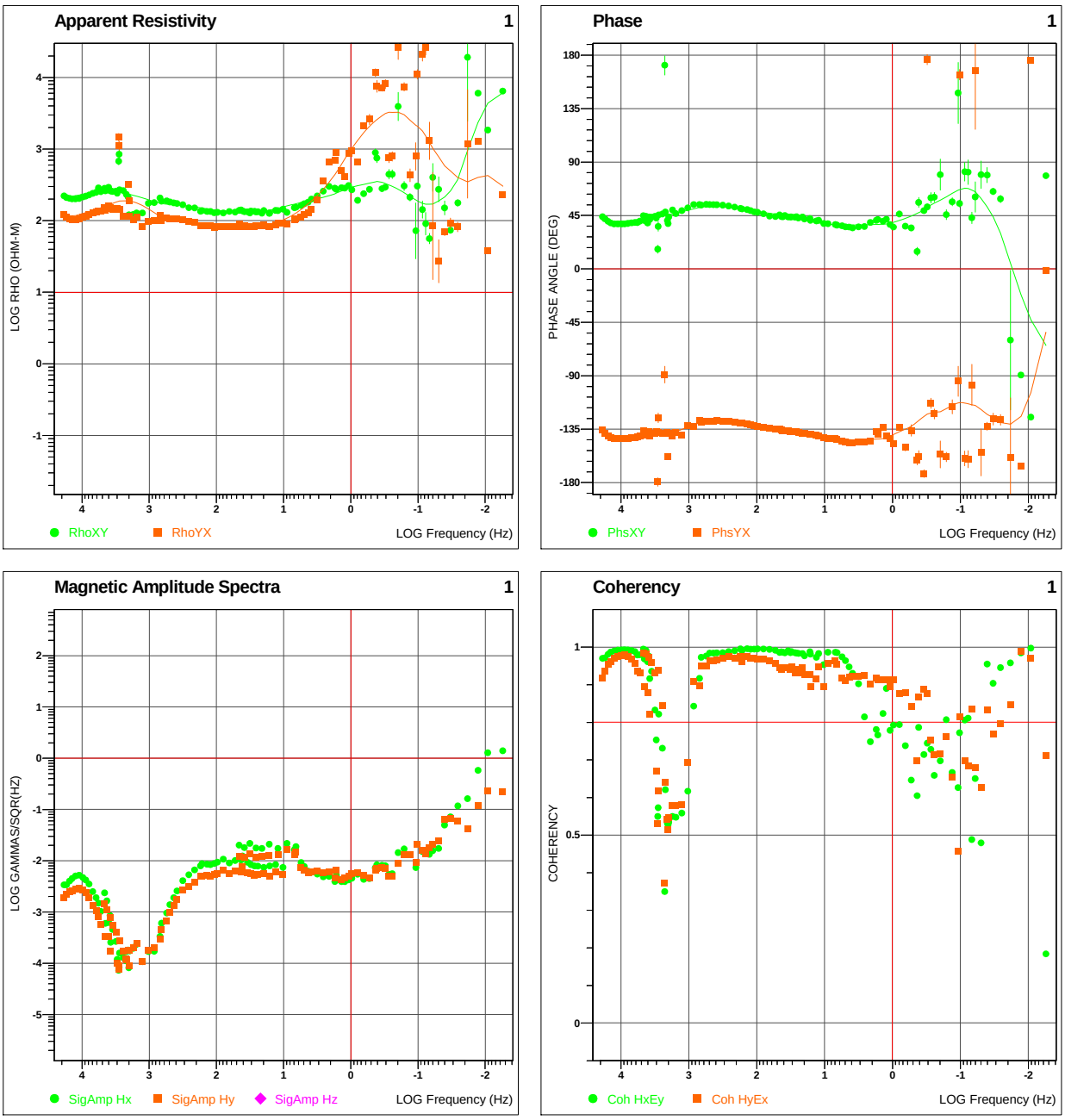

Apparent resistivity, phases, magnetic signal amplitude and off-diagonal coherences of the MT remote, data processed unreferenced.

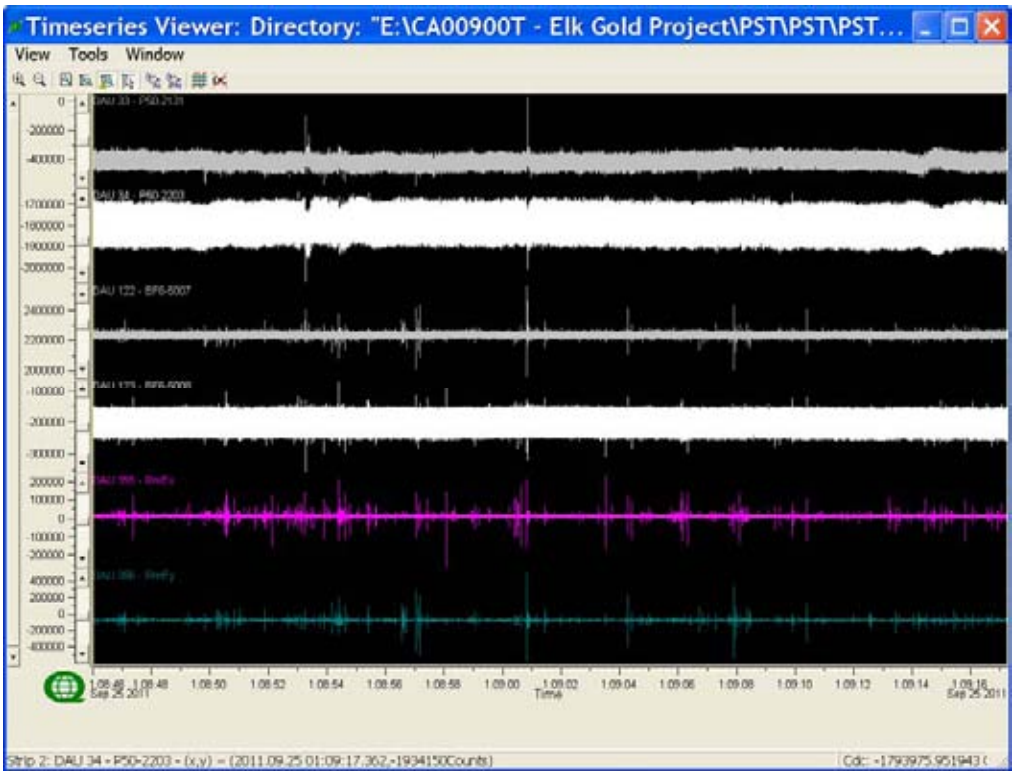

Screen Capture of MT time series, sample rate at 48ksps.

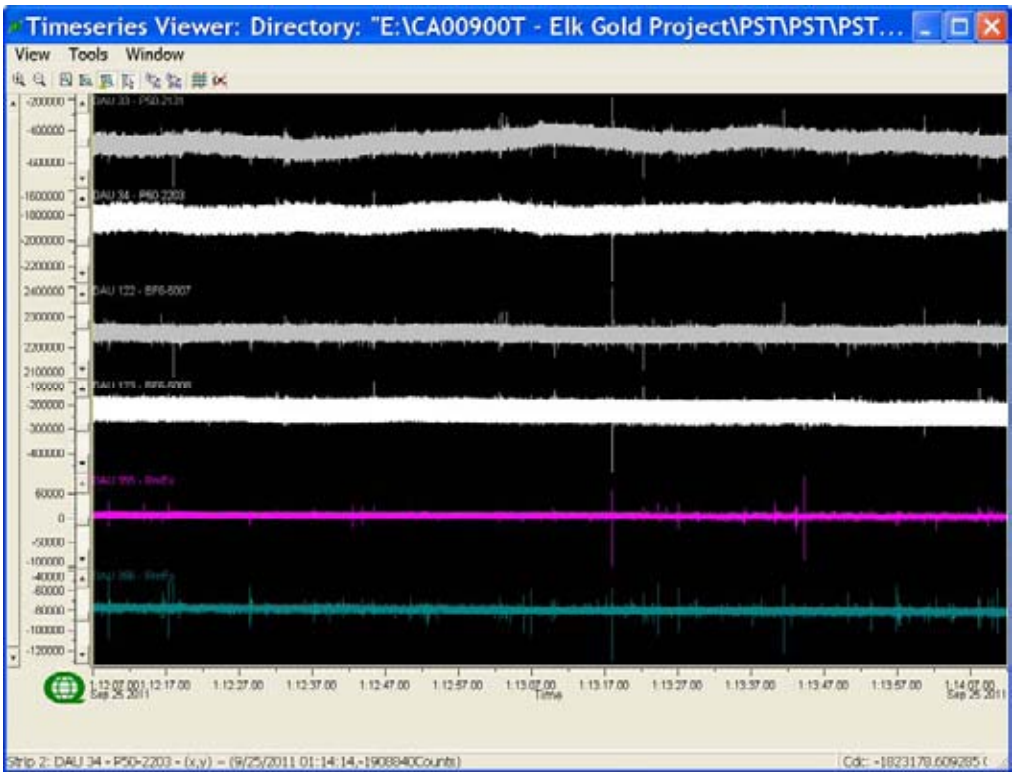

Screen Capture of MT time series, sample rate at 12ksps.

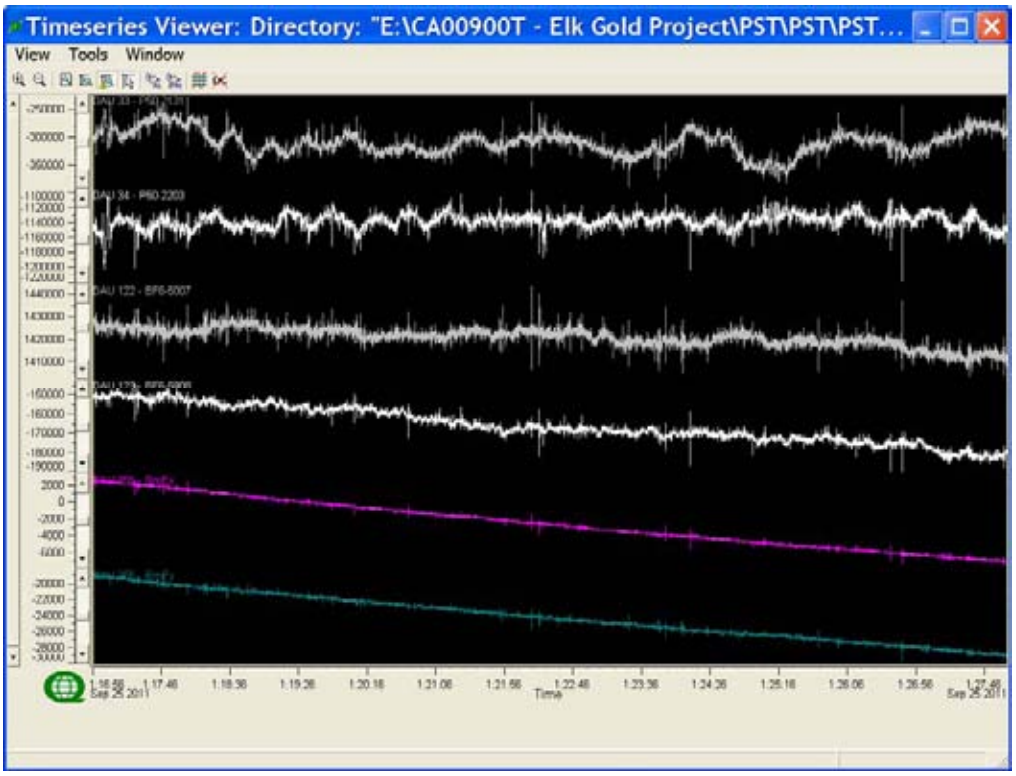

Screen Capture of MT time series, sample rate at 120ksps.

H INSTRUMENTS SPECIFICATIONS

H.1 REF TEK – 120 DATA ACQUISITION SYSTEM

Refraction Technology Inc. – Plano, Texas

Specifications:

Specification	Description
Physical	
Size:	267 x 248 x 184 mm 10.5 x 9.75 x 7.25 in.
Weight:	3.7kg 305 g 8 lbs (2-Channels maximum weight))
Temperature:	-40°C to 60°C operating range.
Environmental:	Operates in 1m of water without leaking for 48 hours. Airtight to 1.0 psi.
Shock:	Remains operational after 1m drop (any corner) onto cement floor.
Connectors	
Line A & Line B:	A pair of identical 10 pin U77/U style connectors. Each connector provides 3 pairs of lines (+): A (+)/B (-) Receive telemetry data and/or commands C (+)/D (-) Transmit telemetry data and/or commands E (+)/F (-) Sync
Power:	PTO7A12-8S style connector. Provides input +12 VDC supplied from battery.
Sensor:	PU283/U style connector. Provides for a direct connection from the AM to the sensor.
Power Requirements	
Battery:	Two 12 volt lead acid battery (7 Ah).
Signal Input	
Input Impedance:	10 megohms, 330pF, differential
Broadband Dynamic Range:	130dB (noise power ratio test @ 125 sample per second [sps])
ADC Type:	Delta-sigma modulation
Sample Rage:	Multiple 50 to 48,000
Gain Settings:	Four – programmable for 1, 4, 16 and 64.

Specification	Description				
Sensor Input Signal Range:	Gain	24-Bit High Speed A/D		24-Bit Low Speed A/D	
		Actual	Reported	Actual	Reported
	1	1.192μV	78.12mV	1.907μV	125.0mV
	4	298.0nV	19.53mV	476.8nV	31.25mV
	16	74.51nV	4.883mV	119.2nV	7.812mV
	64	18.63nV	1.221mV	29.80nV	1.953mV
Data Storage					
Data Size:	32-bit two's compliment.				
Base Memory:	128K EPROM 6.5Mb SRAM				
Base Capacity:	Better than 1.5 million samples or approximately 3 hours 10 minutes continuous data @ 125 sps.				
AM Telemetry					
Protocol:	Full duplex synchronous data link control (SDLC).				
Error Correction:	Packet acknowledge with modulo 8 sliding window.				
Speed	3.072Mb/second				
Encoding:	Bi-phase pulse = 1, missing pulse = 0				
Line Impedance:	100 Ohm				
Synchronization					
Timing:	Each AM on-line is timed and synchronized for simultaneous sampling within + 1.50 μsecond.				
Protection					
Electrical Protection:	Line A and Line B signals circuits are protect by: - A surge arrestor located on the RT514 board (SS1-14). - A line isolation transformer located on the RT514 board (T1-6) with over-voltage diodes (D1-4) on both sides of each secondary windings				
State-of-Health					
Information Provided:	The AM reports information on battery status, clock setting, gain setting, calibration mode and the communications link.				

Acquisition Parameters

Acquisition parameters include the sample rate, transmitter frequency and number of samples desired. The operator can also determine whether the AMs calibration signal is activated during data collection.

In typical use, the acquisition parameters are set according to the specific application configuration and event type. For each event type, several recording sessions are made, each at a different transmitter frequency and sample rate. The recording period is set based on event type and transmitter frequency.

The listing below shows several examples of event type, typical transmitter frequency (Hz), sample rates (with applicable ADC resolution) and the corresponding number of samples (record period).

Event Type	Transmit Frequency	Sample Rate	ADC Resolution	Number of Sample
Geophysical Response	375 Hz	48,000	24	124,032
Gain Test	375	48,000	24	65,536
Geophysical Response	75	9,600	24	130,176
Gain Test	75	9,600	24	65,536
Geophysical Response	25/8	3,200	24	139,264
Gain Test	25/8	3,200	24	32,768
Sensor Impedance	N/A	1,600	24	8,704
Ambient Noise	N/A	1,600	24	8,192
Geophysical Response	25/128	800	24	147,456
Gain Test	25/128	800	24	16,384
Geophysical Response	25/2048	100	24	212,992
Gain Test	25/256	100	24	4,096
Gain Test	N/A	50	24	4,096
Geophysical Response	N/A	50	24	65,536

Sensor Calibration

The AM can source a 12.5Hz, 50μA signal to the sensor input for measuring the source impedance of the attached sensor. The user can also specify frequency in amplitude of calibration signal.

Telemetry Cable

The telemetry cable is a *Category V* specification cable and is supplied by the customer.

Sample Rates

The following table shows all available sample rates, based on a 12.288 Mhz oscillator. A 24-bit resolution ADC is used for sample rates 48000 through 4800 and a 24-bit resolution ADC is used for

sample rates 3200 and below. The correct ADC is selected automatically by the AM, based on the sample rate.

Typically, different sample rates and transmitter frequencies are used in 50 Hz and 60 Hz power environments to minimize AC power effects on the data. In the table, the shaded areas indicate the sample rates typically used in a 60 Hz power environment. A few rates are typically used in both environments.

Sample Rate	Power Line
48000	50 & 60
24000	50 & 60
19200	60
16000	50
12000	50 & 60
9600	50 & 60
6400	50
4800	60
3200	50
1920	60
1600	50
960	60
800	50
480	60
400	50
240	60
200	50
120	60
100	50
60	60
50	50
60/2	60
50/2	50
60/4	60
50/4	50
60/8	60
50/8	50
60/16	60
50/16	50
60/32	60
50/32	50

H.2 BF-6 MAGNETIC FIELD INDUCTION SENSOR

Schlumberger –EMI (Electromagnetic Instruments Inc.)Technology Center

The BF-6 sensor utilizes a magnetic feedback design to provide a stable flat response over several decades of frequency. The sensors respond as a B field detector over the flat band regions. Both the amplitude and phase responses are highly stable with variations of less than 0.1dB in amplitude and +/- one degree in phase between sensors. For the frequencies below the flat response region, the sensor response is proportional to signal frequency so that the sensor acts as a dB/dt detector. The coil is potted with epoxy and housed inside a rugged impact-resistant ABS tube. A matched low noise preamplifier is connected to the coil in a waterproof case and powered by an external +/- 12V power supply.

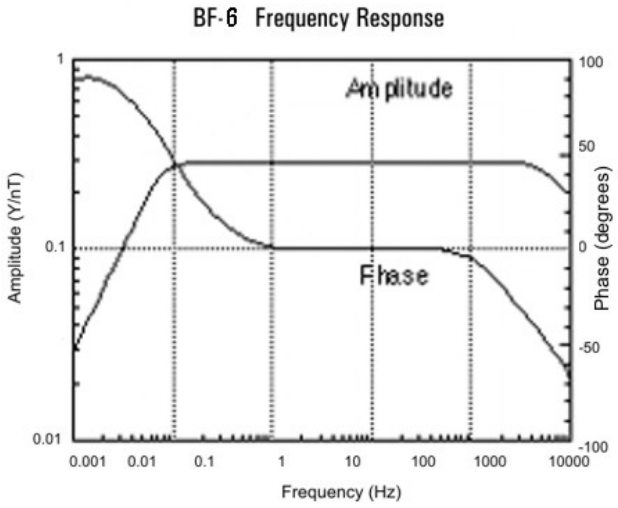

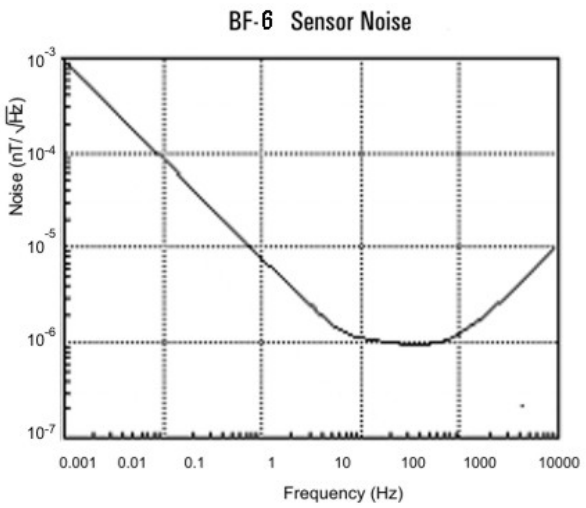

Features

High sensitivity
Very low noise
Magnetic feedback design
Ruggedized and waterproof
Light weight and compact
Low power consumption (210 mW)
Stable phase response

Applications

Magnetotellurics
Audiomagnetotellurics
Controlled-source electromagnetics
Magnetometric resistivity
Time domain electromagnetics

Performance

Frequency Range: 1 Hz to -100 kHz or 1 Hz to 25 kHz
3 dB frequency corners: 10 Hz, 25 kHz or 10 Hz, 100 kHz
Sensitivity (flat region): 0.3 V/nT (standard)
Power consumption: 9mA at +/-12V

Physical

Housing: High Impact ABS Straight Tube
Length: 73 cm (29 inches)
Diameter: 5 cm (2 inches)
Weight: 1.7 kg (3.7 lbs)
Connector: 8-pin Tajimi

H.3 MTC 50 (P50) SERIES MAGNETIC SENSORS

Phoenix Geophysics Ltd

MTC-50 magnetic sensor coils weigh just over 10 kg, and measure only 141 cm. They provide magnetotelluric data at frequencies between 400 Hz to 0.00002 Hz.

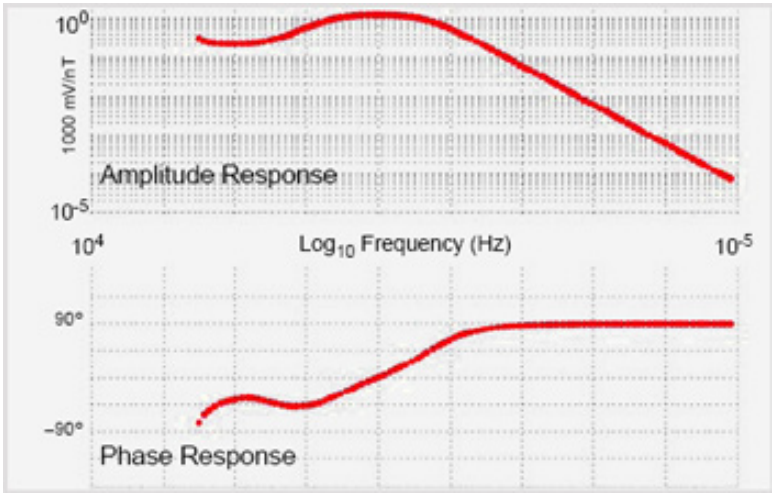

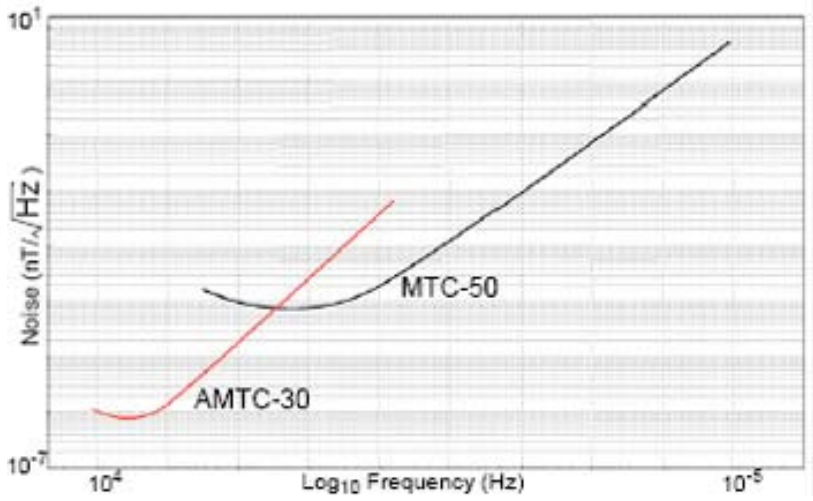

Technical Specifications

Overall Length : 141 cm
Outside Diameter : 6.0 cm
Weight : 10.5 kg
Frequency Range (for MT) :
400 Hz to 0.00002 Hz

I GEOSOFT SECTIONS OF THE 2D MODELS

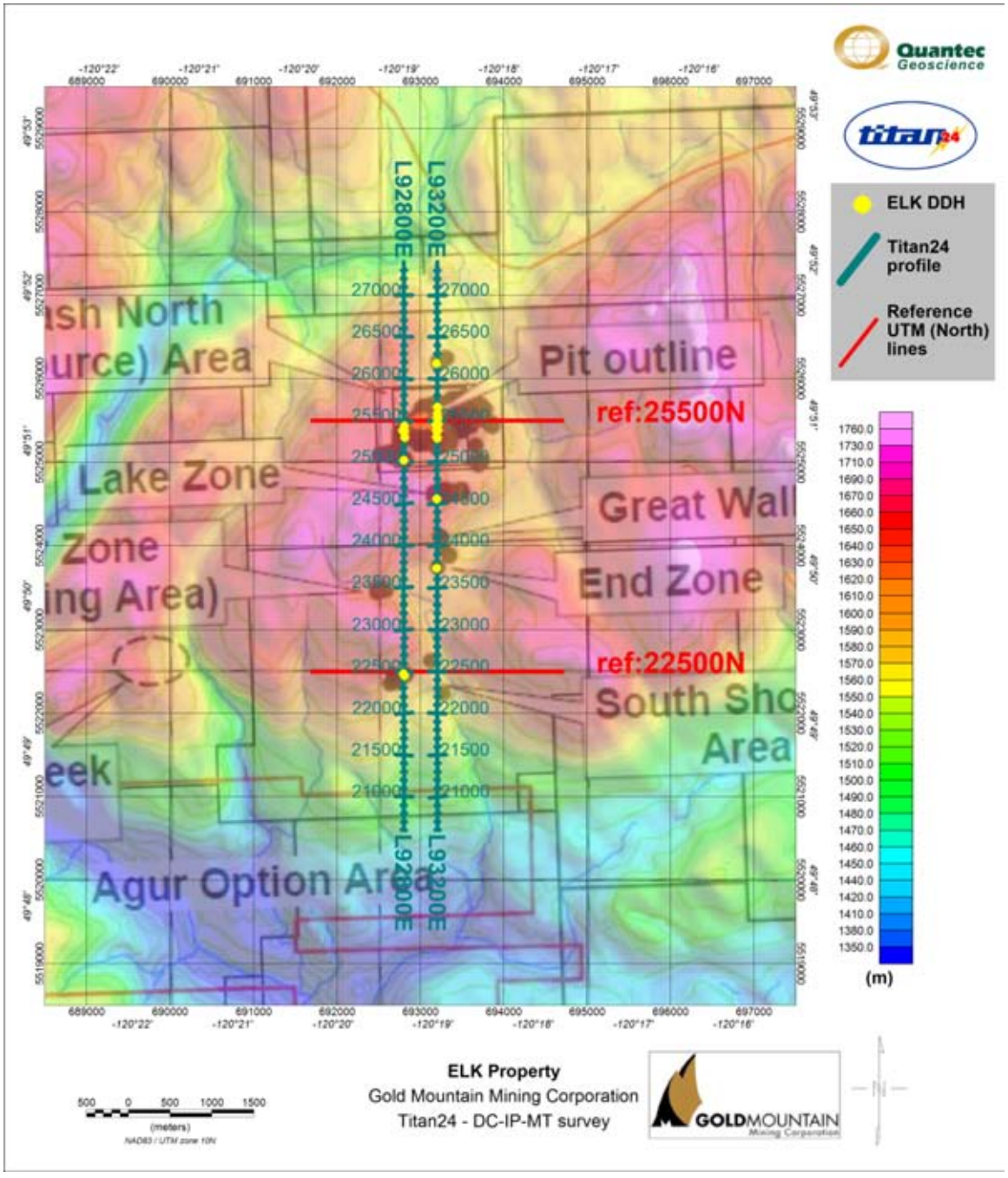

I.1 LINE 28000E

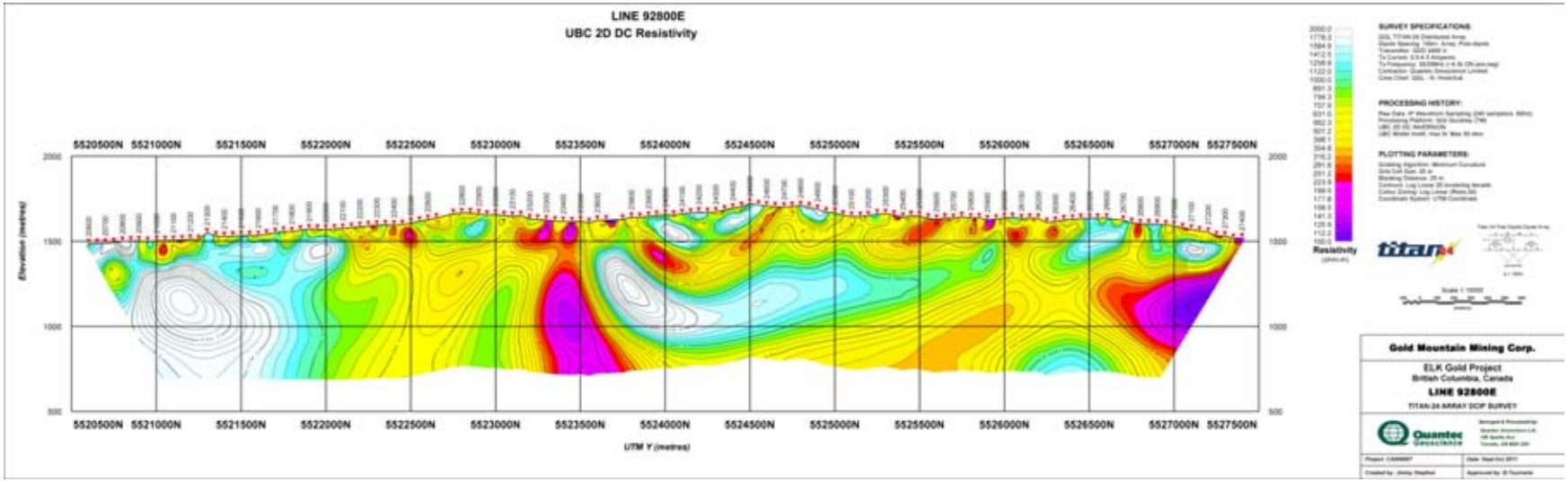

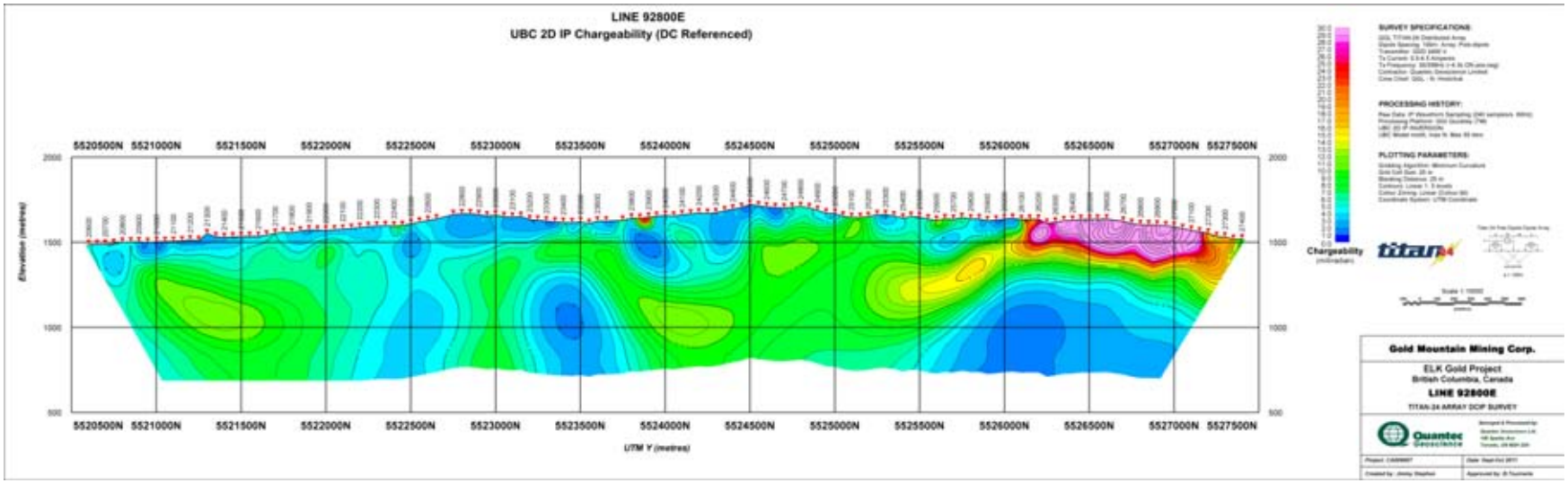
LINE 92800E
UBC 2D IP Chargeability (DC Referenced)
5520500N 5521000N 5521500N 5522000N 5522500N 5523000N 5523500N 5524000N 5524500N 5525000N 5525500N 5526000N 5526500N 5527000N 5527500N
Elevation (metres)
UTM Y (metres)
Chargeability
Gold Mountain Mining Corp.
ELK Gold Project
British Columbia, Canada
LINE 92800E
TITAN-24 ARRAY DCIP SURVEY

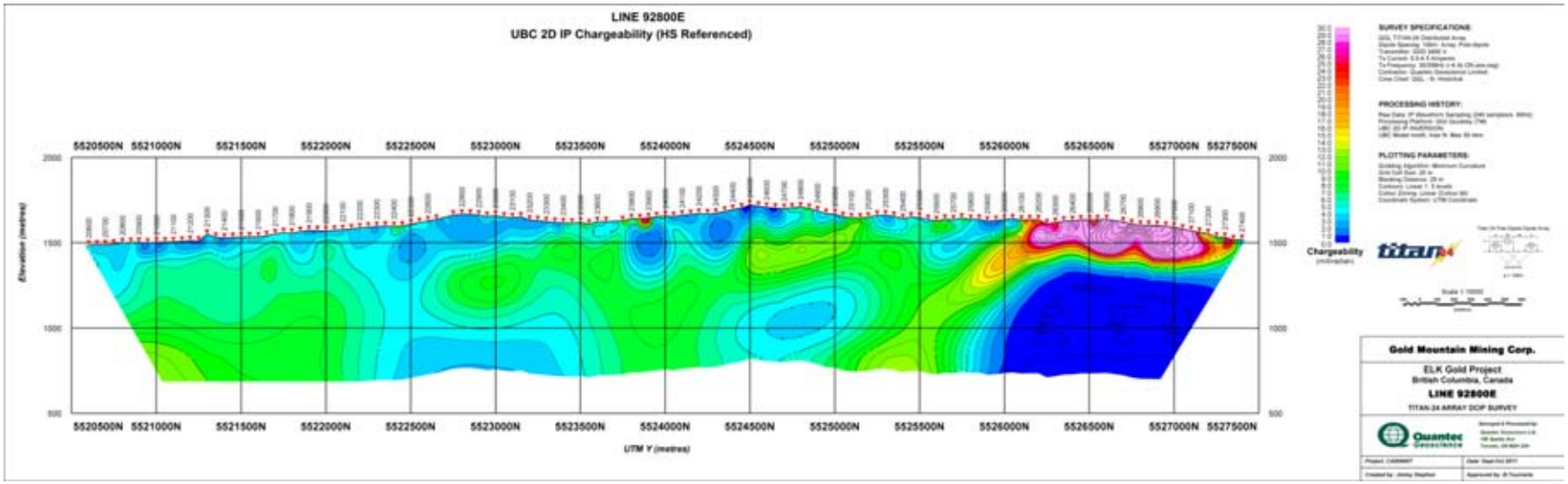
LINE 92800E
UBC 2D IP Chargeability (HS Referenced)
5520500N 5521000N 5521500N 5522000N 5522500N 5523000N 5523500N 5524000N 5524500N 5525000N 5525500N 5526000N 5526500N 5527000N 5527500N
Elevation (metres)
UTM Y (metres)
Chargeability
Gold Mountain Mining Corp.
ELK Gold Project
British Columbia, Canada
LINE 92800E
TITAN-24 ARRAY DCIP SURVEY

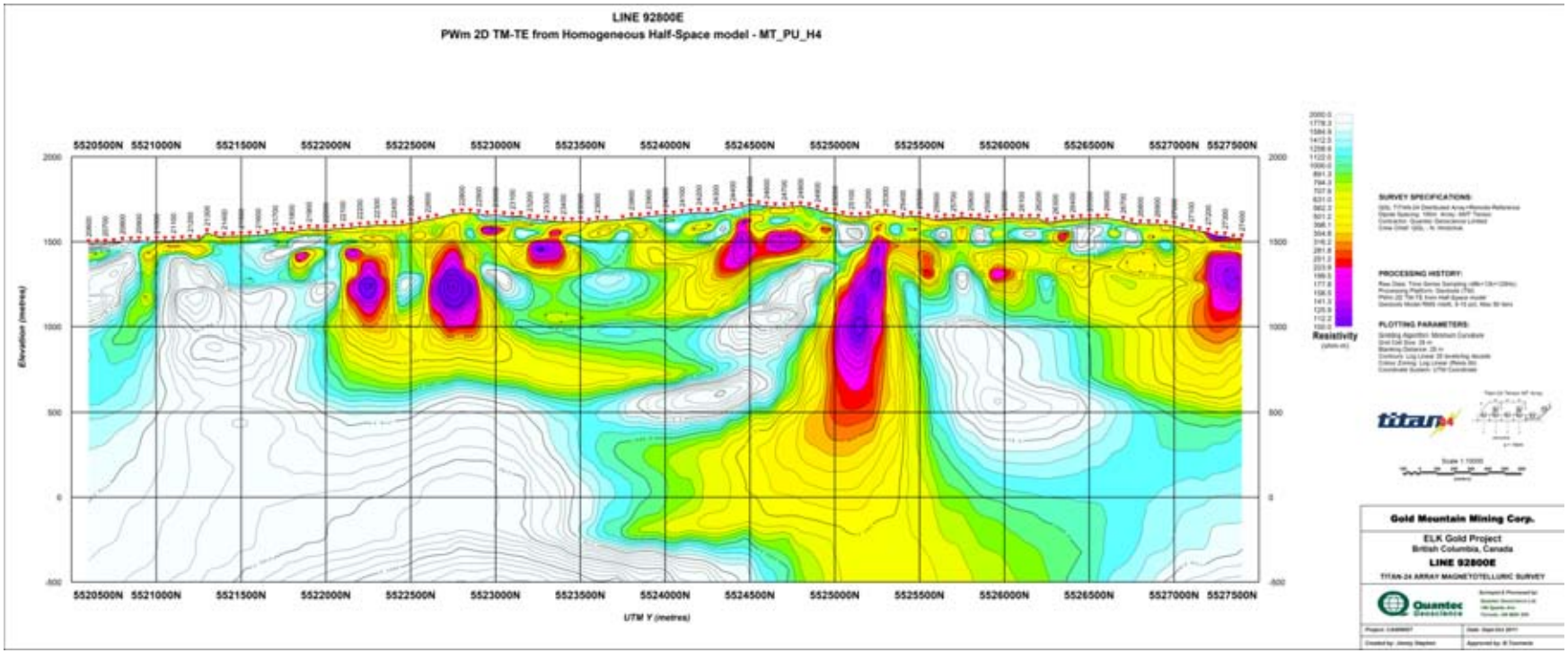
LINE 92800E
PWm 2D TM-TE from Homogeneous Half-Space model - MT_PU_H4
5520500N 5521000N 5521500N 5522000N 5522500N 5523000N 5523500N 5524000N 5524500N 5525000N 5525500N 5526000N 5526500N 5527000N 5527500N
Elevation (metres)
2000
1500
1000
500
0
-500
UTM Y (metres)
Resistivity
SURVEY SPECIFICATIONS:
PROCESSING HISTORY:
PLOTTING PARAMETERS:
titan24
Gold Mountain Mining Corp.
ELK Gold Project
British Columbia, Canada
LINE 92800E
TITAN-24 ARRAY MAGNETOTELLURIC SURVEY
Quantec Geoscience

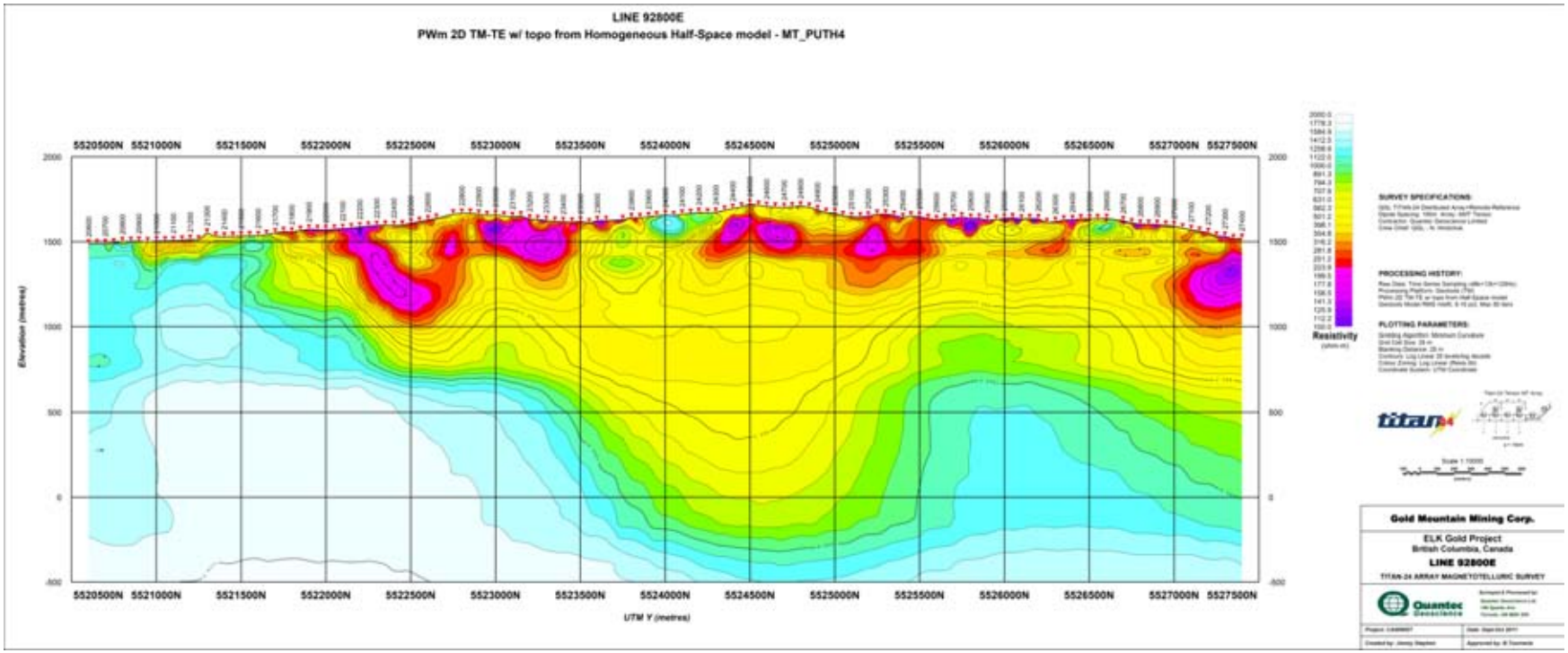
LINE 92800E
PWm 2D TM-TE w/ topo from Homogeneous Half-Space model - MT_PUTH4
5520500N 5521000N 5521500N 5522000N 5522500N 5523000N 5523500N 5524000N 5524500N 5525000N 5525500N 5526000N 5526500N 5527000N 5527500N
Elevation (metres)
UTM Y (metres)
Resistivity
SURVEY SPECIFICATIONS:
PROCESSING HISTORY:
PLOTTING PARAMETERS:
titan24
Gold Mountain Mining Corp.
ELK Gold Project
British Columbia, Canada
LINE 92800E
TITAN-24 ARRAY MAGNETOTELLURIC SURVEY
Quantec Geoscience

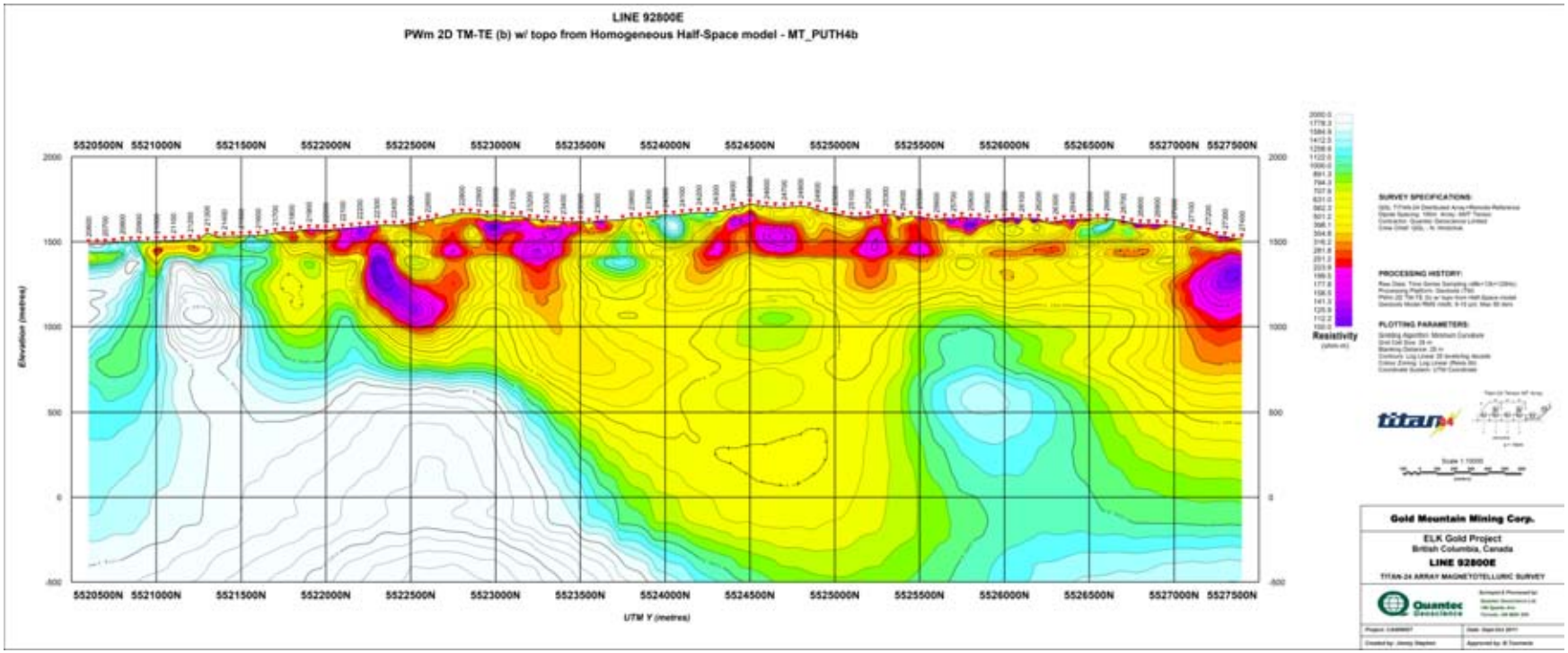
LINE 92800E
PWm 2D TM-TE (b) w/ topo from Homogeneous Half-Space model - MT_PUTH4b
5520500N 5521000N 5521500N 5522000N 5522500N 5523000N 5523500N 5524000N 5524500N 5525000N 5525500N 5526000N 5526500N 5527000N 5527500N
Elevation (metres)
2000
1500
1000
500
0
-500
UTM Y (metres)
Resistivity
SURVEY SPECIFICATIONS:
PROCESSING HISTORY:
PLOTTING PARAMETERS:
titan24
Gold Mountain Mining Corp.
ELK Gold Project
British Columbia, Canada
LINE 92800E
TITAN-24 ARRAY MAGNETOTELLURIC SURVEY
Quantec Geoscience

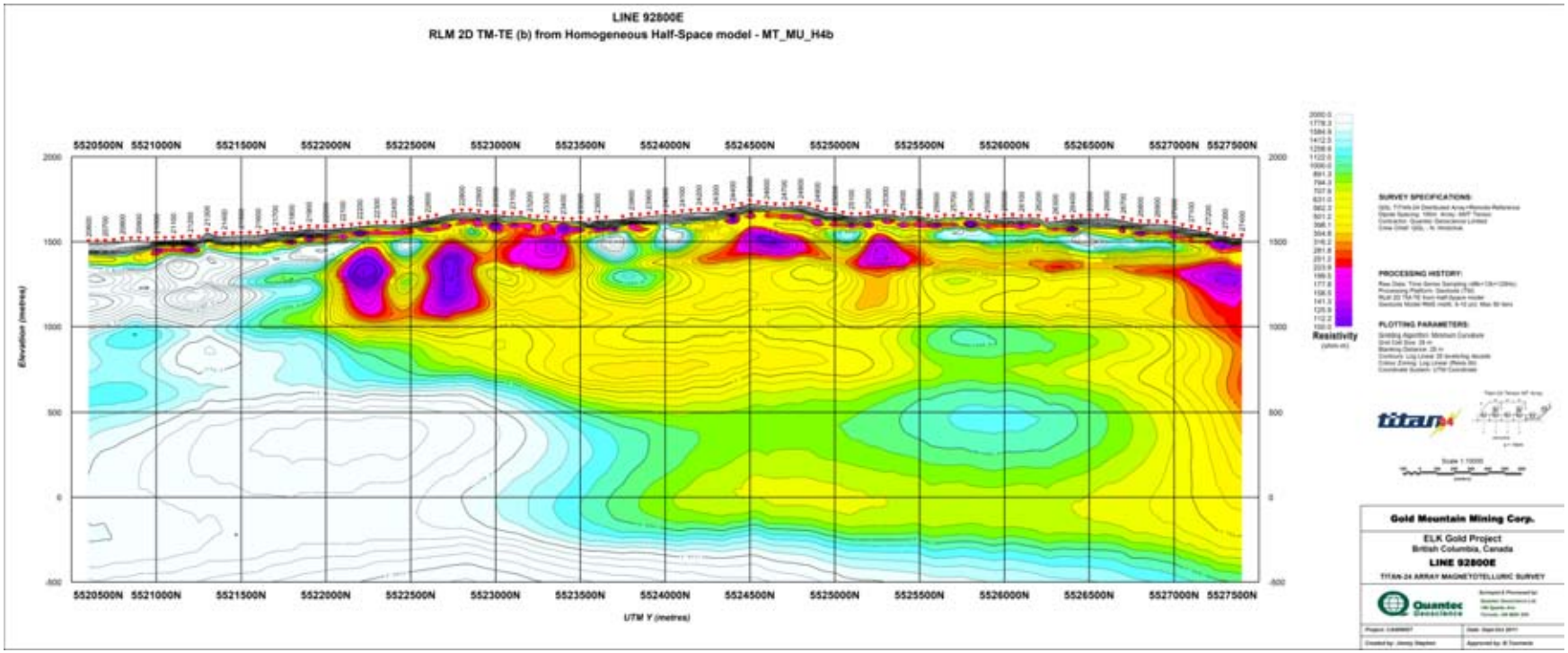
LINE 92800E
RLM 2D TM-TE (b) from Homogeneous Half-Space model - MT_MU_H4b
5520500N 5521000N 5521500N 5522000N 5522500N 5523000N 5523500N 5524000N 5524500N 5525000N 5525500N 5526000N 5526500N 5527000N 5527500N
Elevation (metres)
UTM Y (metres)
Resistivity
titan24
Gold Mountain Mining Corp.
ELK Gold Project
British Columbia, Canada
LINE 92800E
TITAN-24 ARRAY MAGNETOTELLURIC SURVEY
Quantec Geoscience

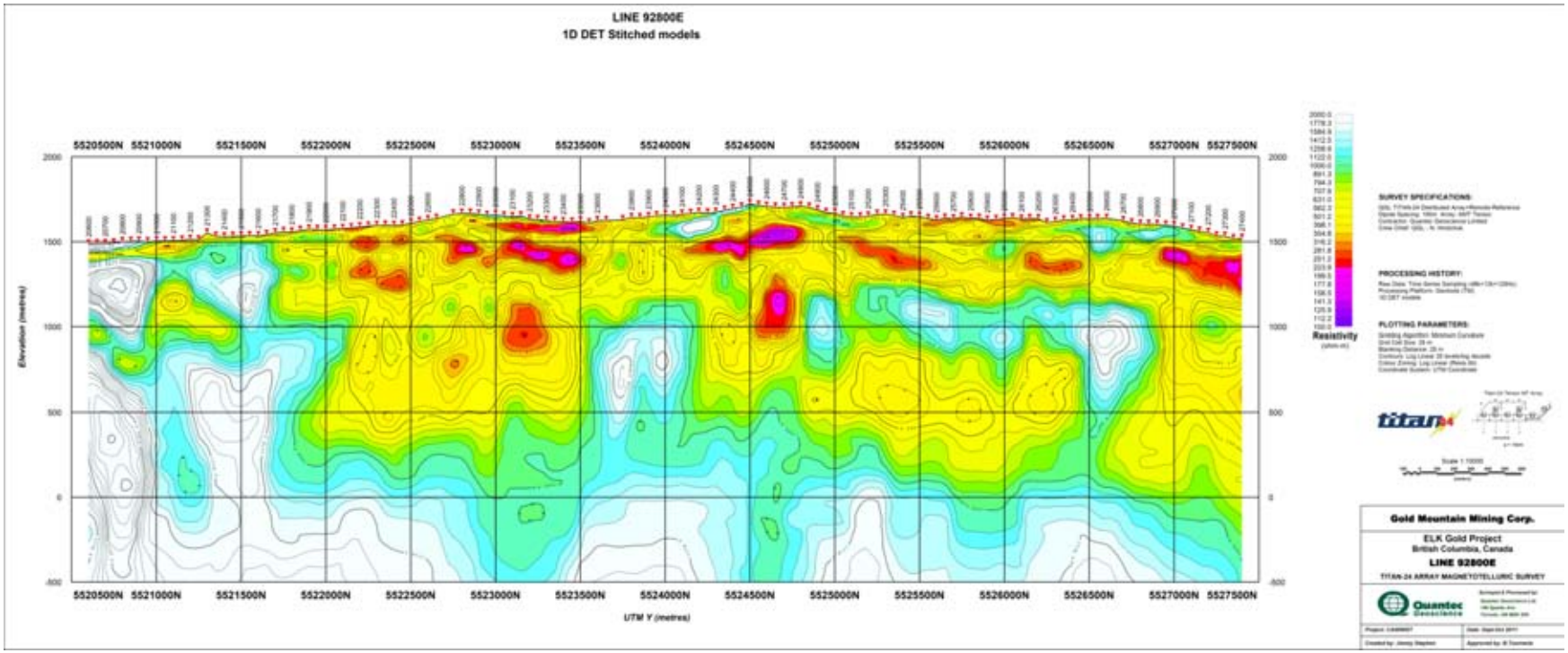
LINE 92800E
1D DET Stitched models
5520500N 5521000N 5521500N 5522000N 5522500N 5523000N 5523500N 5524000N 5524500N 5525000N 5525500N 5526000N 5526500N 5527000N 5527500N
Elevation (metres)
UTM Y (metres)
Resistivity
SURVEY SPECIFICATIONS:
PROCESSING HISTORY:
PLOTTING PARAMETERS:
titan24
Gold Mountain Mining Corp.
ELK Gold Project
British Columbia, Canada
LINE 92800E
TITAN-24 ARRAY MAGNETOTELLURIC SURVEY
Quantec Geoscience

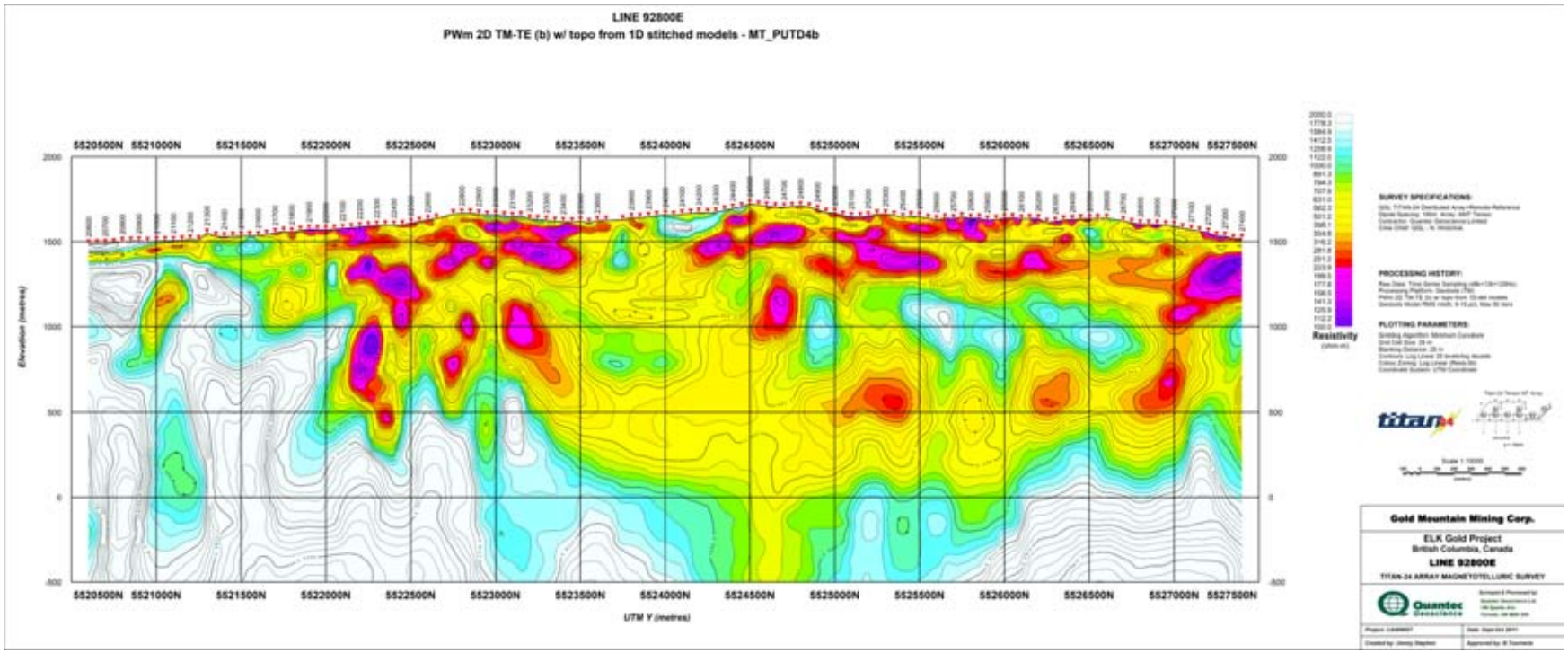
LINE 92800E
PWm 2D TM-TE (b) w/ topo from 1D stitched models - MT_PUTD4b
5520500N 5521000N 5521500N 5522000N 5522500N 5523000N 5523500N 5524000N 5524500N 5525000N 5525500N 5526000N 5526500N 5527000N 5527500N
Elevation (metres)
UTM Y (metres)
Resistivity
SURVEY SPECIFICATIONS:
PROCESSING HISTORY:
PLOTTING PARAMETERS:
titan24
Gold Mountain Mining Corp.
ELK Gold Project
British Columbia, Canada
LINE 92800E
TITAN-24 ARRAY MAGNETOTELLURIC SURVEY
Quantec Geoscience

I.2 LINE 32000E

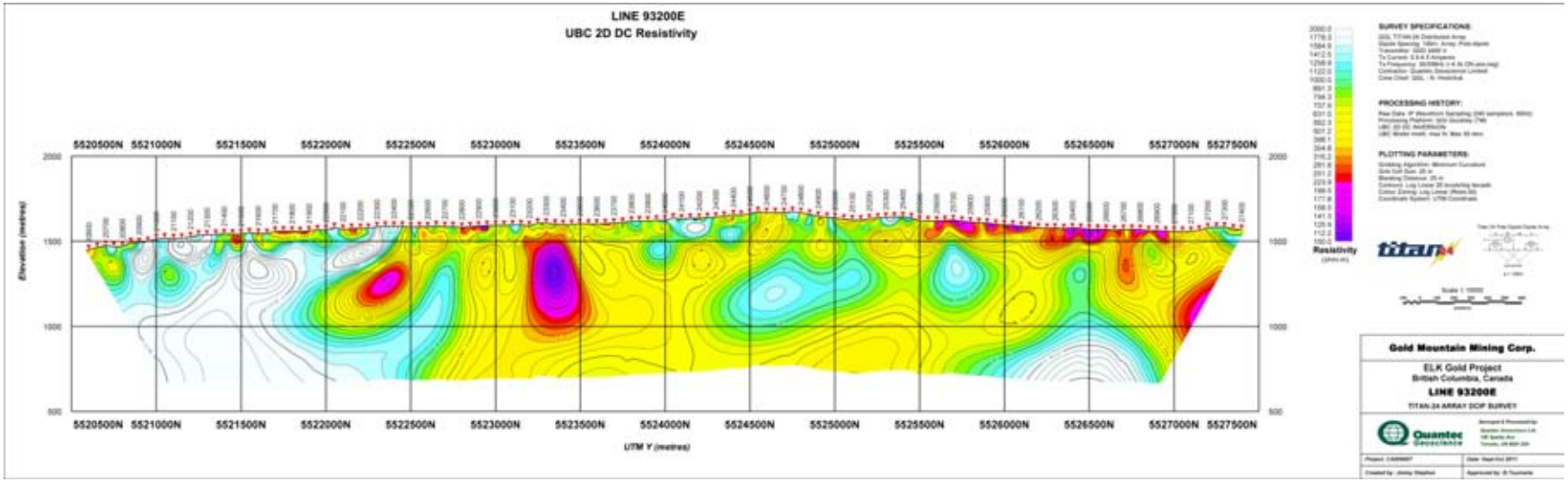

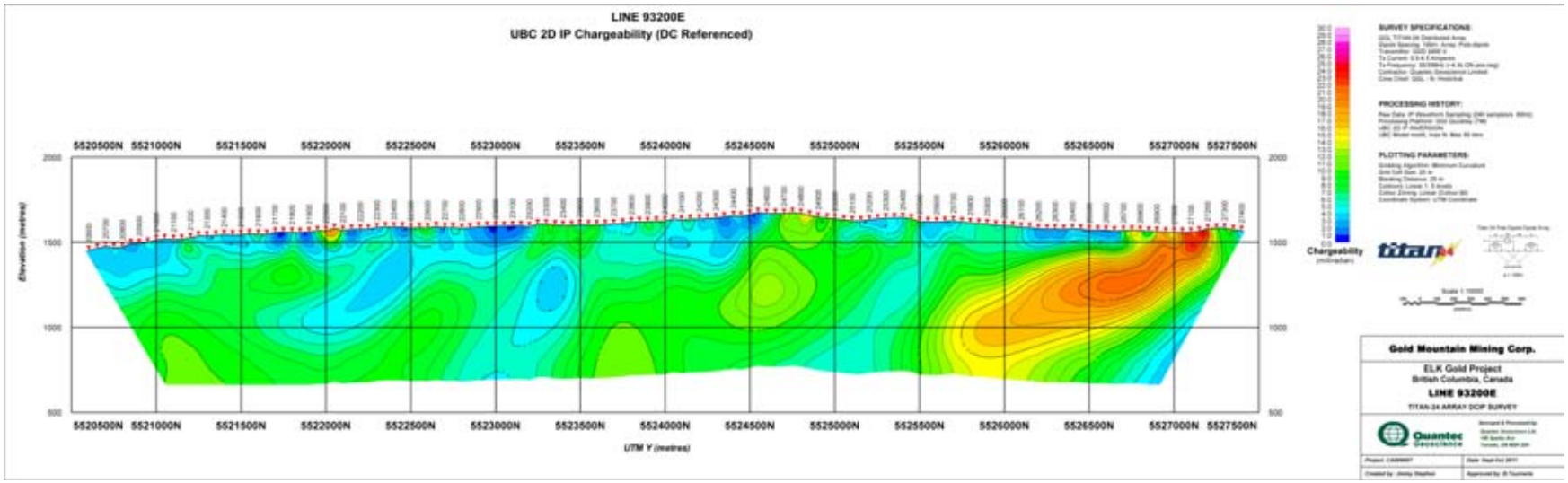
LINE 93200E
UBC 2D IP Chargeability (DC Referenced)
5520500N 5521000N 5521500N 5522000N 5522500N 5523000N 5523500N 5524000N 5524500N 5525000N 5525500N 5526000N 5526500N 5527000N 5527500N
Elevation (metres)
2000
1500
1000
500
UTM Y (metres)
Chargeability
SURVEY SPECIFICATIONS:
PROCESSING HISTORY:
PLOTTING PARAMETERS:
titan24
Gold Mountain Mining Corp.
ELK Gold Project
British Columbia, Canada
LINE 93200E
TITAN-24 ARRAY DCIP SURVEY
Quantec

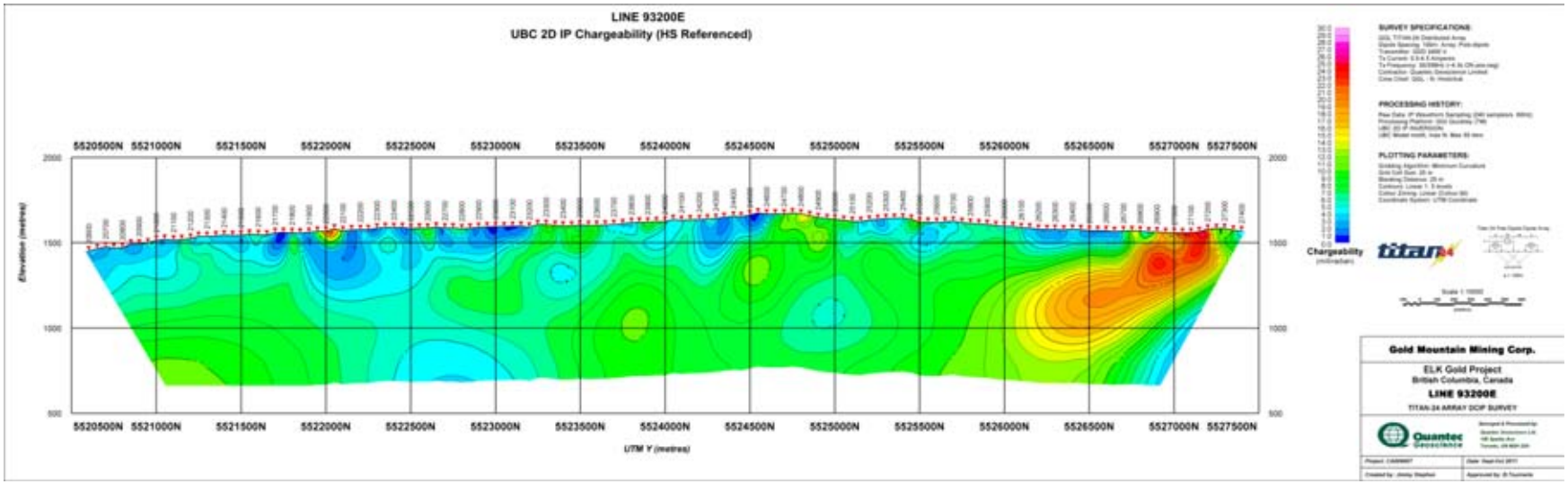
LINE 93200E
UBC 2D IP Chargeability (HS Referenced)
5520500N 5521000N 5521500N 5522000N 5522500N 5523000N 5523500N 5524000N 5524500N 5525000N 5525500N 5526000N 5526500N 5527000N 5527500N
Elevation (metres)
2000
1500
1000
500
UTM Y (metres)
Chargeability
SURVEY SPECIFICATIONS:
PROCESSING HISTORY:
PLOTTING PARAMETERS:
titan24
Gold Mountain Mining Corp.
ELK Gold Project
British Columbia, Canada
LINE 93200E
TITAN-24 ARRAY DCIP SURVEY
Quantec

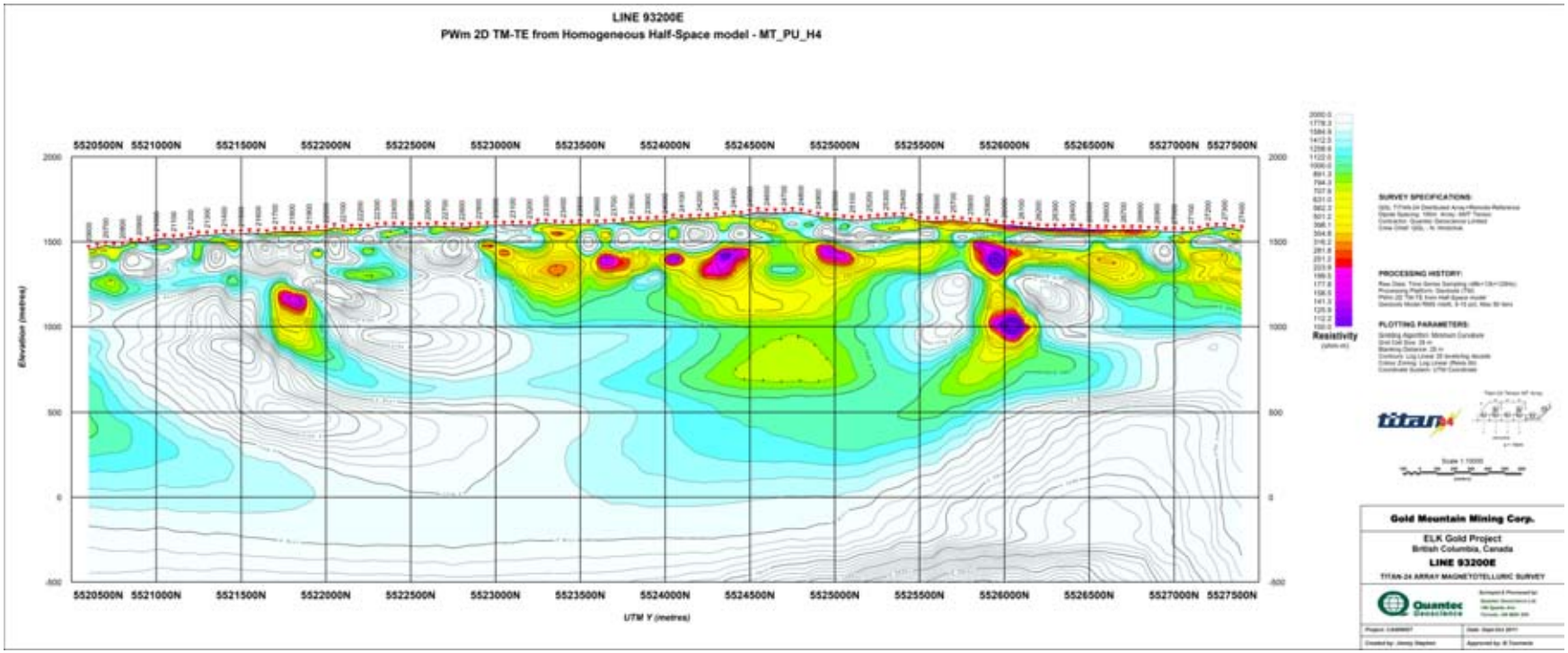
LINE 93200E
PWm 2D TM-TE from Homogeneous Half-Space model - MT_PU_H4
5520500N 5521000N 5521500N 5522000N 5522500N 5523000N 5523500N 5524000N 5524500N 5525000N 5525500N 5526000N 5526500N 5527000N 5527500N
Elevation (metres)
2000
1500
1000
500
0
-500
UTM Y (metres)
Resistivity
titan24
Gold Mountain Mining Corp.
ELK Gold Project
British Columbia, Canada
LINE 93200E
TITAN-24 ARRAY MAGNETOTELLURIC SURVEY
Quantec Geoscience

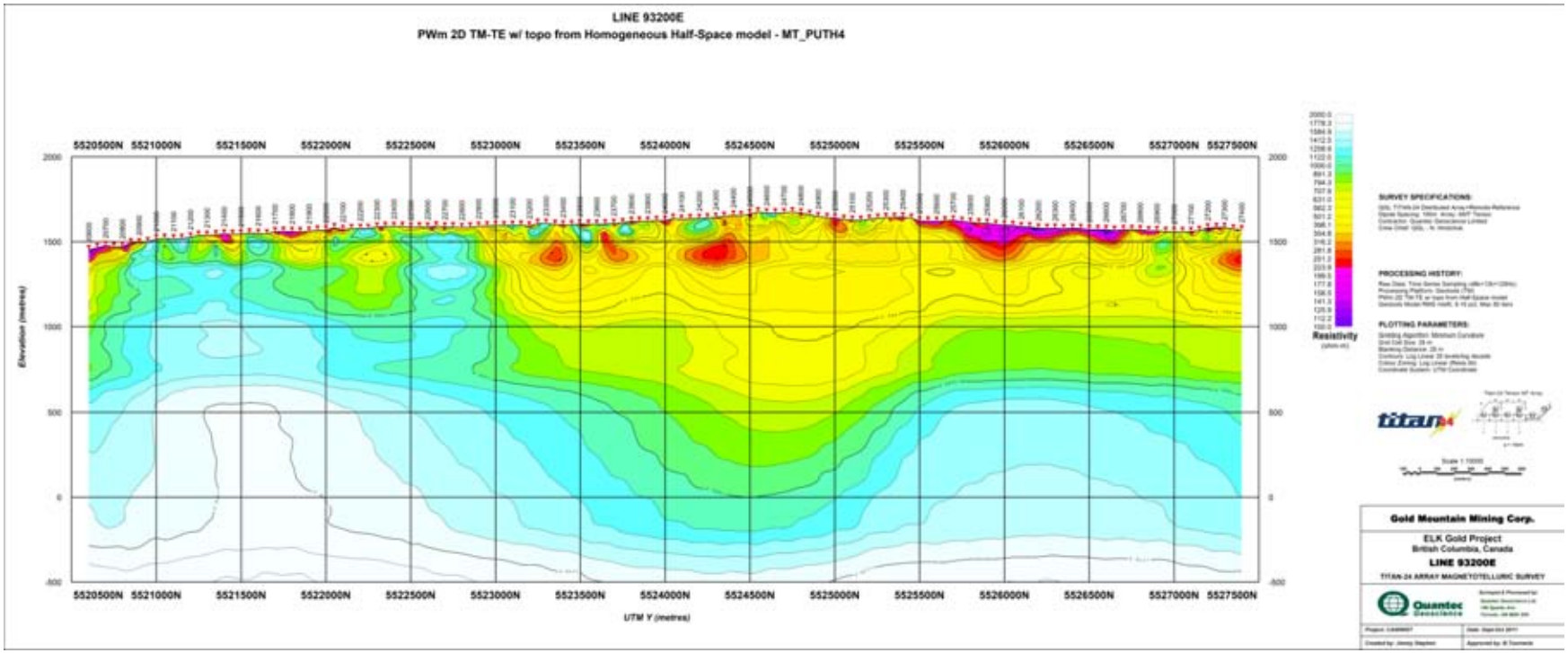
LINE 93200E
PWm 2D TM-TE w/ topo from Homogeneous Half-Space model - MT_PUTH4
5520500N 5521000N 5521500N 5522000N 5522500N 5523000N 5523500N 5524000N 5524500N 5525000N 5525500N 5526000N 5526500N 5527000N 5527500N
Elevation (metres)
UTM Y (metres)
Resistivity
titan24
Gold Mountain Mining Corp.
ELK Gold Project
British Columbia, Canada
LINE 93200E
TITAN-24 ARRAY MAGNETOTELLURIC SURVEY
Quantec Geoscience

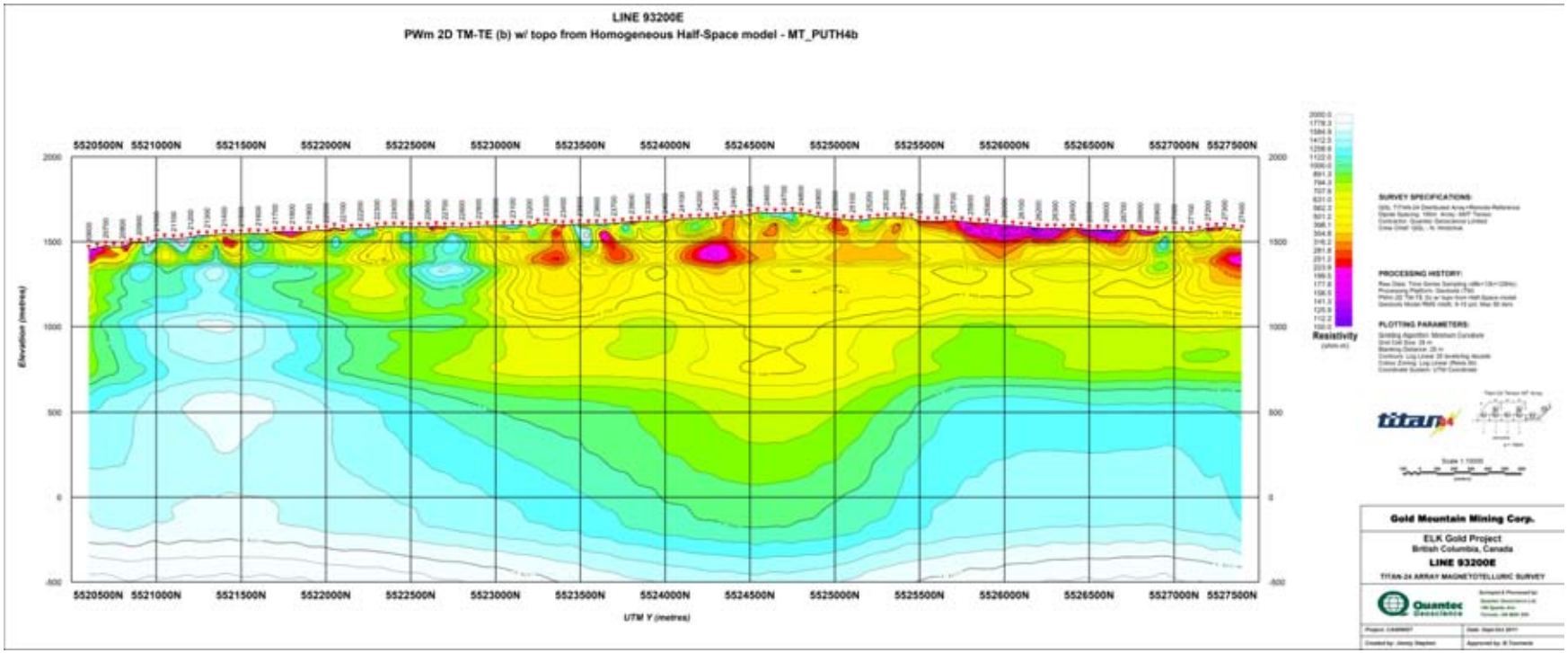
LINE 93200E
PWm 2D TM-TE (b) w/ topo from Homogeneous Half-Space model - MT_PUTH4b
5520500N 5521000N 5521500N 5522000N 5522500N 5523000N 5523500N 5524000N 5524500N 5525000N 5525500N 5526000N 5526500N 5527000N 5527500N
Elevation (metres)
UTM Y (metres)
Resistivity
SURVEY SPECIFICATIONS:
PROCESSING HISTORY:
PLOTTING PARAMETERS:
titan24
Gold Mountain Mining Corp.
ELK Gold Project
British Columbia, Canada
LINE 93200E
TITAN-24 ARRAY MAGNETOTELLURIC SURVEY
Quantec Geoscience

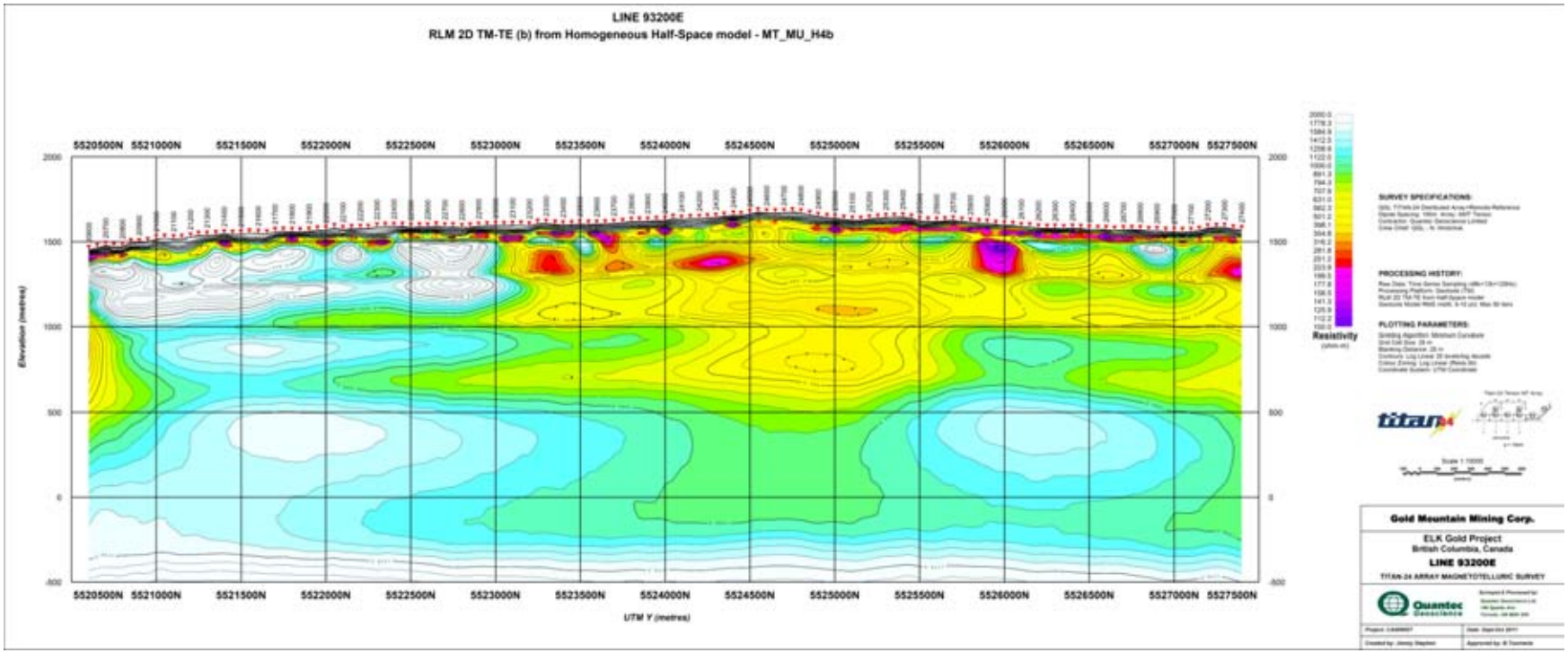
LINE 93200E
RLM 2D TM-TE (b) from Homogeneous Half-Space model - MT_MU_H4b
5520500N 5521000N 5521500N 5522000N 5522500N 5523000N 5523500N 5524000N 5524500N 5525000N 5525500N 5526000N 5526500N 5527000N 5527500N
Elevation (metres)
2000
1500
1000
500
0
-500
UTM Y (metres)
Resistivity
SURVEY SPECIFICATIONS:
PROCESSING HISTORY:
PLOTTING PARAMETERS:
titan24
Gold Mountain Mining Corp.
ELK Gold Project
British Columbia, Canada
LINE 93200E
TITAN-24 ARRAY MAGNETOTELLURIC SURVEY
Quantec Geoscience

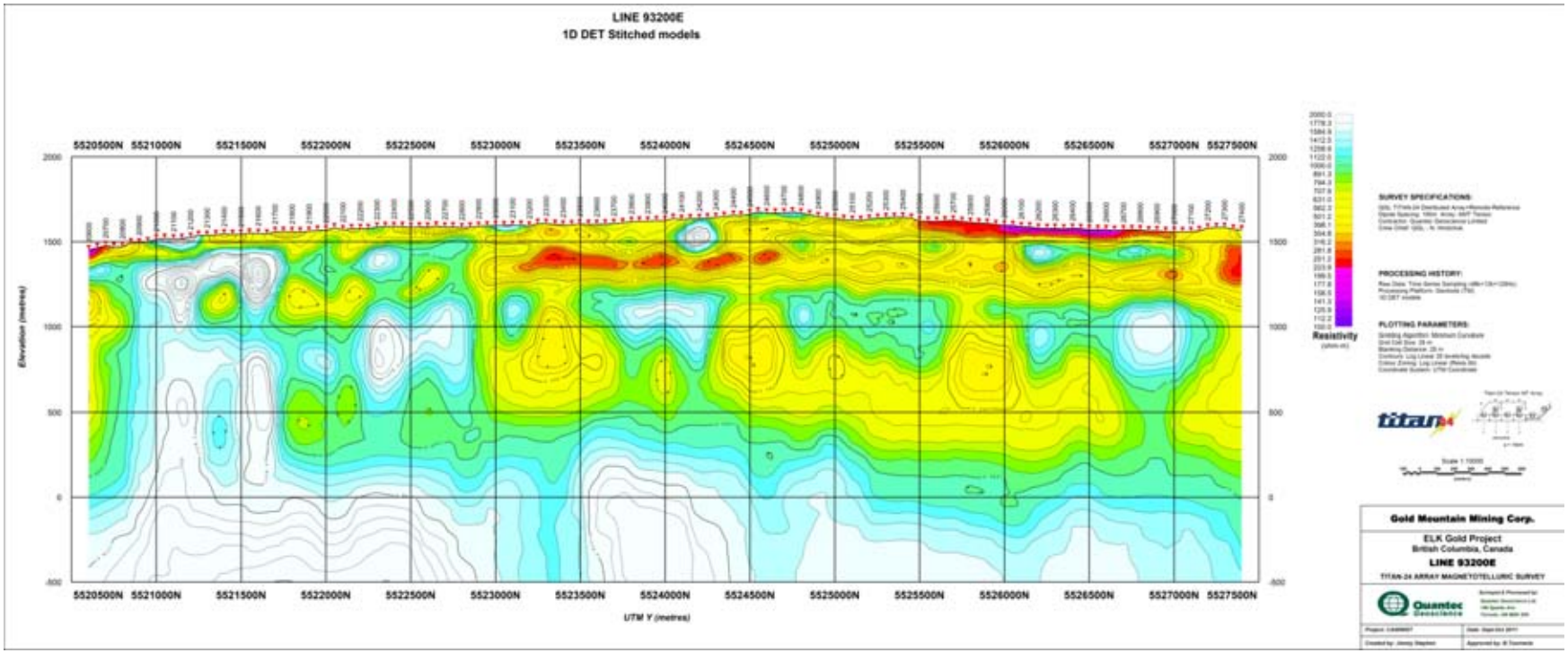
LINE 93200E
1D DET Stitched models
5520500N 5521000N 5521500N 5522000N 5522500N 5523000N 5523500N 5524000N 5524500N 5525000N 5525500N 5526000N 5526500N 5527000N 5527500N
Elevation (metres)
UTM Y (metres)
Resistivity
SURVEY SPECIFICATIONS:
PROCESSING HISTORY:
PLOTTING PARAMETERS:
titan24
Gold Mountain Mining Corp.
ELK Gold Project
British Columbia, Canada
LINE 93200E
TITAN-24 ARRAY MAGNETOTELLURIC SURVEY
Quantec Geoscience

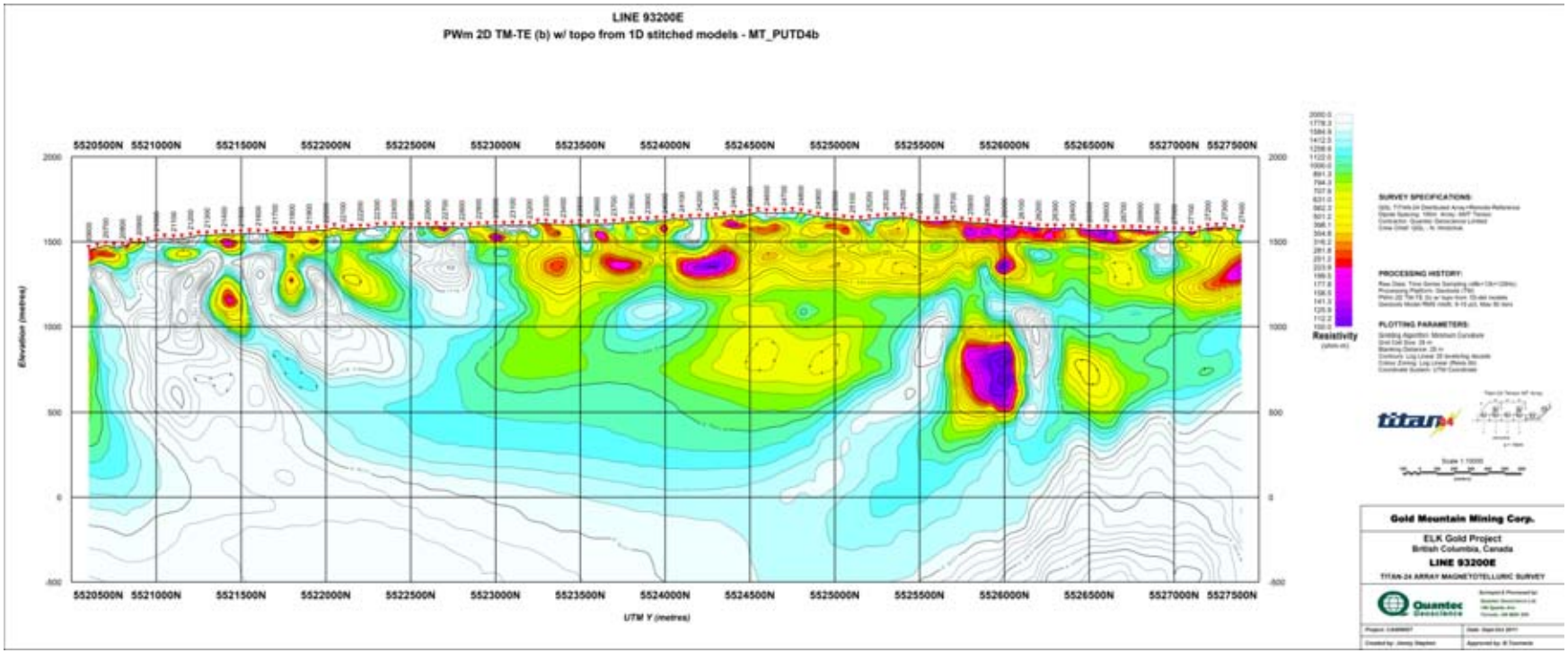
LINE 93200E
PWm 2D TM-TE (b) w/ topo from 1D stitched models - MT_PUTD4b
5520500N 5521000N 5521500N 5522000N 5522500N 5523000N 5523500N 5524000N 5524500N 5525000N 5525500N 5526000N 5526500N 5527000N 5527500N
Elevation (metres)
UTM Y (metres)
Resistivity
titan24
Gold Mountain Mining Corp.
ELK Gold Project
British Columbia, Canada
LINE 93200E
TITAN-24 ARRAY MAGNETOTELLURIC SURVEY
Quantec Geoscience

J AN INTRODUCTION TO TITAN-24 DIRECT CURRENT (DC) RESISTIVITY AND INDUCED POLARISATION (IP) METHODS

J.1 INTRODUCTION

Titan-24 is a 24-bit multi-channel, distributed acquisition system that allows for the collection of high quality Direct Current (DC) Resistivity and Induced Polarization (IP) data (Sheard 1998). The system provides high multiplicity data sets and records full-waveform time-series utilizing 24-bit Sigma Delta Analog to Digital (A/D) conversion. Like other conventional resistivity methods, acquisition is performed by the injection of an artificial controlled source of current, usually a series of full duty cycle[14] square pulses, into the ground through the transmitter electrode. The voltages, normalized by the injected current, are measured at the receiver electrodes as time series.

The use of 24-bit A/D converter allows the Titan-24 system to record the full waveform at the receivers, thus permitting the accurate removal or deconvolution of the source effects from the recorded time series. What is left of the time series after the deconvolution consist of mainly the responses of the ground and noise.

DC resistivity method is quite sensitive to small variations in resistivity near surface, and its effectiveness will be limited by high level of noise in the presence of a shallow conductive layer in the ground. On the other hand, in the desert or coarse-grained sandy environments, DC resistivity method can suffer from poor electrical contact with the ground. As a result, very little or no current can be injected into the ground, and no meaningful data can be collected.

The resistivity is among the most variable of all geophysical parameters, with a range exceeding 10^6 ohm-m. The resistivity of rocks depends primarily on their porosity, permeability and particularly the salinity of fluids contained, according to Archie's Law. Therefore, DC resistivity method can be utilized in a wide variety of applications in mineral exploration, mainly for mapping of resistivity structures and locating of conductive targets.

The chargeability responds to the presence of polarisable minerals (metals, sub-metallic sulphides and oxides, and graphite), in minute amounts. Both the quantity of individual chargeable grains present and their distributions within subsurface current flow paths are significant in controlling the level of response. The IP method can be used to directly detect disseminated to massive sulphides.

More detailed descriptions on the theory and application of the DCIP method can be found in Telford et al. (1976).

[14] Duty cycle is the ratio between the pulse duration and the period of a square waveform.

J.2 TITAN-24 DCIP SURVEY

Titan-24 is a distributed DCIP acquisition system. A typical survey layout, or spread, is 2400m long and has 25 inline (Ex) 100m potential dipoles and the current injections sites. With current extensions, a typical Titan-24 spread can be stretched to 3600m. If requested, the dipole length can be changed to 50m or 200m, and the resulting length Titan-24 spread will be 1200m or 4800m. Also, cross line dipoles (Ey) can be deployed as well.

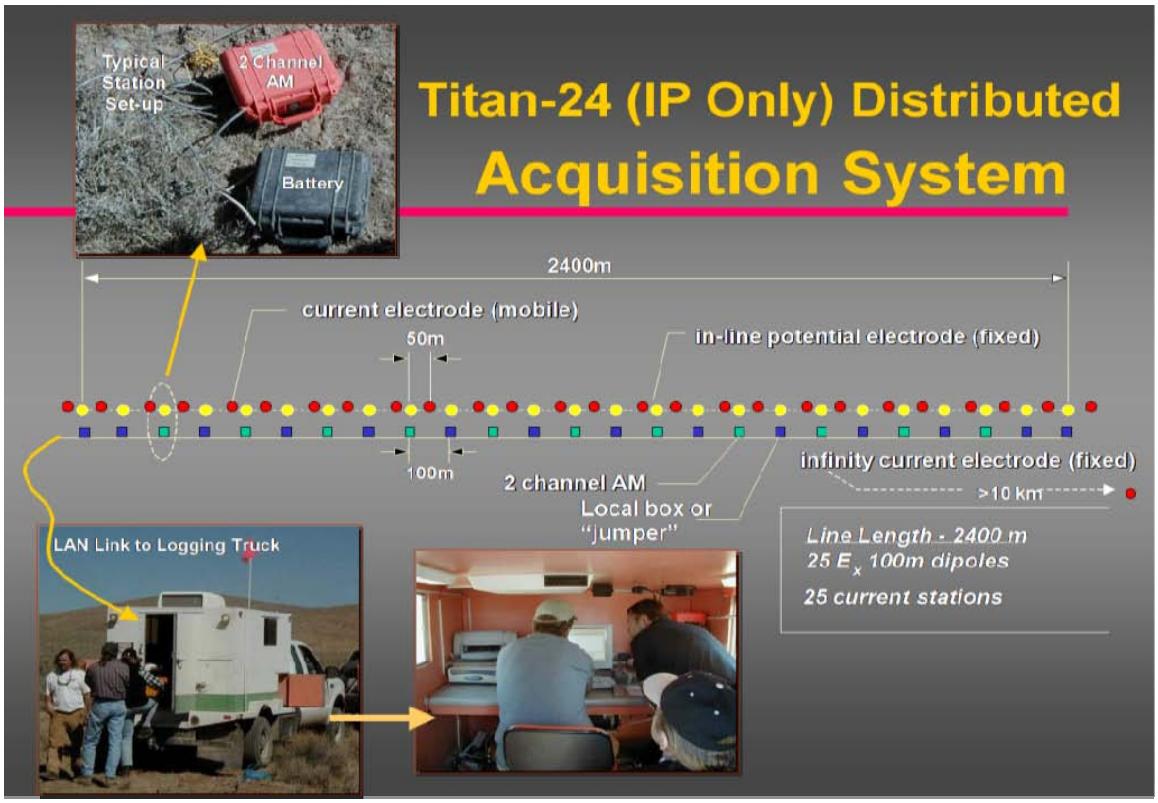

Titan-24 Distributed Acquisition System (IP-only) layout.

In a normal Titan-24 survey, the transmitter (Tx) and receiver (Rx) configuration is the pole-dipole-dipole array, combining pole-dipole right (PDR) and pole-dipole left (PDL). The current is injected at the mid-point between two potential electrodes. However, with special safety arrangements made to the system, the current can be injected at the potential electrode locations.

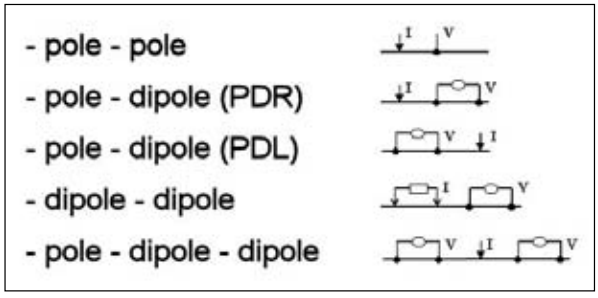

Titan-24 Transmitter (Tx) and Receivers (Rx) configurations.

J.3 TITAN-24 DCIP DATA PROCESSING

For one potential electrode pair, the data acquired with one current injection event is a time series of measured voltages at the electrodes normalized by the current, Vp in mV/A. A typical Titan-24 time series are shown below.

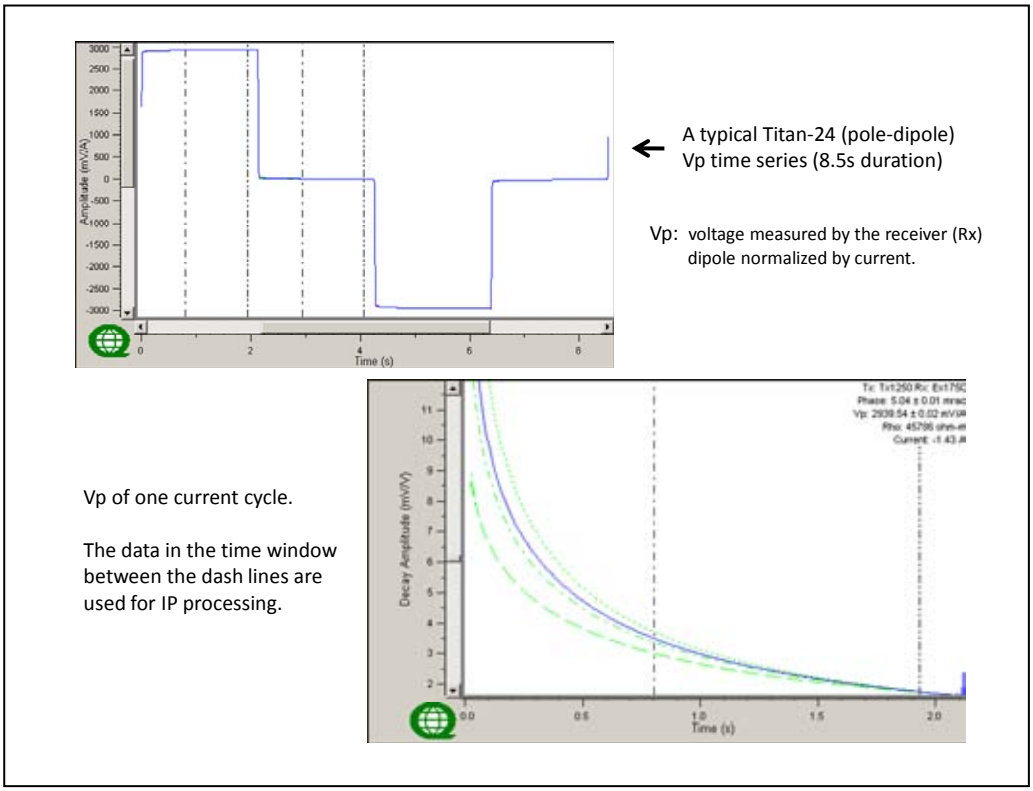

Typical Titan-24 DCIP time series.

A single injection event usually lasts approximately three minutes. The time series of an event are stacked twenty times per second in order to increase the signal to noise (S/N) ratio. The data processing is done in the frequency domain. Current waveform deconvolution and digital filtering of power line noise (60/50Hz, and their harmonics) are applied to the frequency domain data.

J.4 HALVERSON-WAIT CHARGEABILITY

Titan-24 IP chargeability are described using the Halverson-Wait spectral model (Halverson et al., 1981), which is not well known, but is similar to the Cole-Cole model proposed by Pelton et al. (1978) which is a simple relaxation model that fits complex (frequency-dependant) resistivity results.

The time domain chargeability, originally proposed by Siegel (1959), is defined (Telford et al., 1976) as:

$$M = \frac{1}{V_c}\int_{t1}^{t2} V(t)dt$$

where $V(t)$ is the residual or secondary voltage at a time t that is decaying after the current is cut off, between time t_1 and t_2 with the steady voltage V_c during the current flow interval. The ratio $V(t)/V_c$ is expressed in millivolts per volts (mV/V).

In the frequency domain, the "frequency effect" is defined as:

$$FE = \frac{(\rho_{DC} - \rho_{AC})}{\rho_{AC}}$$

where ρ_{DC} and ρ_{AC} are the apparent resistivity's measured at DC and "very high" frequency, usually in the 0.1 to 10 Hz range.

The Cole-Cole model for the chargeability m, as defined by Pelton et al. (1978) is given by the following:

$$Z(\omega) = R_0\left[1 - m\left(1 - \frac{1}{1+(i\omega\tau)^C}\right)\right]$$

where $Z(\omega)$ is the complex impedance with ω the angular frequency in Hz, R_0 the DC resistivity, m the chargeability in volts per volt, τ the time constant in seconds, and c is the frequency dependence (unit less). The latter two physical properties describe the shape of the decay curve in time domain or the phase spectrum in frequency domain, and commonly range between 0.01s to +100s and 0.1 to +0.5, respectively (Johnson, 1984).

The Halverson-Wait model was proposed by Halverson et al. (1981) as an extension to the Wait (1959) model of the impedance of "volume loading" of spheres, given by:

$$Z(\omega) = \frac{\rho}{G}\left[1 - 3\nu\left(1 - \frac{3\delta}{1+2\delta}\right)\right]$$

where G is a geometric factor, ρ the resistivity of the media, ν the volume loading (the volume fraction of chargeable "spheres"), δ the sphere surface impedance. The Wait model was designed to provide an explanation of the differences in the shape of decay curves from different polarisable targets, but does not describe very well the physical attributes of the rocks.

The Halverson-Wait model expands the Wait coated sphere IP model to include a new formulation of the sulphide-rock interface impedance, based on field studies and laboratory tests on samples. It is closely correlated to the Pelton et al. (1978) Cole-Cole model and is given by:

$$Z(\omega) = \frac{\rho}{G}\left[1 - 3\nu\left(1 - \frac{3/2}{1+r[i\omega]^K}\right)\right]$$

where r is the sphere radius and is equivalent to τ - the Cole-Cole time constant ($r = \tau^K$). The volume loading ν compares well to m, the Cole-Cole chargeability (see equation below), and the exponent K is equal to c, the Cole-Cole frequency dependence (Halverson et al., 1981). For sulphide systems, the r -factor reflects the size or inter-connectedness of the sulphide grains and the K -factor reflects the electrical characteristics of the sulphide surfaces.

An example of time domain Halverson-Wait model responses is shown below:

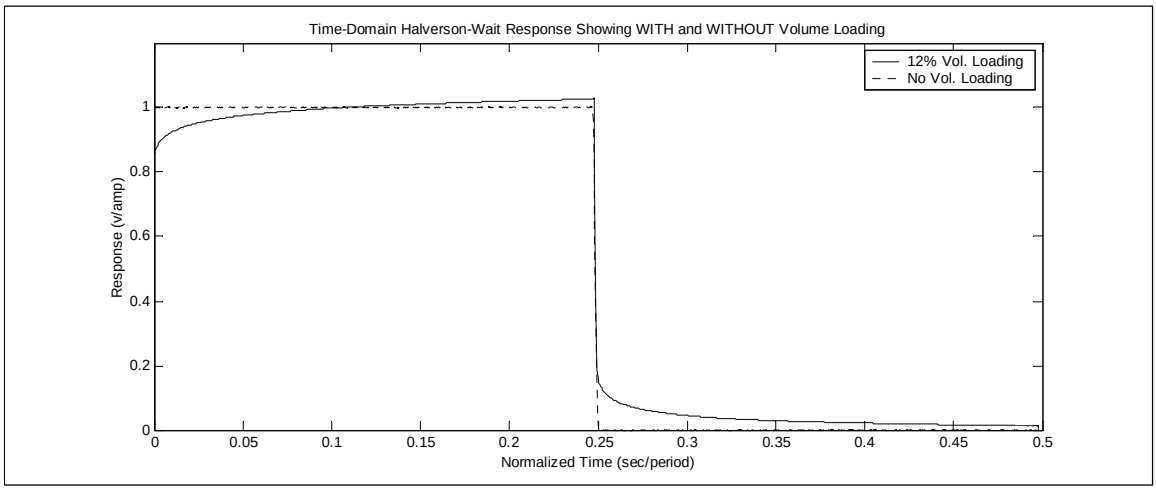

Polarisable versus Non-Polarisable TD-IP response using Halverson-Wait Model.

In the Halverson-Wait model the theoretical Percentage Frequency Effect (PFE)[15] (for infinite bandwidth), which equates to the theoretical chargeability in the Cole-Cole equation, is thereby defined by the volume loading:

$$\frac{PFE_0^{\infty}}{100} = m_0 = \frac{9v}{(2+3v)}$$

and m is output in units of milliradians (mrads).

J.5 TITAN-24 IP CHARGEABILITY DEFINITION (QTN001)

Quantec prefers to estimate IP responses using a time domain half-duty square-wave excitation standard, but convert those chargeability results to units of phase. The specific procedure and algorithm is as follows:

1. Determine the earliest time for which EM coupling has died out sufficiently. This time is called the averaging or integration *start time* t_0. A typical value for t_0 is 0.8s;
2. Determine the latest charge/decay time that is minimally affected by sigma-delta and low-pass (usually Hanning window moving average) filtering, called the averaging or integration *end time* t_1. A typical value for t_1 is 1.95s;
3. Adjust the *start time* (t_0) so that $t_1 - t_0$ (equated to number of samples) exactly spans an integer number of power-line signal periods. This can only be done for transmitted (fundamental) frequencies that are much lower than the power-line frequency;
4. Using the charge and decay sample numbers that equate to the averaging window[16] defined by t_0 and t_1, calculates the average charge and decay voltages. This average may

[15] The classical definition of PFE is $100 \times (\rho_0 - \rho_\infty) / \rho_0$.

[16] In practice this averaging window is tapered slightly to widen the stop-band notches and thereby provide enhanced power-line noise rejection.

involve a non-uniform weighting to further improve rejection of power-line noise;

5. Calculate the theoretical Halverson-Wait half-duty time-domain response using identical filtering to that applied to the measured data response estimate, and presuming the following spectral parameters:
   a. volume loading: 0.125 (this value is not important)
   b. r – value: 1.0
   c. k – value: 0.2
6. For the standard Halverson-Wait spectral parameters mentioned, the synthesized time-domain response and the $t_1 - t_0$ averaging window, convert all estimated/measured charge and decay voltages (using the specified averaging window) to chargeability (millivolts/volt) and then to phase (milliradians).

This is the algorithm used in the Titan-24 data processing. The relationship between Titan-24 chargeability unit, phase in milliradians, and other frequency domain systems is straightforward – Quantec's time-domain based phase equates to frequency domain based phase, see figures below.

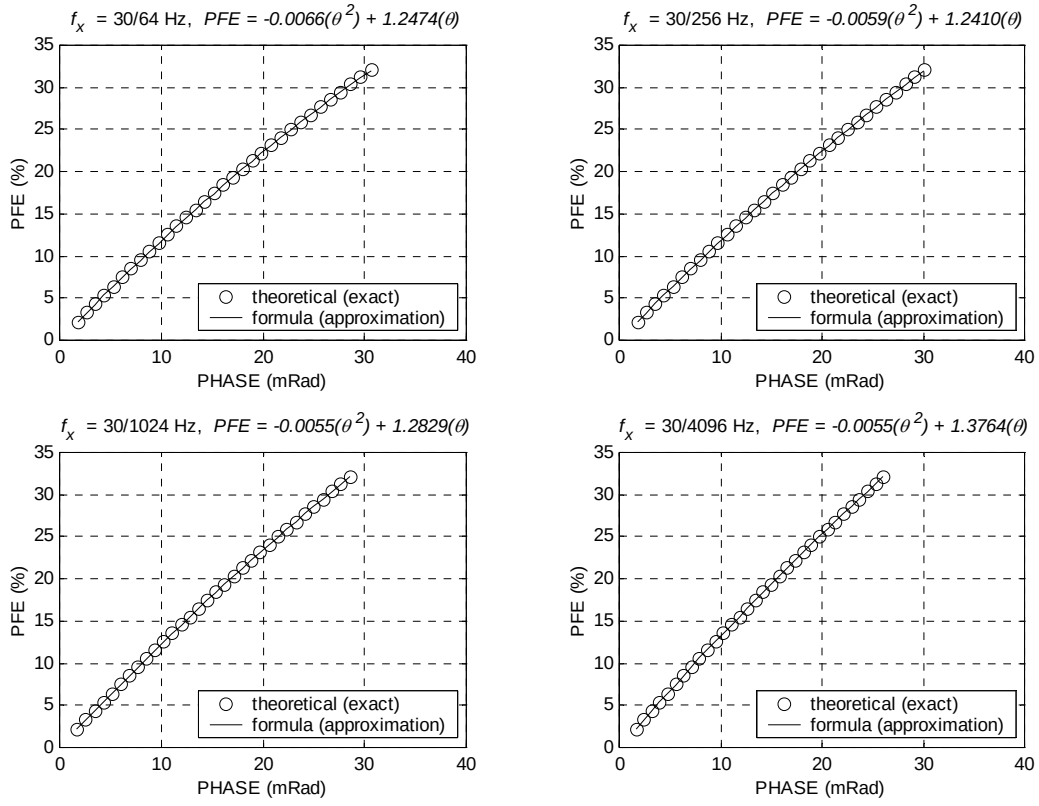

Phase vs. PFE for various pulse lengths and presuming standard Halverson-Wait spectral parameters (r-value = 1.0 and k-value = 0.2).

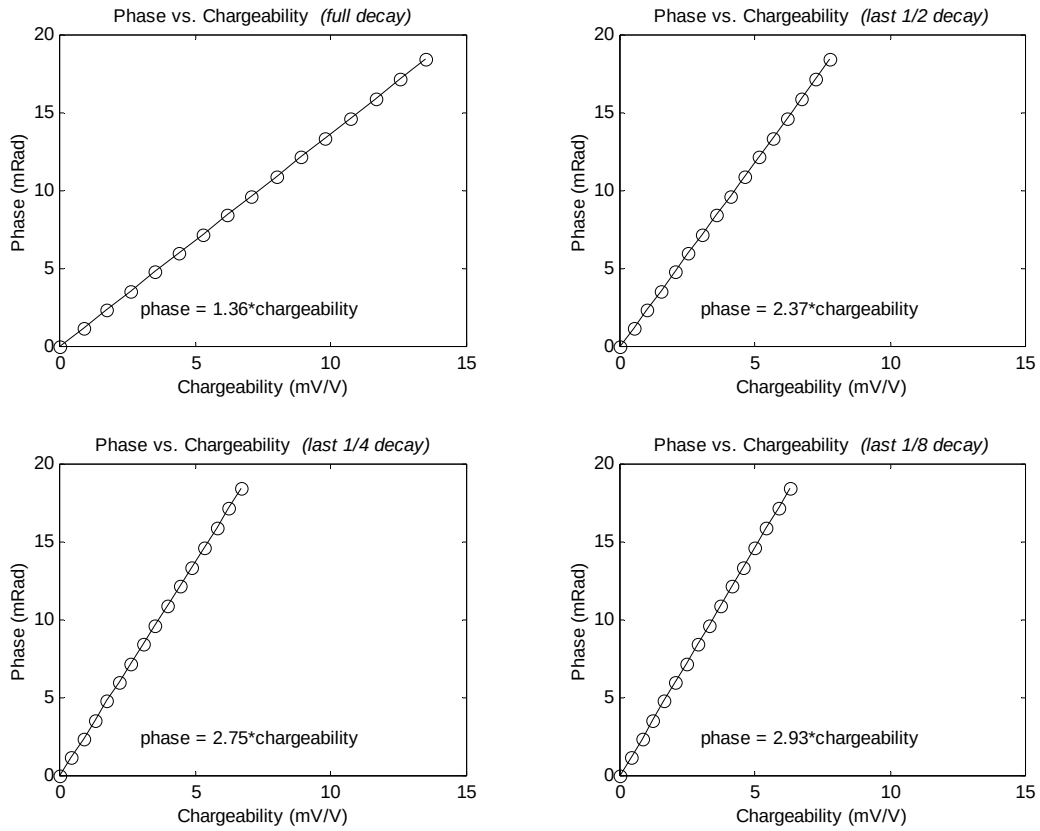

Illustration of the proportional relationship between phase (mrad) and chargeability (mV/V) for various charge/decay averaging windows

J.6 DCIP2D INVERSION

An excellent overview and introduction to both the theory and use of inversions in geophysics is available on the University of British Columbia (UBC) website (Oldenburg et al., 1998).

The DCIP2D inversion algorithms are developed by UBC-Geophysical Inversion Facility.

Mathematically, inversion is the process of fitting the observed data to a model through minimizing a function. The choice of which function to minimize ultimately defines the inversion model. In the inversion algorithm developed by UBC, this function is:

$$\phi = \phi_d + \beta \phi_m = \text{(misfit)} + \beta\,\text{(model norm)}$$
$$0 < \beta < \infty \quad \text{is a constant}$$

The function to be minimized consists of a function, ϕ_d, that minimizes the data misfit, and a function ϕ_m that finds a "smooth" model. Beta, the regularization parameter, represents a relative weighting between fitting the data and smoothing the model.

Clearly, the data misfit function must be defined in more detail. One approach might be

$$\phi_d = \sum_{i=1}^{N} \left(\frac{F_i[m] - d_i^{obs}}{\varepsilon_i} \right)^2 .$$

This function defines the data misfit as the sum of the individual misfits squared (L2 norm), normalized by the errors associated with each data point. It is the least-squares definition of the data misfit.

The model misfit function must also be defined in more detail. One of the most flexible definitions is the one used by UBC

$$\phi_m(m,m_0) = \alpha_s \int_{vol} (m-m_0)^2 dv + \alpha_x \int_{vol} \left(\frac{\partial (m-m_0)}{\partial x} \right)^2 dv + \alpha_z \int_{vol} \left(\frac{\partial (m-m_0)}{\partial z} \right)^2 dv$$

In this definition there are three components to the "model norm" (or "smoothness" constraint, or "regularization"), each of which contains an α constant (α_s, α_x, α_z) that are commonly referred to as "alpha parameters", and a fourth variable m_o that refers to the starting or reference model – either a half-space or geophysical constraint – that also has a profound influence on the model-misfit.

The three "alpha" parameters represent a relative weighting of each component:

- the first component is simply an overall difference between the model and a "target" model;
- the second component is a horizontal smoothness;
- the third component is a vertical smoothness.

J.7 APPARENT RESISTIVITY OF UNIFORM HALF SPACE

From p.636, Telford et al. 1976, the apparent resistivity ρ_a is given as:

$$\rho_a = \frac{2\pi V_p}{G_f}$$

where G_f is the geometric factor defined as:

$$G_f = \left(\frac{1}{r_1} - \frac{1}{r_2}\right) - \left(\frac{1}{r_3} - \frac{1}{r_4}\right)$$

with:

r_1 the distance between current electrode P1 and potential electrode C1;

r_2 the distance between current electrode P1 and potential electrode C2;

r_3 the distance between current electrode P2 and potential electrode C1;

r_4 the distance between current electrode P2 and potential electrode C2;

J.8 DC INVERSION USING A SYNTHETIC MODEL

A synthetic resistivity model and its apparent resistivity pseudo section based on Titan-24 configuration are shown here. The model consists of a background of 1,000 ohm-m and a vertical dyke of 1 ohm-m. The synthetic DC data, V_p's, are computed using UBC's 2D forward modeling tool DCIPF2D

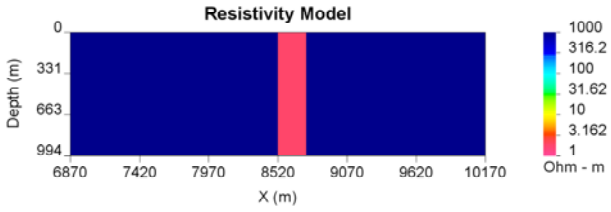

1,000 ohm-m background and 1 ohm-m vertical conductor

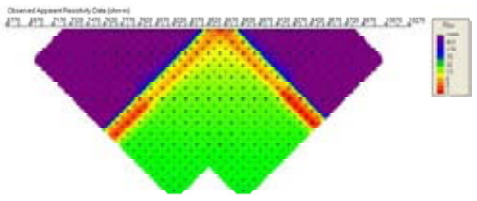

DC Resistivity Pseudo Section
Titan-24 pole-dipole with 500m current extensions

A synthetic model and its apparent resistivity pseudo section

The inverted resistivity model and the convergence curves are displayed below.

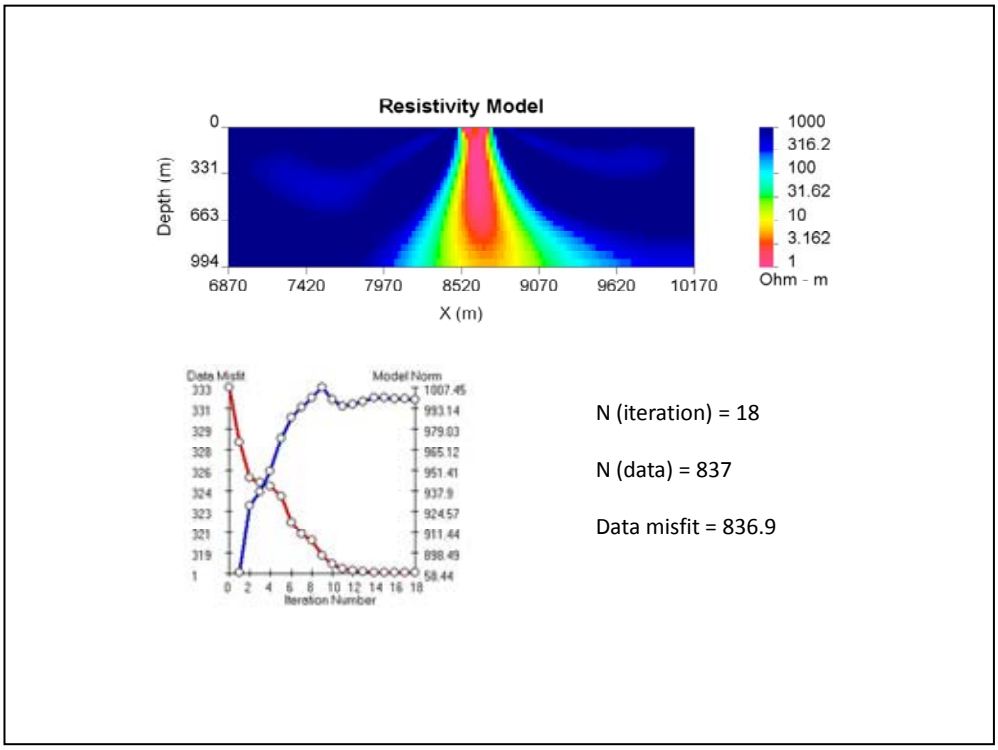

Inversion model, convergence curves and inversion statistics

J.9 IP INVERSIONS

For IP inversions, the apparent chargeability η is computed by carrying out two DC resistivity forward modeling with conductivity distributions $\sigma(x_i, z_j)$ and $(1-\eta)\sigma(x_i, z_j)$ (Oldenburg and Li, 1994), where (x_i, z_j) specifies the location in a 2D mesh.

The conductivity distributions used in IP inversions can be the inverted DC model or a half space of uniform conductivity. The IP inversion, generated through the use of a half space, is called the "NullCon" or "HSref" IP model

K INTRODUCTION TO THE MAGNETOTELLURIC METHOD

K.1 INTRODUCTION

The magnetotelluric (MT) method utilizes time-variations in the Earth's natural electric (E) and magnetic (H) fields to image the resistivity of the subsurface structure. The natural electromagnetic (EM) signals are assumed to be of plane-wave source over the frequency range with which the MT surveys are usually carried out. The plane-wave source is simpler to model compared with the complex transmitter geometries and signals used in the other EM methods. It makes the MT responses easier to understand and interpret with respect to the subsurface resistivity variations.

The E and H fields are measured over a broad range of frequencies. Typically, the frequencies can range from above 10 kHz to below 0.001Hz. Considering the conductivity of the Earth's materials and the frequency range over which the MT data are measured, the EM fields propagate in a diffusive regime. High frequency signals are attenuated more rapidly in the subsurface. Therefore, high frequency data are indicative of shallow resistivity structure while low frequency data are indicative of deep resistivity structure.

At frequencies below 1Hz the EM signal source is due to oscillations of the Earth's ionosphere as it interacts with the solar wind. At frequencies above 1Hz the signal source is due to worldwide lightning activities. There is a lack of natural signal around 1Hz, often referred to as the "hole". Modern 24-bit recording hardware and signal processing techniques, however, have largely eliminated the data quality degradations that have been traditionally seen around the 1Hz signal hole.

Between about 8Hz and 300Hz the signal from worldwide lightning activity propagates in a "resonant" cavity (the resistive atmosphere) between the conductive ionosphere and the conductive Earth's surface. Above 3 kHz the signal propagates as a ground wave. Between 300Hz and 3 kHz there is a "dead-band" where the signal does not propagate well. Despite hardware and signal processing improvements this dead-band remains problematic. When signal (atmospheric activity) is present within several hundreds of miles of the survey area the data quality improves. When no signal is being generated in the vicinity of the survey area the data quality is poor.

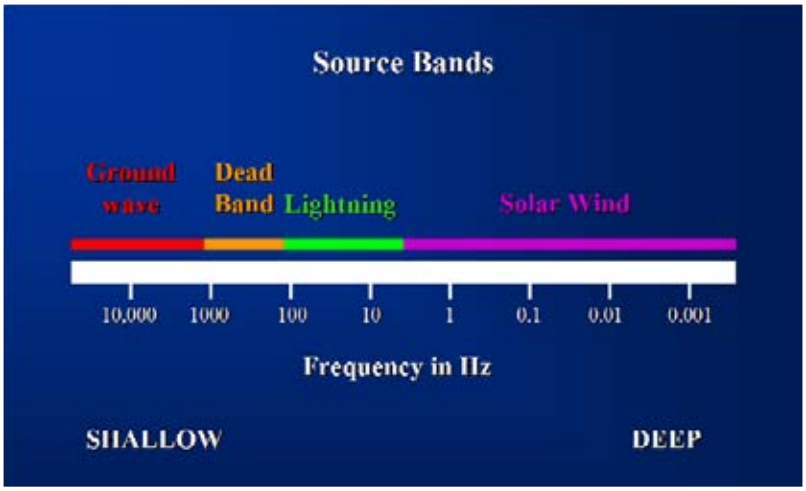

K.2 MEASUREMENTS

Both the electric and magnetic fields are measured at each site. The measured field strengths depend on the ionosphere and lightning activities and are essentially of random nature. While the E and H field strengths are random the ratio of these two fields depends on the frequency and the subsurface resistivity structure. For a homogeneous and a 1D earth resistivity structures, the magnetic field is perpendicular to the electric field. However, it is possible for a complex subsurface resistivity structure to rotate the fields. Therefore, full tensor data, including two perpendicular electric and two perpendicular magnetic fields, are usually measured.

In the field surveys, the electric and magnetic fields are measured as a function of time. The electric field is measured using two orthogonal grounded dipoles. The magnetic field is also measured using induction coils parallel to the electric dipoles.

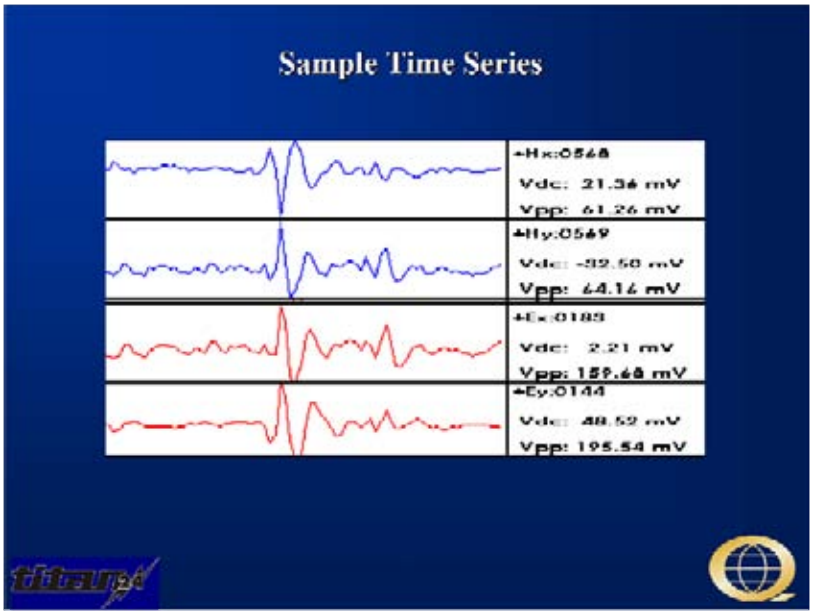

K.3 DATA PROCESSING

Extracting the subsurface resistivity structure from the measured magnetic and electric fields is a multi-step process. First, time series are transformed into frequency domain and sophisticated processing techniques are used to estimate the MT impedance tensor from the electric and magnetic fields. The impedance tensor is then used to calculate the apparent resistivity and phase data. In interpretation stage, inversion techniques are used to invert the apparent resistivity and phase data in to the subsurface true resistivity image. Finally, the resistivity image must be interpreted in terms of geologic units.

In time series processing, the measured magnetic and electric fields are Fourier transformed into the frequency domain. Calibration curves are applied to the measured fields to remove the acquisition system response. The Fourier coefficients represent the amplitude and phase of the electric and magnetic fields as a function of frequency.

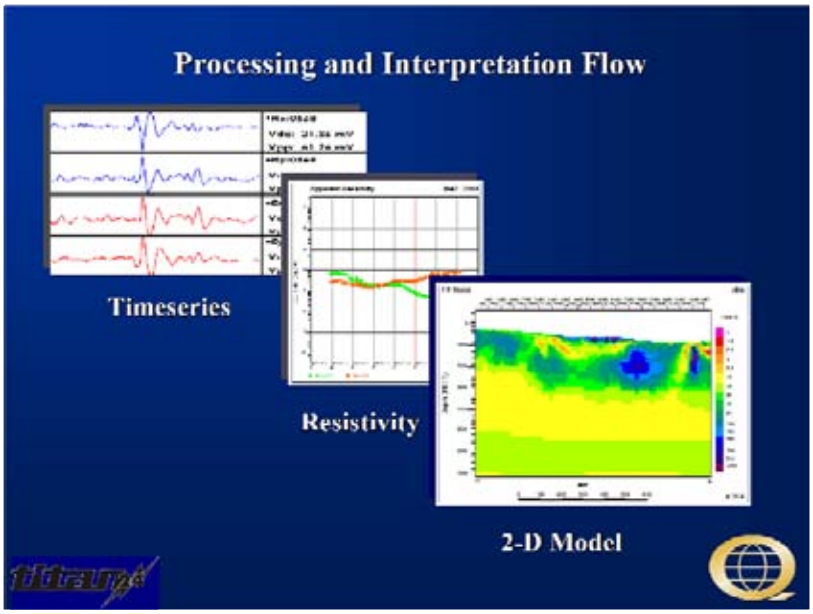

A variety of complex signal processing techniques are used to minimize noise and bias in the estimation of geophysical parameters from the measured fields. The approaches include:

- Spatial isolation of noise. A remote reference magnetic station is used to separate signal from local noise in the magnetic field data;
- Coherency sieves to find coherent signal. First the local and remote magnetic field measurements are compared and coherent signal are kept. Then the local magnetic and electric fields are compared for coherency;
- Frequency isolation of noise. Long Fourier transforms are used to provide extremely sharp isolation of noise in frequency;
- Time isolation of noise. Short Fourier transforms are used to remove noise that is isolated in time (noise spikes, or noise that is randomly turning off and on);
- Robust statistics that minimize biasing effects of a few isolated measurements.

The geophysical parameters are estimated after the processing is completed. In frequency domain, the ratio between the two measured components (E and H) is called electrical impedance (Z) and is defined as $|Z| = |E/H|$. The primary geophysical parameters are usually represented as plots of the apparent resistivity versus frequency and the phase versus frequency. The impedance values are used to calculate apparent resistivity and phase data as follows:

$$\rho_a(\Omega m) = \frac{1}{\mu\omega}|Z|^2 \quad \text{and} \quad \varphi = \arg(Z)$$

The apparent resistivity is a function of the frequency. The apparent resistivity can be considered as a volumetric weighted average of the resistivity and thickness of the rocks being sampled. Consequently, it is a smoothly varying function of the frequency. It can be shown theoretically that on a log-log plot of the apparent resistivity vs. frequency the curve cannot exceed a slope of +/- 45 degrees for a layered earth model. For a homogenous half-space or a one-dimensional (1D) earth the phase is related to the apparent resistivity through the Hilbert transform. This association does not exist for the 2D and the 3D earth models.

K.4 INTERPRETATION

Plots of apparent resistivity and phase data versus frequency in a log-log scale are a conventional way of looking at the data before interpretation. If the survey involves several MT sites located along a line pseudo-sections of the apparent resistivities and phases in both components provides a first impression of the resistivity variation of the subsurface along the survey line.

The depth of penetration of the EM signal depends on the frequency of the data and the resistivity of the subsurface. The depth at which the signal amplitude attenuates to 37% (1/e) of its initial value is called the electromagnetic skin depth (δ) and is defined as:

$$\delta(m) = \sqrt{\frac{2}{\mu\omega\sigma}} = 503\left(\sqrt{\frac{\rho}{f}}\right)$$

where δ (m) is the skin depth, μ the magnetic permeability, σ (S/m) the conductivity (1/resistivity), ω the angular frequency (=2πf), f (Hz) the frequency, and ρ (Ωm) the resistivity (1/conductivity)

The skin depth concept provides an estimation of the maximum depth of investigation of the MT data.

The following plots illustrate example of the apparent resistivity curves for two MT sites as well as the apparent resistivity cross-sections along a MT line over a simple geological model.

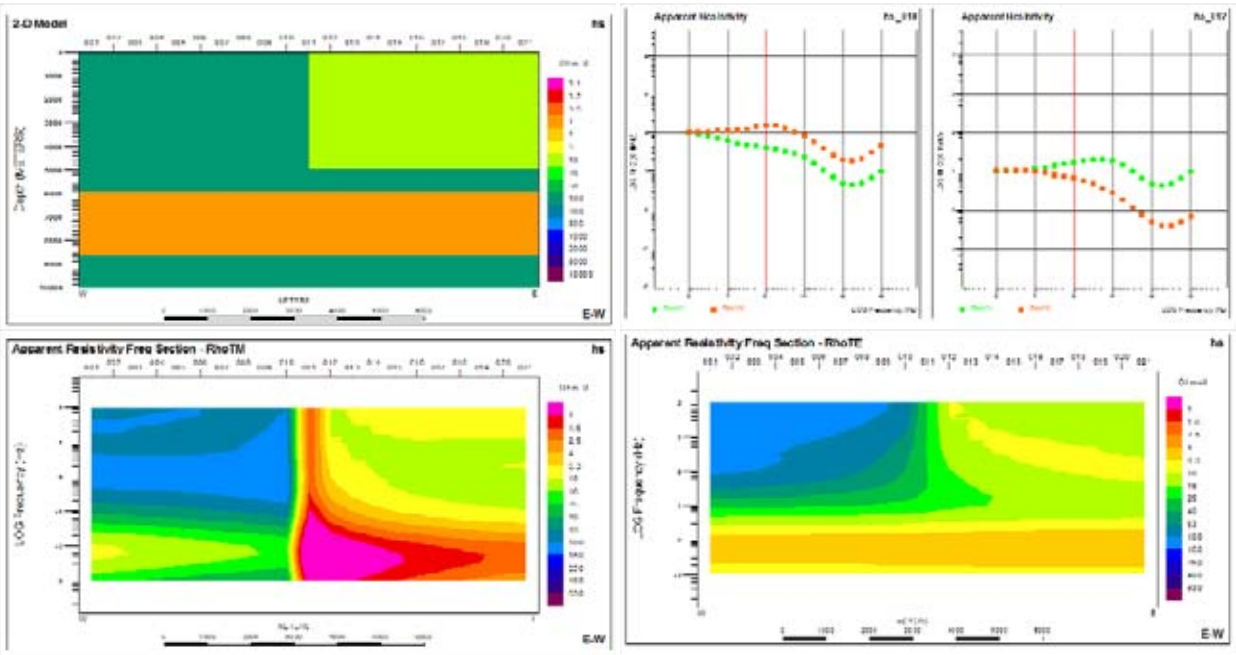

Interpretation of the MT data is performed using the maps of true resistivity of the subsurface. Inversion algorithms in one-dimension (1D), two-dimension (2D), and three-dimension (3D) are used to invert the apparent resistivity and phase data in to the maps of true resistivity of the subsurface. A simple layered subsurface structure generally can adequately be reproduced using the 1D inversion. In the case of more complex 2D or 3D structures, the MT response will be affected by lateral variations in resistivity. Consequently, a 2D or 3D inversion algorithm is required to allow the lateral resistivity variations.

In 1D earth assumption, off-diagonal elements of the impedance tensor are equal and of opposite signs and the diagonal elements are zero. The 1D inversion of the MT data produces a resistivity-depth profile

for each MT site. The results represent a first order approximation of the resistivity variations with depth using a layered-earth model.

If there are lateral variations in the resistivity of the subsurface along one direction only (perpendicular to the strike) then a 2D inversion and interpretation is required. In this case, for a data rotated to the strike direction, off-diagonal elements of the impedance tensor are of opposite signs but not equal and the diagonal elements are zero. Because the electrical conductivity is constant along the strike direction (for example x-direction) all derivatives with respect to x will be zero. Therefore, Maxwell's equations are simplified and can be separated into two distinct modes so-called Transverse Electric (TE) and Transverse Magnetic (TM). The TE-mode represents the condition where the electric field is parallel to the strike direction while the TM-mode represents the condition where the magnetic field is parallel to the strike direction.

A cross-section of the true resistivity variations perpendicular to the assumed strike direction is created in the 2D inversion and is used in interpretation. For more complex geological structures a 3D inversion is essential to adequately describe the resistivity variation of the subsurface. In this case, none of the elements in the impedance tensor are equal or zero.

One of the factors that can affect the multi-dimensional MT data and interpretation is "static shift". The apparent resistivity curves can be biased (shifted up or down) by lateral resistivity contrasts with dimensions smaller than the minimum wavelength of the EM fields. These small features cannot be resolved by the MT data and they introduce a DC shift on the log-log apparent resistivity plots. This effect can be recognized by examining the sounding resistivity curves from the neighbouring MT sites and most be treated before the interpretation. Note that there are no static shift effects in the phase data.

L REFERENCES

L.1 TITAN-24 METHOD AND APPLICATION

Donohue, J.G., and Sheard, S.N., 2001. Geophysics in North West Queensland – Improving the use of electrical geophysics. AIG Journal Paper 2001-01.

Garner, S., and Webb, D., 2000. Broadband MT and IP electrical property mapping with MIMDAS. SEG Technical Program Expanded Abstracts, 1085-1088.

Goldie, M., 2007. A comparison between conventional and distributed acquisition induced polarization surveys for gold exploration in Nevada. The Leading Edge, 26 (2), 180-183.

Hollyer, G, and Hearst, R., 2009. Deep exploration technologies for discovery in the shadow of head frames. First Break, 27 (July), 99-105.

Kingman, J., and Garner, S., 2003. Benefits of large channel capacity systems in electrical geophysics. ASEG 16th Geophysical Conference and Exhibition, Adelaide.

Legault, J., Carriere, D., and Petrie, L., 2008. Synthetic model testing and distributed acquisition dc resistivity results over an unconformity uranium target from the Athabasca Basin, northern Saskatchewan. The Leading Edge, 27 (1), 46-51.

Sheard, N., 1998. MIMDAS: A new direction in geophysics. Proceedings of the ASEG 13th International Conference, Hobart, Tasmania.

White, M., and Gordon, R., 2003. Deep imaging: New technology lowers cost of discovery. Canadian Mining Journal, April, 27-28.

L.2 DIRECT CURRENT (DC) AND INDUCED POLARISATION (IP) METHODS

Cogan, H., 1973, Comparison of IP electrode arrays, Geophysics, 38, p 737 - 761.

Halverson, M.O., Zinn, W.G., McAlister, E.O., Ellis, R., and Yates, W.C., 1981. Assessment of results of broad-band spectral IP field test. In: Advances in Induced Polarization and Complex Resistivity, 295-346, University of Arizona.

Johnson, I.M., 1984. Spectral induced polarization parameters as determined through time-domain measurements. Geophysics, v. 49, 1993-2003.

Langore, L., Alikaj, P., Gjovreku, D., 1989, Achievements in copper sulphide exploration in Albania with IP and EM methods, Geophysical Prospecting, 37, p 925 - 941.

Li, Y., and Oldenburg, W., 2000. 3-D inversion of induced polarization data. Geophysics, v 65 (6), 1931-1945.

Loke, M.H., 2004. Tutorial: 2D and 3D electrical imaging surveys, Res2Dinv and Res3Dinv manual [www.geoelectrical.com].

Oldenburg, D., and Li, Y., 1994. Inversion of induced polarization data. Geophysics, 59, 1327-1341.

Oldenburg, D., Li, Y., and Jones, F., 1998. Tutorial: Inversion (Res/IP) Methodology. In: The UBC-GIF Tutorials [http://www.geop.ubc.ca/ubcgif].

Oldenburg, D., and Li, Y., 1999. Estimating depth of investigation in DC and IP surveys. Geophysics, 64, 403-416.

Pelton, W.H., Ward, S.H., Hallof, P.G., Sill, W.R. and Nelson, P.H., 1978. Mineral discrimination and removal of inductive coupling with multi-frequency IP. Geophysics, v.43, 588-609.

Quantec, 2009. Standard chargeability calculations in Titan-24 IP measurements. Quantec Technical Note 001.

Seigel, H., 1959. Mathematical formulation and type curves for induced polarization. Geophysics, 24, 547-565.

Telford., W.M., Geldart, L., Sheriff, R., and Keys, D., 1976. Applied Geophysics. Cambridge University Press, New York, NY.

Van Blaricom, R., 1992. Practical Geophysics for the Exploration Geologist. Nortwest Mining Association, Spokane, WA.

Wait, J., 1959. Overvoltage Research and Geophysical Applications. Pergammon Press.

L.3 MAGNETOTELLURIC (MT) METHOD

Bahr, K., and Simpson, F., 2005, Practical Magnetotellurics, Cambridge University Press.

Berdichevsky, M.N., Dmitriev, V.I., Pozdnjakova, E.E., 1998. On two-dimensional interpretation of magnetotelluric soundings. Geophys. J. Int. 133, 585–606.

Constable, S.C., Parker, R.L., and Constable, C.G., 1987. Occam's inversion - A practical algorithm for generating smooth models from electromagnetic sounding data. Geophysics, 52 (3), 289-300.

de Lugao, P.P., and Wannamaker, P.E., 1996. Calculating the two-dimensional magnetotelluric Jacobian in finite elements using reciprocity. Geophysical Journal International, 127, 806-810.

Marquardt, D.W., 1963. An algorithm for least-squares estimation of non-linear parameters. J. Sot. Ind. Appl. Math., 11, 431–441.

Nabighian, M.N., 1987. Electromagnetic Methods in Applied Geophysics, Volume 2: Application (Parts A and B). Society of Exploration Geophysicists (SEG), Tulsa.

Orange, A.S., 1989. Magnetotelluric exploration for hydrocarbons. Proceedings of the IEEE, 77, 287-317.

Rodi, W., and Mackie, R.L., 2001. Nonlinear conjugate gradients algorithm for 2D magnetotelluric inversions. Geophysics, 66, 174-187.

Siripunvaraporn, W., Egbert, G., Lenbury, Y., and Uyeshima, M., 2005. Three-Dimensional Magnetotelluric: Data Space Method. Physics of the Earth and Planetary Interiors, 150, 3-14.

Vozoff, K., 1972. The Magnetotelluric method in the Exploration of Sedimentary basins. Geophysics, 37, 98-141.

Wannamaker, P., Hohmann, G., Ward, S., 1984. Magnetotelluric response of three-dimensional bodies in layered earth. Geophysics 49, 1517–1534.

Wannamaker, P.E., Stodt, J.A., and Rijo, L., 1987. A stable finite-element solution for two-dimensional magnetotelluric modeling. Geophysical Journal of the Royal Astronomical Society, 88, 277-296.

Wight, D.E., 1987. MT/EMAP Data Interchange Standard, Revision 1.0. Society of Exploration Geophysicists (SEG). (Document available at the SEG web site: www.seg.org).

L.4 TECHNICAL REPORTS AND ARTICLES

R.Pooley, s-Lomas, G-Hawthorn, and RB-Alexander; NI 43-101 Technical Report for a Preliminary Economic Assessment on the Elk Gold Project, Merritt, British Columbia, Canada, for almaden Minerals. January, 2011.

R.Pooley, s-Lomas, G-Hawthorn, and RB-Alexander; NI 43-101 Technical Report for a Preliminary Economic Assessment on the Elk Gold Project, Merritt, British Columbia, Canada, for almaden Minerals. January, 2011.

Dubé, B; Gosselin, P; Greenstone-hosted Quartz-Carbonate Vein Deposits. In, Mineral deposits of Canada: a synthesis of major deposit-types, district metallogeny, the evolution of geological provinces, and exploration methods; Goodfellow, W D (éd.); Geological Association of Canada, Mineral Deposits Division, Special Publication no. 5, 2007; pages 49-73.

Quantec Geoscience Ltd Summary Table	
CLIENT	
Client / Company Name	Gold Mountain Mining Corporation
Client Main Location	(British Columbia, Canada)
Client Representative	Peter Thiersch Vice President Exploration
Phone Number	(604) 558 4653 x237
Fax Number	(604) 682-2993
Email Contact (if available)	PeterT@aumtn.com
PROJECT	
Project Grid Name	Elk Gold Project
Project Grid Location	(British Columbia, Canada)
Survey Type	Titan-24 DC - IP - MT
Survey Period (YY/MM/DD to YY/MM/DD)	2011/09/24 to 2011/10/10
Quantec Project Number	CA00900T
Responsible Geophysicist	Benoit Tournerie
Data Processor	Wade Lee
REPORT	
Report Date	08/11/2011
Quantec Template Version	2011.2

Inversion Results (Line L92800E)

DC Model

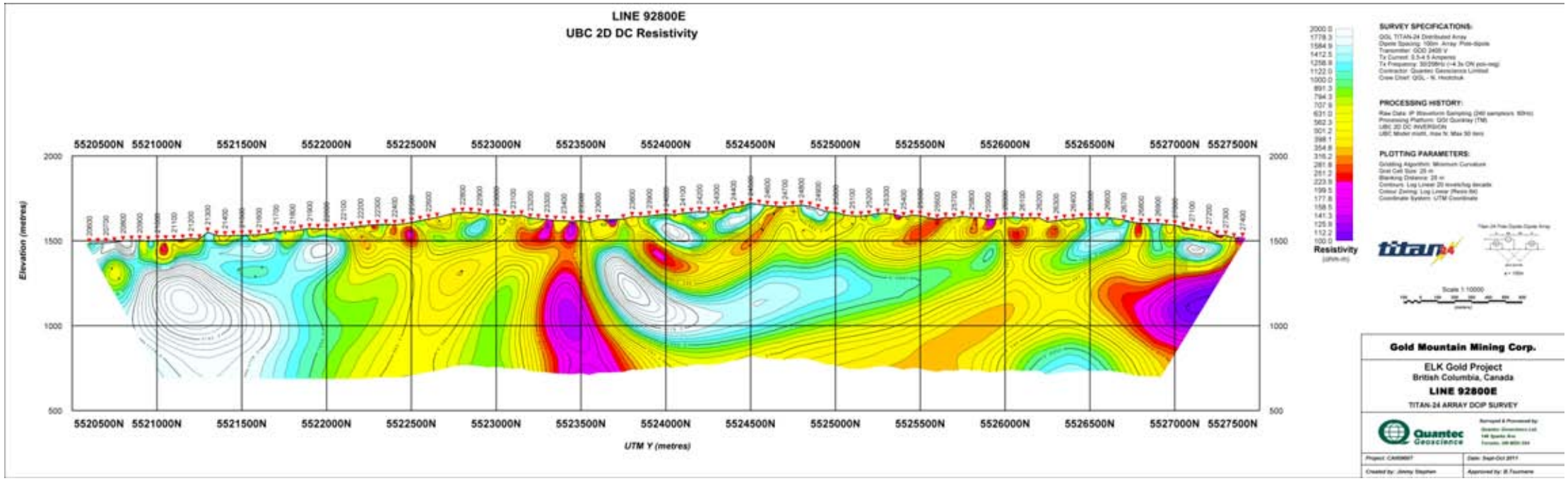

Inversion Results (Line L92800E)

IP Models

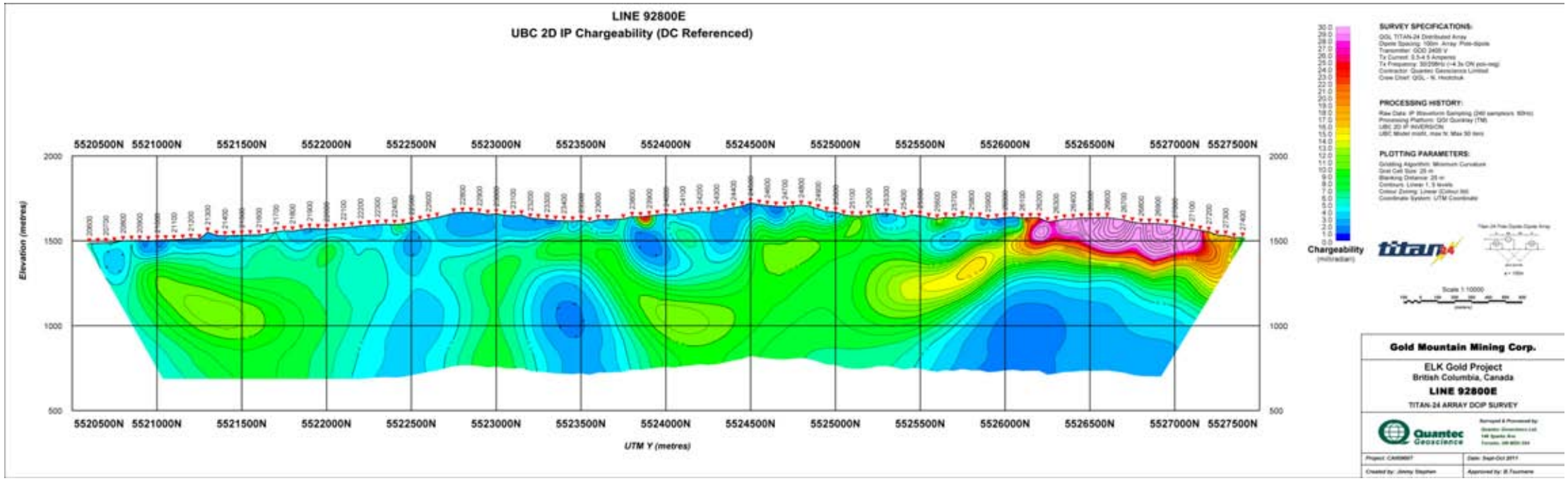

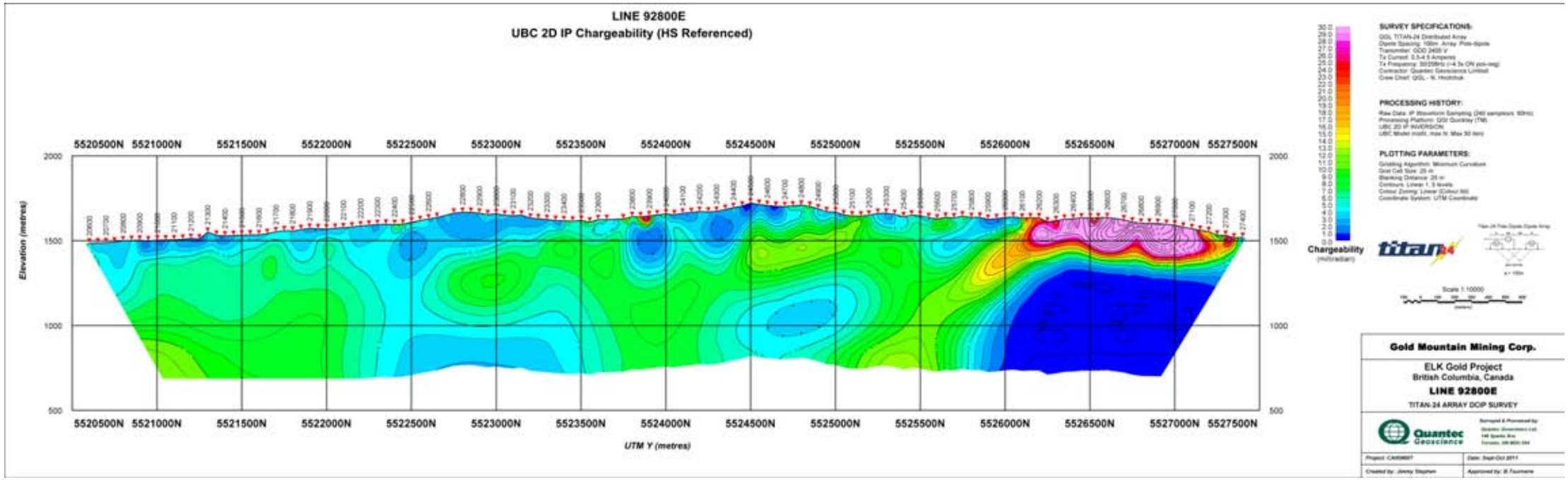

Inversion Results (Line L93200E)

DC Model

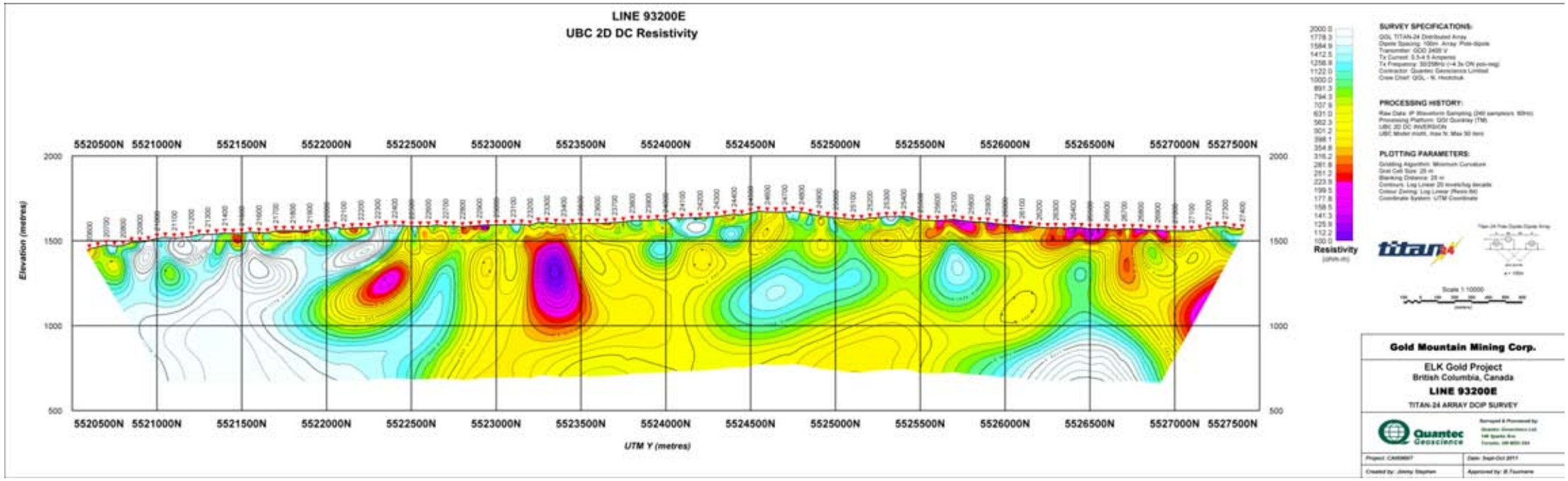

Inversion Results (Line L93200E)

IP Models

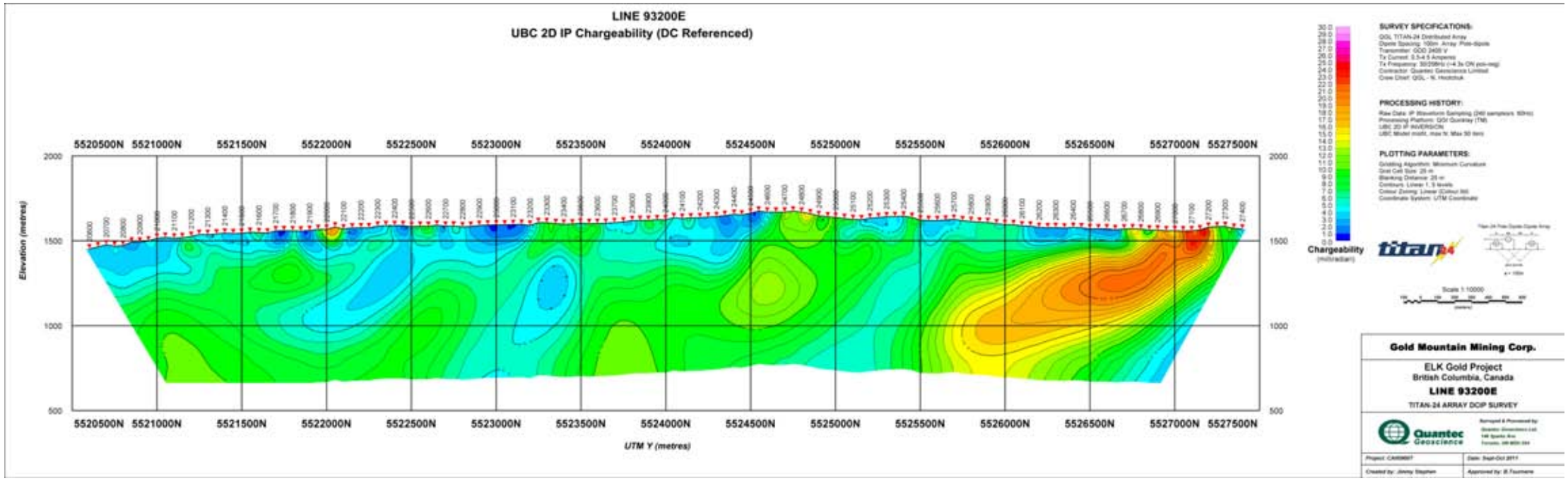

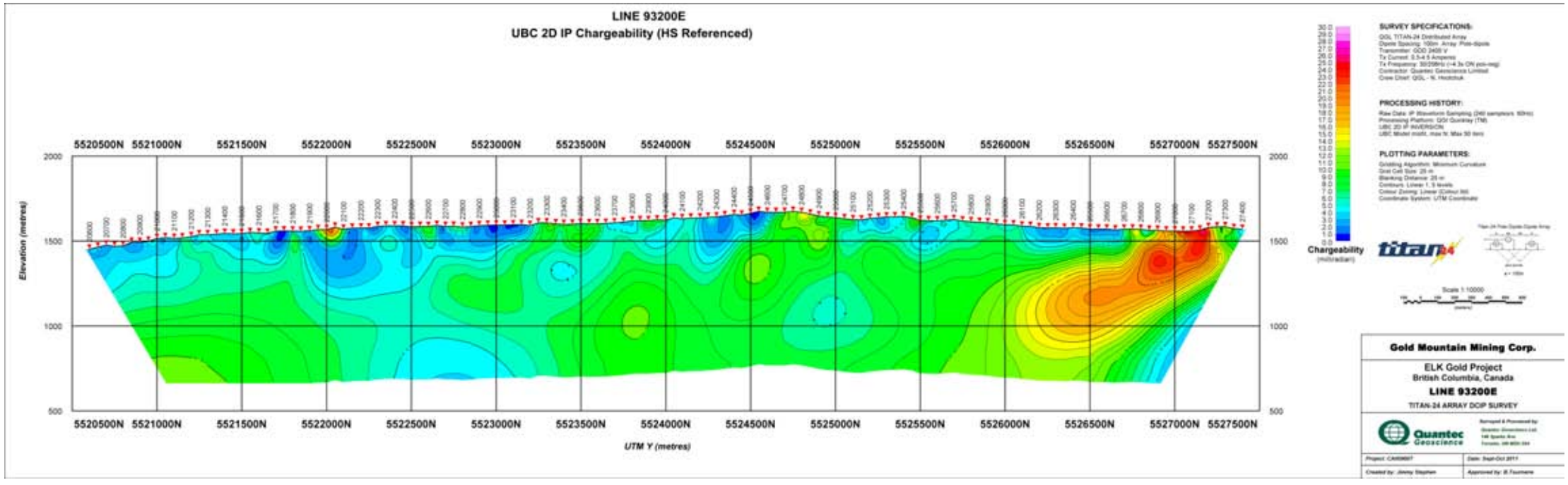

Leaders in Deep Exploration
Quantec Geoscience

GOLD MOUNTAIN MINING CORPORATION

ELK GOLD PROJECT

BRITISH COLUMBIA, CANADA
TITAN-24 DC / IP / MT

INVERSION RESULTS
DCIP MODELS

ELK Property Location

Leaders in Deep Exploration
Quantec Geoscience

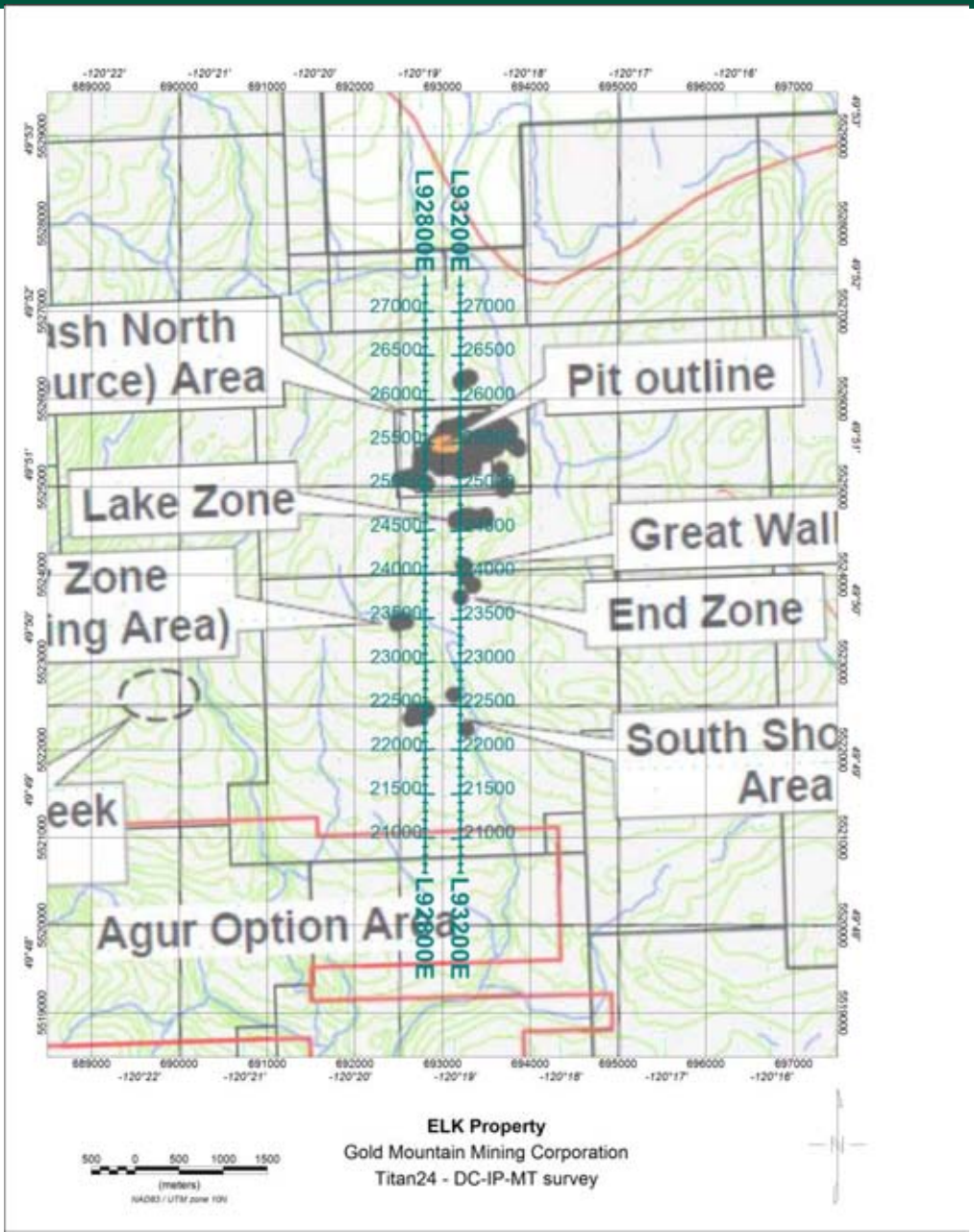

LINE L92800E
DC MODEL

Leaders in Deep Exploration
Quantec Geoscience

2013-03-25

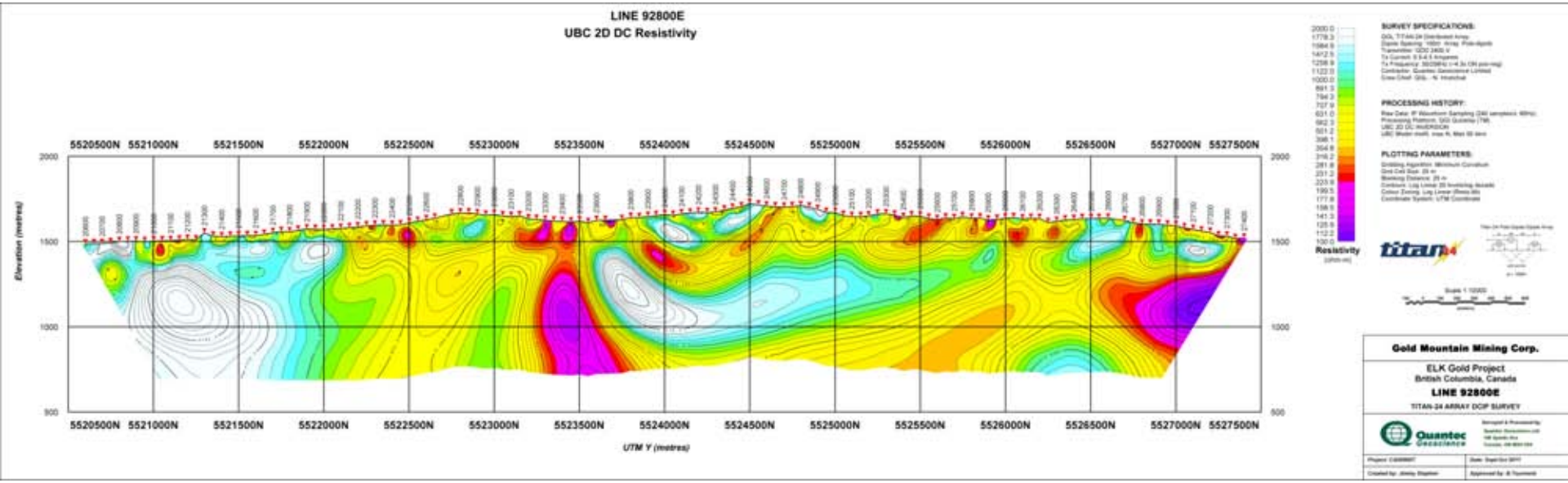

LINE L92800E
IP_DCREF MODEL

Leaders in Deep Exploration
Quantec Geoscience

2013-03-25

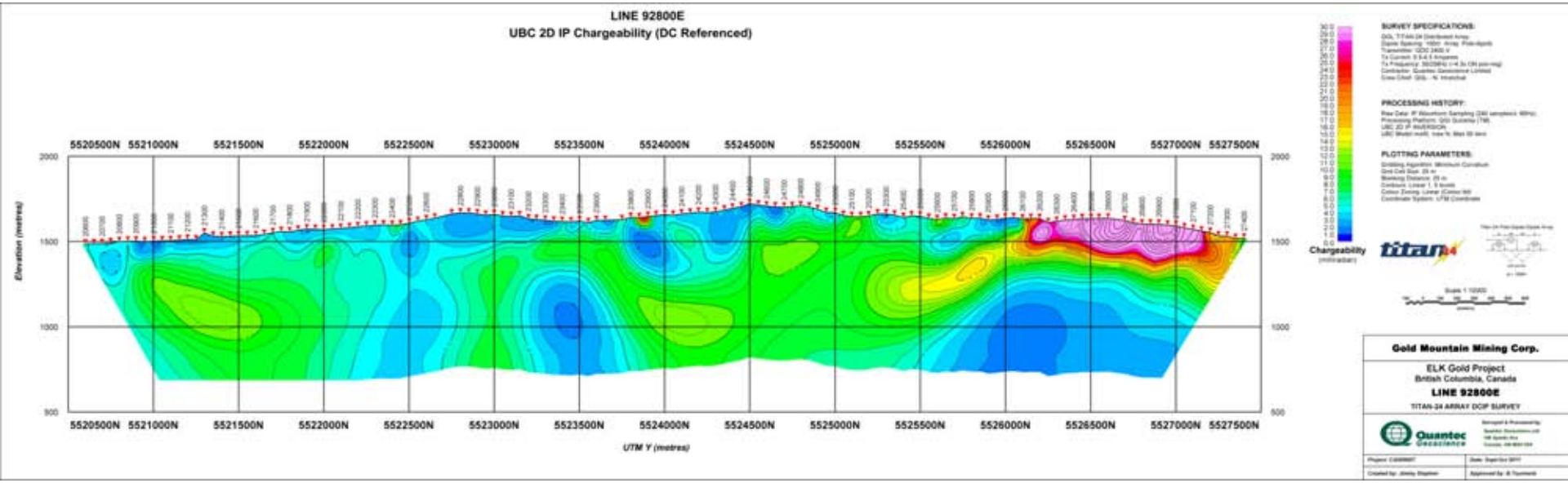

LINE L92800E
IP_HSREF MODEL

Leaders in Deep Exploration
Quantec Geoscience

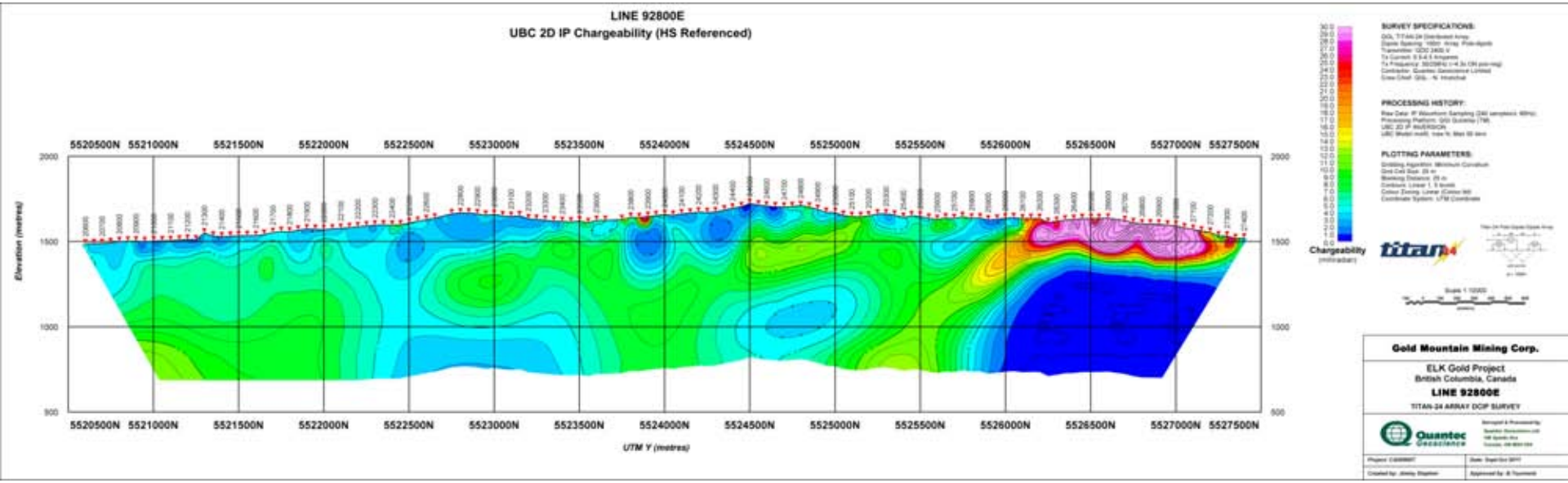

LINE L93200E
DC MODEL

Leaders in Deep Exploration
Quantec Geoscience

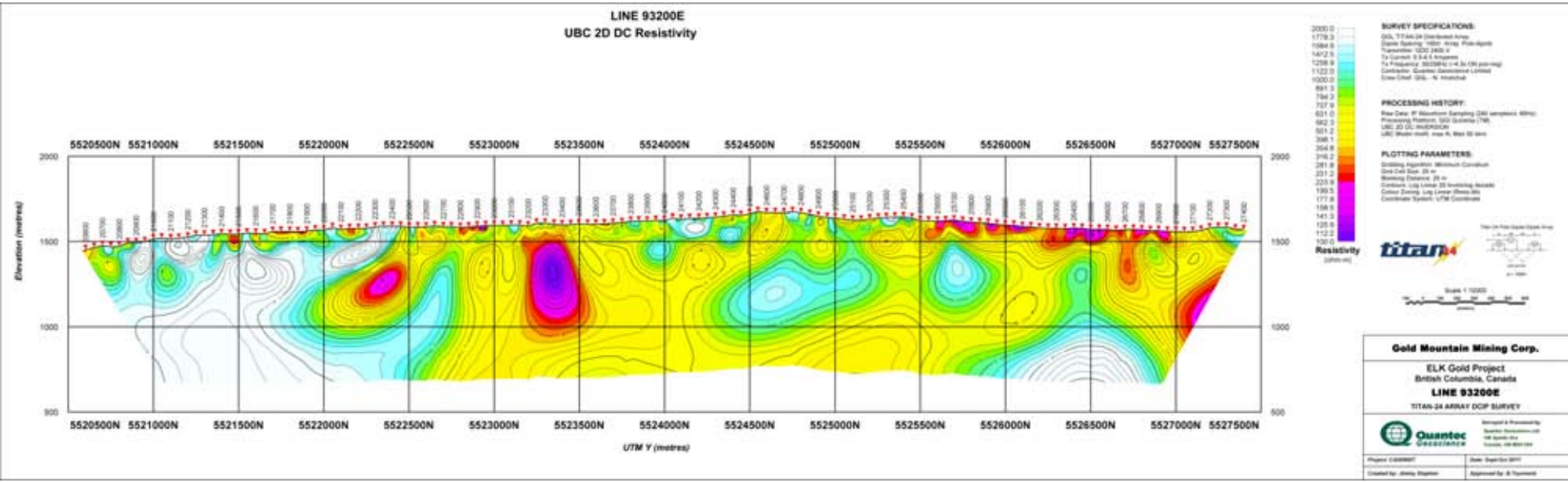

LINE L93200E
IP_DCREF MODEL

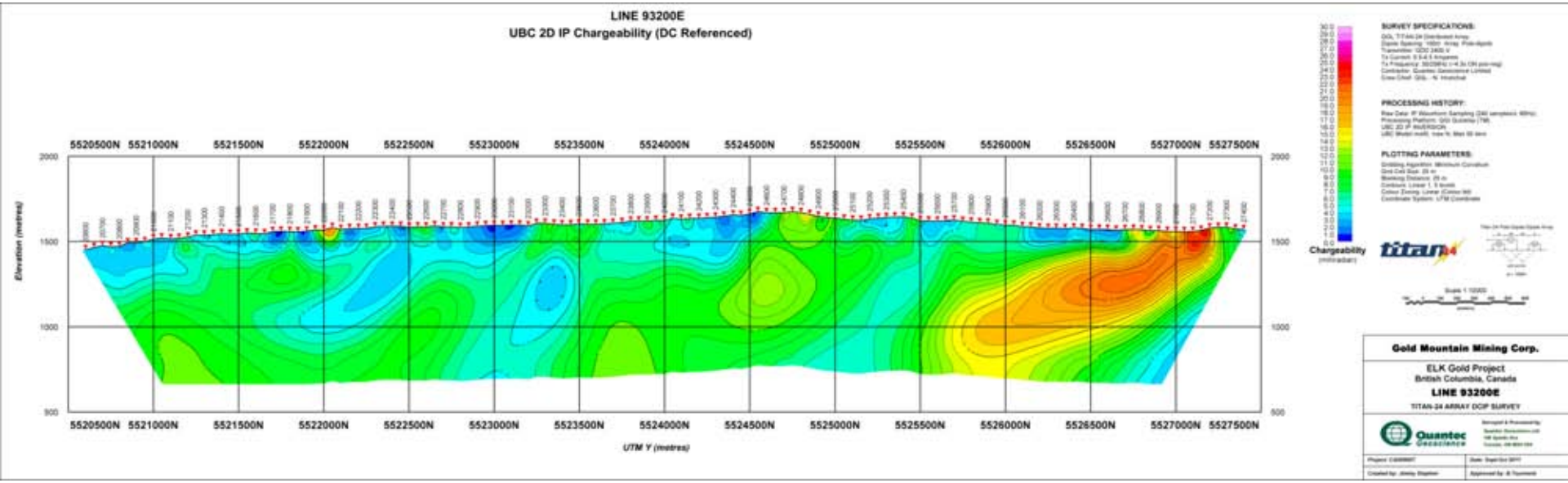

LINE L93200E
IP_HSREF MODEL

Leaders in Deep Exploration
Quantec Geoscience